Analysis of Structures Subjected to Moving Loads

Olsson, Mats

1986

Document Version:
Publisher's PDF, also known as Version of record

[Link to publication](#)

LUND INSTITUTE OF TECHNOLOGY
Division of Structural Mechanics
Report TVSM-1003
LUND SWEDEN 1986
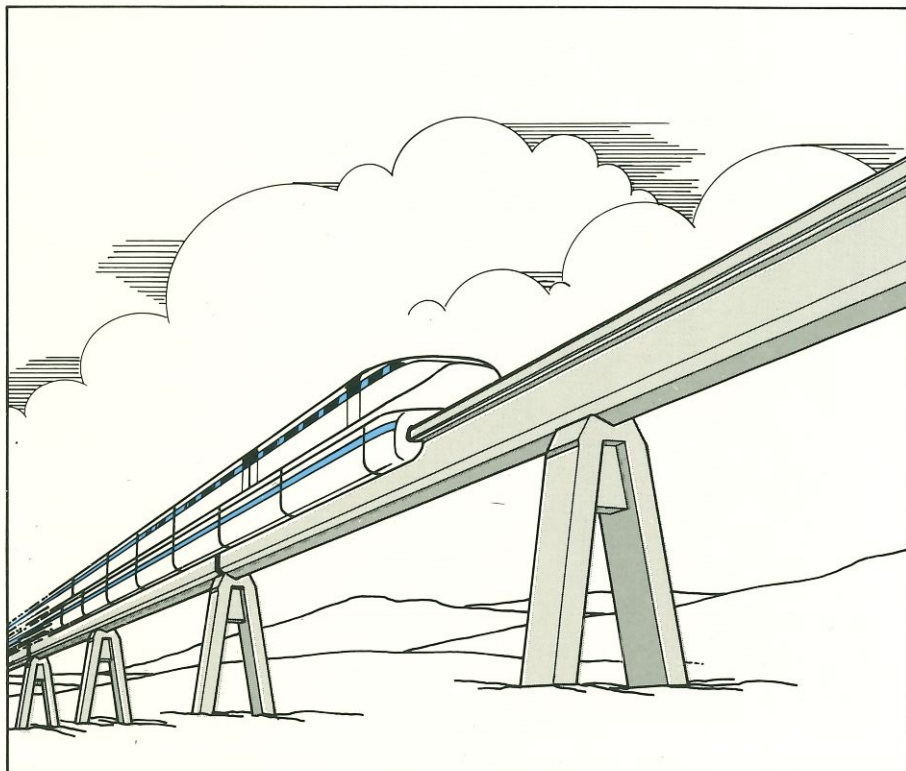
MATS OLSSON

ANALYSIS OF STRUCTURES SUBJECTED TO MOVING LOADS

Structure-Vehicle Interaction
Finite Element Formulations
Numerical Simulations

LUND INSTITUTE OF TECHNOLOGY
Division of Structural Mechanics
Report TVSM-1003

CODEN: LUTVDG/(TVSM-1003)/1-246/(1986)

MATS OLSSON

ANALYSIS OF STRUCTURES
SUBJECTED TO MOVING LOADS

Structure-Vehicle Interaction
Finite Element Formulations
Numerical Simulations

ACKNOWLEDGEMENTS

CONTENTS

ACKNOWLEDGEMENTS

ABSTRACT

ABSTRACT

Analysis of structures subjected to moving loads is presented. In particular, structural effects due to structure-vehicle interaction are studied. The basic equations of the structure-vehicle system are derived by means of continuum mechanics, the finite element method and multibody dynamics.

In order to consider the interaction between structure and vehicle in a straightforward way, a special structure-vehicle finite element is derived in general terms. To the author's knowledge this is a new way to describe the moving load problem.

For the structural part a hierarchical finite beam element is derived. Polynomial terms and, as a special feature, eigenfunctions can be used as hierarchical functions. The element is capable of handling coupled vibrations and warping torsion. The element has a number of options which makes it flexible in use.

Numerical results are mainly presented in terms of time histories and dynamic magnification factors for structural displacements and moments as functions of different models and parameters. Structural effects due to different vehicle models are studied in particular. In the verification examples, present results show good agreement with theoretical and experimental results of other investigators. To some extent, the present results are compared with structural design codes.

Key words

Moving loads, bridge, guideway, structural dynamics, structure-vehicle interaction, finite element method, modal analysis, beams, frames, torsion, warping, braking, numerical simulations, dynamic magnification, design.

1. INTRODUCTION

1.1 Analysis of structures subjected to moving loads

Structures in the field of transportation are subjected to moving loads. In contrast to other dynamic loads these loads vary not only in magnitude but also in position. In Fig. 1.1 four examples of structures subjected to moving loads are illustrated: guideways, bridges, cranes and cableways. Other examples are rails, sleepers, roadways, airport runways and pipelines.
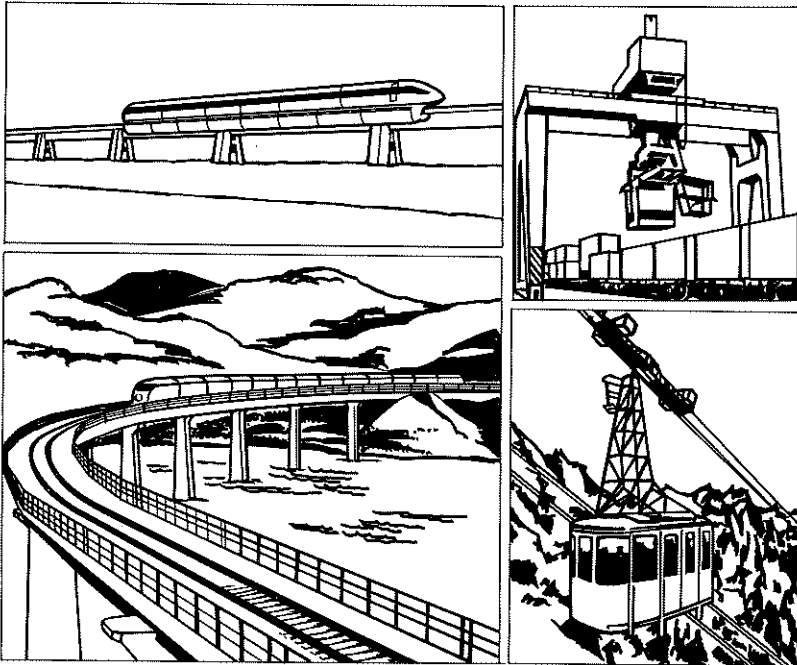
Figure 1.1. Structures subjected to moving loads.

Analyses of structures subjected to moving loads have been carried out ever since the first railway bridges were built in the early 19th century. Since that time the moving load problem has become more and more dynamic in character. This is mainly due to increased

vehicle speed and structural slenderness. In fact, high-speed facilities with vehicle speeds over 400 km/h do not seem to be unrealistic in the near future.

The increasing dynamic nature of the moving load problem has focused interest on the structure–vehicle interaction. Thus the forces between structure and vehicle depend on the motions of both the structure and the vehicle. This means that structural and vehicle analysis should not be carried out independently. Many problems of advanced transportation systems such as fatigue, wear, comfort, stability, costs, noise radiation and trip time are directly related to the structural and vehicle designs and, consequently, also to the dynamic interaction.

In the present study attention is paid to bridge and guideway structures and to the structure–vehicle interaction problem, mainly through theoretical studies. A large number of studies of the moving load problem are referred to in the excellent monograph by Frýba [38]. (A reference list is given in Appendix E). Developments and results in the present field can also be found in a number of state-of-the-art reviews: Huang [51], Kortüm and Wormley [60], Kortüm [61], Richardson and Wormley [101], Ting et al. [123]–[125] and through the committee work "Dynamics of steel elevated guideways – An overview" [32]. Previous studies are considered in greater detail in the following.

1.2   Methods of analysis

As in most other problems, the success in analysing structures subjected to moving loads is closely related to the purpose of the analysis, the choice of models and input data and the methods of analysis available. Up to the 1940s analysts had to rely almost

entirely on analytical methods. Thus, only simple bridge and vehicle models could be treated, for instance a simply supported beam subjected to moving constant forces (static axle loads). Most of the analytical methods used are described by Frýba [38].

A more general analysis, however, calls for numerical methods. Since computers came into use in the 1950s such methods have been used to treat more realistic structural and vehicle models and, in particular, the structure–vehicle interaction. The discretizations introduced in connection with numerical methods are related to either the space domain or the time domain. The space domain discretization of the vehicle often results in a vehicle model in terms of a number of rigid bodies connected by massless springs and dampers (Sec. 2.3). While leaving comments on the discretization in time until Chapter 5, the rest of this section is devoted to methods of discretization in space of the structure. The most important methods used in analysis of structures subjected to moving loads are described and compared below.

The lumped mass method

In modelling the structure its mass may be concentrated or lumped at a limited number of points, see for example Clough and Penzien [17]. A limited number of ordinary differential equations, related to the translations of these mass points, is obtained in this way. Damping and external loads may also be lumped at these points while the distributed stiffness is often handled by means of influence coefficients. For structures with a large proportion of their total mass actually concentrated at a few discrete points this method may be advantageous. In connection with the moving load problem this method has been used by e.g. Chu et al. [15], Kishan and Traill–Nash [55] and Veletsos and Huang [129].

The integral formulation method

In treating distributed mass, damping and loads, the equations of motion of a simple structure may be written in the form of integral-differential equations, see for instance Genin and Maybee [40]. The integrals represent these distributions and the inertia, damping and load effects are described by means of influence functions. The discretization in space gives ordinary differential equations similar to those obtained for the lumped mass method in combination with influence coefficients. The integral formulation method is applied to the moving load problem principally by Genin et al. [41][42] and Ting et al. [122]-[124].

The method of generalized displacements

A further method that can be used in analysing simple structures, such as simply supported beams, with distributed properties is the method of generalized displacements, see for example Clough and Penzien [17]. The deflection of such structures can be expressed by means of a set of shape functions. Like the influence functions mentioned above these functions are defined for all points of the structure and must satisfy the boundary conditions. For instance, a limited set of eigenfunctions is often used in dynamic analysis. A large number of reports and papers in connection with the moving load problem are based on the method of generalized displacements, see e.g. Arpe [3], Blejwas et al. [9][10], Wormley et al. [14][60] [101][110], Dahlberg [23], Hillerborg [47] and Popp et al. [93][95].

The finite element method

In the finite element method (FEM), see for example Zienkiewicz [141], the structure is divided into a number of finite elements. The elements may be one-, two- or three-dimensional and can thus describe any structure. Each element has a number of degrees of

freedom and a shape function is related to each of these. Thus, in contrast to the influence and shape functions above the present functions often only describe a part of the structure. In addition, the boundary conditions are not introduced until the resulting system of equations is solved. Certain features of the lumped mass method may be adopted in the finite element method. FEM has been applied to the moving load problem by e.g. Dailey et al. [27], Filho [35], Hino et al. [48], Malsch [70], the author [83][85], Ripegård [102], Schneider et al. [108] and Yoshida et al. [139][140].

The finite strip method

This method, see Cheung [13] and Loo and Cusens [65], is most often applied to bridge analysis. The finite strip method (FSM) can be regarded as a combination of the last two methods above: in considering a bridge structure, its behaviour along the longitudinal direction is described in terms of generalized displacements while its cross section is divided into finite elements. Thus a number of finite strips, each of them reaching from one end of the bridge to the opposite one, are introduced. FSM is especially powerful if the two ends of the bridge are simply supported and when there are no intermediate supports. For other cases FSM is quite cumbersome. FSM in moving load analysis has been used by e.g. Mulcahy [77], Smith [111] and Srinivasan and Munaswamy [113].

Comparison of methods

A comparison between the five methods described favours the finite element method due to its versatility. However, the role of FEM in dynamic analysis of structures subjected to moving loads has not been so dominant as may be expected. The main reasons for this are: 1) for design studies dynamic magnification factors are used; thus FEM is used for static analysis only in such studies, 2) modern FEM packages are not suited for the moving load problem, especially when

the structure-vehicle interaction is to be considered and 3) much of the theoretical efforts up to now have been concentrated on the determination of dynamic magnification factors as functions of a limited set of parameters; thus studies have to be made of simple structural models, which often favours the method of generalized displacements.

1.3 Aim and scope of the present study

The aim of the present study is twofold. Firstly, attempts are made to formulate refined analysis tools for quite general studies of the moving load problem. Secondly, the aim of the study is to investigate the behaviour of structures under moving loads by means of numerical simulations and a number of different structural and vehicle models. Basic restrictions inherent in the study are linear elastic structural material, vehicle modelled as rigid bodies connected by linear springs and dampers, small deformations and maintenance of contact between the vehicle (moving load) and the structure during passage.

With regard to the refined analysis tools the finite element method is adopted due to its usefulness. As indicated in Sec. 1.2, however, FEM is not immediately applicable to the moving load problem. For this purpose a special coupling element, a so-called structure-vehicle finite element, is derived to demonstrate the capability of FEM in moving load analysis. Any structural finite element may be incorporated in this special element. However, the continued analysis in this study is restricted to beam structures. A finite beam element, based on a quite extensive beam theory, for analysis of beams and beam structures in general has been developed and is adopted here.

As far as the second aim is concerned, time histories and dynamic magnification factors are presented as functions of a limited set of

parameters for quite simple but representative structure and vehicle models. However, special emphasis is put on comparing different vehicle models in this study. In particular, efforts are made to investigate under which circumstances the effects of structure-vehicle interaction are significant and when a simpler vehicle model neglecting these effects may be sufficient. To some extent the theoretical results are compared with experiments and structural design codes.

For some of the problems studied, the use of FEM may seem to be extravagant. However, the methodology of the present study is directed towards the more general moving load problem for which the versatile FEM is clearly favourable. It is believed to be fruitful to formulate the moving load problem in quite general terms although some of the problems treated in this study are limited in scope to permit verifications and insight into the moving load problem.

1.4 Summary of the contents

In Chapter 2 the basic equations for the structure, the vehicle and their interaction are derived by means of continuum mechanics, the finite element method and multibody dynamics. At this stage the structure is regarded as a general body of linear elastic material while the vehicle is modelled as a number of rigid bodies connected by linear springs and dampers. A structure-vehicle finite element is derived to handle the structure-vehicle interaction effectively. The structural equations are transformed into a limited number of modal coordinates so as to keep the computational efforts to a minimum.

In the continued analysis beams and beam structures are considered. In Chapter 3 a finite beam element is derived giving an effective analysis tool. The beam theory introduced allows for coupled vibrations and warping torsion. A special feature of the finite element, in addition to its being based on a rather extensive beam

theory, is its ability to incorporate additional displacement functions (and additional degrees of freedom) to improve its accuracy. Polynomial terms and, as a special feature, eigenfunctions can be used as additional (hierarchical) functions. In this way effective hierarchical finite elements can be used giving a minimum number of elements. The element has a number of options which makes it flexible in use.

Different vehicle models are described and their applicability is discussed in Chapter 4. The models are divided into three groups: suspension, moving mass and moving force models. The vehicle model used as a starting point for the numerical examples and a number of special cases of this model are described in particular.

In Chapter 5 the numerical procedure containing the discretization in time is presented. The equations to be solved constitute a set of linear ordinary second–order differential equations with non-constant (time–dependent) coefficients. The step–by–step algorithm used for this purpose as well as the computer implementation are described.

In Chapter 6 time histories and dynamic magnification factors are determined by numerical simulations using a number of different structure and vehicle models. The different theoretical models are compared with one another and, to some extent, with design codes. The in–plane as well as the out–of–plane structural behaviour are studied. In addition, a large scale beam structure is studied in order to demonstrate the capability of the refined analysis tools developed in a more general moving load problem.

Finally, Chapter 7 gives concluding remarks concerning the developed analysis tools and the numerical results. Possible future developments are also indicated.

2.   BASIC EQUATIONS

2.1   Introduction

In this chapter the basic equations for the structure, the vehicle and their interaction are derived. Thus it serves as a base for the continued study. Starting from a general moving load problem a number of assumptions enter the derivation. The assumptions gradually introduced in this chapter are listed at the end of this section. A special feature of the present chapter is the derivation of a structure–vehicle finite element (Sec. 2.4). By means of this analysis tool the structure–vehicle interaction can be studied in a simple and straightforward way.

The starting point in deriving the basic equations is thus the general moving load problem as shown in Fig. 2.1. (Notations are listed in Appendix A). The structure is modelled as a three-dimensional continuum supported on parts of its boundary surface. The vehicle mainly consists of a number of three–dimensional bodies ($b = 1,2...n_b$). At this stage, these bodies may also be considered as continuous and deformable. In addition, the vehicle model contains connecting elements such as springs and dampers (not shown in Fig. 2.1) that tie the vehicle bodies to each other. The vehicle moves along a path on the structure.

A Lagrangian description of motion, see e.g. Malvern [71] and Spencer [112], is chosen for both the structure and the vehicle. Thus the motion of each material point of the structure or vehicle is described by means of a reference configuration. As shown in Fig. 2.1 a right–handed rectangular Cartesian reference frame X is introduced to describe the motion of the structure and of the vehicle (unit base vectors e_{Xi}). This frame is earth fixed, and thus inertial, and the position of each material point in the undeformed configuration can be identified by a vector X. The reference frame Y
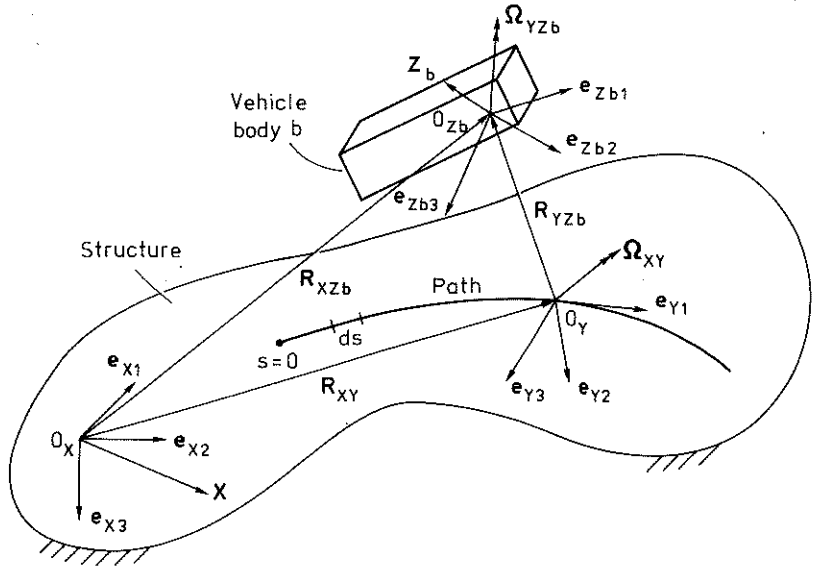
<u>Figure 2.1</u>. Reference frames for a general moving load problem. Only one vehicle body is indicated. For a railway vehicle the body may model the vehicle cabin, a bogie or a wheel. Connecting elements such as springs and dampers are not shown.

is, however, moving with the vehicle and is in general noninertial (accelerated). The same applies to the reference frames Z_b ($b = 1,2...n_b$). In this way the absolute motion of the structure and vehicle can be measured in the frame X whereas the relative motion of the moving vehicle is measured in Y or Z_b.

As implied above the origin O_Y of the frame Y moves at the vehicle speed along the vehicle path on the structure, see Fig. 2.1. The structural surface deformations and irregularities are not included in this referential (nominal) path. For tracked vehicles the path may, for instance, coincide with the track centre line. The position of O_Y is described by means of the position vector R_{XY} or the curvilinear coordinate s. Measured from the fixed frame X, the

vehicle reference frame Y not only translates but in general also rotates. This rotation is represented by the angular velocity vector Ω_{XY} (Fig. 2.1). The rotations of the base vectors $\mathbf{e}_{Yi}$ (Y-axes) are related to the nominal vehicle path and structural surface as follows: the vector $\mathbf{e}_{Y1}$ is tangential to the vehicle path at O_Y and directed in the forward vehicle direction (speed vector $v\mathbf{e}_{Y1}$ if the vehicle speed is denoted by v). The vector $\mathbf{e}_{Y2}$ is orthogonal to $\mathbf{e}_{Y1}$, lies in the tangent plane to the structural surface at O_Y and is directed to the right as seen from the forward vehicle direction. Finally, the unit base vector $\mathbf{e}_{Y3}$ completes a right-handed reference frame.

In analogy, each vehicle body reference frame Z_b is related to the overall vehicle frame Y through a position vector $\mathbf{R}_{YZb}$ and an angular velocity vector Ω_{YZb} (Fig. 2.1). Further, a vector Z_b can identify each vehicle material point in the undeformed configuration. As shown in Fig. 2.1 the position of the origin O_{Zb} can be related to the frame X through the vectors $\mathbf{R}_{XY}$ and $\mathbf{R}_{YZb}$ or directly through the vector $\mathbf{R}_{XZb}$.

After this introductory description of the general moving load problem the basic equations will be derived for the structure (Sec. 2.2), the vehicle (Sec. 2.3) and their interaction (Sec. 2.4). A number of assumptions are introduced to cope with this. The assumptions adopted in this chapter are:

- small structural strains and rotations (Subsec. 2.2.1)
- geometric effects of the structure are negligible (2.2.2)
- initially unstressed and unstrained structure (2.2.3)
- linear elastic and isotropic structural material (2.2.3)
- separable space and time discretizations of structure (2.2.4)
- prescribed vehicle path and speed (2.3.1)
- rigid vehicle bodies (2.3.1)
- small relative motions of the vehicle bodies (2.3.1)

- linear viscous dampers and linear elastic springs are the only
  connecting elements of the vehicle (2.3.3)
- holonomic constraints (maintained contact) (2.4.1)
- structural irregularities are not considered (2.4.3).

These assumptions, which enter the derivation gradually, are under-
lined and further commented on in the following text. A summary of
Chapter 2 is given in Sec. 2.5.

2.2   Structure

The basic equations describing the structural behaviour are derived
in this section. These equations are presented within the framework
of continuum mechanics in the first three subsections: kinematic
equations (2.2.1), equations of motion (2.2.2) and constitutive
equations (2.2.3). With regard to continuum mechanics, see e.g.
Malvern [71], Peterson [91], Spencer [112] and Truesdell [127]. The
last part of this section, Subsec. 2.2.4, gives the basic equations
within the concept of the finite element method.

2.2.1 Kinematic equations

With the fixed Cartesian reference frame X introduced in Sec. 2.1
the absolute motion of a material point of the structure at
reference position X and at time t can be expressed by

$$x = x(X, t).\tag{2.1}$$

Thus the vector x represents the current position of the material
point or particle. (As far as possible, reference quantities are
denoted by capital letters and current quantities by lower-case
letters). The displacement components $u_i(X, t)$ of a particle can be
defined by

$$x_i = X_i + u_i \tag{2.2}$$

where x_i, X_i and u_i refer to the same base vector (e_{Xi}). Further, the deformation gradient tensor F is defined by

$$F_{iJ} = \frac{\partial x_i}{\partial X_J} = \delta_{iJ} + \frac{\partial u_i}{\partial X_J} \tag{2.3}$$

where δ_{iJ} is the Kronecker delta. As a measure of strain the Green strain tensor E is used. Hence

$$E = \frac{1}{2}(F^T F - 1) \tag{2.4}$$

where 1 is the unit tensor. In component form Eq. (2.4) is given by

$$E_{IJ} = \frac{1}{2}\left(\frac{\partial u_J}{\partial X_I} + \frac{\partial u_I}{\partial X_J} + \frac{\partial u_K}{\partial X_I}\frac{\partial u_K}{\partial X_J}\right). \tag{2.5}$$

For the problem studied it is reasonable to assume small structural strains and rotations, i.e.

$$\left|\frac{\partial u_i}{\partial X_J}\right| \ll 1. \tag{2.6}$$

Thus Eq. (2.5) can be written as

$$E_{IJ} = \frac{1}{2}\left(\frac{\partial u_J}{\partial X_I} + \frac{\partial u_I}{\partial X_J}\right). \tag{2.7}$$

2.2.2 Equations of motion

The Piola–Kirchhoff stress quantities are related to the undeformed configuration. The second Piola–Kirchhoff stress tensor, $\tilde{T}$, is

chosen here as stress quantity since it is symmetric. With respect to the reference (undeformed) volume V of the structure the equations of motion are

$$\frac{\partial}{\partial X_J}(\tilde{T}_{JI}\,\frac{\partial x_i}{\partial X_I}) + U_i = \rho\,\frac{d^2 x_i}{dt^2} \tag{2.8}$$

where U_i and ρ are the body load components and the mass density respectively, both measured with respect to the reference frame X. With reference to the boundary surface S of the structure the stress boundary conditions may be written as

$$\tilde{t}_I = \hat{N}_J \tilde{T}_{JI} \tag{2.9}$$

in which $\tilde{t}_I$ are the second Piola–Kirchhoff traction components and $\hat{N}_J$ the direction cosines between the X_J-axis and the normal to the surface dS. It is now assumed that geometric effects can be neglected. This means that the deformation gradient tensor can be replaced by the unit tensor in the equations of motion. Further, it is observed from Eq. (2.2) that the relation

$$\frac{d^2 x_i}{dt^2} = \frac{\partial^2 u_i}{\partial t^2} \tag{2.10}$$

must hold since the material coordinates X_i are independent of time (fixed frame X). Thus Eq. (2.8) can be written as

$$\frac{\partial}{\partial X_J}(\tilde{T}_{Ji}) + U_i = \rho\,\frac{\partial^2 u_i}{\partial t^2}. \tag{2.11}$$

2.2.3 Constitutive equations

If initial strains and stresses are neglected and linear elastic material is assumed for the structure the constitutive equations, related to the reference configuration, can be written as

$$\tilde{T}_{IJ} = C_{IJKL} E_{KL} \tag{2.12}$$

where C_{IJKL} are the fourth-order material tensor components relating the strain components E_{KL} to the stress components $\tilde{T}_{IJ}$. Since the tensors $\tilde{T}$ and E are symmetric the relations

$$C_{IJKL} = C_{JIKL} \tag{2.13a}$$

and

$$C_{IJKL} = C_{IJLK} \tag{2.13b}$$

must hold. If further the symmetric condition

$$C_{IJKL} = C_{KLIJ} \tag{2.13c}$$

is imposed and if the structural material is assumed to be isotropic Eq. (2.12) turns into Hooke's law (see Malvern [71])

$$\tilde{T}_{IJ} = \lambda \delta_{IJ} E_{KK} + 2\mu E_{IJ} \tag{2.14}$$

in which λ and μ are the Lamé elastic constants. These constants are related to the elastic modulus E, Poisson's ratio υ and the shear modulus G as follows:

$$\lambda = \frac{\upsilon E}{(1+\upsilon)(1-2\upsilon)} \tag{2.15a}$$

and

$$\mu = G = \frac{E}{2(1+\nu)}.$$ (2.15b)

2.2.4 Finite element discretization

As implied in Sec. 1.2 the finite element method is very suitable when the spatial discretization process is concerned. The method is described in many text books, see e.g. Bathe [5], Segerlind [109], Thelandersson [118], Vichnevetsky [130] and Zienkiewicz [141]. Only a brief summary, based on the previous equations in Sec. 2.2 and weighted residuals, is given here.

First multiply the equations of motion in Eq. (2.11) by weighting functions $W_{imp}(X,t)$ (i=1,2,3; m=1,2...; p=1,2...) and integrate over the reference volume V of the structure and the actual time range, say $0 \leq t \leq \bar{t}$:

$$\int_0^{\bar{t}}\int_V W_{imp} \frac{\partial}{\partial X_J} \tilde{T}_{Ji} \, dVdt + \int_0^{\bar{t}}\int_V W_{imp} \, U_i \, dVdt$$

$$= \int_0^{\bar{t}}\int_V W_{imp} \, \rho \, \frac{\partial^2 u_i}{\partial t^2} \, dVdt.$$ (2.16)

Here it should be noted that if Eq. (2.16) holds for any set of weighting functions $(W_{1mp}, W_{2mp}, W_{3mp})$ it is equivalent to Eq. (2.11) (i.e. the residuals are zero). Now assume that the space dependence and time dependence of the quantities in Eq. (2.16) can be separated. This separation of variables means that the space discretization and time discretization can be treated separately. In this subsection the spatial discretization is handled whereas the time discretization is left to Sec. 5.2.

In the finite element discretization the domain V is divided into subdomains V^e called finite elements. For an arbitrary element and point of time Eq. (2.16) turns into

$$\int_{V^e} W_{im}^X \frac{\partial}{\partial X_J} \tilde{T}_{Ji} dV^e + \int_{V^e} W_{im}^X U_i \, dV^e$$

$$= \int_{V^e} W_{im}^X \rho \frac{\partial^2 u_i}{\partial t^2} \, dV^e \qquad (2.17)$$

where W_{im}^X is related to W_{imp} through

$$W_{imp}(X,t) = W_{im}^X(X) W_p^t(t). \qquad (2.18)$$

Then integration by parts of the first term in Eq. (2.17) yields

$$\int_{V^e} \frac{\partial W_{im}^X}{\partial X_J} \left[\lambda \delta_{Ji} \frac{\partial u_K}{\partial X_K} + \mu \delta_{iI} \left(\frac{\partial u_I}{\partial X_J} + \frac{\partial u_J}{\partial X_I} \right) \right] dV^e$$

$$+ \int_{V^e} W_{im}^X \rho \frac{\partial^2 u_i}{\partial t^2} \, dV^e = \int_{V^e} W_{im}^X U_i \, dV^e + \int_{S^e} W_{im}^X \tilde{t}_i \, dS^e \qquad (2.19)$$

in which Eqs. (2.7), (2.9) and (2.14) have been utilized and where S^e denotes the boundary surface of the element. The displacements u_i are now approximated within the element (displacement formulation) as

$$u_i(X,t) = \sum_n N_{in}^e(X) u_n^e(t) \qquad (2.20)$$

where N_{in}^e and u_n^e are the shape functions and displacement variables of the element respectively. The summation index n implies summation over all degrees of freedom of the element. If the shape functions also serve as weighting functions of the element according to Galerkin (see for instance Zienkiewicz [141]), that is if

$$W_{im}^X = N_{im}^e \tag{2.21}$$

Eq. (2.19) is turned into the finite element matrix equations of the structure (subscript s stands for structure)

$$M_s^e \ddot{u}_s^e + K_s^e u_s^e = P_s^e + P_{qs}^e \tag{2.22}$$

with components

$$M_{s,mn}^e = \int_{V^e} N_{im}^e \, \rho \, N_{in}^e \, dV^e, \tag{2.23a}$$

$$K_{s,mn}^e = \int_{V^e} \left[\frac{\partial N_{Jm}^e}{\partial X_J} \lambda \frac{\partial N_{Kn}^e}{\partial X_K} + \frac{\partial N_{Im}^e}{\partial X_J} \mu \left(\frac{\partial N_{In}^e}{\partial X_J} + \frac{\partial N_{Jn}^e}{\partial X_I} \right) \right] dV^e \tag{2.23b}$$

and

$$P_{s,m}^e + P_{qs,m}^e = \int_{S^e} N_{im}^e \, \tilde{t}_i \, dS^e + \int_{V^e} N_{im}^e \, U_i \, dV^e. \tag{2.23c}$$

In Eq. (2.22) $\ddot{u}_s^e$ is the second time derivative of the displacement vector u_s^e of the structural element; $u_s^e = [u_1^e \, u_2^e \ldots]^T$. Further M_s^e, K_s^e, P_s^e and P_{qs}^e are the mass matrix, stiffness matrix, force vector and load vector respectively of the element. Note that all quantities in Eq. (2.22) refer to a global coordinate system defined by the reference frame X according to Fig. 2.1.

In Eq. (2.23c) the element force vector components $P_{s,m}^e$ correspond to tractions $\tilde{t}_i$ on those parts of S^e which the element studied has in common with neighbouring elements. Thus the element force vectors cancel out in the finite element assembly procedure, see Subsec. 2.4.3.

Finally, it should also be noted that viscous damping effects may be introduced on the left-hand side of Eq. (2.22) by a term $C_s^e \dot{u}_s^e$. The damping effects of the structure are discussed in some more detail in Subsec. 2.4.3.

2.3   Vehicle

In this section the basic equations describing the behaviour of a moving vehicle are derived. In analogy with the structure (Sec. 2.2) there are three subsections called: kinematic equations (2.3.1), equations of motion (2.3.2) and constitutive equations (2.3.3). However, a finite element discretization (cf. Subsec. 2.2.4) is not performed here since the spatial discretization consists of an assumption of rigid vehicle bodies introduced in Subsec. 2.3.1. Systems with rigid bodies as fundamental building blocks are usually referred to as multibody systems.

Although the assumption of rigid bodies and a number of other assumptions are adopted in this section (cf. the list in Sec. 2.1) the derivation of the basic vehicle equations becomes rather extensive. This is because additional reference frames (Y and Z_b in Fig. 2.1) must, in general, be introduced to analyse the moving vehicle. To limit the extent of this section explicit or component expressions of most of the vectors, tensors and matrices introduced are therefore left to Appendix B.

Much literature is available in the field of vehicle dynamics. It should be noted that in most studies the vehicle is considered as a multibody system. References in the present field are e.g. Cooperrider and Law [18], Kortüm and Richter [59], Schiehlen [106] [107] and the report VDI–Berichte 510 [128]. See also Meriam [76].

2.3.1 Kinematic equations

In addition to the fixed reference frame X, the frames Y and Z_b have been introduced to describe the motion of the moving vehicle, see Fig. 2.1. The vehicle frame Y moves at the vehicle speed along the nominal vehicle path on the structure. It is here assumed that the vehicle path and speed are prescribed. This means that neither the path nor the speed of the vehicle are affected by the structural and vehicle responses but are known in advance (no active control). As far as the frames Z_b are concerned each vehicle body (b = 1,2...n_b) is associated with such a reference frame. The motion of the ends of the connecting elements, such as springs and dampers, can be expressed in terms of the body motion quantities (see Subsec. 2.3.3 and Appendix B). Thus, it is sufficient to derive the kinematic equations for a single vehicle body.

The reference frames X, Y and Z_b are closely connected to each other as indicated in Fig. 2.1. Hence the absolute reference translations of the origin O_{Zb} are given by the vector

$$\mathbf{R}_{XZb} = \mathbf{R}_{XY} + \mathbf{R}_{YZb} \tag{2.24a}$$

while the absolute reference rotations of the frame Z_b can be expressed by the tensor

$$\mathbf{S}_{XZb} = \mathbf{S}_{YZb}\,\mathbf{S}_{XY}. \tag{2.24b}$$

The rotation tensors in Eq. (2.24b) consist of nine direction

cosines. For instance, S_{XY} consists of direction cosines referring the X_i-axes (e_{Xi}) to the Y_j-axes (e_{Yj}). In Appendix B the nine cosines of S_{XY} are expressed in terms of three consecutive rotations ($A(s)$, $B(s)$ and $\Gamma(s)$). These rotations are also related to more convenient vehicle path parameters in Appendix B. The three prescribed parameters consist of two radii of curvature and a superelevation angle ($R(s)$, $H(s)$ and $Q(s)$).

The relative motion of a material point or particle of the vehicle body, measured in the moving reference frame Z_b, is expressed by the current position vector (cf. Eq. (2.1))

$$z_b = z_b(Z_b, t). \tag{2.25}$$

In analogy with Eq. (2.2), the relative displacements of a vehicle particle labelled by Z_b can be defined by

$$z_b = Z_b + w_b \tag{2.26}$$

where $w_b = w_b(Z_b, t)$ is the vector of relative displacements. The absolute motion of a vehicle particle, measured in the fixed reference frame X, is given by

$$r_b = R_{XZb} + z_b. \tag{2.27}$$

Insertion of Eqs. (2.24a) and (2.26) into Eq. (2.27) consequently yields

$$r_b = R_{XY} + R_{YZb} + Z_b + w_b. \tag{2.28}$$

Two basic assumptions regarding the vehicle bodies are now introduced. First, it is assumed that the vehicle bodies are rigid. Since it is not the purpose of the present study to predict the internal stresses of these bodies this assumption is not

unrealistic. Further, the frequency content of the structural input
to the vehicle is concentrated at low frequencies when the
structural irregularities are moderate (see also Subsec. 2.4.3). The
input frequencies are further lowered for the suspended vehicle
bodies. This means that the excitation of the elastic body modes is
usually negligible when compared with the low frequency rigid body
modes. For instance, Schiehlen [106] justifies the rigid body
concept (multibody system method) if the load input frequencies are
less than 50 Hz. Other investigators who also demonstrate the
applicability of this concept are for example Duffek et al. [30] and
Dössing [33].

A second assumption is the assumption of <u>small relative motions of
the vehicle bodies</u> when measured in the reference frame Y. Choosing
the position vector R_{YZb} and the rotation tensor S_{YZb} as time-
independent with respect to the frame Y and the position vector Z_b
as time-independent with respect to the frame Z_b, this assumption
implies that the relative displacements of w_b are small. For
convenience S_{YZb} is set equal to the unit tensor meaning that
$e_{Zbi} = e_{Yi}$. The above assumption also implies that the finite rigid
body rotations of wheels cannot be considered, see also Subsec.
2.4.2. With the interest focused on the overall behaviour of
structures subjected to moving loads the present assumption is in
general reasonable.

The two assumptions introduced above simplify the continued analysis
considerably. As indicated above, however, the main characteristics
of the vehicle are believed to be retained so that the vehicle
influence on the structure can be modelled in an acceptable way.
These assumptions imply that the relative displacements of each
vehicle body can be described by only six properly chosen displace-
ment quantities. Here these are chosen to be the three translations
contained in the vector $w_{bo} = w_b(0,t)$ and the three (small) rota-
tions of a rotation vector ψ_b. In this way the spatial discre-

tization (cf. Subsec. 2.2.4) has been performed resulting in six degrees of freedom for each vehicle body element. The absolute translations of the material point labelled by $Z_b = 0$ (or O_{Zb}) may now be written as (cf. Eq. (2.28))

$$r_{bo} = R_{XY} + R_{YZb} + w_{bo} \qquad (2.29a)$$

whereas the absolute rotations of the body are given by

$$s_b = \zeta_b S_{XZb} = \zeta_b S_{YZb} S_{XY} \qquad (2.29b)$$

in which Eq. (2.24b) has been used. In Eq. (2.29b) the infinitesimal rotation tensor ζ_b corresponds to the small rotation vector ψ_b just mentioned, see Appendix B.

The absolute translational velocities of the vehicle body are now found by time differentiation of Eq. (2.29a). Hence

$$v_{bo} = (\frac{d}{dt} r_{bo})_X = (\frac{d}{dt} R_{XY})_X + \Omega_{XY} \times (R_{YZb} + w_{bo}) + (\frac{d}{dt} w_{bo})_{Zb}$$

$$(2.30a)$$

where Ω_{XY} is the angular velocity vector describing the rotation of the frame Y relative to the frame X, see Fig. 2.1 and Appendix B. In Eq. (2.30a) the relations $(\frac{d}{dt} R_{YZb})_Y = 0$ and $\Omega_{YZb} = 0$ (due to $S_{YZb}=1$) have been utilized. The subscripts $(\ )_X$, $(\ )_Y$ and $(\ )_{Zb}$ mean that the vectors within parentheses are considered in relation to the reference system X, Y and Z_b respectively. The absolute rotational (angular) velocities of the vehicle body can be expressed by a skew spin tensor $A_b = (\frac{d}{dt} s_b)_X s_b^T$ where s_b is given by Eq. (2.29b). However, it is more convenient to express the three independent velocities in A_b by an angular velocity vector, ω_b. For small relative body rotations ω_b can be written approximately as

$$\omega_b = \Omega_{XY} + (\frac{d}{dt} \psi_b)_{Zb}. \tag{2.30b}$$

To evaluate the time−dependent referential vectors $\mathbf{R}_{XY}$ and Ω_{XY} in Eqs. (2.30a−b), the vehicle speed $(v(t))$ must be known. Thus, in addition to the three path parameters mentioned above a fourth prescribed or known parameter, the vehicle speed, enters the analysis.

Time differentiation of Eqs. (2.30a−b) results in the absolute acceleration vectors

$$\dot{\mathbf{v}}_{bo} = (\frac{d^2}{dt^2} r_{bo})_X = (\frac{d^2}{dt^2} \mathbf{R}_{XY})_X + (\frac{d}{dt} \Omega_{XY})_Y \times (\mathbf{R}_{YZb} + \mathbf{w}_{bo})$$

$$+ \Omega_{XY} \times (\Omega_{XY} \times (\mathbf{R}_{YZb} + \mathbf{w}_{bo})) + 2\Omega_{XY} \times (\frac{d}{dt} \mathbf{w}_{bo})_{Zb} + (\frac{d^2}{dt^2} \mathbf{w}_{bo})_{Zb}$$

$$\tag{2.31a}$$

and

$$\dot{\omega}_b = (\frac{d}{dt} \omega_b)_X = (\frac{d}{dt} \Omega_{XY})_Y + \Omega_{XY} \times (\frac{d}{dt} \psi_b)_{Zb} + (\frac{d^2}{dt^2} \psi_b)_{Zb}$$

$$\tag{2.31b}$$

where the relation $(\frac{d}{dt} \Omega_{XY})_X = (\frac{d}{dt} \Omega_{XY})_Y$, due to $\Omega_{XY} \times \Omega_{XY} = 0$, has been used. Hence Eqs. (2.31a−b) define the absolute accelerations of the vehicle body in terms of the known reference quantities $\mathbf{R}_{XY}$, $\mathbf{R}_{YZb}$ and Ω_{XY} and the unknown relative displacement vectors $\mathbf{w}_{bo}$ and ψ_b (six degrees of freedom). In Eq. (2.31a) the components of the vector $2\Omega_{XY} \times (\frac{d}{dt} \mathbf{w}_{bo})_{Zb}$ may be recognized as the Coriolis accelerations.

2.3.2 Equations of motion

After that the kinematic relations have been established it is possible to formulate the equations of motion for a rigid vehicle body. If the centre of gravity of the vehicle body is labelled by O_{Zb} the six equations of motion can be expressed according to Newton and Euler, that is

$$m_b \dot{v}_{bo} = F_b + F_{qb} \tag{2.32a}$$

and

$$I_{bo}\dot{\omega}_b + \omega_b \times (I_{bo}\omega_b) = M_{bo} + M_{qbo}. \tag{2.32b}$$

The new quantities introduced in Eqs. (2.32a–b) are, to start with, the body mass m_b and the inertia tensor I_{bo} with respect to the centre of gravity of the body. Further, F_b and M_{bo} are force and moment vectors associated with the connection to other vehicle elements such as springs and dampers. The weight of the body and possibly external loads are represented by the load vectors F_{qb} and M_{qbo}. Substitution of Eqs. (2.30b) and (2.31a–b) into Eqs. (2.32a–b) yields, after some rearranging, the second-order differential equations in w_{bo} and ψ_b

$$m_b \ddot{w}_{bo} + m_b(2\Omega_{XY} \times \dot{w}_{bo}) + m_b(\Omega_{XY} \times (\Omega_{XY} \times w_{bo}) + \dot{\Omega}_{XY} \times w_{bo})$$

$$= F_b + F_{qb} - m_b(\ddot{R}_{XY} + \Omega_{XY} \times (\Omega_{XY} \times R_{YZb}) + \dot{\Omega}_{XY} \times R_{YZb}) \tag{2.33a}$$

and

$$I_{bo}\ddot{\psi}_b + I_{bo}(\Omega_{XY}\times\dot{\psi}_b) + \Omega_{XY} \times (I_{bo}\dot{\psi}_b) + \dot{\psi}_b \times (I_{bo}\Omega_{XY})$$

$$+ \dot{\psi}_b \times (I_{bo}\dot{\psi}_b) = M_{bo} + M_{qbo} - I_{bo}\dot{\Omega}_{XY} - \Omega_{XY} \times (I_{bo}\Omega_{XY}) \quad (2.33b)$$

respectively. In Eqs. (2.33a-b) the dots represent time differentiation with respect to the frame Z_b for w_{bo} and ψ_b, with resepect to Y for Ω_{XY} and, finally, with respect to the fixed frame X for R_{XY}. It should also be noted that a rotating reference frame Y (due to a curved path for instance), represented by Ω_{XY}, does not only affect the right-hand sides of Eqs. (2.33a-b) but also gives rise to coupled terms with the fundamental unknowns w_{bo} and ψ_b on the left-hand sides. A further complication appears in Eq. (2.33b) due to the nonlinear term $\dot{\psi}_b\times(I_{bo}\dot{\psi}_b)$. However, since small relative body motions are assumed this term can be neglected.

Since the rigid vehicle bodies are not associated with any constitutive equations (cf. Subsec. 2.3.3), Eqs. (2.33a-b) can be turned into matrix form now. The matrix relation for a rigid body vehicle element may be written as (cf. Subsec. 2.2.4)

$$M_v^e\ddot{u}_v^e + C_v^e\dot{u}_v^e + K_v^e u_v^e = P_v^e + P_{qv}^e - P_Z^e \quad (2.34)$$

in which the 6×1 displacement vector u_v^e contains the components of w_{bo} and ψ_b (subscript v stands for vehicle). These components are here related to the base vectors e_{Zbi}. The mass matrix M_v^e in Eq. (2.34) is symmetric and although time-independent only in a body fixed frame, it may be approximated as time-independent since the chosen frame Z_b only differs from the body fixed frame by small displacements. Both the damping matrix C_v^e and the stiffness matrix K_v^e of the body element are, however, in general unsymmetric and time-dependent. Note that the matrices associated with velocities

and displacements are called damping matrix and stiffness matrix for the sake of consistency with the structural terminology, although the underlying phenomena of these vehicle matrices are completely different from those of the structure. The matrices $\mathbf{M}_v^e$, $\mathbf{C}_v^e$ and $\mathbf{K}_v^e$ for the rigid body element are given in explicit form in Appendix B.

On the right-hand side of Eq. (2.34) the element force vector $\mathbf{P}_v^e$ contains the components of $\mathbf{F}_b$ and $\mathbf{M}_{bo}$ while the element load vector $\mathbf{P}_{qv}^e$ contains the components of $\mathbf{F}_{qb}$ and $\mathbf{M}_{qbo}$. The element noninertia load vector $\mathbf{P}_Z^e$ corresponds to the remaining terms of the right-hand sides of Eqs. (2.33a-b). These terms appear if the moving reference frame Z_b is noninertial, see also Appendix B. The computer commands VEM3EI and VEM3EN used for generating the inertial and noninertial matrices and vectors in Eq. (2.34) are described in Sec. 5.4.

2.3.3 Constitutive equations

The complete vehicle model consists of rigid body elements and elements that connect the body elements to each other. In contrast to the rigid body elements, the connecting elements are associated with constitutive equations. Many types of connecting devices are available in modern vehicles. In modelling these devices, one may distinguish between active and passive elements. Active elements have feedback (active control) whereas the passive ones have not. The most common passive elements are springs and dampers. For a more extensive description of different connecting elements, see for example Duffek et al. [30].

To limit the scope of the present study <u>only linear viscous dampers and linear elastic springs will be considered</u>. It is believed that this assumption is reasonable so that the main structural behaviour due to the moving vehicle is retained in the model. The constitutive equations for the selected connecting elements may be written as

$$C_v^e \dot{u}_v^e + K_v^e u_v^e = P_v^e - P_Z^e \qquad (2.35a)$$

and

$$K_v^e u_v^e = P_v^e \qquad (2.35b)$$

for a damper and a spring element respectively. Note that the quantities in Eqs. (2.35a–b) are different from those in Eq. (2.34) although the same notations are used. In addition, the matrix $\mathbf{K}_v^e$ in Eq. (2.35a) differs from the one in Eq. (2.35b). In Eqs. (2.35a–b) u_v^e is a 12×1 displacement vector containing the six displacements of each of the two connected rigid body elements. As shown in Appendix B (Subsecs. B.3.2–4) the global vector u_v^e is related to a local 6×1 displacement vector $\bar{u}_v^e$, describing the translations of the two ends of the connecting element, through a transformation matrix $\mathbf{Q}$. The damping matrix C_v^e in Eq. (2.35a) and the stiffness matrix K_v^e in Eq. (2.35b) are the only matrices obtained if the reference frames Z_b are inertial. As for the rigid body element, however, additional matrices and vectors are introduced for the damping element due to noninertial effects. Hence the damper element is associated with a "stiffness matrix" K_v^e and a noninertia load vector P_Z^e. The matrix K_v^e for the spring element, the matrices C_v^e and K_v^e for the damper element and the vector P_Z^e are given explicitly in Appendix B. The computer commands VEC3EI and VEC3EN for the damper element and VEK3E for the spring element are described in Sec. 5.4.

Three different vehicle elements have been considered in Sec. 2.3: rigid body elements, damper elements and spring elements. The basic equations of these elements are expressed by Eqs. (2.34), (2.35a) and (2.35b) respectively. The six degrees of freedom (DOF) of each rigid body element serve as global DOF for the vehicle. Thus the

vehicle has $6n_b$ DOF if n_b is the number of rigid body elements of the vehicle. In Sec. 2.4 this number as well as the number of structural DOF is decreased due to different kinds of constraints.

2.4   Structure−vehicle interaction

The basic matrix equations of the structure−vehicle system are founded on the equations of its components, that is structural elements (Eq. (2.22)), vehicle body elements (Eq. (2.34)) and vehicle damper and spring elements (Eqs. (2.35a−b)). Of the global structure and vehicle coordinates or DOF some are constrained. Subsec. 2.4.1 of this section deals with these constraints in general terms while Subsec. 2.4.2 concentrates on the constraints associated with structure−vehicle interaction. A special structure− vehicle finite element is derived in that subsection. Finally, Subsec. 2.4.3 contains a modal coordinate formulation of the structure and also of the structure−vehicle element.

2.4.1 Constraints

The constraints may be classified in different types, see e.g. Blejwas [9], Greenwood [44] and Schiehlen [107]. First one should distinguish between holonomic and nonholonomic constraints. Holo- nomic constraints can be expressed by equality relations in terms of displacement coordinates and constant or time−dependent coefficients only. If the constraints are not holonomic they are called non- holonomic. Only holonomic constraints will be considered in this study. A consequence of this restriction is that the vehicle must be in contact with the structure during the entire traversing time since contact losses are associated with inequality relations. (For levitated vehicles a maintained fictitious contact is assumed, see Chapter 4). Another possible classification is into scleronomic and rheonomic holonomic constraints. For scleronomic constraints the co- efficients just mentioned are constants while they (or at least one

coefficient) are time-dependent for rheonomic ones. Both these types are considered in this study. It should be mentioned that the type of constraints considerably affects the complexity of the structure-vehicle analysis and the numerical procedure (see Chapter 5).

The simplest scleronomic constraint is to prescribe a displacement component to zero. For instance some of the structural displacements contained in $\mathbf{u}_s$ should be set to zero to define the boundary conditions (indicated in Fig. 2.1). A further example is that all out-of-plane displacement components of the structure and vehicle can be deleted in a plane structure-vehicle analysis. Another scleronomic constraint is that of two vehicle bodies being directly connected to each other through a hinge. In this way the original DOF are not independent and three DOF can be eliminated (two DOF for plane analysis). The reduction of the number of DOF associated with scleronomic constraints is most often performed on the global level, that is on the global displacements $\mathbf{u}_s$ and $\mathbf{u}_v$ of the structure and vehicle respectively. If all constraints are scleronomic no updating of the reduced global matrices is required since the pertinent coefficients are time-independent.

A further reduction of the number of DOF can be made by considering the constraints that tie the structure and vehicle together. These constraints are rheonomic, unless the vehicle is at rest, and of main interest in the present study. Since the rheonomic constraint coefficients are time-dependent, updating of the further reduced global matrices is necessary at every time step. (See Sec. 5.2 for time discretization). In general, however, the time dependence only affects a small portion of the matrix components. This implies that the elimination of DOF associated with the present rheonomic constraints is not performed so efficiently on the global level. Instead the elimination procedure should be performed on the local or element level. Hence only structure and vehicle elements in connection with the eliminated DOF are incorporated. In this way

so-called structure-vehicle finite elements can be derived, see the author [83][85]. Thus these elements make the structure-vehicle analysis more effective. A more general derivation of a structure-vehicle element than those of the author [83][85] is shown in the next subsection.

Finally, it should be noted that it is not necessary to eliminate the DOF associated with holonomic constraints. Instead the Lagrange multiplier method, see for instance Blejwas [9] and Greenwood [44], may be applied. However, an increased number of differential equations must be solved by this method.

2.4.2 Structure-vehicle finite element

The nature of structure-vehicle interaction is very complex. A detailed interaction analysis of, for instance, rail and vehicle requires a careful study of the contact between rail and wheel, see e.g. Cooperrider and Law [18]. Such an analysis, which puts emphasis on the contact problem, should be called rail-wheel interaction analysis in contrast to the more global term structure-vehicle interaction. For studies of the contact problem, see also Nilsson [81].

In this study the global structure-vehicle interaction is analysed. The contact vehicle bodies (wheels) are modelled as concentrated or lumped masses, that is the rotations of the wheels are not considered (3 DOF). For many structure-vehicle problems this restriction is of no consequence. In some cases, however, contact losses may occur due to this simplified model. It should also be kept in mind that the problems associated with contact masses do not apply to levitated vehicles, see Chapter 4.

As mentioned in the previous subsection the vehicle must be in contact with the structure due to the restriction to holonomic

constraints. In addition, it must follow a prescribed nominal path at a prescribed speed (see Subsec. 2.3.1). Each contact mass point of the vehicle is related to this common path through its position vector R_{YZb} (constant in the frame Y). In this way a nominal path can be assigned to each contact point. The only allowable departures from these nominal paths are those due to structural surface irregularities and structural deformations. While the irregularities are time−independent when measured in X, the structural deformations and displacements vary with time and depend upon the magnitudes and positions of the contact forces. The (nominal) positions are known in advance due to the prescribed vehicle path and speed. The magnitudes, however, depend on the relative motions of the vehicle bodies and also on the structural motions themselves. This coupling effect has the result that the structure and the vehicle cannot be analysed separately but the problem becomes a structure−vehicle interaction one. It should be noted that the contact forces obtained from a structure−vehicle analysis must be checked to verify that the normal contact forces are compressive and that the tangential ones are below the actual capacity (e.g. frictional capacity).

The three (translational) DOF of each contact mass point are constrained, as indicated above, and can thus be eliminated. According to the previous subsection this elimination is most effectively carried out on the element level giving so−called structure−vehicle finite elements. The derivation of such an element is shown below.

The DOF of interest in deriving a structure−vehicle finite element are the DOF of a loaded structural element, the DOF of the contact masses on the structural element in question and, finally, the DOF of the vehicle body elements which are connected to the actual contact masses through damper and spring elements. A simple example of a structure−vehicle element is shown in Fig. 2.2.
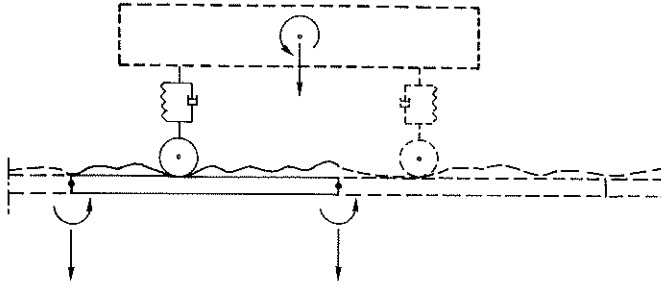
<u>Figure 2.2</u>. Plane structure–vehicle finite element (example). The element is illustrated by full lines and consists of a beam element, a contact mass element, a damper element and a spring element. The pertinent 6 DOF and structural irregularities are indicated.

In Fig. 2.2 it should be noted that the out-of-plane and longitudinal DOF have been constrained to zero (scleronomic constraints) whereas the vertical contact mass DOF has been eliminated by demanding structural contact (rheonomic constraint). For structure and vehicle models in general, a structure–vehicle element can be derived through first establishing the pertinent unconstrained equations of motion as

$$
\begin{bmatrix} M_s^e & 0 \\ 0 & M_v^e \end{bmatrix} \begin{bmatrix} \ddot{u}_s^e \\ \ddot{u}_{vc}^e \\ \ddot{u}_{vb}^e \end{bmatrix} + \begin{bmatrix} C_s^e & 0 \\ 0 & C_v^e \end{bmatrix} \begin{bmatrix} \dot{u}_s^e \\ \dot{u}_{vc}^e \\ \dot{u}_{vb}^e \end{bmatrix}
$$

$$
+ \begin{bmatrix} K_s^e & 0 \\ 0 & K_v^e \end{bmatrix} \begin{bmatrix} u_s^e \\ u_{vc}^e \\ u_{vb}^e \end{bmatrix} = \begin{bmatrix} P_s^e \\ 0 \\ P_{vb}^e \end{bmatrix} + \begin{bmatrix} P_{qs}^e \\ P_{qvc}^e \\ 0 \end{bmatrix} - \begin{bmatrix} 0 \\ P_{Zc}^e \\ P_{Zb}^e \end{bmatrix}. \qquad (2.36)
$$

The structural equations can be identified as Eq. (2.22) with a possible extension for damping effects. It should be noted that these equations are not associated with any noninertial terms (zero subvector in the rightmost vector of Eq. (2.36)) since $\mathbf{u}_s^e$ and its time derivatives $\dot{\mathbf{u}}_s^e$ adn $\ddot{\mathbf{u}}_s^e$ refer to the earth fixed reference frame X. The displacement vector $\mathbf{u}_{vc}^e$ contains the DOF of the contact masses on the structural element while $\mathbf{u}_{vb}^e$ contains displacements of the vehicle body elements which are connected to the contact masses through damper and spring elements. Thus the corresponding matrices $\mathbf{M}_v^e$, $\mathbf{C}_v^e$ and $\mathbf{K}_v^e$ are, in general, assemblages of many contact masses, springs and dampers. (Note that the DOF of $\mathbf{u}_{vc}^e$ are already eliminated in Fig. 2.2 and that only one vehicle element of each type is present). The fact that vehicle elements have been assembled can be seen from the subvector of zeroes in the element force vector. It should be noted that if the reference frames Z_b, to which $\mathbf{u}_{vc}^e$ and $\mathbf{u}_{vb}^e$ and their derivatives refer, are noninertial the contact masses will contribute to $\mathbf{C}_v^e$, $\mathbf{K}_v^e$ and $\mathbf{P}_{Zc}^e$ while the connecting dampers will contribute to $\mathbf{K}_v^e$, $\mathbf{P}_{Zc}^e$ and $\mathbf{P}_{Zb}^e$ (cf. Eqs. (2.34) and (2.35a)).

While the structural and vehicle equations of Eq. (2.36) are uncoupled on the left-hand side they are coupled through the load vectors $\mathbf{P}_{qs}^e$ and $\mathbf{P}_{qvc}^e$ which both contain the unknown contact forces. By eliminating the constrained contact DOF of $\mathbf{u}_{vc}^e$, however, the unknown forces are also eliminated. (The contact forces can be evaluated after the global equations of motion have been solved). For convenience, only one contact mass is considered in the following (as in Fig. 2.2). Hence $\mathbf{u}_{vc}^e$ is a 3×1 vector with components referring to base vectors $\mathbf{e}_{Zbi}$. The structural displacements at the point of contact are given by

$$u_{sc}^e = N_c^e \, u_s^e \tag{2.37}$$

which is Eq. (2.20) evaluated at the point of contact. Thus the components of u_{sc}^e refer to base vectors e_{Xi}. To match the components of u_{vc}^e the vector u_{sc}^e must be represented by a vector, $\tilde{u}_{sc}^e$, with components related to e_{Zbi}. According to Appendix B the change of basis from X to Z_b is described by the transpose of the rotation tensor S_{XY} ($S_{YZb} = 1$). Hence the components of $\tilde{u}_{sc}^e$ are related to those of u_{sc}^e implied by

$$\tilde{u}_{sc}^e = S_{XY}^T \, u_{sc}^e . \tag{2.38}$$

If the vector $\tilde{r}_{sc}^e$ contains the structural surface irregularities of the point of contact (base vectors e_{Zbi}), the constraint equations for maintained contact can be written in vector form as

$$u_{vc}^e = \tilde{u}_{sc}^e + \tilde{r}_{sc}^e \tag{2.39}$$

which also holds for each component. Equation (2.39) states, as mentioned above, that the motion of the contact mass deviates from its nominal path due to structural displacements (deformations) and irregularities. The structural irregularities are discussed in more detail in Subsec. 2.4.3. Introduction of Eqs. (2.37) and (2.38) into Eq. (2.39) yields the rheonomic constraint equations as

$$u_{vc}^e = T_{cu} u_s^e + T_{cr} r_{sc}^e \tag{2.40}$$

where

$$T_{cu} = S_{XY}^T N_c^e \tag{2.41a}$$

and

$$T_{cr} = S_{XY}^T \tag{2.41b}$$

are time-dependent transformation matrices since the point of contact and, in general, S_{XY} change with time. ($\tilde{r}_{sc}^e = S_{XY}^T r_{sc}^e$ in analogy with Eq. (2.38)). The first and second time derivatives of u_{vc}^e, when measured in the moving reference frame Z_b, thus become

$$\dot{u}_{vc}^e = \dot{T}_{cu} u_s^e + T_{cu} \dot{u}_s^e + \dot{T}_{cr} r_{sc}^e + T_{cr} \dot{r}_{sc}^e \tag{2.42a}$$

and

$$\ddot{u}_{vc}^e = \ddot{T}_{cu} u_s^e + 2\dot{T}_{cu} \dot{u}_s^e + T_{cu} \ddot{u}_s^e$$

$$+ \ddot{T}_{cr} r_{sc}^e + 2\dot{T}_{cr} \dot{r}_{sc}^e + T_{cr} \ddot{r}_{sc}^e \tag{2.42b}$$

respectively. Here

$$\dot{T}_{cu} = \frac{d}{dt}(T_{cu}(X_c(t))) = \sum_{i=1}^{3} \frac{dT_{cu}}{dX_{ci}} \frac{dX_{ci}}{dt} \tag{2.43a}$$

and

$$\ddot{T}_{cu} = \frac{d}{dt}(\dot{T}_{cu}(X_c(t))) = \sum_{i=1}^{3} \left[\sum_{j=1}^{3} \frac{d^2 T_{cu}}{dX_{ci} dX_{cj}} \frac{dX_{cj}}{dt} \right] \frac{dX_{ci}}{dt}$$

$$+ \sum_{i=1}^{3} \frac{dT_{cu}}{dX_{ci}} \frac{d^2 X_{ci}}{dt^2} \tag{2.43b}$$

whereas the expressions for $\dot{T}_{cr}$, $\ddot{T}_{cr}$, $\dot{r}^e_{sc}$ and $\ddot{r}^e_{sc}$ are analogous with Eqs. (2.43a–b). Inserting Eqs. (2.40) and (2.42a–b) into Eq. (2.36) and premultiplying by T^T_{cu} for the contact mass equations, one obtains the equations of motion for the structure–vehicle finite element as

$$M^e \ddot{u}^e + C^e \dot{u}^e + K^e u^e = P^e + P^e_q - P^e_Z \tag{2.44}$$

where

$$u^e = \left[\begin{array}{c} u^e_s \\ \hline u^e_{vb} \end{array} \right], \tag{2.45a}$$

$$M^e = \left[\begin{array}{c|c} M^e_s & 0 \\ \hline 0 & 0 \end{array} \right] + \left[\begin{array}{c|c} T^T_{cu} M^e_{vcc} T_{cu} & 0 \\ \hline 0 & 0 \end{array} \right], \tag{2.45b}$$

$$C^e = \left[\begin{array}{c|c} C^e_s & 0 \\ \hline 0 & C^e_{vbb} \end{array} \right] + \left[\begin{array}{c|c} T^T_{cu}(2M^e_{vcc}\dot{T}_{cu} & T^T_{cu}C^e_{vcb} \\ +C^e_{vcc}T_{cu}) & \\ \hline C^e_{vbc}T_{cu} & 0 \end{array} \right], \tag{2.45c}$$

$$K^e = \left[\begin{array}{c|c} K^e_s & 0 \\ \hline 0 & K_{vbb} \end{array} \right] + \left[\begin{array}{c|c} T^T_{cu}(M^e_{vcc}\ddot{T}_{cu} & T^T_{cu}K_{vcb} \\ +C^e_{vcc}\dot{T}_{cu} & \\ +K^e_{vcc}T_{cu}) & \\ \hline C^e_{vbc}\dot{T}_{cu}+K^e_{vbc}T_{cu} & 0 \end{array} \right], \tag{2.45d}$$

$$P^e = \left[\begin{array}{c} P^e_s \\ \hline P^e_{vb} \end{array} \right], \tag{2.45e}$$

$$P^e_q = \left[\begin{array}{c} P^e_{qs} + T^T_{cu} P^e_{qvc} \\ \hline 0 \end{array} \right] \tag{2.45f}$$

and

$$P^e_Z = \left[\begin{array}{c} T^T_{cu} P^e_{Zc} \\ \hline P^e_{Zb} \end{array} \right]$$

$$+ \left[\begin{array}{c} T^T_{cu}[M^e_{vcc}(\ddot{T}_{cr} r^e_{sc} + 2\dot{T}_{cr} \dot{r}^e_{sc} + T_{cr} \ddot{r}^e_{sc}) + C^e_{vcc}(\dot{T}_{cr} r^e_{sc} + T_{cr} \dot{r}^e_{sc}) + K^e_{vcc} T_{cr} r^e_{sc}] \\ \hline C^e_{vbc}(\dot{T}_{cr} r^e_{sc} + T_{cr} \dot{r}^e_{sc}) + K^e_{vbc} T_{cr} r^e_{sc} \end{array} \right].$$

$$\tag{2.45g}$$

In order to arrive at Eqs. (2.44) and (2.45a–g) the matrices M^e_v, C^e_v and K^e_v in Eq. (2.36) have also been decomposed into submatrices which correspond to the vectors u^e_{vc} and u^e_{vb} in that equation. For instance K^e_v is decomposed into K^e_{vcc}, K^e_{vcb}, K^e_{vbc} and K^e_{vbb}. Note that M^e_{vcb}, M^e_{vbc} and M^e_{vbb} are zero matrices (cf. Fig. 2.2).

As can be seen from Eqs. (2.45b–d) the element matrices of the structure-vehicle finite element have been divided into two parts: a noninteraction part and an interaction part. If u^e_{vc} is set to a zero vector, the interaction part defined by the second matrices in Eqs. (2.45b–d) vanishes and the structure-vehicle interaction is

neglected. If, on the other hand, u_{vc}^e is given by Eq. (2.40), the interaction is considered and both parts have an influence on the element matrices. In Sec. 2.3 it was noted that rigid body elements and damper elements give rise to unsymmetric and time-dependent element matrices in the case of noninertial vehicle motion. The structure–vehicle element matrices derived above are, however, unsymmetric (except for $\dot{M}^e$) and time-dependent already for the case of inertial vehicle motion. A further contrast to rigid body and damper elements is that the physical DOF of a structure–vehicle element change when the contact point leaves one structural element and enters another one.

On the right-hand side of Eq. (2.44), the load vector P_q^e is not affected by the unknown contact forces as pointed out above. This circumstance can be seen from Eq. (2.45f) since the sum $P_{qs}^e + T_{cu}^T P_{qvc}^e$ is a zero vector for the contact forces. Besides the contact forces P_{qvc}^e contains the weight of the contact mass. It should also be noted that, for convenience, the irregularity effects are included in the noninertia load vector P_Z^e, see Eqs. (2.44) and (2.45g).

The expressions given in Eqs. (2.45a–g) for the matrices and vectors in Eq. (2.44) are those for a single contact point (mass) on a structural element as mentioned above. However, the inclusion of more contact points in the structure–vehicle element is straight-forward. A further note is that updating of the time-dependent terms of the present element can be reduced to a minimum if the terms associated with DOF constrained to zero (scleronomic constraints) are not considered, cf. Fig. 2.2.

The element equations of the structure–vehicle finite element, Eq. (2.44), compose a set of linear ordinary second-order differential equations with nonconstant (time-dependent) coefficients. In

addition to the time dependence, the unsymmetry of the element matrices C^e and K^e complicates the analysis. Thus the choice of solution algorithm for solving the equations of motion of the whole structure−vehicle system is important, see Sec. 5.2. The computer commands SVE3EM and SVE3EV used for generating the element matrices (interaction part) and the element vectors of Eq. (2.44) are described in Sec. 5.4.

The structure−vehicle finite element derived in this subsection, see also the author [83][85], is believed to be novel. In Duffek and Jaschinski [31] a similar element can be found which models the contact between rail and wheel ("Radsatz−Gleiselement"). The rail, which rests on springs and dampers, is however modelled as rigid. This means that the rail (structure) only contributes with a mass matrix to the rail−wheel element and that terms which are associated with deformations of the rail are neglected. A procedure similar to the one shown in this subsection can be found in Dailey et al. [27], Filho [35] and Yoshida et al. [139][140]. However, the elimination of the contact DOF is performed for the global structure−vehicle system and no special structure−vehicle finite element can be ident−ified. As mentioned in Subsec. 2.4.1, for the present rheonomic con−straints, elimination on the global level is in general less effec−tive than on the element level.

The structure−vehicle finite element formulated in the present study means that the moving load problem and, in particular, the structure−vehicle interaction can be studied within the finite element concept. Although the element matrices may be both time−dependent and unsymmetric, this means that structure−vehicle problems can be solved quite easily by persons familiar with the finite element method. As mentioned in Sec. 1.2, however, modern FEM packages are not suited for the structure−vehicle interaction problem. (Some of the difficulties in implementing routines for the present problem are shown in Schneider et al. [108]). The present

coupling element should be considered as an analysis tool which makes it possible to study structure–vehicle interaction problems, by means of FEM, in a straightforward way. A number of verification examples of the structure–vehicle element are given in Appendix D.

Even though the derivation of the finite element has been performed in rather general terms a number of assumptions, as listed in Sec. 2.1, have been introduced. However, the general approach in deriving such an element holds even if most of the restrictions are released. For instance, effects due to nonlinear structural material or nonlinear vehicle springs and dampers may be included while still using a structure–vehicle finite element. If, however, the structural material assumption of linearity is retained a modal coordinate formulation can be performed as shown in the next subsection.

2.4.3 Modal coordinate formulation of structure

The global equations of motion of the structure can be written as

$$M_s \ddot{u}_s + C_s \dot{u}_s + K_s u_s = P_{qs} \qquad (2.46)$$

which is an assemblage of the element equations in Eq. (2.22) with a possible extension for damping effects. Note that P_{qs} is an assemblage of P_{qs}^e and possibly nodal loads only, since the element force vectors P_s^e cancel out. Since linear structural behaviour is assumed in Sec. 2.2, Eq. (2.46) can be transformed into a set of modal equations. In this subsection the modal coordinate formulation of the structure is shown. Moreover, the structure–vehicle finite element derived in the previous subsection is given in terms of modal coordinates.

For linear structural behaviour it is well-known, see for instance Clough and Penzien [17], that the displacement vector $\mathbf{u}_s$ can be expressed as

$$\mathbf{u}_s = \Phi \mathbf{u}_s^m \tag{2.47}$$

where $\Phi = [\varphi_1 \ \varphi_2 \ldots]$ is a set of eigenvectors and $\mathbf{u}_s^m$ contains the corresponding modal displacements or coordinates. The (time-independent) eigenvectors φ_i as well as the pertinent circular eigenfrequencies ω_i are obtained as the solution of the generalized eigenvalue problem (cf. Eq. (2.46))

$$M_s \ddot{\mathbf{u}}_s + K_s \mathbf{u}_s = 0 \tag{2.48}$$

in which the (scleronomic) constraints of $\mathbf{u}_s$ must be considered. Introduction of Eq. (2.47) into Eq. (2.46) and premultiplication by Φ^T yields the uncoupled modal equations

$$M_{si}^m \ddot{\mathbf{u}}_{si}^m + 2\xi_i \omega_i M_{si}^m \dot{\mathbf{u}}_{si}^m + \omega_i^2 M_{si}^m \mathbf{u}_{si}^m = P_{qsi}^m \tag{2.49}$$

provided the damping matrix C_s in Eq. (2.46) has orthogonality properties. In Eq. (2.49) the orthogonal damping is expressed by modal damping ratios ξ_i. Further, M_{si}^m and P_{qsi}^m are the modal mass and modal load respectively of structural vibration mode number i given by

$$M_{si}^m = \varphi_i^T M_s \varphi_i \tag{2.50a}$$

and

$$P_{qsi}^m = \varphi_i^T P_{qs}. \tag{2.50b}$$

As is well-known, uncoupled modal equations are advantageous from a numerical point of view. However, even though orthogonal damping is supposed this advantage cannot be utilized here since the structure-vehicle interaction couples the modal equations. This should be obvious by inspection of Eqs. (2.45b-d), see also the end of this subsection.

However, the modal coordinate formulation often has another major advantage: the structural response can be described reasonably well in terms of the lowermost vibration modes only. Thus the number of equations of motion to be solved can be drastically reduced. This truncation requires the loads acting on the structure to be low frequent in character. In the present study the loads, i.e. the vehicle loads, vary both in position and magnitude and the high frequency content of the loads may be significant in the case of high vehicle speed in combination with large structural irregularities. In order to limit the scope of the study the structural irregularities introduced in Subsec. 2.4.2 are not considered in the following. This also means that a truncation of most of the modes described by Eq. (2.48) should be justified and that the modal formulation turns out to be favourable. (Also note that contact losses cannot be considered in this study, see Subsec. 2.4.1).

It is difficult to estimate to what extent the structural surface irregularities affect the contact forces and, consequently, the vehicle loads on the structure. Even though the irregularities were considered according to Subsec. 2.4.2 in an analysis, see for instance the author [83][85], the results of such a deterministic analysis can be questioned. To cope with both the stochastic nature of the irregularities and the structure-vehicle interaction, Popp [94] suggests that the analysis be divided into two cases: analysis of effects due to stochastic irregularities on a rigid structure and analysis of effects due to a deformable structure without irregularities. Thus it is the second case that is considered in the

present study. Although the principle of superposition does not apply for the two cases, results from an analysis of the first case may be added to results of the present analysis. Hence a rough estimate of the effects of the structural irregularities may be gained in this way.

A modal coordinate formulation of the structure is very common in structure–vehicle analysis. As pointed out in Sec. 1.2, a modal formulation is often used for simple structures in combination with the method of generalized displacements. With regard to the structure–vehicle element derived in Subsec. 2.4.2, the expressions for this element are altered due to the modal formulation. The modal version of the structure–vehicle finite element is given below as completion of the subsection.

The displacement vector u^e of the structure–vehicle element, see Eq. (2.44), can be written in view of the modal formulation as

$$u^e = \begin{bmatrix} u^e_s \\ \hline u^e_{vb} \end{bmatrix} = \begin{bmatrix} \Phi^e & 0 \\ \hline 0 & 1 \end{bmatrix} \begin{bmatrix} u^m_s \\ \hline u^e_{vb} \end{bmatrix} \tag{2.51}$$

where Φ^e is a submatrix of Φ in accordance with the DOF of the loaded structural element. Introducing Eq. (2.51) into Eq. (2.44) and premultiplying by the transpose of the matrix in Eq. (2.51), one obtains the modal version of the structure–vehicle element as (cf. Eqs. (2.44) and (2.45a–g))

$$M^{em}\ddot{u}^{em} + C^{em}\dot{u}^{em} + K^{em}u^{em} = P^{em} + P^{em}_q - P^{em}_Z \tag{2.52}$$

where

$$u^{em} = \left[\begin{array}{c} u_s^m \\ \hline u_{vb}^e \end{array} \right], \tag{2.53a}$$

$$M^{em} = \left[\begin{array}{c|c} \Phi^{eT} M_s^e \Phi^e & 0 \\ \hline 0 & 0 \end{array} \right] + \left[\begin{array}{c|c} T_{cu}^{mT} M_{vcc}^e T_{cu}^m & 0 \\ \hline 0 & 0 \end{array} \right], \tag{2.53b}$$

$$C^{em} = \left[\begin{array}{c|c} \Phi^{eT} C_s^e \Phi^e & 0 \\ \hline 0 & C_{vbb}^e \end{array} \right] + \left[\begin{array}{c|c} T_{cu}^{mT}(2M_{vcc}^e \dot{T}_{cu}^m & T_{cu}^{mT} C_{vcb}^e \\ +C_{vcc}^e T_{cu}^m) & \\ \hline C_{vbc}^e T_{cu}^m & 0 \end{array} \right], \tag{2.53c}$$

$$K^{em} = \left[\begin{array}{c|c} \Phi^{eT} K_s^e \Phi^e & 0 \\ \hline 0 & K_{vbb}^e \end{array} \right] + \left[\begin{array}{c|c} T_{cu}^{mT}(M_{vcc}^e \ddot{T}_{cu}^m & T_{cu}^{mT} K_{vcb} \\ +C_{vcc}^e \dot{T}_{cu}^m & \\ +K_{vcc}^e T_{cu}^m) & \\ \hline C_{vbc}^e \dot{T}_{cu}^m + K_{vbc}^e T_{cu}^m & 0 \end{array} \right], \tag{2.53d}$$

$$P^{em} = \left[\begin{array}{c} \Phi^{eT} P_s^e \\ \hline P_{vb}^e \end{array} \right], \tag{2.53e}$$

$$P_q^{em} = \left[\begin{array}{c} \Phi^{eT} P_{qs}^e + T_{cu}^{mT} P_{qvc}^e \\ \hline 0 \end{array} \right], \tag{2.53f}$$

$$P_Z^{em} = \left[\begin{array}{c} T_{cu}^{mT} P_{Zc}^e \\ \hline P_{Zb}^e \end{array} \right] \tag{2.53g}$$

and

$$T_{cu}^{m} = T_{cu}\Phi^{e}. \tag{2.54}$$

In Eq. (2.53g) the structural irregularities are not considered as implied above (cf. Eq. (2.45g)). The first matrices on the right-hand side of Eqs. (2.53b-d) are diagonal, provided C_s is chosen appropriately, whereas the second ones are not. Thus the modal equations of the structure–vehicle finite element, given by Eq. (2.52), are coupled. As indicated above, however, a reduction of the number of vibration modes included is possible. In this way the number of modal equations can be considerably reduced. Verification examples of the structure–vehicle finite element, in the modal version, are shown in Appendix D.

2.5   Summary

In this chapter the basic equations for the structure, the vehicle and their interaction are derived. Starting from a general moving load problem assumptions according to the list in Sec. 2.1 enter the derivation. The structure and the vehicle and also their interaction are regarded as assemblages of elements which, in turn, can be described by element equations. In this way the moving load problem can be studied within the well-known finite element concept.

In Sec. 2.2 the basic structural equations are derived. In the first three subsections continuum mechanics relations constitute the kinematic equations, the equations of motion and the constitutive equations respectively. On the basis of these equations the finite element equations of a structural element are derived in the last subsection. The five assumptions introduced in this section are listed in Sec. 2.1.

The basic equations for the vehicle are then derived in Sec. 2.3. The assumption of rigid vehicle bodies should be seen as a spatial discretization corresponding to the finite element discretization of the structure described in Subsec. 2.2.4. In this way Sec. 2.3 is only divided into three subsections in analogy with Sec. 2.2. Since the vehicle bodies are assumed to be rigid, the motion of the vehicle can be described by means of three translations and three rotations of each body. The six equations of motion for each rigid body are seen as element equations of a rigid body element. The corresponding six degrees of freedom consist of (small) relative displacements. Thus additional matrices (C_v^e and K_v^e) and an additional vector (P_Z^e) are introduced in the case of noninertial reference motion of the vehicle. The "new" element matrices are in general time-dependent and unsymmetric. Constitutive equations are also given for the two connecting element types considered in this study: damper element and spring element. Explicit expressions for the three different vehicle elements are given in Appendix B.

In Sec. 2.4 the structure–vehicle interaction phenomenon is studied. After a general discussion of different kinds of constraints, the constraints associated with permanent contact between the vehicle and the structure are treated in Subsec. 2.4.2. By means of the contact constraints, the contact DOF of the vehicle can be eliminated. In this way structure–vehicle finite elements can be derived. Such a derivation is shown in Subsec. 2.4.2. The matrices of a structure–vehicle element are time-dependent due to the introduction of rheonomic contact constraints. In addition, the damping and stiffness matrices are unsymmetric (cf. the rigid body element). The structure–vehicle finite element derived is believed to be novel. The element formulation means that the interaction problem can be studied within the finite element concept and that updating at each time step can be reduced to a minimum. A modal

coordinate formulation of the structure and the structure–vehicle elements is also shown. The possible truncation of higher vibration modes means that the number of modes included can be considerably reduced. Verification examples of the structure–vehicle finite element (modal version) are shown in Appendix D.

3.   STRUCTURAL MODELS

3.1   Introduction

In Chapter 2 the basic equations for the structure, the vehicle and their interaction were derived. These equations serve as a base for the present chapter as well as for Chapters 4 and 5. The structural models formulated in this chapter are based on the equations in Sec. 2.2. In that section the kinematic equations, the equations of motion and the constitutive equations for an infinitesimal structural element $dX_1 dX_2 dX_3$ were derived (Subsecs. 2.2.1-3) and followed by a finite element discretization (Subsec. 2.2.4). The assumptions introduced in Sec. 2.2 are listed in Sec. 2.1.

In this chapter further structural assumptions enter the analysis. A main source of these assumptions is the restriction from a general three-dimensional structural body (Chapter 2) to beam structures. Thus the structures considered here are three-dimensional bodies with one dimension significantly larger than the other two. In general a length to width (height) ratio of 5-10 of the structural members is sufficient. This means that the structures subjected to moving loads, such as bridges and guideways, which are studied here are often well qualified for being modelled as beam structures. The assumptions introduced in this chapter are listed at the end of this section (cf. Chapter 2).

Since beam structures are assumed the space discretization (cf. Subsec. 2.2.4) is divided into two steps. First a discretization of the beam cross section is performed. For this an infinitesimal beam lamina is considered, formulating the beam theory. Secondly, a finite element discretization in the longitudinal direction of the beam is performed giving a finite beam element. The two steps are described in Sec. 3.2 and Secs. 3.3-3.4 respectively. Section 3.5 contains a summary of Chapter 3. The present three-dimensional beam

element is implemented through the computer commands BEAM3E, BEAM3C, BEAM3R and BEAM3S according to Sec. 5.4. Verification examples for the element are given in Appendix C.

Beyond the fundamental beam theory according to Euler-Bernoulli and Saint Venant, the formulation in Sec. 3.2 includes warping (Vlasov) torsion and coupled vibrations. Rotatory inertia according to Rayleigh and warping inertia are also included as a consequence of the kinematic assumptions in Subsec. 3.2.1 but may be omitted if desired. The formulation is not limited to any special type of beam cross section. It should also be noted that the Saint Venant torsional moment enters the analysis through the kinematic assumptions and is not, as is common, tacitly introduced in the equations of motion, see e.g. Murray [78] and Tralli [126].

In Secs. 3.3 and 3.4 a hierarchical finite beam element is formulated. This special feature means that the accuracy of the basic displacement fields can be improved by introducing hierarchical or additional displacement functions. For a given number of degrees of freedom a minimum number of hierarchical elements yield, in general, better results than a subdivision into many conventional elements, see Sec. C.2 and Meirovitch and Baruh [75]. Two sets of additional functions can be chosen in the present study: polynomial terms and, in particular, eigenfunctions. The formulation with additional eigenfunctions as shown in Secs. 3.3 and 3.4 is believed to be novel. For the example of Sec. C.2, application of these functions gives excellent results when compared with the polynomials.

The finite beam element formulated in this chapter has several options: the type of torsion (Saint Venant torsion or warping torsion or both), whether rotatory and warping inertia should be included and whether additional displacement functions should be used (plus the type and the number of these functions). One may also

choose the position of the reference axes for the cross sectional displacements, and the position of the common point of beam end displacements needed in the transformation into a global coordinate system. In this way the present finite beam element becomes flexible in use giving a number of different structural models. In a previous version of the element, see the author [86][88], geometric effects (neglected here in Subsec. 2.2.2) and bending shear effects (to be neglected in Subsec. 3.2.1) might be included as well.

The assumptions introduced in this chapter are:

- initially straight beam (Subsec. 3.2.1)
- separable cross sectional and longitudinal discretizations (3.2.1)
- undeformable beam cross section (3.2.1)
- shear strains according to Saint Venant (3.2.1)
- direction cosine n_x = 0 along the contour of a beam lamina (3.2.2)
- constant material properties over the beam cross section (3.2.3).

As in Chapter 2 the assumptions are underlined in the following.

3.2   Beam theory formulation

In this section the partial differential equations of a beam are formulated. As in Secs. 2.2 and 2.3 the formulation contains the subsections: kinematic equations (3.2.1), equations of motion (3.2.2) and constitutive equations (3.2.3). To give the differential equations explicitly these three groups of equations are combined in the last part, Subsec. 3.2.4. Beam theory in general has been treated by several authors. Some references are Benscoter [7], Chen and Atsuta [12], Gjelsvik [43], Kollbrunner and Hajdin [56][57], Murray [78], Oden and Ripperger [82], the author [86][88], Petersson [92], Rayleigh [100], Thelandersson [119], Timoshenko et al. [120][121], Vlasov [131], von Karman and Christensen [132] and Åkesson [144].

3.2.1 Kinematic equations

The beam structures to be considered are assumed to consist of initially straight beams. For an initially straight beam it is convenient to introduce a local rectangular Cartesian reference frame. Denoting the coordinates by x, y and z, the x-axis may be chosen as the longitudinal axis and thus the y- and z-axes become cross sectional axes. In general the global coordinates X_1, X_2 and X_3 in Chapter 2 differ from the local ones x, y and z. The pertinent transformation from local to global coordinates is shown in Subsec. 3.4.2.

Other global quantities in Sec. 2.2 correspond to local ones (given by engineering notations) as follows: u_1, u_2, u_3 correspond to u, v, w; E_{11}, E_{22}, E_{33} to ϵ_x, ϵ_y, ϵ_z; $2E_{12} = 2E_{21}$ to γ_{xy}; $2E_{13} = 2E_{31}$ to γ_{xz}; $2E_{23} = 2E_{32}$ to γ_{yz}; $\tilde{T}_{11}$, $\tilde{T}_{22}$ $\tilde{T}_{33}$ to σ_x, σ_y, σ_z; $\tilde{T}_{12} = \tilde{T}_{21}$ to τ_{xy}; $\tilde{T}_{13} = \tilde{T}_{31}$ to τ_{xz}; $\tilde{T}_{23} = \tilde{T}_{32}$ to τ_{yz}; U_1, U_2, U_3 to $\bar{U}_x$, $\bar{U}_y$, $\bar{U}_z$; W_{im}^X to $\bar{\bar{W}}_{im}$; N_{in}^e to $\bar{N}_{in}$ and finally u_s^e to $\bar{u}_s^e$.

In local quantities, Eq. (2.20) can be written as

$$\bar{u} = \bar{N}\bar{u}_s^e \tag{3.1}$$

where $\bar{u} = [u\ v\ w]^T$ and the size of $\bar{N}$ is 3×NDOFSE (NDOFSE = number of degrees of freedom of the structural (beam) element). It is now assumed that the cross sectional and longitudinal discretizations are separable, that is

$$\bar{N}(x,y,z) = \bar{N}_{yz}(y,z)\bar{N}_x(x). \tag{3.2}$$

Introduction of Eq. (3.2) into Eq. (3.1) yields

$$\bar{u} = \bar{N}_{yz}\bar{u}_x \tag{3.3}$$

where

$$\bar{u}_x = \bar{N}_x \bar{u}_s^e \tag{3.4}$$

contains the cross sectional beam displacements, $\bar{u}_x = \bar{u}_x(x,t)$. The cross sectional discretization, represented by Eq. (3.3), is performed in this section whereas the longitudinal discretization (Eq. (3.4)) is carried out in Secs. 3.3 and 3.4.

The shape function matrix $\bar{N}_{yz}$ can be evaluated by means of two kinematic assumptions. Assume first, as in most beam theories, that the beam cross section is undeformable. This means that

$$\epsilon_y (x,y,z,t) = 0, \tag{3.5a}$$

$$\epsilon_z (x,y,z,t) = 0 \tag{3.5b}$$

and

$$\gamma_{yz}(x,y,z,t) = 0. \tag{3.5c}$$

In order to express the corresponding displacement field $\bar{u}$, beam cross sectional displacements must be defined. Four independent beam displacements are defined in Fig. 3.1 for an arbitrary cross section. With the definitions according to Fig. 3.1 the displacements of $\bar{u}$ corresponding to Eqs. (3.5a-c) may be written (see the author [86]) as
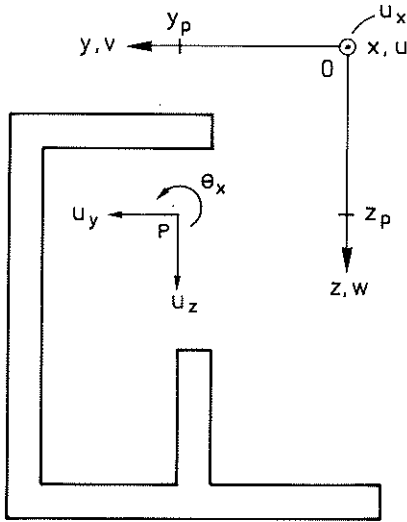
Figure 3.1. Displacements u_x, u_y, u_z and θ_x of an arbitrary beam cross section. The x-axis and the pole axis $(y,z) = (y_p, z_p)$ can be chosen arbitrarily.

$$
\begin{bmatrix} u \\ v \\ w \end{bmatrix} = \begin{bmatrix} 1 & 0 & 0 & 0 & -y & -z & -\bar{\Omega} \\ 0 & 1 & 0 & -(z-z_p) & 0 & 0 & 0 \\ 0 & 0 & 1 & (y-y_p) & 0 & 0 & 0 \end{bmatrix} \begin{bmatrix} u_x \\ u_y \\ u_z \\ \theta_x \\ u'_y \\ u'_z \\ \theta'_x \end{bmatrix} + \begin{bmatrix} u_\gamma \\ 0 \\ 0 \end{bmatrix}
\tag{3.6}
$$

where the sign $'$ denotes differentiation with respect to the longitudinal coordinate x and where

$$
\bar{\Omega}(y,z) = \int\limits_{(0,0)}^{(y,z)} [(\bar{y}-y_p)d\bar{z} - (\bar{z}-z_p)d\bar{y}]
\tag{3.7}
$$

and

$$u_\gamma(x,y,z,t) = \int_{(0,0)}^{(y,z)} [\gamma_{xy}(x,\bar{y},\bar{z},t)d\bar{y} + \gamma_{xz}(x,\bar{y},\bar{z},t)d\bar{z}] \qquad (3.8)$$

are two line integrals. The first integral, Eq. (3.7), may be identified as the sectorial coordinate of a beam of open thin–walled cross section, see Vlasov [131], provided the path of integration follows the midsurface of the walls. (A special midsurface coordinate, often denoted s, is usually introduced for thin–walled beams). The second integral, Eq. (3.8), describes the warping of the cross section due to the shear strains γ_{xy} and γ_{xz}. In accordance with the above assumption of separable variables, u_γ may be written as

$$u_\gamma = \psi_1(y,z)\chi_1(x,t) + \psi_2(y,z)\chi_2(x,t) + \ldots \qquad (3.9)$$

where ψ_i (i = 1,2...) are additional cross sectional shape functions and χ_i additional cross sectional displacement variables. Since the integral in Eq. (3.7) is not independent of the path of integration, however, u_γ must be chosen so that the sum $-\bar{\Omega}\theta_x' + u_\gamma$ in Eq. (3.6) is path independent. A second kinematic assumption saying that <u>the shear strains equal those predicted by Saint Venant</u> satisfies this requirement (provided that the line integrals in Eqs. (3.7) and (3.8) are carried out along the same path). In addition, this approximation of the shear strains is often acceptable. The assumption may be expressed as

$$\gamma_{xy}(x,y,z,t) = -\phi_{svy}(y,z)\theta_x'(x,t) \qquad (3.10a)$$

and

$$\gamma_{xz}(x,y,z,t) = \phi_{svz}(y,z)\theta_x'(x,t) \qquad (3.10b)$$

where ϕ_{svy} and ϕ_{svz} are functions which describe the cross sectional Saint Venant shear strain distributions. Thus bending shear strains are neglected; cf. for instance Magrab [69], the author [86][88] and Timoshenko [120]. Substituting Eqs. (3.10a–b) into Eq. (3.8) and introducing that equation into Eq. (3.6), one obtains

$$\bar{u} = \bar{N}_{yz}\bar{u}_x \tag{3.3}$$

or explicitly

$$\begin{bmatrix} u \\ v \\ w \end{bmatrix} = \begin{bmatrix} 1 & 0 & 0 & 0 & -y & -z & -\Omega \\ 0 & 1 & 0 & -(z-z_p) & 0 & 0 & 0 \\ 0 & 0 & 1 & (y-y_p) & 0 & 0 & 0 \end{bmatrix} \begin{bmatrix} u_x \\ u_y \\ u_z \\ \theta_x \\ u'_y \\ u'_z \\ \theta'_x \end{bmatrix} \tag{3.11}$$

where

$$\Omega(y,z) = \int\limits_{(0,0)}^{(y,z)} [(\bar{y}-y_p-\phi_{svz})d\bar{z} - (\bar{z}-z_p-\phi_{svy})d\bar{y}] \tag{3.12}$$

is the warping coordinate (Saint Venant warping function). It can be shown, see for instance the author [86], that this coordinate is independent of the path of integration (the integrand is an exact differential). It should be noted, however, that a complication occurs if the integral starting point (0,0) is situated outside the beam cross section, see for instance Fig. 3.1. In such cases one usually chooses a starting point on the cross section so that the

functions ϕ_{svy} and ϕ_{svz} can be defined. On the midsurface of an open thin-walled beam, the warping coordinate Ω coincides with the sectorial coordinate $\bar{\Omega}$ due to Vlasov [131] since $\phi_{svy} = \phi_{svz} = 0$ on the midsurface. On the midsurface of a closed thin-walled beam the warping coordinate coincides with the coordinate formulated by Benscoter [7] and von Karman and Christensen [132]. Since the warping coordinate Ω is here defined for every point on the beam cross section secondary warping effects may be included, see for instance Gjelsvik [43] and Oden and Ripperger [82].

When comparing Eq. (3.11) with Eq. (3.6) it can be seen that the assumption in Eqs. (3.10a-b) gives no additional displacement variable since this assumption is associated with the already existing variable θ'_x. The assumption according to Eqs. (3.10a-b) is the one introduced by Vlasov [131] and von Karman and Christensen [132] for thin-walled open and closed beams, respectively.

The nonzero strains may now be written as (cf. Eq. (2.7))

$$\epsilon = \begin{bmatrix} \epsilon_x \\ \gamma_{xy} \\ \gamma_{xz} \end{bmatrix} = \begin{bmatrix} \dfrac{\partial}{\partial x} & 0 & 0 \\ \dfrac{\partial}{\partial y} & \dfrac{\partial}{\partial x} & 0 \\ \dfrac{\partial}{\partial z} & 0 & \dfrac{\partial}{\partial x} \end{bmatrix} \begin{bmatrix} u \\ v \\ w \end{bmatrix}. \qquad (3.13)$$

Substitution of Eq. (3.11) into Eq. (3.13) results in

$$\epsilon = \nabla_b \bar{u}_x \qquad (3.14)$$

or explicitly

$$\begin{bmatrix} \epsilon_x \\ \gamma_{xy} \\ \gamma_{xz} \end{bmatrix} = \begin{bmatrix} \frac{\partial}{\partial x} & 0 & 0 & 0 & -y\frac{\partial}{\partial x} & -z\frac{\partial}{\partial x} & -\Omega\frac{\partial}{\partial x} \\ 0 & 0 & 0 & 0 & 0 & 0 & -\phi_{svy} \\ 0 & 0 & 0 & 0 & 0 & 0 & \phi_{svz} \end{bmatrix} \begin{bmatrix} u_x \\ u_y \\ u_z \\ \theta_x \\ u'_y \\ u'_z \\ \theta'_x \end{bmatrix}. \qquad (3.14')$$

Note that the relations

$$\frac{\partial \Omega}{\partial y} = -(z - z_p - \phi_{svy}) \qquad (3.15a)$$

and

$$\frac{\partial \Omega}{\partial z} = (y - y_p - \phi_{svz}) \qquad (3.15b)$$

derived from Eq. (3.12) have been used in Eq. (3.14').

3.2.2 Equations of motion

According to Eqs. (2.21) and (3.2) it can be concluded that the weighting function matrix $\overline{\overline{W}}$ can be written as

$$\overline{\overline{W}}(x,y,z) = \overline{\overline{W}}_{yz}(y,z)\overline{\overline{W}}_x(x). \qquad (3.16)$$

Then Eq. (2.17) may be formulated in local coordinates as

$$\int_{V^e} \overline{\overline{w}}^T \widetilde{\nabla}\widetilde{\sigma} \, dV^e + \int_{V^e} \overline{\overline{w}}^T \overline{\overline{U}} \, dV^e = \int_{V^e} \overline{\overline{w}}^T \rho \ddot{\overline{u}} \, dV^e \qquad (3.17)$$

where

$$\widetilde{\widetilde{\mathbf{v}}}\boldsymbol{\sigma} = \begin{bmatrix} \dfrac{\partial}{\partial x} & 0 & 0 & \dfrac{\partial}{\partial y} & \dfrac{\partial}{\partial z} & 0 \\[2mm] 0 & \dfrac{\partial}{\partial y} & 0 & \dfrac{\partial}{\partial x} & 0 & \dfrac{\partial}{\partial z} \\[2mm] 0 & 0 & \dfrac{\partial}{\partial z} & 0 & \dfrac{\partial}{\partial x} & \dfrac{\partial}{\partial y} \end{bmatrix} \begin{bmatrix} \sigma_x \\[1mm] \sigma_y \\[1mm] \sigma_z \\[1mm] \tau_{xy} \\[1mm] \tau_{xz} \\[1mm] \tau_{yz} \end{bmatrix} \qquad (3.18)$$

corresponds to the first term in Eq. (2.11). If each of the volume integrals in Eq. (3.17) is now replaced by an integral along the beam (length L) and an integral over the beam cross sectional area $A = A(x)$, Eq. (3.17) can be expressed as

$$\int_0^L \bar{\mathbf{W}}_x^T (\int_A \bar{\mathbf{W}}_{yz}^T \widetilde{\widetilde{\mathbf{v}}}\boldsymbol{\sigma} \; dA)dx + \int_0^L \bar{\mathbf{W}}_x^T (\int_A \bar{\mathbf{W}}_{yz}^T \bar{\mathbf{U}} \; dA)dx$$

$$= \int_0^L \bar{\mathbf{W}}_x^T (\int_A \bar{\mathbf{W}}_{yz}^T \rho \ddot{\bar{\mathbf{u}}} \; dA)dx \qquad (3.19)$$

by substitution of Eq. (3.16). In this section a beam lamina Adx is considered meaning that the integration with respect to x in Eq. (3.19) are left to Secs. 3.3 and 3.4. In analogy with Eq. (2.21), $\bar{\mathbf{W}}_{yz}^T$ in Eq. (3.19) can be substituted by $\bar{\mathbf{N}}_{yz}^T$ which is given by Eq. (3.11). Thus the integrals

$$\int_A \bar{\mathbf{N}}_{yz}^T \widetilde{\widetilde{\mathbf{v}}}\boldsymbol{\sigma} \; dA + \int_A \bar{\mathbf{N}}_{yz}^T \bar{\mathbf{U}} \; dA = \int_A \bar{\mathbf{N}}_{yz}^T \rho \ddot{\bar{\mathbf{u}}} \; dA \qquad (3.19')$$

are first evaluated. Several of the 42 terms of the matrix $\bar{\mathbf{N}}_{yz}^T \widetilde{\mathbf{v}}$ in Eq. (3.19') contain the operators $\dfrac{\partial}{\partial y}$ or $\dfrac{\partial}{\partial z}$. If these terms are

integrated by parts it can be shown that Eq. (3.19') can be transformed into

$$\int_A \mathbf{v}_a^T \sigma \ dA + \int_A \bar{\mathbf{N}}_{yz}^T \bar{\mathbf{U}} \ dA + \int_{\mathcal{L}} \bar{\mathbf{N}}_{yz}^T \bar{\mathbf{U}}_{\mathcal{L}} \ d\mathcal{L} = \int_A \bar{\mathbf{N}}_{yz}^T \rho \ddot{\bar{\mathbf{u}}} \ dA \qquad (3.20)$$

where

$$\mathbf{v}_a^T = \begin{bmatrix} \dfrac{\partial}{\partial x} & 0 & 0 \\[2ex] 0 & \dfrac{\partial}{\partial x} & 0 \\[2ex] 0 & 0 & \dfrac{\partial}{\partial x} \\[2ex] 0 & -(z-z_p)\dfrac{\partial}{\partial x} & (y-y_p)\dfrac{\partial}{\partial x} \\[2ex] -y\dfrac{\partial}{\partial x} & 1 & 0 \\[2ex] -z\dfrac{\partial}{\partial x} & 0 & 1 \\[2ex] -\Omega\dfrac{\partial}{\partial x} & \dfrac{\partial\Omega}{\partial y} & \dfrac{\partial\Omega}{\partial z} \end{bmatrix}, \qquad (3.21)$$

$$\sigma = \begin{bmatrix} \sigma_x \\ \tau_{xy} \\ \tau_{xz} \end{bmatrix} \qquad (3.22)$$

and

$$\bar{\mathbf{U}}_{\mathcal{L}} = \begin{bmatrix} \bar{U}_{\mathcal{L}x} \\ \bar{U}_{\mathcal{L}y} \\ \bar{U}_{\mathcal{L}z} \end{bmatrix} = \begin{bmatrix} \tau_{xy}n_y + \tau_{xz}n_z \\ \sigma_y n_y + \tau_{yz}n_z \\ \tau_{yz}n_y + \sigma_z n_z \end{bmatrix}. \qquad (3.23)$$

The integral $\displaystyle\int_{\mathcal{L}}$ in Eq. (3.20) is the contour integral of the beam cross section while n_y and n_z in Eq. (3.23) are direction cosines of

this contour. It is here presupposed that $\underline{n_x = 0 \text{ along the contour}}$ $\underline{\text{of each beam lamina}}$. This also implies that $n_x = \pm 1$ at the beam end surfaces.

The first integral in Eq. (3.20) may alternatively be written as

$$
\int_A \mathbf{v}_a^T \sigma \; dA = \bar{\sigma} =
\begin{bmatrix}
\dfrac{\partial N}{\partial x} \\[2ex]
\dfrac{\partial V_y}{\partial x} \\[2ex]
\dfrac{\partial V_z}{\partial x} \\[2ex]
\dfrac{\partial T}{\partial x} \\[2ex]
\dfrac{\partial M_z}{\partial x} + V_y \\[2ex]
-\dfrac{\partial M_y}{\partial x} + V_z \\[2ex]
-\dfrac{\partial B}{\partial x} + T_w
\end{bmatrix}
\tag{3.24}
$$

where

$$
N \;=\; \int_A \sigma_x \; dA,
\tag{3.25a}
$$

$$
V_y \;=\; \int_A \tau_{xy} \; dA,
\tag{3.25b}
$$

$$
V_z \;=\; \int_A \tau_{xz} \; dA,
\tag{3.25c}
$$

$$
T \;=\; \int_A [(y-y_p)\tau_{xz} - (z-z_p)\tau_{xy}]dA,
\tag{3.25d}
$$

$$M_z = \int_A -y \ \sigma_x \ dA, \qquad\qquad (3.25e)$$

$$M_y = \int_A z \ \sigma_x \ dA, \qquad\qquad (3.25f)$$

$$B = \int_A \Omega \ \sigma_x \ dA \qquad\qquad (3.25g)$$

and

$$T_w = \int_A (\frac{\partial \Omega}{\partial y} \ \tau_{xy} + \frac{\partial \Omega}{\partial z} \ \tau_{xz}) dA \qquad\qquad (3.25h)$$

are the chosen stress resultants: normal force, shear forces, torsional moment, bending moments, bimoment and warping torsional moment. The quantity T_w in Eq. (3.25h) is named warping torsional moment since it is related to the warping coordinate Ω, see also Subsec. 3.2.4.

3.2.3 Constitutive equations

From Eqs. (2.14) and (2.15a–b) one obtains the constitutive relation

$$\sigma = D\epsilon \qquad\qquad (3.26)$$

where

$$D = \begin{bmatrix} \bar{E} & 0 & 0 \\ 0 & G & 0 \\ 0 & 0 & G \end{bmatrix} \qquad\qquad (3.27)$$

is the material matrix. The modified elastic modulus $\bar{E}$ in Eq. (3.27)

is equal to $\dfrac{E(1-v)}{(1+v)(1-2v)}$ if Eqs. (3.5a–c) are adopted. For instance, $\bar{E} = 1.35E$ for $v = 0.3$ in this case. For thin-walled beams the definition of $\bar{E}$ above may yield too high values for $\bar{E}$. According to Vlasov [131], $\bar{E}$ may be defined as $E/(1-v^2)$ for such beams ($\bar{E} = 1.10E$ for $v = 0.3$). Often $\bar{E}$ is simply approximated by E in order to consider that $\sigma_y \approx \sigma_z \approx 0$ rather than retaining the assumptions that $\epsilon_y = \epsilon_z = 0$, see Chapter 6 and Appendices C and D.

In Subsec. 3.2.4, Eq. (3.26) will be substituted into the stress resultant equations (3.25a–h). To simplify these integral expressions <u>constant material properties over the beam cross section</u> are assumed. Thus E ($\bar{E}$) and G as well as the mass density ρ are constant over the cross section.

3.2.4 Combined equations

It may be argued that there is no need to combine the resulting equations of Subsecs. 3.2.1–3 since the final goal of this chapter is to formulate a finite beam element. However, it is important to identify the partial differential equations, including the material and cross sectional constants, of a beam lamina. In addition, it is of interest to identify the Saint Venant torsional moment T_{sv} which has not yet appeared in the analysis.

To express the partial differential equations it should be noted that the seven equations of motion in Eq. (3.20) correspond to the seven cross sectional displacements in Eqs. (3.11) and (3.14'). As indicated above, however, these displacements are not independent but can be expressed as

$$
\begin{bmatrix} u_x \\ u_y \\ u_z \\ \theta_x \\ u'_y \\ u'_z \\ \theta'_x \end{bmatrix} = \begin{bmatrix} 1 & 0 & 0 & 0 \\ 0 & 1 & 0 & 0 \\ 0 & 0 & 1 & 0 \\ 0 & 0 & 0 & 1 \\ 0 & \dfrac{\partial}{\partial x} & 0 & 0 \\ 0 & 0 & \dfrac{\partial}{\partial x} & 0 \\ 0 & 0 & 0 & \dfrac{\partial}{\partial x} \end{bmatrix} \begin{bmatrix} u_x \\ u_y \\ u_z \\ \theta_x \end{bmatrix}
\tag{3.28}
$$

or briefly

$$
\bar{u}_x = \bar{v}_b \, \bar{\bar{u}}_x .
\tag{3.28'}
$$

Thus only four differential equations are necessary. In analogy with Eq. (3.28), the seven stress resultant expressions in Eq. (3.24) should be reduced to four. Premultiplication of Eq. (3.24) by an appropriate operation matrix gives

$$
\begin{bmatrix} 1 & 0 & 0 & 0 & 0 & 0 & 0 \\ 0 & -1 & 0 & 0 & \dfrac{\partial}{\partial x} & 0 & 0 \\ 0 & 0 & -1 & 0 & 0 & \dfrac{\partial}{\partial x} & 0 \\ 0 & 0 & 0 & -1 & 0 & 0 & \dfrac{\partial}{\partial x} \end{bmatrix}
\begin{bmatrix} \dfrac{\partial N}{\partial x} \\ \dfrac{\partial V_y}{\partial x} \\ \dfrac{\partial V_z}{\partial x} \\ \dfrac{\partial T}{\partial x} \\ \dfrac{\partial M_z}{\partial x} + V_y \\ -\dfrac{\partial M_y}{\partial x} + V_z \\ -\dfrac{\partial B}{\partial x} + T_w \end{bmatrix}
=
\begin{bmatrix} \dfrac{\partial N}{\partial x} \\ \dfrac{\partial^2 M_z}{\partial x^2} \\ -\dfrac{\partial^2 M_y}{\partial x^2} \\ -\dfrac{\partial^2 B}{\partial x^2} - \dfrac{\partial}{\partial x}(T-T_w) \end{bmatrix}
\tag{3.29}
$$

or

$$\bar{\mathbf{v}}_a^T \bar{\boldsymbol{\sigma}} = \bar{\bar{\boldsymbol{\sigma}}}. \tag{3.29'}$$

The choice of $\bar{\mathbf{v}}_a^T$ according to Eq. (3.29) leads to elimination of the shear forces V_y and V_z from $\bar{\bar{\boldsymbol{\sigma}}}$. This elimination is necessary here since these forces are not associated with any shear strains (cf. Eqs. (3.10a–b)). Further, the torsional moments T and T_w are collected to a term $T - T_w$ in $\bar{\bar{\boldsymbol{\sigma}}}$. Often this term is presupposed to be equal to the Saint Venant torsional moment T_{sv}. In general, however, this is not true but depends on the definition of Ω. For this reason, no such interpretation is presupposed here.

Combining the equations by premultiplying Eq. (3.20) by $\bar{\mathbf{v}}_a^T$ and substituting Eqs. (3.26), (3.14), (3.3) and (3.28'), one obtains

$$(\bar{\mathbf{v}}_a^T \int_A \mathbf{v}_a^T \, \mathbf{D} \, \mathbf{v}_b \, dA \, \bar{\mathbf{v}}_b) \bar{\bar{\mathbf{u}}}_x - (\bar{\mathbf{v}}_a^T \int_A \bar{\mathbf{N}}_{yz}^T \, \rho \, \bar{\mathbf{N}}_{yz} \, dA \, \bar{\mathbf{v}}_b) \ddot{\bar{\bar{\mathbf{u}}}}_x$$

$$= -\bar{\mathbf{v}}_a^T \int_A \bar{\mathbf{N}}_{yz}^T \, \bar{\mathbf{U}} \, dA - \bar{\mathbf{v}}_a^T \int_{\mathscr{L}} \bar{\mathbf{N}}_{yz}^T \, \bar{\mathbf{U}}_{\mathscr{L}} \, d\mathscr{L}. \tag{3.30}$$

Evaluation of this expression gives

$$\mathbf{v}_\epsilon^T \, \mathbf{D}_\epsilon \, \mathbf{v}_\epsilon \, \bar{\bar{\mathbf{u}}}_x - \mathbf{v}_\gamma^T \, \mathbf{D}_\gamma \, \mathbf{v}_\gamma \, \bar{\bar{\mathbf{u}}}_x$$

$$+ \mathbf{v}_p^T \, \mathbf{D}_p \, \mathbf{v}_p \, \ddot{\bar{\bar{\mathbf{u}}}}_x - \mathbf{v}_s^T \, \mathbf{D}_s \, \mathbf{v}_s \, \ddot{\bar{\bar{\mathbf{u}}}}_x = \mathbf{v}_{q1}^T \, \bar{\bar{\mathbf{q}}}_{x1} + \mathbf{v}_{q2}^T \, \bar{\bar{\mathbf{q}}}_{x2} \tag{3.31}$$

or explicitly

$$\begin{bmatrix} \dfrac{\partial}{\partial x} & 0 & 0 & 0 \\[4pt] 0 & \dfrac{\partial^2}{\partial x^2} & 0 & 0 \\[4pt] 0 & 0 & \dfrac{\partial^2}{\partial x^2} & 0 \\[4pt] 0 & 0 & 0 & \dfrac{\partial^2}{\partial x^2} \end{bmatrix} \left(\int_A \bar{E} \begin{bmatrix} 1 & -y & -z & -\Omega \\ -y & y^2 & yz & y\Omega \\ -z & yz & z^2 & z\Omega \\ -\Omega & y\Omega & z\Omega & \Omega^2 \end{bmatrix} dA \right) \begin{bmatrix} \dfrac{\partial}{\partial x} & 0 & 0 & 0 \\[4pt] 0 & \dfrac{\partial^2}{\partial x^2} & 0 & 0 \\[4pt] 0 & 0 & \dfrac{\partial^2}{\partial x^2} & 0 \\[4pt] 0 & 0 & 0 & \dfrac{\partial^2}{\partial x^2} \end{bmatrix} \begin{bmatrix} u_x \\ u_y \\ u_z \\ \theta_x \end{bmatrix}$$

$$- \begin{bmatrix} 0 & 0 & 0 & 0 \\ 0 & 0 & 0 & 0 \\ 0 & 0 & 0 & 0 \\ 0 & 0 & 0 & \dfrac{\partial}{\partial x} \end{bmatrix} \left(\int_A G \begin{bmatrix} 0 & 0 & 0 & 0 \\ 0 & 0 & 0 & 0 \\ 0 & 0 & 0 & 0 \\ 0 & 0 & 0 & \phi_{svy}^2 + \phi_{svz}^2 \end{bmatrix} dA \right) \begin{bmatrix} 0 & 0 & 0 & 0 \\ 0 & 0 & 0 & 0 \\ 0 & 0 & 0 & 0 \\ 0 & 0 & 0 & \dfrac{\partial}{\partial x} \end{bmatrix} \begin{bmatrix} u_x \\ u_y \\ u_z \\ \theta_x \end{bmatrix}$$

$$+ \begin{bmatrix} 1 & 0 & 0 & 0 \\ 0 & 1 & 0 & 0 \\ 0 & 0 & 1 & 0 \\ 0 & 0 & 0 & 1 \end{bmatrix} \left(\int_A \rho \begin{bmatrix} -1 & 0 & 0 & 0 \\ 0 & 1 & 0 & -(z-z_p) \\ 0 & 0 & 1 & (y-y_p) \\ 0 & -(z-z_p) & (y-y_p) & (y-y_p)^2 + (z-z_p)^2 \end{bmatrix} dA \right) \begin{bmatrix} 1 & 0 & 0 & 0 \\ 0 & 1 & 0 & 0 \\ 0 & 0 & 1 & 0 \\ 0 & 0 & 0 & 1 \end{bmatrix} \begin{bmatrix} \ddot{u}_x \\ \ddot{u}_y \\ \ddot{u}_z \\ \ddot{\theta}_x \end{bmatrix}$$

$$- \begin{bmatrix} 1 & 0 & 0 & 0 \\ 0 & \dfrac{\partial}{\partial x} & 0 & 0 \\[4pt] 0 & 0 & \dfrac{\partial}{\partial x} & 0 \\[4pt] 0 & 0 & 0 & \dfrac{\partial}{\partial x} \end{bmatrix} \left(\int_A \rho \begin{bmatrix} 0 & -y & -z & -\Omega \\ -y & y^2 & yz & y\Omega \\ -z & yz & z^2 & z\Omega \\ -\Omega & y\Omega & z\Omega & \Omega^2 \end{bmatrix} dA \right) \begin{bmatrix} 1 & 0 & 0 & 0 \\ 0 & \dfrac{\partial}{\partial x} & 0 & 0 \\[4pt] 0 & 0 & \dfrac{\partial}{\partial x} & 0 \\[4pt] 0 & 0 & 0 & \dfrac{\partial}{\partial x} \end{bmatrix} \begin{bmatrix} \ddot{u}_x \\ \ddot{u}_y \\ \ddot{u}_z \\ \ddot{\theta}_x \end{bmatrix}$$

$$
= \begin{bmatrix} -1 & 0 & 0 & 0 \\ 0 & 1 & 0 & 0 \\ 0 & 0 & 1 & 0 \\ 0 & 0 & 0 & 1 \end{bmatrix} \left(\int_A \begin{bmatrix} \bar{U}_x \\ \bar{U}_y \\ \bar{U}_z \\ (y-y_p)\bar{U}_z - \\ (z-z_p)\bar{U}_y \end{bmatrix} dA + \int_{\mathscr{L}} \begin{bmatrix} \bar{U}_{\mathscr{L}x} \\ \bar{U}_{\mathscr{L}y} \\ \bar{U}_{\mathscr{L}z} \\ (y-y_p)\bar{U}_{\mathscr{L}z} - \\ (z-z_p)\bar{U}_{\mathscr{L}y} \end{bmatrix} d\mathscr{L} \right)
$$

$$
+ \begin{bmatrix} 0 & 0 & 0 & 0 \\ 0 & -\dfrac{\partial}{\partial x} & 0 & 0 \\ 0 & 0 & \dfrac{\partial}{\partial x} & 0 \\ 0 & 0 & 0 & \dfrac{\partial}{\partial x} \end{bmatrix} \left(\int_A \begin{bmatrix} 0 \\ -y\bar{U}_x \\ z\bar{U}_x \\ \Omega\bar{U}_x \end{bmatrix} dA + \int_{\mathscr{L}} \begin{bmatrix} 0 \\ -y\bar{U}_{\mathscr{L}x} \\ z\bar{U}_{\mathscr{L}x} \\ \Omega\bar{U}_{\mathscr{L}x} \end{bmatrix} d\mathscr{L} \right) \qquad (3.31')
$$

where Eqs. (3.15a–b) have been used. The first two terms in Eq. (3.31) are related to the normal strain ϵ_x and to the shear strains γ_{xy} and γ_{xz} respectively. It should be noted that only the Saint Venant quantities ϕ_{svy} and ϕ_{svz} enter the shear strain integral since only Saint Venant shear strains have been considered, see Eqs. (3.10a–b). The last terms on the left–hand side of Eq. (3.31) represent primary and secondary dynamic effects. The (small) secondary effects are due to rotatory inertia according to Rayleigh, warping inertia as well as coupling terms. The right–hand side consists of the external loadings on the beam lamina.

If $\bar{E}(E)$, G and ρ are constant over the cross section as assumed in Subsec. 3.2.3, the symmetric beam property matrices D_ϵ, D_γ, D_p and D_s become

$$\mathbf{D}_\epsilon = \bar{E}\begin{bmatrix} A & -S_z & -S_y & -S_\Omega \\ -S_z & I_z & I_{yz} & I_{y\Omega} \\ -S_y & I_{yz} & I_y & I_{z\Omega} \\ -S_\Omega & I_{y\Omega} & I_{z\Omega} & I_\Omega \end{bmatrix}, \quad \mathbf{D}_\gamma = G\begin{bmatrix} 0 & 0 & 0 & 0 \\ 0 & 0 & 0 & 0 \\ 0 & 0 & 0 & 0 \\ 0 & 0 & 0 & K_v \end{bmatrix} \quad (3.32a,b)$$

and

$$\mathbf{D}_p = \rho\begin{bmatrix} -A & 0 & 0 & 0 \\ 0 & A & 0 & -\bar{S}_y \\ 0 & 0 & A & \bar{S}_z \\ 0 & -\bar{S}_y & \bar{S}_z & I_p \end{bmatrix}, \quad \mathbf{D}_s = \rho\begin{bmatrix} 0 & -S_z & -S_y & -S_\Omega \\ -S_z & I_z & I_{yz} & I_{y\Omega} \\ -S_y & I_{yz} & I_y & I_{z\Omega} \\ -S_\Omega & I_{y\Omega} & I_{z\Omega} & I_\Omega \end{bmatrix} \quad (3.32c,d)$$

where the cross sectional constants can be identified by means of Eq. (3.31') (see Appendix A for notations). In particular, it can be seen that the assumed cross sectional shear strain functions ϕ_{svy} and ϕ_{svz} result in the Saint Venant torsion constant K_v because

$$K_v = \int_A (\phi_{svy}^2 + \phi_{svz}^2)dA. \quad (3.33)$$

This relation can be verified through the use of the Prandtl stress function concept, see for instance Krenk [63]. The term $\int_A G(\phi_{svy}^2 + \phi_{svz}^2)dA \, \theta_x' = GK_v\theta_x'$ in Eq. (3.31') equals $T-T_w$ in Eq. (3.29) and thus it is shown that

$$T = T_{sv} + T_w \quad (3.34)$$

since $T_{sv} = GK_v\theta_x'$. In conclusion, the (total) torsional moment T equals the sum of the Saint Venant torsional moment T_{sv} and the warping torsional moment T_w for the present choice of warping coordinate Ω (Eq. (3.12)). Note that no such assumption has been

presupposed here and introduced in Eq. (3.29) but has been derived from the kinematic assumptions. Also note that the Saint Venant torsion is, in general, associated with cross sectional warping. In contrast to the warping torsion, however, the Saint Venant torsion is not associated with any normal stresses (σ_x) or strains (ϵ_x). For open thin–walled beams warping torsion is often called Vlasov torsion, see Vlasov [131].

Finally, it should be noted that the four partial differential equations in Eq. (3.31) are in general coupled as can be seen from the off–diagonal nonzero terms in Eqs. (3.31') and (3.32). Even though the x–axis (see Fig. 3.1) can be chosen to coincide with the centroidal axis $(S_y = S_z = 0)$, the y– and z–axes are principal axes $(I_{yz} = 0)$, the pole axis is the shear centre axis $(I_{y\Omega} = I_{z\Omega} = 0)$ and the warping coordinate is normalized $(S_\Omega = 0)$, the beam vibrations may be coupled. This is the case when the centroidal axis and the shear centre axis do not coincide $(\bar{S}_y \neq 0$ and/or $\bar{S}_z \neq 0)$, see Secs. 6.4 and C.3.

3.3   Finite element formulation

The second spatial discretization step of the beam is performed in this and the following section. Based on the beam theory formulated in Sec. 3.2, the first discretization step, a finite beam element is formulated. The present formulation proceeds in analogy with the one in Sec. 3.2. Thus kinematic equations, equations of motion and constitutive equations are derived (Subsecs. 3.3.1–3) and combined (Sec. 3.4).

Several three–dimensional finite beam elements have been formulated for dynamic analysis during the last twenty years. Most formulations are restricted to uncoupled vibrations and Saint Venant torsion.

Some references are Bhatt [8], Craig [19], Friberg [37], Kolousek [58], Lundén and Åkesson [66], Mei [74], the author [86][88], Paz [89] and Przemieniecki [96]. References in connection with hierarchical finite elements, a special feature of the present beam element, are given in Subsec. 3.3.1.

3.3.1 Kinematic equations

The second discretization step means that the beam displacements in $\bar{u}_x(\bar{\bar{u}}_x)$ are to be replaced by a set of finite beam element displacements $\bar{u}_s^e$. According to Eq. (3.4) a new set of shape functions, $\bar{N}_x$, must be defined for that purpose. Since the displacements in $\bar{u}_x$ are not independent, it is convenient to establish the analogous expression

$$\bar{\bar{u}}_x = \bar{\bar{N}}_x \, \bar{u}_s^e \tag{3.35}$$

for the independent displacement variables in $\bar{\bar{u}}_x$. It can then be seen from Eqs. (3.28') and (3.4) that the two shape function matrices are related to each other as

$$\bar{N}_x = \bar{v}_b \, \bar{\bar{N}}_x. \tag{3.36}$$

Thus once $\bar{\bar{N}}_x$ has been chosen $\bar{N}_x$ can be evaluated from Eq. (3.36). Usually the shape functions in $\bar{\bar{N}}_x$ are chosen as polynomials in the longitudinal coordinate x. Here the following displacement relation is introduced

$$
\begin{bmatrix} u_x \\ u_y \\ u_z \\ \theta_x \end{bmatrix} = \begin{bmatrix} 1 & 0 & 0 & 0 & 0 & 0 & x & 0 & 0 & 0 & 0 & 0 & 0 & 0 \\ 0 & 1 & 0 & 0 & 0 & x & 0 & x^2 & 0 & 0 & 0 & x^3 & 0 & 0 \\ 0 & 0 & 1 & 0 & x & 0 & 0 & 0 & x^2 & 0 & x^3 & 0 & 0 & 0 \\ 0 & 0 & 0 & 1 & 0 & 0 & 0 & 0 & 0 & x & 0 & 0 & x^2 & x^3 \end{bmatrix} \begin{bmatrix} \alpha_1 \\ \alpha_2 \\ : \\ : \\ \alpha_{14} \end{bmatrix} + \begin{bmatrix} A_{ux} \\ A_{uy} \\ A_{uz} \\ A_{\theta x} \end{bmatrix}
$$

$$(3.37)$$

or

$$\bar{\bar{u}}_x = \bar{\bar{N}}_{\alpha 1}\,\alpha_1 + A. \tag{3.37'}$$

Thus linear and cubic polynomials are chosen as basic displacement fields, cf. Bengtsson [6]. However, additional displacements fields, given by A, may be included to improve the accuracy of the approximate basic fields (cf. Eq. (3.9)). In this way a hierarchical finite element can be formulated, see e.g. Meirovitch and Baruh [75], Möller [79], Szabo [115] and Zienkiewicz et al. [142]. The hierarchical refinement (p-refinement) stands in contrast to an improved accuracy through a finite element mesh refinement (h-refinement). Often the p-refinement yields better results, for instance in terms of eigenfrequencies, than the h-refinement. An example of this feature is shown in Sec. C.2 for a simple beam structure.

By means of the hierarchical element concept, symbolized through Eq. (3.37'), a physical beam or column can be represented accurately by only one finite beam element. Thus in addition to giving better numerical results, the p-refinement should result in simpler input data preparation in a computer run. This last advantage is also valid in the dynamic stiffness method, see e.g. Friberg [37], Howson and Williams [50], Kolousek [58] and Lundén and Åkesson [66].

Moreover, 14 displacement variables (cf. Eq. (3.37)) are sufficient to give exact numerical results in the dynamic stiffness method (within the beam theory chosen). However, in this method the element matrices are frequency-dependent, yielding a nonlinear eigenvalue problem. In addition, an exact beam element is very difficult, if not impossible, to formulate for generally coupled beam vibrations. For a further discussion of the merits of approximate and exact finite beam elements, see for instance Sadek [103]. See also the verification examples in Secs. C.3 and C.4.

The hierarchical or additional displacement fields in Eq. (3.37) may be of different kinds. Usually the basic polynomials are extended to higher-order polynomials, see for instance Lees and Thomas [64]. In the present beam element this possibility is included. Also, however, another set of additional functions has been proposed by the author [86][88]. This set consists of the eigenfunctions describing free uncoupled vibrations of a uniform beam clamped at both ends. These functions are also known as antiresonance forms in the dynamic stiffness method, see Kolousek [58]. For tension and pure Saint Venant torsion these functions are sine functions. For bending and warping torsion, however, they contain trigonometric as well as hyperbolic functions, see e.g. Paz [89] and Fig. 3.3. To the author's knowledge the use of additional eigenfunctions results in a finite beam element not formulated previously. A limited numerical study, see the author [86] and Appendix C, suggests that the hierarchical functions in terms of eigenfunctions should be used in preference to polynomials in dynamic beam and frame analysis.

The additional fields in Eq. (3.37') may be written as

$$A = \overline{\overline{N}}_{\alpha 15} \alpha_{15} \tag{3.38}$$

---

where the functions in $\overset{=}{N}_{\alpha 15}$ may be polynomial terms (x^2, x^3... in tension; x^4, x^5... in bending etc.) or eigenfunctions. Substituting Eq. (3.38) into Eq. (3.37'), one finds that

$$\overset{=}{\bar{u}}_x = \left[\overset{=}{N}_{\alpha 1} \mid \overset{=}{N}_{\alpha 15} \right] \begin{bmatrix} \alpha_1 \\ - \\ \alpha_{15} \end{bmatrix} = \overset{=}{N}_\alpha \alpha. \qquad (3.39)$$

In order to describe kinematic and static quantities at the beam ends the variables in α_1 are replaced by the 14 displacement variables $\bar{u}_1$ to $\bar{u}_{14}$ defined as

$$\bar{u}_1(t) = u_x(0,t), \qquad\qquad \bar{u}_7(t) = u_x(L,t), \qquad (3.40a,b)$$

$$\bar{u}_2(t) = u_y(0,t), \qquad\qquad \bar{u}_8(t) = u_y(L,t), \qquad (3.40c,d)$$

$$\bar{u}_3(t) = u_z(0,t), \qquad\qquad \bar{u}_9(t) = u_z(L,t), \qquad (3.40e,f)$$

$$\bar{u}_4(t) = \theta_x(0,t), \qquad\qquad \bar{u}_{10}(t) = \theta_x(L,t), \qquad (3.40g,h)$$

$$\bar{u}_5(t) = -u_z'(0,t), \qquad\qquad \bar{u}_{11}(t) = -u_z'(L,t), \qquad (3.40i,j)$$

$$\bar{u}_6(t) = u_y'(0,t), \qquad\qquad \bar{u}_{12}(t) = u_y'(L,t) \qquad (3.40k,l)$$

and

$$\bar{u}_{13}(t) = \theta_x'(0,t), \qquad\qquad \bar{u}_{14}(t) = \theta_x'(L,t). \qquad (3.40m,n)$$

These new displacement variables introduced in the finite element formulation are illustrated in Fig. 3.2 (cf. Fig. 3.1). With the local element displacement vector defined as $\bar{u}_s^e = [\bar{u}_1 \ \bar{u}_2 ... \bar{u}_{14} \ \alpha_{15} \ \alpha_{16}...]^T$ its relation to α may be evaluated from Eqs. (3.39) and (3.40) and written as
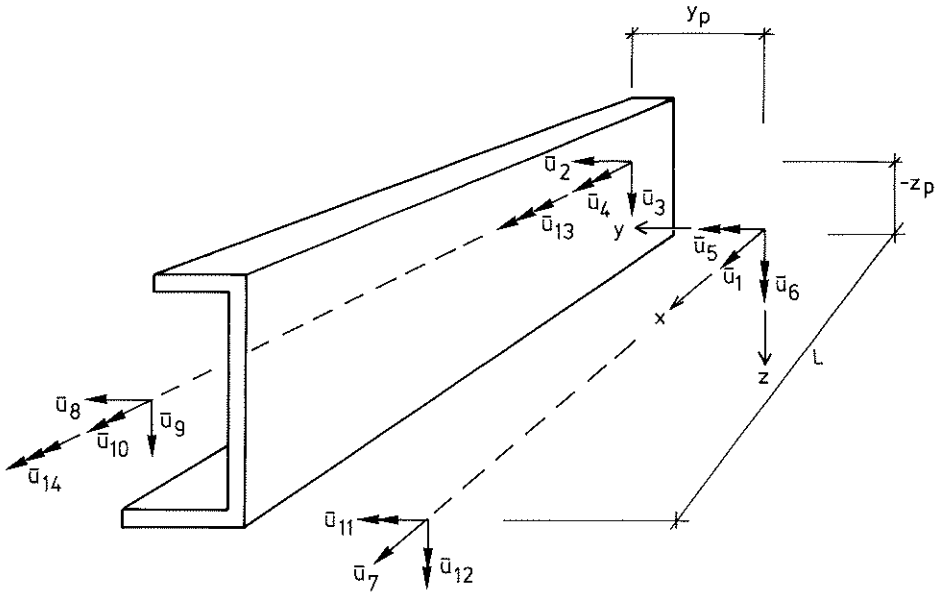
Figure 3.2. Definition of local degrees of freedom $\bar{u}_1$ to $\bar{u}_{14}$. $\bar{u}_{13}$ and $\bar{u}_{14}$ are optional. Beam element length L.

$$\alpha = H \, \bar{u}_s^e \tag{3.41}$$

where H is a transformation matrix depending only upon the beam element length L and the type of additional displacement fields. Introduction of Eq. (3.41) into Eq. (3.39) yields

$$\bar{\bar{u}}_x = \bar{\bar{N}}_x \, \bar{u}_s^e \tag{3.35}$$

where

$$\bar{\bar{N}}_x = \bar{\bar{N}}_\alpha \, H \tag{3.42}$$

is a shape function matrix related to $\bar{N}_x$ according to Eq. (3.36).

Polynomial terms   Eigenfunctions
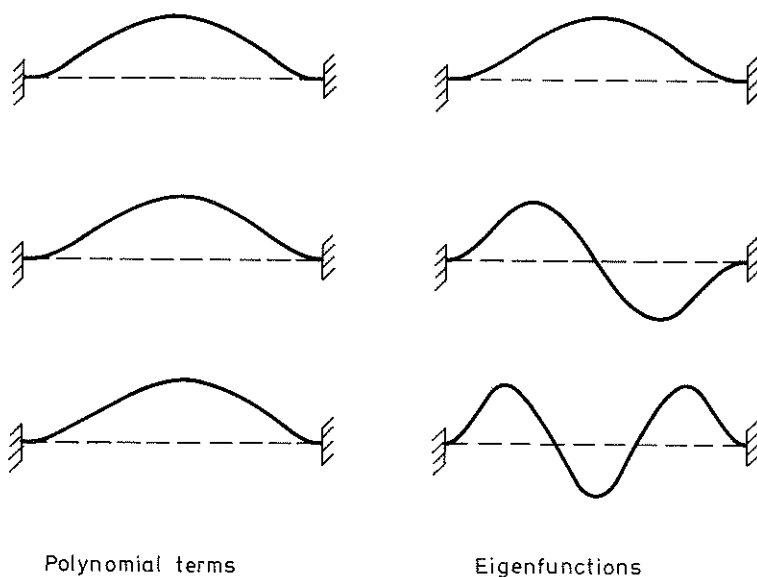
<u>Figure 3.3</u>. First three additional (hierarchical) shape functions in
bending based on polynomial terms and eigenfunctions.

For illustration the first three additional shape functions in
bending (u_y or u_z) are shown in Fig. 3.3. Both sets of additional
functions are represented. It is noticeable from Fig. 3.3 how
similar the polynomial shape functions are. Inclusion of an x^4-term,
the top figure, gives a symmetric shape function whereas the x^5- and
x^6-terms, the figures below, have their maximum only a small
distance to the right of the midpoint (hardly visible). The
eigenfunctions, however, can be clearly distinguished from each
other.

3.3.2 Equations of motion

The finite element discretization requires a choice of a new set of
weighting functions, $\bar{\bar{W}}_x$, as is indicated in Eqs. (3.16) and (3.19).
In analogy with Subsec. 3.2.2 these functions are made to coincide

with the corresponding shape functions, that is $\overline{\mathbf{W}}_x = \overline{\mathbf{N}}_x$. Thus premultiplication of Eq. (3.20) by $\overline{\mathbf{W}}_x^T = \overline{\mathbf{N}}_x^T$ and integration over the element length according to Eq. (3.19), plus partial integration of the first integral give, after some manipulations,

$$
\int_0^L (\mathbf{v}_\epsilon \overline{\overline{\mathbf{N}}}_x)^T \overline{\overline{\mathbf{P}}}_{x\epsilon} dx + \int_0^L (\mathbf{v}_\gamma \overline{\overline{\mathbf{N}}}_x)^T \overline{\overline{\mathbf{P}}}_{x\gamma} dx
$$

$$
+ \int_0^L (\mathbf{v}_p \overline{\overline{\mathbf{N}}}_x)^T \overline{\mathbf{D}}_p \mathbf{v}_p \overline{\overline{\ddot{\mathbf{u}}}}_x dx + \int_0^L (\mathbf{v}_s \overline{\overline{\mathbf{N}}}_x)^T \mathbf{D}_s \mathbf{v}_s \overline{\overline{\ddot{\mathbf{u}}}}_x dx
$$

$$
= \int_0^L (\overline{\mathbf{v}}_{q1} \overline{\overline{\mathbf{N}}}_x)^T \overline{\overline{\mathbf{q}}}_{x1} dx - \int_0^L (\mathbf{v}_{q2} \overline{\overline{\mathbf{N}}}_x)^T \overline{\overline{\mathbf{q}}}_{x2} dx
$$

$$
+ \left[(\overline{\mathbf{v}}_{q1} \overline{\overline{\mathbf{N}}}_x)^T \overline{\overline{\mathbf{P}}}_{x1} \right]_0^L - \left[(\mathbf{v}_{q2} \overline{\overline{\mathbf{N}}}_x)^T \overline{\overline{\mathbf{P}}}_{x2} \right]_0^L \tag{3.43}
$$

in which Eqs. (3.3), (3.11), (3.24), (3.28'), (3.31), (3.32) and (3.36) have been utilized. For a more detailed derivation, see the author [86]. The new quantities in Eq. (3.43) $\overline{\overline{\mathbf{P}}}_{x\epsilon}$, $\overline{\overline{\mathbf{P}}}_{x\gamma}$, $\overline{\overline{\mathbf{P}}}_{x1}$ and $\overline{\overline{\mathbf{P}}}_{x2}$ are given by

$$
\overline{\overline{\mathbf{P}}}_{x\epsilon} = \begin{bmatrix} N \\ M_z \\ -M_y \\ -B \end{bmatrix}, \quad \overline{\overline{\mathbf{P}}}_{x\gamma} = \begin{bmatrix} 0 \\ 0 \\ 0 \\ T_{sv} \end{bmatrix} \tag{3.44a,b}
$$

and

$$\overline{\overline{P}}_{x1} = \begin{bmatrix} N \\ V_y \\ V_z \\ T \end{bmatrix}, \quad \overline{\overline{P}}_{x2} = \begin{bmatrix} 0 \\ M_z \\ M_y \\ B \end{bmatrix} \qquad\qquad (3.45a,b)$$

while $\overline{\overline{D}}_p$ differs from D_p (Eq. (3.32c)) only in that the term $-A$ is replaced by A. The operator $\overline{v}_{q1}$ is an identity matrix. Equation (3.43) constitutes a set of equations of motion for the beam element. The number of equations equals the number of degrees of freedom of the element.

3.3.3 Constitutive equations

The generalized constitutive equations are already implicitly given in Eq. (3.31). If this equation is compared with Eqs. (3.29), (3.34) and (3.44a–b) it can be seen that

$$\overline{\overline{P}}_{x\epsilon} = D_\epsilon \nabla_\epsilon \overline{\overline{u}}_x, \qquad \overline{\overline{P}}_{x\gamma} = D_\gamma \nabla_\gamma \overline{\overline{u}}_x. \qquad\qquad (3.46a,b)$$

3.4   Finite beam element

3.4.1 Local coordinate system

In analogy with Sec. 3.2 the kinematic equations (Subsec. 3.3.1), the equations of motion (3.3.2) and the constitutive equations (3.3.3) are combined. Since these equations are expressed in local quantities their combination yields finite element equations in local coordinates. These finite beam element equations are given in this subsection while global equations are derived in Subsec. 3.4.2.

Thus substitution of Eqs. (3.46a–b) and (3.35) into Eq. (3.43) yields

$$\bar{M}_s^e \ddot{\bar{u}}_s^e + \bar{K}_s^e \bar{u}_s^e = \bar{P}_s^e + \bar{P}_{qs}^e \tag{3.47}$$

where

$$\bar{M}_s^e = \int_0^L (\mathbf{v}_p \bar{\bar{N}}_x)^T \bar{\bar{D}}_p (\mathbf{v}_p \bar{\bar{N}}_x) dx$$

$$+ \int_0^L (\mathbf{v}_s \bar{\bar{N}}_x)^T \bar{\bar{D}}_s (\mathbf{v}_s \bar{\bar{N}}_x) dx, \tag{3.48a}$$

$$\bar{K}_s^e = \int_0^L (\mathbf{v}_\epsilon \bar{\bar{N}}_x)^T D_\epsilon (\mathbf{v}_\epsilon \bar{\bar{N}}_x) dx$$

$$+ \int_0^L (\mathbf{v}_\gamma \bar{\bar{N}}_x)^T D_\gamma (\mathbf{v}_\gamma \bar{\bar{N}}_x) dx, \tag{3.48b}$$

$$\bar{P}_s^e = \left[(\bar{\mathbf{v}}_{q1} \bar{\bar{N}}_x)^T \bar{\bar{P}}_{x1} \right]_0^L - \left[(\mathbf{v}_{q2} \bar{\bar{N}}_x)^T \bar{\bar{P}}_{x2} \right]_0^L \tag{3.48c}$$

and

$$\bar{P}_{qs}^e = \int_0^L (\bar{\mathbf{v}}_{q1} \bar{\bar{N}}_x)^T \bar{\bar{q}}_{x1} dx - \int_0^L (\mathbf{v}_{q2} \bar{\bar{N}}_x)^T \bar{\bar{q}}_{x2} dx \tag{3.48d}$$

are the mass matrix, stiffness matrix, force vector and load vector respectively of the beam element. The bars included in the notations of Eq. (3.47) indicate that the matrices and vectors are related to the local coordinate system shown in Fig. 3.2. The element forces $\bar{P}_{s,1}^e$ to $\bar{P}_{s,14}^e$ can be identified as (cf. Eqs. (3.40a-n))

$$\bar{P}^e_{s,1}(t) \;=\; -N(0,t), \qquad \bar{P}^e_{s,7}(t) \;=\; N(L,t), \qquad (3.49a,b)$$

$$\bar{P}^e_{s,2}(t) \;=\; -V_y(0,t), \qquad \bar{P}^e_{s,8}(t) \;=\; V_y(L,t), \qquad (3.49c,d)$$

$$\bar{P}^e_{s,3}(t) \;=\; -V_z(0,t), \qquad \bar{P}^e_{s,9}(t) \;=\; V_z(L,t), \qquad (3.49e,f)$$

$$\bar{P}^e_{s,4}(t) \;=\; -T(0,t), \qquad \bar{P}^e_{s,10}(t) \;=\; T(L,t), \qquad (3.49g,h)$$

$$\bar{P}^e_{s,5}(t) \;=\; -M_y(0,t), \qquad \bar{P}^e_{s,11}(t) \;=\; M_y(L,t), \qquad (3.49i,j)$$

$$\bar{P}^e_{s,6}(t) \;=\; -M_z(0,t), \qquad \bar{P}^e_{s,12}(t) \;=\; M_z(L,t) \qquad (3.49k,l)$$

and

$$\bar{P}^e_{s,13}(t) \;=\; B(0,t), \qquad \bar{P}^e_{s,14}(t) \;=\; -B(L,t) \qquad (3.49m,n)$$

while the remaining forces, present when the option of additional displacement functions is utilized, are zero. It can be seen that the element or member forces contained in $\bar{P}^e_s$ can be evaluated from Eq. (3.47) once the structural displacements (and accelerations) are known. The stress resultants in $\bar{\bar{P}}_{X\epsilon}$ and $\bar{\bar{P}}_{X\gamma}$ (Eqs. (3.44a–b)) may also be determined from Eqs. (3.46a–b) where $\bar{\bar{u}}_x$ is calculated from Eq. (3.35). However, although additional displacement functions may be included, $\bar{\bar{u}}_x$ is only an approximation. Since the stress resultants depend upon derivatives of $\bar{\bar{u}}_x$ this approximation can be rather rough. Instead, the equations of motion (3.20) are used here to get more reasonable results. This is, in fact, the way V_y, V_z and T_w must be evaluated since these stress resultants are not associated with any strains.

3.4.2 Global coordinate system

The global coordinate system is represented by the reference frame X in Fig. 2.1. In general, the structural elements must refer to such a frame in order to make the finite element assembly procedure

possible. Thus the local finite element equations (3.47) must be transformed into a global coordinate system. This transformation must be performed in two steps: 1) transformation of all degrees of freedom at each beam end to a common point (cf. Fig. 3.2) and 2) transformation of these new DOF into global DOF u_s^e. Thus the total transformation may be represented by the relation

$$\bar{u}_s^e = T u_s^e \tag{3.50}$$

where

$$T = T_1 T_2 \tag{3.51}$$

is the transformation matrix composed of T_1 and T_2 due to the two transformation steps above. If the common point in the first (intermediate) transformation step is denoted (y_I, z_I), the only elements $T_1(i,j)$ which distinguish T_1 from a unit matrix can be found to be

$$T_1(1,5) = T_1(7,11) = -z_I, \tag{3.52a}$$

$$T_1(1,6) = T_1(7,12) = y_I, \tag{3.52b}$$

$$T_1(1,13) = T_1(7,14) = z_I \dot{y}_p - y_I z_p, \tag{3.52c}$$

$$T_1(2,4) = T_1(8,10) = z_I - z_p, \tag{3.52d}$$

$$T_1(3,4) = T_1(9,10) = -(y_I - y_p), \tag{3.52e}$$

$$T_1(5,13) = T_1(11,14) = y_I - y_p \tag{3.52f}$$

and

$$T_1(6,13) = T_1(12,14) = z_I - z_p \qquad (3.52g)$$

provided that the difference in warping displacement between $(0,0)$ and (y_I, z_I) can be neglected. The transformation matrix $\mathbf{T}_2$ may be written in submatrices as

$$\mathbf{T}_2 = \begin{bmatrix} \begin{array}{|c|c|c|c|} \hline \mathbf{n} & 0 & 0 & 0 \\ \hline 0 & \mathbf{n} & 0 & 0 \\ \hline 0 & 0 & \mathbf{n} & 0 \\ \hline 0 & 0 & 0 & \mathbf{n} \\ \hline \end{array} & \mathbf{0} \\ \mathbf{0} & 1 \end{bmatrix} \qquad (3.53)$$

in which $\mathbf{n}$ is the well-known 3×3 direction cosines matrix defining the relations between the local and global coordinate axes.

It can be concluded from Eqs. (3.52a-g) and the unit matrix in Eq. (3.53) that the DOF $\bar{u}^e_{s,13}$ and $\bar{u}^e_{s,14}$ (angles of twist per unit length) as well as the additional DOF are not altered through the entire transformation but remain local quantities. As far as the additional DOF are concerned this is natural since the corresponding shape functions do not affect the beam end displacements (clamped at both ends, see Fig. 3.3). However, the DOF $\bar{u}^e_{s,13}$ and $\bar{u}^e_{s,14}$ do affect these displacements through the warping coordinate Ω as can be seen from Eq. (3.11). Whereas the first 12 DOF of the element correspond to rigid body motions of the beam end laminas the DOF $\bar{u}^e_{s,13}$ and $\bar{u}^e_{s,14}$ describe end deformations. This fact complicates the element assembly procedure. If two beam elements with equal cross section and reference axes are assembled to a continuous beam the DOF $\bar{u}^e_{s,13}$ or $\bar{u}^e_{s,14}$ of the beams at the connection may be considered as global ones and made equal to guarantee warping continuity. If, however, the beam cross sections or reference axes are different or if the

beam elements do not form a continuous beam it is difficult to formulate appropriate boundary conditions. Some kind of judgement must be introduced here (cf. Sec. 6.5).

The global set of finite element equations is now obtained by introducing Eq. (3.50) into Eq. (3.47) and premultiplying by T^T, giving

$$M_s^e \ddot{u}_s^e + K_s^e u_s^e = P_s^e + P_{qs}^e \tag{3.54}$$

where

$$M_s^e = T^T \bar{M}_s^e T, \tag{3.55a}$$

$$K_s^e = T^T \bar{K}_s^e T, \tag{3.55b}$$

$$P_s^e = T^T \bar{P}_s^e \tag{3.55c}$$

and

$$P_{qs}^e = T^T \bar{P}_{qs}^e \tag{3.55d}$$

are the mass matrix, stiffness matrix, force vector and load vector of the beam element, all with reference to a global coordinate system. Note that Eq. (3.54) is in agreement with the general equation (2.22). It should be obvious that the matrices and vectors above can be obtained from Eqs. (2.23a–c) by means of a global shape function matrix N^e defined as

$$N^e = n^T \bar{N}_{yz} \tilde{N}_x T \tag{3.56}$$

in which n is given by Eq. (3.53), $\bar{N}_{yz}$ by Eq. (3.11), $\bar{N}_x$ by Eqs. (3.36)−(3.42) and T by Eqs. (3.51)−(3.53). In Eq. (2.23c) the integral over the beam end surfaces corresponds to P_s^e whereas the remainder of the right−hand side is related to P_{qs}^e.

As mentioned in Subsec. 2.2.4 external viscous damping effects may be introduced on the left−hand side of Eq. (3.54) (Eq. (2.22)) through a term $C_s^e \dot{u}_s^e$. In the present study, however, the damping effects are incorporated by means of modal damping ratios according to Subsec. 2.4.3.

Both the local and global element matrices of the finite element, according to Subsec. 3.4.1 and 3.4.2 respectively, can be obtained through the computer command BEAM3E (see Sec. 5.4).

3.5   Summary

In this chapter a finite beam element is derived. Thus, after a general description in Chapter 2, the analysis of structures sub− jected to moving loads is applied to beam structures (see Chapter 6 and Appendix D). The element derivation is divided into two steps: beam theory formulation (Sec. 3.2) and finite element formulation resulting in the finite beam element (Secs. 3.3 and 3.4). Assumptions introduced in this chapter are listed in Sec. 3.1.

In Sec. 3.2 the beam theory formulation includes warping torsion, in addition to Saint Venant torsion, and coupled vibrations (the reference axes can be chosen arbitrarily). Rotatory inertia according to Rayleigh and warping inertia may also be included. The formulation is not limited to any special type of beam cross section.

In Secs. 3.3 and 3.4 a hierarchical finite beam element, based on the theory in Sec. 3.2, is derived. Two sets of hierarchical or additional functions are available in the present element: polynomial terms and eigenfunctions (antiresonance forms). In Sec. 3.4 the element is represented in local as well as in global coordinates. The pertinent computer commands of the beam element (BEAM3E, BEAM3C, BEAM3R and BEAM3S) are described in Sec. 5.4.

Special features of the present beam element are that

- problems with coupled beam equations can be treated
- the Saint Venant torsion enters the derivation logically
- hierarchical functions simplify and improve the analysis
  (the formulation with eigenfunctions is believed to be novel)
- several options are available which make the element flexible in
  use giving a number of structural models (see Sec. 5.4).

The simplification in using hierarchical beam elements lies in the minimum number of elements to be handled. Further, the improvement in numerical results, as compared with a subdivision into many conventional beam elements with the same number of total degrees of freedom, has been shown by many authors (see e.g. Lees and Thomas [64], Meirovitch and Baruh [75] and the author [86]). In particular additional functions in terms of eigenfunctions, as proposed in this study, yield excellent results and should be preferred in dynamic beam and frame analysis. Three verification examples of the present element are shown in Appendix C. It should also be noted that in a previous version of the element, see the author [86][88], geometric and bending shear effects are also included.

4.   VEHICLE MODELS

4.1   Introduction

In the same way as the structural models in Chapter 3, the vehicle
models in this chapter are related to the basic equations of Chapter
2. In Chapter 3 structural models consisting of finite beam elements
were considered with special emphasis put on the derivation of the
finite element. In this chapter the rigid body element, the damper
element and the spring element derived in Sec. 2.3 (and Appendix B)
are used to describe different kinds of vehicle models. Just as the
structural models should be regarded as finite (beam) element
assemblages the vehicle models should be seen as assemblages of the
three element types. As pointed out in Sec. 2.3, however, a non-
inertial (nominal) vehicle motion gives rise to additional element
damping and stiffness matrices as well as to element noninertia load
vectors. A similar complexity is introduced when the interaction
between the structure and the moving vehicle, inertial or non-
inertial motion, is to be considered (Sec. 2.4).

In the present chapter different vehicle models are described and
their applicability is discussed. Different vehicle models are
compared in most of the examples of Chapter 6 and Appendix D. From a
structural analyst's point of view it is of great importance to
understand the limitations and the applicability of different
vehicle models in modelling the moving load effects on the
structure.

In Sec. 4.2 suspension models are considered. Often, most of the
vehicle mass is suspended by means of springs and dampers in such
models. Note that all the mass should be regarded as suspended for
models of levitated vehicles. The vehicle model used as a starting
point for the numerical examples, as well as a number of special
cases of this model, are shown in this section. The following two
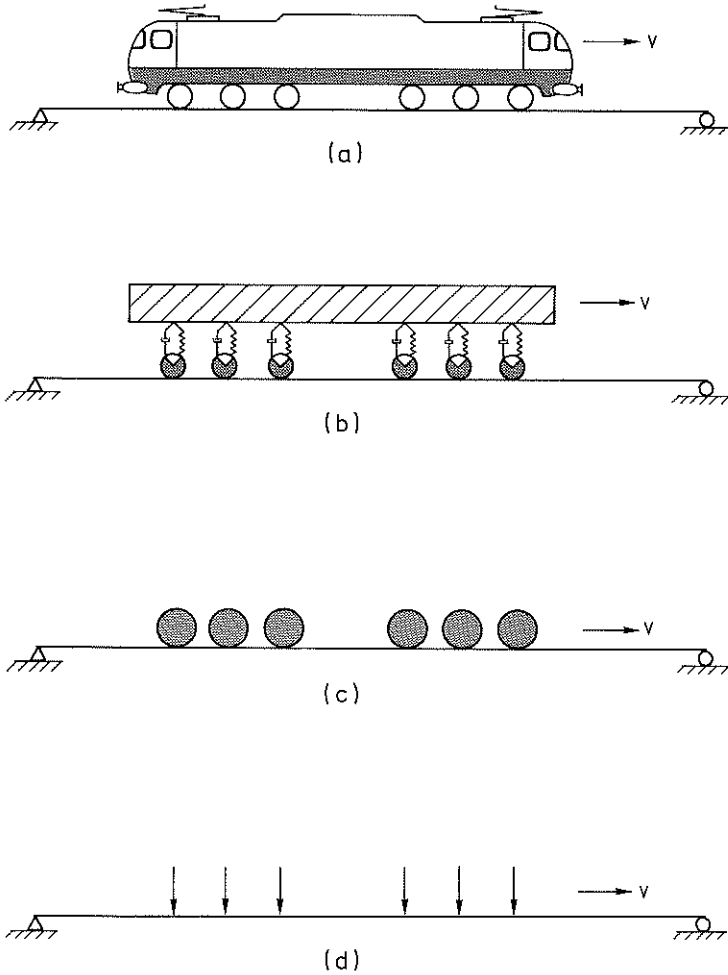
Figure 4.1. Vehicle models (examples).

      (a) Vehicle travelling at speed v.

      (b) Suspension model.

      (c) Moving mass model.

      (d) Moving force model.

sections, Secs. 4.3 and 4.4, describe two other special cases of the suspension models: moving mass models and moving force models, respectively. In the moving mass models no mass is suspended but is directly in contact with the structure. A further simplification is the moving force models in which the contact forces are not dependent on the structural motion but are assumed to be known in advance. In Fig. 4.1 examples of the three different types of vehicle models are given. Studies of structures subjected to moving loads are referred to, with respect to the three different model types, at the end of Secs. 4.2–4.4.

4.2   Suspension models

A wide variety of vehicle models can be applied by using different combinations of rigid body elements, damper elements and spring elements. More advanced elements such as active control elements, see for example Duffek et al. [30], may further widen the spectrum of suspension models. The combination of the above three element types means that element equations according to Eqs. (2.34) and (2.35a–b) are assembled giving

$$\mathbf{M}_v \ddot{\mathbf{u}}_v + \mathbf{C}_v \dot{\mathbf{u}}_v + \mathbf{K}_v \mathbf{u}_v = \mathbf{P}_{qv} - \mathbf{P}_Z. \tag{4.1}$$

This expression thus constitutes the equations of motion for the vehicle (cf. Eqs. (2.46) or (2.49) for the structure). Note that Eq. (4.1) refers to the moving reference frame Y (Z_b) and that the element force vectors $\mathbf{P}_v^e$ in Eqs. (2.34) and (2.35a–b) do not enter Eq. (4.1). The load vector $\mathbf{P}_{qv}$ contains vehicle loads, principally dead weight loads, and contact forces. The contact forces should be seen as reaction forces due to the constrained contact DOF according to Eqs. (2.40) and (2.42a–b). From these equations it is realized that the relative motions of the contact DOF are zero for the limiting case of an infinitely stiff structure and a smooth

structural surface. For such a case the vehicle behaviour can be analysed by means of Eq. (4.1) solely by simply deleting rows and columns corresponding to the contact DOF. For a flexible structure, however, the contact DOF are associated with rheonomic constraints. In Chapter 5 it is described how Eq. (4.1) is generated and how the vehicle elements which are associated with the contact DOF are assembled into structure–vehicle elements.

One suspension model is shown in Fig. 4.1. Three more in–plane suspension models are given in Fig. 4.2. All the models in Fig. 4.2 are made up by the three vehicle elements considered in the present study. The model in Fig. 4.2a consists of a trailer hinged on a tractor. These two parts are suspended on three wheel axles. Note that in addition to these secondary suspensions, primary suspensions are included to model the tyres of the wheels. In this way no mass in the vehicle model is in direct contact with the structure. In general, this is favourable for both the structure and the vehicle.

Figures 4.2b and 4.2c show suspension models for railway vehicles. In Fig. 4.2b bogies are introduced in addition to the vehicle cabin and the wheel axles. Since the railway wheels are very stiff, no wheel flexibilities are introduced here in contrast to Fig. 4.2a. In Fig. 4.2b the suspensions between bogies and wheel axles constitute the primary suspension system. The last model, Fig. 4.2c, is a model of a magnetically levitated vehicle introduced in high–speed transportation, see for instance Kortüm [61], Matsuura [73] and Schiehlen [105]. Also see the author [87]. The gap between the track (structure) and the levitated vehicle is modelled in Fig. 4.2c as distributed springs (fictitious contact). In general the laws relating the "contact" forces to the gap height are very complex and may differ significantly from that of a linear spring. As a rough model, however, the distributed springs may be adequate. A similar introduction of fictitious springs as primary suspensions may be used for models of air cushion levitated vehicles, see Sec. 6.2.
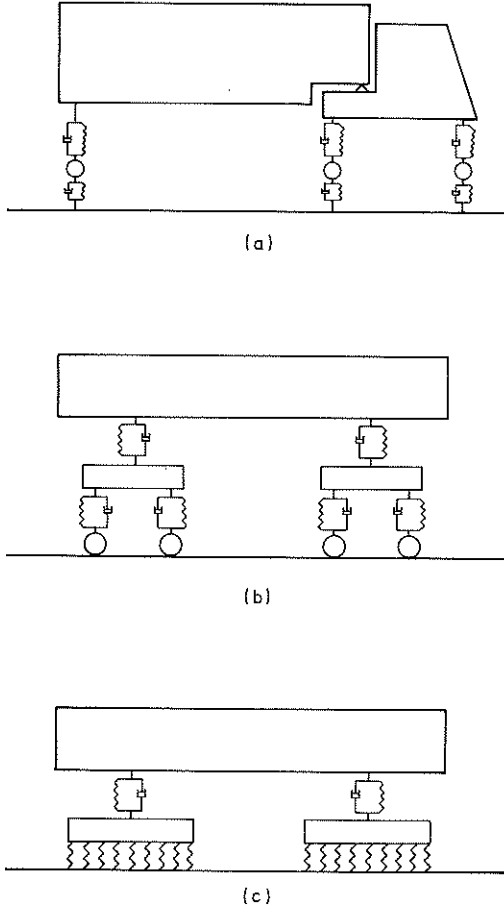
Figure 4.2. Vehicle suspension models (examples).
    (a) Tractor-trailer vehicle (cf. Mulcahy [77]).
    (b) Wheel suspended train (Matsuura [73]).
    (c) Magnet suspended train (Matsuura [73]).

For suspension models in general about 70 to 100 per cent of the total vehicle mass is suspended. The upper limit is applicable for levitated vehicle models as mentioned above. With regard to the suspension stiffness the secondary suspension stiffness is mostly considerably smaller than the primary one. In particular this is relevant for passenger vehicles, see for example Figs. 4.2b and

4-2c. A 10 or even 20 times lower secondary suspension stiffness is not unusual in order to satisfy comfort requirements. Such requirements can be found, for instance, in "Guide for Evaluation of Human Exposure to Whole Body Vibration" [45]. A good guidance for choosing vehicle parameters in numerical simulations can be found in Wormley et al. [14][101], Frýba [38] and Schiehlen [105] among others.

The vehicle model used as a starting point for the numerical examples in Chapter 6 is shown in Fig. 4.3. The two-axle suspension model presented contains both primary and secondary suspensions. For convenience, it has been given double symmetric properties. The figure also shows that the model has 5 masses, 4 linear dampers, 8 linear springs and 30 degrees of freedom. Longitudinal and lateral dampers and springs are, however, not indicated in Fig. 4.3. Such devices are activated when longitudinal and lateral forces or displacements affect the vehicle. Examples of such forces (loads) are: vehicle dead weight components for nonhorizontal structural surface, wind loads, braking contact forces and centripetal contact forces. Effects due to the displacements discussed are mostly related to structural irregularities and flexibilities in the longitudinal-lateral plane. In general, the stiffness k_s in Fig. 4.3 is much less than the longitudinal and lateral stiffnesses. In addition to data of the "new" devices, vehicle height dimensions are needed. Longitudinal (relative) motions of the vehicle are studied to some extent in Sec. 6.3.

If the longitudinal and lateral dampers and springs are not activated, this implies that 19 of the 30 DOF in Fig. 4.3 can be set to zero, cf. Subsec. 2.4.1 (the notation u_1 is short for $u_{v,1}$ etc.):

$$u_1 = u_2 = u_6 = 0, \tag{4.2a}$$

$$u_7 = u_8 = u_{10} = u_{11} = u_{13} = u_{14} = u_{16} = u_{17} = 0 \tag{4.2b}$$
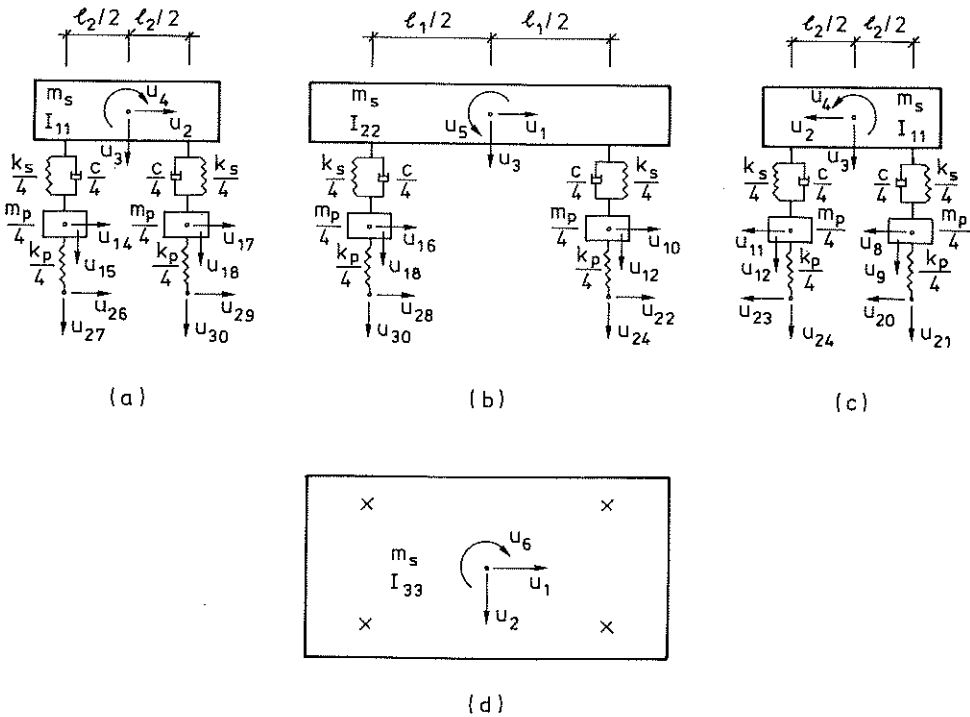
Figure 4.3. Basic vehicle suspension model for the numerical examples, 30 DOF (u_7, u_{13}, u_{19} and u_{25} are not shown). Secondary suspension mass m_s, damping c and stiffness k_s. Principal moments of inertia I_{11}, I_{22} and I_{33}. Primary suspension mass m_p and stiffness k_p. (Longitudinal and lateral dampers and springs are not indicated in the figure).

(a) Rear view.

(b) Side view.

(c) Front view.

(d) Top view.

and

$$u_{19} = u_{20} = u_{22} = u_{23} = u_{25} = u_{26} = u_{28} = u_{29} = 0. \qquad (4.2c)$$

The 3 DOF in Eq. (4.2a) are the longitudinal displacement, the lateral displacement and the yaw rotation respectively of the vehicle cabin. The 8 DOF in Eqs. (4.2b) and (4.2c) are the longitudinal and lateral displacements associated with the primary suspension masses $m_p/4$ and the contact points respectively. The simplification expressed by Eqs. (4.2a–c) significantly decreases the complexity of the vehicle model.

For some studies the remaining 11 vehicle DOF may be further decreased in number. Often it is of interest to study the in-plane (longitudinal–vertical plane) vehicle behaviour. Figure 4.4 shows four different plane vehicle suspension models derived from the model in Fig. 4.3.

Of the remaining 11 DOF five have been removed to give the model in Fig. 4.4a: the roll rotation u_4 is set to zero and the displacements u_9, u_{15}, u_{21} and u_{27} are equal to u_{12}, u_{18}, u_{24} and u_{30} respectively. Thus all external effects must enter the vehicle symmetrically with respect to a longitudinal–vertical plane through the centre of gravity of the vehicle cabin. In other cases the plane model is not valid. The model in Fig. 4.4a is used in Sec. 6.2.

The three models in Figs. 4.4b–d are special cases of the model in Fig. 4.4a. If the primary suspensions are very stiff, e.g. very stiff wheels, u_{24} equals u_{12} and u_{30} equals u_{18} and the 4 DOF model in Fig. 4.4b is obtained. Another simplification may be introduced according to Fig. 4.4c. Here the two–axle model in Fig. 4.4a has been turned into a one–axle model ($u_5 = 0$, $u_{18} = u_{12}$, $u_{30} = u_{24}$). Such a model may be reasonable when the vehicle length is small compared to the bridge or guideway span, see e.g. Frýba [38]. The 2 DOF model in Fig. 4.4d is a combination of the two simplifications above.
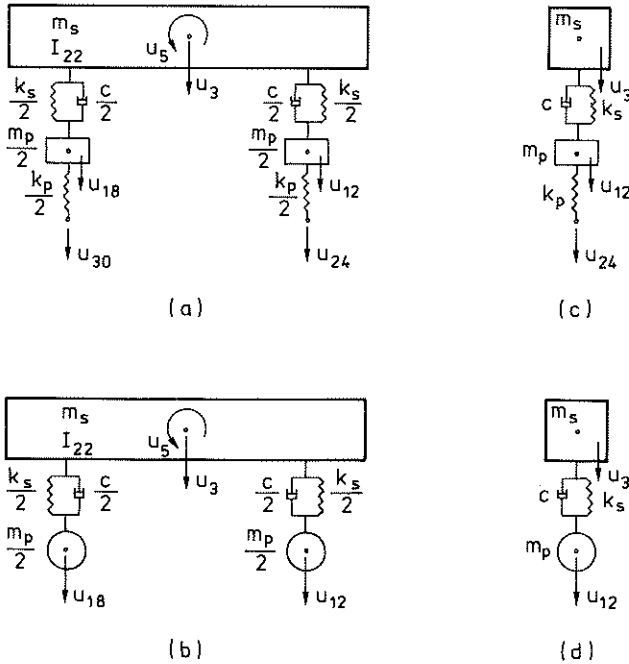
Figure 4.4. Plane vehicle suspension models derived from the model in Fig. 4.3.

(a) Two-axle model, 6 DOF.

(b) Two-axle model, 4 DOF ($k_p = \infty$).

(c) One-axle model, 3 DOF.

(d) One-axle model, 2 DOF ($k_p = \infty$).

As mentioned the contact DOF displacements, see Figs. 4.3 and 4.4, can be set to zero provided that the structure is infinitely stiff and the structural surface is smooth. If the structure is flexible, however, the contact displacements are not constrained to zero but expressed in terms of the structural displacements according to Eq. (2.40). For the suspension models in Figs. 4.3, 4.4a and 4.4c only the primary suspension springs enter the structure–vehicle element derived in Subsec. 2.4.2. For the models in Figs. 4.4b and 4.4d, however, both springs and dampers as well as contact masses are included, cf. Fig. 2.2.

Much more complex models than the one shown in Fig. 4.3 can be treated by means of the concept in Chapter 2 and the computer program in Chapter 5. However, for the problems studied in Chapter 6, the model in Fig. 4.3 and its special cases in Fig. 4.4 are judged to be sufficient. Even simpler models, as described in Secs. 4.3 and 4.4, may also be used.

Some moving load studies in which vehicle suspension models are used are mentioned above. However, a great number of such studies are available. Some of them are: Wormley et al. [14][110], Chung and Genin [16][41], Dailey et al. [27], Filho [35], Traill-Nash et al. [46][55], Hillerborg [47], Joseph and Wilson [52], Popp [93], Smith [111], Tan and Shore [117] and Veletsos and Huang [129]. Further, more recent investigations have been undertaken by: Arpe [3], Dahlberg [23], Garg et al. [39], Genin et al. [42], Hino et al. [48], Machida and Matsuura [67], the author [83][85] and Popp et al. [95]. In most of the above studies the structure is modelled as a beam structure.

4.3   Moving mass models

Since the main interest of the present study is focused on analysis of structures subjected to moving loads the vehicle models shown in Sec. 4.2 may be further simplified. Such models are moving mass models (Sec. 4.3) and moving force models (Sec. 4.4), cf. Fig. 4.1. In fact, one objective of the present study is to investigate how accurately the structural behaviour can be predicted by means of the "noninteractive" moving force model.

As indicated in Fig. 4.1c, for moving mass models all the vehicle mass is in direct contact with the structure. In general, the dynamic structure-vehicle interaction predicted by such models is very strong, see for instance the author [83]. Since most of the

mass of most vehicles is suspended on rather weak secondary
suspension springs the interaction is in general overestimated. A
better model may be obtained by neglecting the inertia effects of
the suspended masses and considering only their dead weights.

Many studies in connection with moving mass models are classical and
referred to by Frýba [38]. Other moving mass studies have been
performed by, for instance: Blejwas et al. [8][9], Dahlberg [23],
Filho [35], Malsch [70], the author [83][85], Schneider et al.
[108], Stanisic [114], Ting et al. [122] and Yoshida et al.
[139][140]. With regard to experimental work the studies by Ayre et
al. [4], Fleming and Romualdi [36], Hillerborg [47], Matsuura [72]
and Wilson [134] should be mentioned.

4.4   Moving force models

The simplest dynamic vehicle models are the moving force models, cf.
Fig. 4.1d. In most moving force models the magnitudes of the contact
forces are constant in time. Thus the structure is affected
dynamically through the moving character of the vehicle only. A
common feature of all moving force models is that the forces are
known in advance. Thus structure–vehicle interaction cannot be
considered. On the other hand the moving force models are very
simple to use and yield reasonable structural results in some cases,
cf. Chapter 6.

The magnitudes of the moving forces to be used in a structural
analysis may be calculated from Eq. (4.1) by setting $\dot{u}_v = \ddot{u}_v = 0$ and
by constraining all contact displacements to zero. The reaction
forces obtained by solving the system of equations are thus the
forces sought. For inertial vehicle motion and no external loads the
moving forces originate from the dead weight of the vehicle only.

As for the moving mass models many classical studies concerning moving force models are referred to by Frýba [38]. Analysis of structures subjected to moving forces has also been carried out by, for instance: Wormley et al. [14][110], Das [28], Filho [34][35], Fleming and Romualdi [36], Khouday and Proulx [54], Rabizadeh et al. [97][98], Srinivasan and Munaswamy [113], Warburton [133], Wilson et al. [135][136] and Yoshida et al. [139][140]. More recent investigations are undertaken by Aida [1], Dahlberg [23], Karaolides and Kounadis [53], Machida and Matsuura [67] and the author [83][85].

5.   NUMERICAL PROCEDURE

5.1   Introduction

In Chapter 2 the basic equations for the structure, the vehicle and their interaction were derived in general terms. By means of these equations, the equations of motion of the structure-vehicle system can be formulated. The procedure for solving these equations of motion is described in this chapter. The computer program and computer commands used for creating and solving these equations are also described. The numerical procedure described aims at a quite general analysis of structures subjected to moving loads (cf. the list of assumptions at the end of Sec. 2.1). When the numerical procedure is developed numerical examples of the moving load problem can be studied, see Chapter 6 and Appendix D.

In Sec. 5.2 the solution algorithm for solving the equations of motion is described. The time discretization is performed in analogy with the spatial discretization through choices of displacement field and weighting function. A single step procedure with a cubic displacement field is chosen. Depending on the choice of weighting function different algorithms may then be obtained. In this study a weighting function giving an unconditionally stable algorithm, at least for the special case of time-independent global matrices M and K and no damping, is chosen.

The last two sections of this chapter, Secs. 5.3 and 5.4, deal with the computer implementation of the problem described up to Sec. 5.2. A computer program CAMFEM (Computer Aided Modelling based on the Finite Element Method), see Dahlblom et al. [24][25], is used as a base for the implementation. This program is based on a command language. In addition to the existing problem-independent commands, about 25 commands are implemented for the problem analysed in this

study. The build-up of the computer program created in this way is described in Sec. 5.3 and the most important problem-dependent commands are described in Sec. 5.4.

5.2   Solution algorithm

The equations of motion to be solved may be seen as an assemblage of the global structural and the global vehicle equations according to Eq. (2.46), or (2.49), and Eq. (4.1) respectively. As mentioned in Sec. 2.4, however, the rheonomic constraints associated with the vehicle contact DOF and the structure-vehicle interaction are best handled on the element level. This means that it is most appropriate to consider the global system as an assemblage of structural elements, vehicle elements and structure-vehicle elements with the vehicle contact DOF already eliminated (cf. Fig. 2.2). This assemblage thus corresponds to Eqs. (2.22), (2.34), (2.35a-b) and (2.44) with the structure-vehicle interaction represented by the time-dependent matrices in Eqs. (2.45b-d). If the structure is described in terms of modal coordinates, which is the case in the following, the structure-vehicle element equations are given by Eq. (2.52). Further, the modal contributions from the structural elements are analogous with the structural part of the modal structure-vehicle element, see Eqs. (2.53a-f).

Assembly of the three types of elements (structural, vehicle and structure-vehicle elements) gives the equations of motion of the structure-vehicle system as

$$\mathbf{M}(t)\ddot{\mathbf{u}}(t) + \mathbf{C}(t)\dot{\mathbf{u}}(t) + \mathbf{K}(t)\mathbf{u}(t) = \mathbf{P}(t) \tag{5.1}$$

in which the time dependence is expressed explicitly for clarity. The vector $\mathbf{u}(t)$ in Eq. (5.1) only contains unconstrained displacements. Thus both scleronomic and rheonomic constraints have been

considered in Eq. (5.1). The fact that the DOF associated with rheonomic constraints (the vehicle contact DOF) have been eliminated can be seen from the time-dependent mass matrix which is otherwise constant. (The time dependence of C and K may also be due to noninertial vehicle motion).

The equations of motion according to Eq. (5.1) constitute a set of linear ordinary second-order differential equations with nonconstant (time-dependent) coefficients. Also note that symmetry of the global matrices cannot be utilized in the solution of the equations since C and K are, in general, unsymmetric.

In order to solve Eq. (5.1) a time discretization is necessary. This discretization can be seen as a subdivision of the time domain into points of time with each point associated with one or more sets of time DOF (displacements, velocities etc.). The time discretization can be performed conveniently in analogy with the spatial discretization of the structure, see Subsec. 2.2.4 and Zienkiewicz [141]. If the time weighting functions $W_p^t(t)$ in Eq. (2.18) are utilized for the vehicle DOF as well, it should be obvious from Eqs. (2.16) and (5.1) that the time weighted residuals of the equations of motion can be written as

$$\int_0^{\bar{t}} W_p^t(M\ddot{u} + C\dot{u} + Ku)dt = \int_0^{\bar{t}} W_p^t \ P \ dt. \tag{5.2}$$

In Eq. (5.2) the time weighting applies to the whole time domain of interest in the problem studied. However, it is often sufficient and convenient to limit the weighting procedure to a single time step, that is to the time domain between two adjacent points of time. In this way a step-by-step procedure can be used to solve the equations of motion. For a single time step Eq. (5.2) may be written as

$$\int_0^1 W_p^t (M\ddot{u} + C\dot{u} + Ku)d\xi = \int_0^1 W_p^t \ P \ d\xi \qquad (5.3)$$

where

$$\xi(t) = \frac{t-t_0}{\Delta t} \quad (0 \le \xi \le 1) \qquad (5.4)$$

is a nondimensional time parameter defined for $t_0 \le t \le t_1$ where $t_1 = t_0 + \Delta t$. It should be noted that in contrast to multistep algorithms, such as the central difference method and the Houbolt method (see Bathe [5]), the time step Δt may easily be altered through the solution process in single step algorithms. For such algorithms each time step can be considered as a finite element in time.

As for the spatial finite element discretization in Subsec. 2.2.4, a displacement field is chosen here so as to make a solution to Eq. (5.3) possible. A cubic displacement field is chosen according to (cf. Eq. (3.37))

$$u(t) = \beta_1 + \beta_2\xi + \beta_3\xi^2 + \beta_4\xi^3 \qquad (5.5a)$$

where β_i (i = 1,2,3,4) are time-independent displacement vectors. Thus the velocity and acceleration vectors become

$$\dot{u}(t) = (\beta_2 + 2\beta_3\xi + 3\beta_4\xi^2)/\Delta t \qquad (5.5b)$$

and

$$\ddot{u}(t) = (2\beta_3 + 6\beta_4\xi)/\Delta t^2 \qquad (5.5c)$$

in which the relation $d\xi/dt = 1/\Delta t$ from Eq. (5.4) has been used. The vectors $\boldsymbol{\beta}_i$ can now be replaced by vectors ${}^{0}\mathbf{u}$, ${}^{0}\dot{\mathbf{u}}$, ${}^{0}\ddot{\mathbf{u}}$ and ${}^{1}\mathbf{u}$ defined by (cf. Eqs. (3.40a-n))

$$
{}^{0}\mathbf{u} = \mathbf{u}(t_0) = \boldsymbol{\beta}_1 , \tag{5.6a}
$$

$$
{}^{0}\dot{\mathbf{u}} = \dot{\mathbf{u}}(t_0) = \boldsymbol{\beta}_2/\Delta t , \tag{5.6b}
$$

$$
{}^{0}\ddot{\mathbf{u}} = \ddot{\mathbf{u}}(t_0) = 2\boldsymbol{\beta}_3/\Delta t^2 \tag{5.6c}
$$

and

$$
{}^{1}\mathbf{u} = \mathbf{u}(t_1) = \boldsymbol{\beta}_1 + \boldsymbol{\beta}_2 + \boldsymbol{\beta}_3 + \boldsymbol{\beta}_4 \tag{5.6d}
$$

where Eqs. (5.5a-c) are utilized. Evaluating $\boldsymbol{\beta}_i$ from Eqs. (5.6a-d) in terms of the vectors ${}^{0}\mathbf{u}$, ${}^{0}\dot{\mathbf{u}}$, ${}^{0}\ddot{\mathbf{u}}$ and ${}^{1}\mathbf{u}$, and introducing the expressions for $\boldsymbol{\beta}_i$ into Eqs. (5.5a-c) yields

$$
\mathbf{u}(t) = {}^{0}N_u\,{}^{0}\mathbf{u} + {}^{0}N_{\dot{u}}\,{}^{0}\dot{\mathbf{u}} + {}^{0}N_{\ddot{u}}\,{}^{0}\ddot{\mathbf{u}} + {}^{1}N_u\,{}^{1}\mathbf{u} , \tag{5.7a}
$$

$$
\dot{\mathbf{u}}(t) = {}^{0}\dot{N}_u\,{}^{0}\mathbf{u} + {}^{0}\dot{N}_{\dot{u}}\,{}^{0}\dot{\mathbf{u}} + {}^{0}\dot{N}_{\ddot{u}}\,{}^{0}\ddot{\mathbf{u}} + {}^{1}\dot{N}_u\,{}^{1}\mathbf{u} \tag{5.7b}
$$

and

$$
\ddot{\mathbf{u}}(t) = {}^{0}\ddot{N}_u\,{}^{0}\mathbf{u} + {}^{0}\ddot{N}_{\dot{u}}\,{}^{0}\dot{\mathbf{u}} + {}^{0}\ddot{N}_{\ddot{u}}\,{}^{0}\ddot{\mathbf{u}} + {}^{1}\ddot{N}_u\,{}^{1}\mathbf{u} \tag{5.7c}
$$

in which the shape functions and their time derivatives are given by the relations

$$\left. \begin{aligned} {}^0N_u &= 1 - \xi^3 \\[6pt] {}^0N_{\dot{u}} &= (1 - \xi^2)\xi\Delta t \\[6pt] {}^0N_{\ddot{u}} &= \tfrac{1}{2}(1 - \xi)\xi^2\Delta t^2 \\[6pt] {}^1N_u &= \xi^3 \end{aligned} \right\}, \tag{5.8a}$$

$$\left. \begin{aligned} {}^0\dot{N}_u &= -3\xi^2/\Delta t \\[6pt] {}^0\dot{N}_{\dot{u}} &= 1 - 3\xi^2 \\[6pt] {}^0\dot{N}_{\ddot{u}} &= (1 - \tfrac{3}{2}\xi)\xi\Delta t \\[6pt] {}^1\dot{N}_u &= 3\xi^2/\Delta t \end{aligned} \right\} \tag{5.8b}$$

and

$$\left. \begin{aligned} {}^0\ddot{N}_u &= -6\xi/\Delta t^2 \\[6pt] {}^0\ddot{N}_{\dot{u}} &= -6\xi/\Delta t \\[6pt] {}^0\ddot{N}_{\ddot{u}} &= 1 - 3\xi \\[6pt] {}^1\ddot{N}_u &= 6\xi/\Delta t^2 \end{aligned} \right\}. \tag{5.8c}$$

The shape functions of Eq. (5.8a) are illustrated in Fig. 5.1 in connection with the choice of weighting function W_p^t ($p = 1$). Note that only one weighting function is necessary since for the initial value problem at hand only the vector ${}^1u$ is unknown. (The vectors ${}^0u$, ${}^0\dot{u}$ and ${}^0\ddot{u}$ are either initial vectors ($t=0$) or vectors determined in the previous time step).

Before paying attention to the choice of weighting function the time dependence of $\mathbf{M}$, $\mathbf{C}$, $\mathbf{K}$ and $\mathbf{P}$ in Eq. (5.3) must, however, be considered. It is often reasonable to assume that the load vector $\mathbf{P}$ varies linearly within the time step, see for instance Zienkiewicz et al. [143]. Here such a linear distribution is assumed for $\mathbf{P}$ as well as for the global matrices $\mathbf{M}$, $\mathbf{C}$ and $\mathbf{K}$. In analogy with the procedure followed above for $\mathbf{u}$, $\dot{\mathbf{u}}$ and $\ddot{\mathbf{u}}$ one obtains

$$\mathbf{M}(t) = {}^0\!N\,{}^0\!\mathbf{M} + {}^1\!N\,{}^1\!\mathbf{M}, \qquad (5.9a)$$

$$\mathbf{C}(t) = {}^0\!N\,{}^0\!\mathbf{C} + {}^1\!N\,{}^1\!\mathbf{C}, \qquad (5.9b)$$

$$\mathbf{K}(t) = {}^0\!N\,{}^0\!\mathbf{K} + {}^1\!N\,{}^1\!\mathbf{K} \qquad (5.9c)$$

and

$$\mathbf{P}(t) = {}^0\!N\,{}^0\!\mathbf{P} + {}^1\!N\,{}^1\!\mathbf{P} \qquad (5.9d)$$

with

$$\left.\begin{array}{l} {}^0\!N = 1 - \xi \\[2mm] {}^1\!N = \xi \end{array}\right\}. \qquad (5.10)$$

The left superscripts 0 and 1 in Eqs. (5.9a–d) and (5.10) refer, as before, to the points of time t_0 ($\xi = 0$) and t_1 ($\xi = 1$) respectively.

The parameters $\bar{\alpha}$, α, β, γ and δ are then introduced as

$$\bar{\alpha} = \int_0^1 W_p^t \xi^4 d\xi, \tag{5.11a}$$

$$\alpha = \int_0^1 W_p^t \xi^3 d\xi, \tag{5.11b}$$

$$\beta = \int_0^1 W_p^t \xi^2 d\xi, \tag{5.11c}$$

$$\gamma = \int_0^1 W_p^t \xi d\xi \tag{5.11d}$$

and

$$\delta = \int_0^1 W_p^t d\xi. \tag{5.11e}$$

Introduction of Eqs. (5.7) to (5.10) into Eq. (5.3) then gives

$$\hat{K} \, ^1u = \hat{P} \tag{5.12}$$

with an effective stiffness matrix

$$\hat{K} = 6\gamma \, \frac{1}{\Delta t^2} \, ^0M + 6\beta \, \frac{1}{\Delta t^2} \, \Delta M + 3\beta \, \frac{1}{\Delta t} \, ^0C + 3\alpha \, \frac{1}{\Delta t} \, \Delta C$$

$$+ \, \alpha \, ^0K + \bar{\alpha} \, \Delta K \tag{5.13a}$$

and an effective load vector

$$\hat{P} = \delta \ {}^{0}P + \gamma \ \Delta P$$

$$+ \left[6\gamma \ \frac{1}{\Delta t^{2}} \ {}^{0}M + 6\beta \ \frac{1}{\Delta t^{2}} \ \Delta M + 3\beta \ \frac{1}{\Delta t} \ {}^{0}C + 3\alpha \ \frac{1}{\Delta t} \ \Delta C \right.$$

$$\left. + \ (\alpha - \delta) {}^{0}K + (\bar{\alpha} - \gamma)\Delta K \right] {}^{0}u$$

$$+ \left[6\gamma \ \frac{1}{\Delta t} \ {}^{0}M + 6\beta \ \frac{1}{\Delta t} \ \Delta M + (3\beta - \delta) \ {}^{0}C + (3\alpha - \gamma)\Delta C \right.$$

$$\left. + \ (\alpha - \gamma)\Delta t \ {}^{0}K + (\bar{\alpha} - \beta)\Delta t \ \Delta K \right] {}^{0}\dot{u}$$

$$+ \left[(3\gamma - \delta) \ {}^{0}M + (3\beta - \gamma)\Delta M + (\frac{3}{2}\beta - \gamma)\Delta t \ {}^{0}C + (\frac{3}{2}\alpha - \beta)\Delta t \ \Delta C \right.$$

$$\left. + \ (\frac{1}{2}\alpha - \frac{1}{2}\beta)\Delta t^{2} \ {}^{0}K + (\frac{1}{2}\bar{\alpha} - \frac{1}{2}\alpha)\Delta t^{2} \ \Delta K \right] {}^{0}\ddot{u}. \qquad (5.13b)$$

The increments ΔM, ΔC, ΔK and ΔP in Eqs. (5.13a–b) are defined as $\Delta M = {}^{1}M - {}^{0}M$ etc.. Thus provided that ${}^{0}M$, ${}^{1}M$, ${}^{0}C$, ${}^{1}C$, ${}^{0}K$, ${}^{1}K$, ${}^{0}P$, ${}^{1}P$, ${}^{0}u$, ${}^{0}\dot{u}$ and ${}^{0}\ddot{u}$ are known, the displacement vector ${}^{1}u$ can be determined from Eq. (5.12) for a given choice of parameters $\bar{\alpha}$, α, β, γ and δ. The velocity vector ${}^{1}\dot{u}$ and the acceleration vector ${}^{1}\ddot{u}$, which serve as input quantities for the following time step, can then be evaluated from Eqs. (5.7b–c) and (5.8b–c) as

$$^{1}\dot{u} = \dot{u}(t_{1}) = -3 \ \frac{1}{\Delta t} \ {}^{0}u - 2 {}^{0}\dot{u} - \frac{1}{2} \ \Delta t \ {}^{0}\ddot{u} + 3 \ \frac{1}{\Delta t} \ {}^{1}u \qquad (5.14a)$$

and

$$^{1}\ddot{u} = \ddot{u}(t_{1}) = -6 \ \frac{1}{\Delta t^{2}} \ {}^{0}u - 6 \ \frac{1}{\Delta t} \ {}^{0}\dot{u} - 2 {}^{0}\ddot{u} + 6 \ \frac{1}{\Delta t^{2}} \ {}^{1}u. \qquad (5.14b)$$

The rest of this section is devoted to the choice of parameters $\bar{\alpha}$, α, β, γ and δ and thus to the choice of weighting function W_p^t (p = 1), see Eqs. (5.11a-e). To simplify the choice of W_1^t attention is called to the special and well-known case of time-independent global matrices M, C and K. For this case the effective quantities $\hat{K}$ and $\hat{P}$ in Eqs. (5.13a-b) are given by

$$\hat{K} = 6\gamma \frac{1}{\Delta t^2} M + 3\beta \frac{1}{\Delta t} C + \alpha K \tag{5.15a}$$

and

$$\hat{P} = \delta\ ^0P + \gamma\ \Delta P$$

$$+ \left[6\gamma \frac{1}{\Delta t^2} M + 3\beta \frac{1}{\Delta t} C + (\alpha-\delta)K\right]^0u$$

$$+ \left[6\gamma \frac{1}{\Delta t} M + (3\beta-\delta)C + (\alpha-\gamma)\Delta t\ K\right]^0\dot{u}$$

$$+ \left[(3\gamma-\delta)M + (\tfrac{3}{2}\beta-\gamma)\Delta t\ C + (\tfrac{1}{2}\alpha - \tfrac{1}{2}\beta)\Delta t^2\ K\right]^0\ddot{u} \tag{5.15b}$$

where M, C and K are now constant matrices. Note that the weighting parameter $\bar{\alpha}$, defined in Eq. (5.11a), does not appear in Eqs. (5.15a-b). Of the remaining four parameters α, β, γ and δ the parameter δ can be seen as a normalizing factor (provided $\delta \neq 0$) giving three independent parameters α/δ, β/δ and γ/δ. These normalized parameters can be identified in Eqs. (5.15a-b) if $\hat{K}$ and $\hat{P}$ are divided by δ.

A number of different weighting functions W_1^t are illustrated in Fig. 5.1 and pertinent values of α, β, γ and δ are given, cf. Zienkiewicz [141].
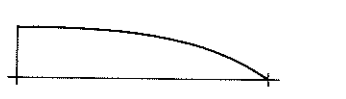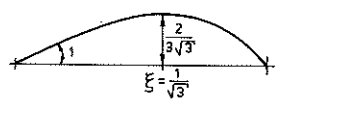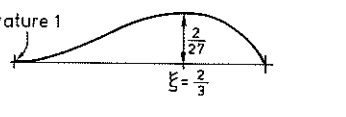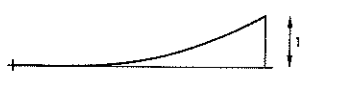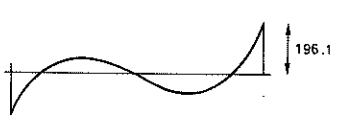
W_1^t	α	β	γ	δ	
	1	1	1	1	Newmark linear acceleration
	1	1	1	0	Newmark linear acceleration (incremental)
	$\frac{3}{28}$	$\frac{1}{6}$	$\frac{3}{10}$	$\frac{3}{4}$	Galerkin ${}^0N_u$
	$\frac{2}{35}$	$\frac{1}{12}$	$\frac{2}{15}$	$\frac{1}{4}$	Galerkin ${}^0\dot{N}_u/\Delta t$
	$\frac{1}{84}$	$\frac{1}{60}$	$\frac{1}{40}$	$\frac{1}{24}$	Galerkin ${}^0\ddot{N}_u/\Delta t^2$
	$\frac{1}{7}$	$\frac{1}{6}$	$\frac{1}{5}$	$\frac{1}{4}$	Galerkin ${}^1N_u$
	6	$\frac{11}{3}$	2	1	Houbolt (corresponding)
	4	$\frac{8}{3}$	2	1	Zienkiewicz (corresponding)

<u>Figure 5.1</u>. Weighting functions for single step algorithms. The parameters α, β, γ and δ are related to W_1^t according to Eqs. (5.11b–e) (p = 1).

Choosing the top weighting function in Fig. 5.1 gives an algorithm which coincides with the Newmark linear acceleration method, see Bathe [5] and Newmark [80]. This circumstance should be evident since a linear acceleration field is assumed through Eq. (5.5c) and in the Newmark method the weight is concentrated at $\xi = 1$, cf. Fig. 5.1. The coincidence can also be verified by inserting $\alpha = \beta = \gamma = \delta = 1$ in Eqs. (5.15a–b) and comparing with the Newmark linear acceleration method ($\beta_N = 1/6$, $\gamma_N = 1/2$). As is well-known this method also coincides with the Wilson θ method with $\theta = 1$. The next weighting function in Fig. 5.1 gives an incremental form of the Newmark linear acceleration method, cf. the author [85]. Note that $\delta = 0$ for this solution algorithm.

The following four functions in Fig. 5.1 are the Galerkin functions, i.e. the shape functions introduced in the displacement field formulation, see Eqs. (5.7a) and (5.8a). The last two weighting functions in Fig. 5.1 are also cubic polynomials. These functions are normalized by setting $\delta = 1$. According to Wood [138] and Zienkiewicz et al. [143], $\alpha/\delta = 6$, $\beta/\delta = 11/3$ and $\gamma/\delta = 2$ gives an algorithm which corresponds to the multistep Houbolt method; see Bathe [5], Houbolt [49] and Zienkiewicz [141]. A somewhat different algorithm is obtained for $\alpha/\delta = 4$, $\beta/\delta = 8/3$ and $\gamma/\delta = 2$ (see Fig. 5.1). This algorithm corresponds to a multistep method proposed by Zienkiewicz [141] ($\alpha_Z = 22$, $\beta_Z = 8$, $\gamma_Z = 3$).

An important aspect in the choice of weighting function is the stability of the resulting algorithm. For a cubic displacement field Wood [137][138] has investigated the stability of different algorithms. In these studies no damping and constant mass and stiffness matrices are presupposed. Although both damping and time-dependent matrices appear in the present study the studies by Wood serve as a guide for the choice of weighting function.

According to Wood [137][138], the algorithms resulting from the first six weighting functions are only conditionally stable. The last two functions, however, give unconditionally stable algorithms. Thus a weighting function according to Galerkin does not seem to be the best choice here, cf. the spatial discretization in Subsec. 2.2.4. Instead the last weighting function in Fig. 5.1 is chosen here due to a very satisfactory performance as shown by Zienkiewicz [141]. Although a good performance is not guaranteed for the present case of time-dependent matrices this choice should be reasonable provided an appropriate time step Δt is chosen.

In conclusion, a single step solution algorithm based on a cubic displacement field and a weighting function giving $\alpha = 4$, $\beta = 8/3$, $\gamma = 2$ and $\delta = 1$ (see Fig. 5.1) is chosen in this section. It can be shown that the present weighting function gives $\bar{\alpha} \approx 5.13$, see Eq. (5.11a). Thus Eq. (5.12), Eqs. (5.13a-b) with the five parameter values just mentioned and Eqs. (5.14a-b) represent the solution algorithm to be used. As a final remark, it should be mentioned that algorithms based on other than cubic displacement fields are described by Zienkiewicz et al. [143].

5.3   Computer program

Most of existing computer programs for the analysis of structures subjected to moving loads are only quasistatic. This means that static vehicle loads are placed at a number of positions on the structure to give influence lines for different structural quantities. In order to consider the dynamic effects of the moving vehicle these quantities are then multiplied by dynamic magnification factors given in different codes (cf. Subsec. 6.2.4). On the other hand, most vehicle system dynamics programs cannot be used in case of flexible structures, see Kortüm and Schiehlen [62].

The possibility that just a slight modification can be made to some existing computer program for the present study is therefore out of the question. In this study the computer program CAMFEM (Computer Aided Modelling based on the Finite Element Method), see Dahlblom et al. [24][25], is used as a base for the computer implementation. As mentioned in Sec. 5.1 this base consists of a number of problem–independent commands. In this way development work for matrix manipulations, assembly, eigenvalue solution and other basic operations can be saved. The program CAMFEM has served as a basic computer tool in many research works, see e.g. Dahlblom [26], the author [85][88], Peterson [91] and Sandberg [104]. The build–up of the present computer program is described in this section, and some of the problem–dependent commands developed are decribed in Sec. 5.4.

The command language of CAMFEM means that the computer program can be seen as a series of commands. In turn, each command calls a driver subroutine with one or more underlying executive subroutines. CAMFEM also offers the possibility of defining a sequence of commands as a macro command. The present computer program is activated by the macro command EMACRO PROG (execute macro PROG). The macro PROG contains the sequence of commands as shown in Fig. 5.2.

```
MATRIX PROG              5 ROWS
===============================

   1 EMACRO INIT
   2 EMACRO STRUCT
   3 EMACRO VEHICO
   4 EMACRO TIMEST NTSTEP
   5 EMACRO OUTPUT
```

Figure 5.2. Macro PROG.

As can be seen from Fig. 5.2 a macro can itself contain macro commands. In this way many levels of commands may be used. The text matrix (vector) PROG in Fig. 5.2 defines the five main steps of the computer program as described below.

The macro INIT creates some additional input data based on input data matrices restored from an external file. Several numerical matrices and vectors to be used in the analysis are also initialized in this macro.

The macro STRUCT generates the element matrices of the structural elements through the command BEAM3E (cf. Chapter 3 and Sec. 5.4). Further, the element matrices are assembled to form the global matrices of the structure. This macro also contains the eigenvalue solution for the modal coordinate formulation of the structure (Subsec. 2.4.3).

The global vehicle matrices and vectors of Eq. (4.1) are formulated and evaluated at time $t = 0$ in the macro VEHICO. The time $t = 0$ is defined as the time point when the vehicle is just about to enter the structure. As for the structure the global matrices and vectors are assemblages of the element matrices and vectors. The commands for generating the vehicle element matrices and vectors consist of VEK3E (spring element), VEC3EI and VEC3EN (damper element) and VEM3EI and VEM3EN (rigid body element); see Sec. 5.4. It should be noted that constant noninertial vehicle motion, i.e. steady state curving or steady state acceleration, or inertial vehicle motion is assumed when the vehicle enters the structure. Since the entrance to the structure is assumed rigid and smooth the initial quantities $\dot{u}_v(0)$ and $\ddot{u}_v(0)$, see Eq. (4.1), can be set to zero vectors.

The time stepping procedure of the structure–vehicle interaction analysis is executed through the macro TIMEST. As may be concluded from Fig. 5.2, this macro is executed not only once but NTSTEP times (NTSTEP = number of time steps). The use of macro commands is especially effective for such repetitive operations. For nonconstant noninertial vehicle motion the matrices C_v and K_v as well as the vectors P_{qv} and P_Z in Eq. (4.1) are different at the beginning and end of each time step. This means that the quantities ΔC, ΔK and ΔP in Eqs. (5.13a–b) do not become zero matrices and a zero vector respectively. After this updating if necessary, the macro TIMEST handles the structure–vehicle interaction. This phenomenon makes the uncoupled structure and vehicle equations at $t = 0$ coupled and gives further contributions to ΔC, ΔK and ΔP (plus ΔM) even in the case of inertial vehicle motion. The interaction is effectively treated by means of structure–vehicle finite elements as derived in Subsec. 2.4.2. Evaluation of the structural shape function values of N_c^e, see Eqs. (2.37) and (2.41a), is performed through the command BEAM3C. Further, the interaction parts of the matrices in Eqs. (2.45b–d) are handled by the command SVE3EM and the vectors in Eqs. (2.45f–g) (no irregularities) by SVE3EV, see Sec. 5.4. After transformation of the interaction matrices and vectors into modal coordinates (Eqs. (2.53b–d, f–g)) the macro TIMEST solves Eq. (5.12), updates velocity and acceleration vectors according to Eqs. (5.14a–b) and determines contact forces. Finally, beam displacements and member forces are evaluated through the commands BEAM3R and BEAM3S.

The macro OUTPUT, the final macro in Fig. 5.2, prints out the quantities of interest saved in macro TIMEST. For instance vehicle and beam displacements, contact forces and beam member forces are saved. Both the entire time histories and the maxima of the quantities are in general saved and printed out.

5.4 Computer commands

As pointed out in Secs. 5.1 and 5.3 problem-dependent computer commands have been developed in addition to the existing problem-independent ones of the original version of CAMFEM. Some of the about 25 commands developed have been mentioned in the previous text, particularly in Sec. 5.3. These commands are demonstrated and described in this section.

The commands associated with the structural elements (here three-dimensional beam elements) are

    BEAM3E EPS EKS [ECS][EMS][ERS][J]
    BEAM3C EPS ENS PDOFS ISE XC AVC XYZC NC NCT NCTT J
    BEAM3R EPS ISEV XYZC CF SXY
    BEAM3S EPS ENS US [UST][USTT][NS][J[OUT]]

with bracketed arguments being optional. In all the above four beam commands the argument EPS is the element property matrix with each row describing the properties of a single structural (beam) element. The input data of EPS are divided into six groups: general, geometric, cross sectional and material, damping, displacement function and element load information group. Options such as warping torsion, rotatory/warping inertia and additional displacement functions may be introduced by giving appropriate data to the general information group. For a more extensive description of EPS see the author [86].

In the present study the command BEAM3E, included in the macro STRUCT (see Fig. 5.2), computes element stiffness matrix EKS and element mass matrix EMS for the beam element defined by row number J

of the matrix EPS. These matrices are the matrices K_s^e and M_s^e respectively in Eq. (3.54). The optional damping matrix ECS and load vector ERS in BEAM3E above are not used since the damping is defined through modal damping ratios ξ_i (see Subsec. 2.4.3) and the vehicle loads on the structure (contact forces) are not in general known in advance. A loop over all beam elements $(J = 1,2...)$ gives all the element matrices needed.

BEAM3C, the next beam command listed above, is included in the macro TIMEST and evaluates the local coordinates (XYZC) and shape function values (NC, NCT and NCTT) for contact point number J. The matrix NC is the matrix N_c^e introduced in Eq. (2.37), see also Eq. (3.56). NCT and NCTT are first and second time derivatives respectively of N_c^e. Only values of shape functions corresponding to nonprescribed DOF are determined. These DOF can be identified through the topology matrix ENS, the vector of prescribed DOF of the structure PDOFS and the number of the structural element associated with the contact point ISE. XC contains global coordinates and AVC global accelerations and velocities of the contact points.

When structural and vehicle motion components have been determined in the macro TIMEST (cf. Sec. 5.3) the contact forces can be determined. The command BEAM3R is then used to modify the matrix EPS so as to include the now known element loads (contact forces). The contact forces of matrix CF are transformed from the frame Y to the frame X by means of the matrix SXY (S_{XY}). Then, from known local coordinates (XYZC) and structural element numbers (ISEV) of the contact points, the matrix EPS can be modified due to element loads.

The final beam command developed, BEAM3S, calculates member forces and beam displacements at the beam ends (according to Eqs. (3.49a–n) and (3.40a–n)) as well as along the beam element. Input matrices and vectors of BEAM3S are the property matrix EPS, the topology matrix

ENS and the structural displacement, velocity and acceleration vectors US, UST and USTT (u_s, $\dot{u}_s$ and $\ddot{u}_s$). In addition the matrix NS defines the number of beam sections where member forces and displacements must be calculated while J defines the element to be treated in analogy with BEAM3E.

It should be noted that the set of beam commands listed above and introduced into the present computer program can be accompanied, or replaced, by sets of commands for element types other than beams. In this way a library of structural element commands may be established to cope with more general moving load problems. Also note that the commands BEAM3E and BEAM3S, applicable in analysis of beam structures in general, are further described by the author [86][88].

The commands developed for the <u>vehicle elements</u> are

> VEK3E EPVK EKV J
> VEC3EI EPVC ECV J
> VEC3EN EPVC EKV EPZ OMEGA J
> VEM3EI EPVM EMV EPQV SXY J
> VEM3EN EPVM ECV EKV EPZ AVS OMEGA J

These commands generate element matrices and vectors for the three vehicle element types considered in this study: spring element, damper element and rigid body (mass) element. They are included in the macro VEHICO and are analogous with the command BEAM3E for the structural elements.

The command <u>VEK3E</u> computes the 12×12 element stiffness matrix EKV for a spring element, see Subsecs. 2.3.3 and B.3.3. The input data, spring end coordinates and spring stiffness, are given by the element property matrix EPVK.

For damper elements of the vehicle the commands <u>VEC3EI</u> and <u>VEC3EN</u> are utilized. For inertial vehicle motion only VEC3EI is needed while the command VEC3EN also must be used for noninertial motion. The command VEC3EI creates the 12×12 element damping matrix ECV for a damper element analogous with VEK3E, see Subsecs. 2.3.3 and B.3.2. For noninertial vehicle motion an element stiffness matrix EKV (see Eqs. (B.26b) and (B.31b)) and an element noninertial load vector EPZ (see Eqs. (B.26d) and (B.31e)) are created by the command VEC3EN for each damper element. The matrix OMEGA, which contains the angular velocity vector Ω_{XY}, is needed to compute these noninertial quantities.

<u>VEM3EI</u> and <u>VEM3EN</u>, the last vehicle commands listed above, are used for rigid body masses of the vehicle in analogy with damper elements. In addition to the 6×6 element mass matrix EMV an element load vector EPQV is created in the command VEM3EI. For element loads referring to the frame X the transformation matrix SXY (S_{XY}) must be utilized. For noninertial vehicle motion the damping matrix ECV, the stiffness matrix EKV and the noninertia load vector EPZ are created by the command VEM3EN for each rigid body element. Acceleration, velocity and position (AVS) of the vehicle (origin O_Y, see Fig. 2.1) as well as angular velocities and accelerations (OMEGA) are needed to determine these noninertial quantities. The quantities EMV, ECV, EKV, EPQV and EPZ correspond to M_v^e, C_v^e, K_v^e, P_{qv}^e and P_Z^e respectively of Eq. (2.34), see also Subsec. B.3.1. Note that the noninertial commands VEC3EN and VEM3EN are also needed in the time stepping procedure (macro TIMEST).

For <u>structure-vehicle elements</u> two commands are developed:

  SVE3EM MVC CVC KVC EMSV ECSV EKSV ENSVV TCU TCUT
     TCUTT PDOFV NDFSER J
  SVE3EV PQVC PZC EPQSV EPZSV ENSVV TCU PDOFV NDFSER J

The interaction parts of the element matrices in Eqs. (2.45b–d) are created and stored in EMSV, ECSV and EKSV through the command SVE3EM. As input quantities the lower right submatrices in Eq. (2.36) (MVC, CVC and KVC) and the transformation matrices of Eqs. (2.41a) and (2.43a–b) (TCU, TCUT and TCUTT) are needed. Since SVE3EM is performed at each time step EMSV, ECSV and EKSV only contain elements corresponding to nonprescribed structural and vehicle DOF. Greater computational efficiency can be achieved in this way. To arrive at these reduced element matrices a topology matrix ENSVV for the vehicle DOF of the structure–vehicle elements is used. The vector of prescribed DOF of the vehicle PDOFV and the reduced number of DOF of the structural element in question NDFSER are also needed. The last argument, J, is the contact point number.

The vectors of Eqs. (2.45f–g) are computed by the command SVE3EV in analogy with SVE3EM. Note that, according to Subsec. 2.4.3, no structural irregularities are included in EPZSV (P_Z^e). As pointed out in Sec. 5.3, the structure–vehicle element matrices and vectors obtained by the commands SVE3EM and SVE3EV are later transformed into modal coordinates of the structure (unchanged vehicle DOF).

6.   NUMERICAL EXAMPLES

6.1   Introduction

In this chapter four numerical examples concerning analysis of structures subjected to moving loads are given. One purpose of the present chapter is to demonstrate some of the capabilities of the analysis tools developed in Chapters 2 to 5. Another is to investigate time histories and dynamic magnification factors of structural quantities for different models and parameters.

While introductory moving load problems are studied in Appendix D as verification examples, more complex ones are analysed in this chapter. However, the numerical examples here are believed to be simple enough to retain the physical insight into the moving load problem. As in Appendix D, the modal coordinate formulation of the structure (and the structure-vehicle element) described in Subsec. 2.4.3 is applied in this chapter. Output quantities such as normalized displacements, moments and contact forces are presented as time histories and dynamic magnification factors.

In Sec. 6.2 the structure-vehicle interaction is studied in terms of nondimensional input and output parameters (cf. Appendix D). The use of nondimensional parameters means that it is simpler to identify the main characteristics of the moving load problem. In the in-plane problem studied in Sec. 6.2 the structure is modelled as three consecutive two span beams while the model in Fig. 4.4a is adopted for the vehicle. The results associated with this suspension vehicle model are compared with moving force and quasistatic results as well as with structural design code criteria.

The behaviour of a plane frame subjected to a braking vehicle is analysed in Sec. 6.3. Thus the vehicle motion studied is non-inertial. The plane frame studied in detail in Sec. C.4 and the

vehicle model according to Fig. 4.4b, extended by longitudinal springs, are used. Suspension and moving force model results are compared with each other and with quasistatic results.

In Sec. 6.4 the interest is focused on the out-of-plane structural behaviour. Bending and Saint Venant torsion of a simple beam structure are studied in this way. The torsion of the structure is caused by a vehicle moving along a curved path. The vehicle model used is restricted to a moving force model. The moving force results are compared with quasistatic ones.

Finally, in Sec. 6.5 a large scale beam structure under moving loads is studied. The main aim of this numerical example is to demonstrate in a more general moving load problem the capability of the theory and tools developed. Theoretical results associated with suspension and moving force vehicle models are compared with quasistatic results and structural design criteria.

6.2   Structure-vehicle interaction study in terms of nondimensional parameters

6.2.1 General remarks

In the present section nondimensional input and output parameters are utilized to study structure-vehicle interaction in order to identify main characteristics of the moving load problem. The structure and vehicle models studied in the present problem as well as the definition of the pertinent nondimensional parameters are described in Subsec. 6.2.2. Numerical results of mainly structural quantities are then given in terms of time histories and dynamic magnification factors in Subsec. 6.2.3. Finally, Subsec. 6.2.4 contains a discussion of the structural results obtained by the suspension vehicle model, the pertinent moving force model and structural design criteria.

6.2.2 Models and nondimensional parameters

The structure studied in this numerical example consists of three consecutive and identical two span beam structures. The in-plane model of the structure is shown in Fig. 6.1. The structure in Fig. 6.1a can be seen as either a bridge structure or as part of a guide-
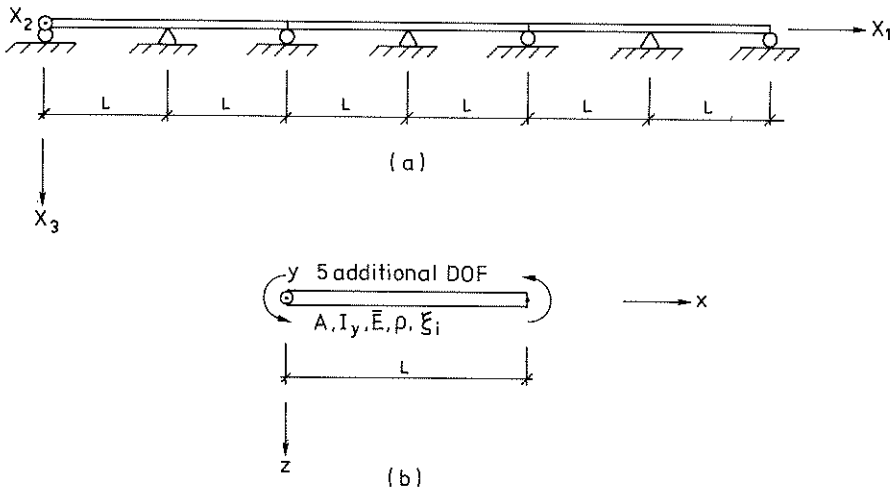
Figure 6.1. Structural model.

(a) The structure consists of three consecutive and uniform two span beams of length 2L. Global reference coordinate system (X_1,X_2,X_3). The beam structure is initially at rest.

(b) Each span is modelled as a single finite (Euler-Bernoulli) beam element with five additional eigenfunctions. The unconstrained beam DOF are indicated. Local coordinate system (x,y,z). Beam cross sectional area A, moment of inertia I_y, elastic modulus $\bar{E}$, mass density ρ and modal damping ratios ξ_i.

way structure. It is noted from Fig. 6.1b that the hierarchical concept of the finite beam element derived in Chapter 3 is adopted thus giving a minimum number of beam elements. In this way the structure is modelled by means of six beam elements, each of them consisting of seven unconstrained DOF in the bending action (cf. Appendix C). Each of the three independent two span beams is thus modelled by 13 DOF. Through the modal coordinate formulation, introduced in Subsec. 2.4.3, eight modes are truncated here giving only five modal DOF for each two span beam. In total, the structure is thus described by 15 DOF in this example.

The vehicle travelling over the present structure is modelled in two different ways according to Fig. 6.2.
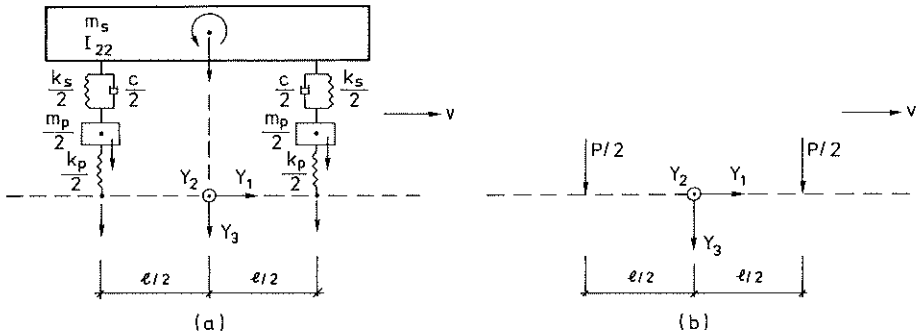
Figure 6.2. Vehicle models. The vehicle is moving at constant speed v. Axle distance ℓ. Reference coordinate system (Y_1, Y_2, Y_3) (cf. Fig. 2.1).

(a) Suspension model. Secondary suspension mass m_s, damping c and stiffness k_s. Principal moment of inertia I_{22}. Primary suspension mass m_p and stiffness k_p. The six nonzero DOF are indicated. The vehicle is at rest in the vertical direction when it enters the structure.

(b) Moving force model. Vehicle weight $P = (m_p + m_s)g$.

The two-axle plane suspension vehicle model introduced is recognized as the model of Fig. 4.4a. The model of Fig. 6.2a should be seen as an assemblage of nine (finite) elements: four spring elements, two damper elements and three mass elements. (As pointed out in the previous chapter, the element matrices/vectors of these three element types are generated by means of the computer commands VEK3E, VEC3EI and VEM3EI respectively). In addition, two fictitious zero mass elements have to be used in order to define the two contact points. The model of Fig. 6.2a is primarily intended to model an air cushion vehicle, cf. Smith et al. [110]. Depending on the choice of parameter values, however, the model may also be appropriate for other vehicle types, cf. Sec. 4.2.

The moving force vehicle model of Fig. 6.2b constitutes a special case of the present suspension model, cf. Chapter 4 and Appendix D. Thus the deviation from the magnitude P/2 of the two contact forces, due to the structural deflections, is ignored.

The quantities of the structural model in Fig. 6.1 and of the suspension vehicle model in Fig. 6.2a can now be expressed in terms of nine nondimensional input parameters for the sake of clarity. The nine parameters are defined in Table 6.1, cf. the author [83][85] and Smith et al. [110].

Representative values of the parameters in Table 6.1 are given in Subsec. 6.2.3. If the moving force model in Fig. 6.2b is applied it should be noted that only three of the parameters in Table 6.1 are needed: α, λ and ξ_i. (Also only a limited number of the parameters in Table 6.1 are needed in Appendix D). As in most of the examples in this work, the output parameters are nondimensional (normalized), see Subsec. 6.2.3.

Parameter		Definition
α	vehicle to structure velocity ratio	$v\pi/\omega_1 L$
κ	vehicle to structural span mass ratio	$(m_p+m_s)/\rho AL$
κ_0	vehicle primary to secondary suspension mass ratio	m_p/m_s
κ_1	vehicle moment of inertia ratio	$12I_{22}/m_s\ell^2$
λ	vehicle axle distance to structural span ratio	ℓ/L
ξ_i	modal damping ratio(s) of structure	$C_{si}^m/2M_{si}^m\omega_i$
ξ_v	vehicle damping ratio	$c/2m_s\omega_v$
χ	vehicle primary to secondary suspension stiffness ratio	k_p/k_s
Ω	structure to vehicle frequency ratio	ω_1/ω_v

Table 6.1. Nondimensional input parameters of the moving load problem in Sec. 6.2. Circular eigenfrequencies of Ω are defined as $\omega_1 = \pi^2\sqrt{\overline{EI}_y/\rho AL^4}$ and $\omega_v = \sqrt{k_s/m_s}$. (For other notations see Figs. 6.1 and 6.2a and Appendix A).

The vehicle model in Fig. 6.2a has been used in previous studies by for instance Frýba [38] and Smith et al. [110]. Similar models are reported by e.g. Arpe [3], Garg et al. [39] and Matsuura [73] (see Fig. 4.2), while a corresponding one-axle vehicle is used in e.g. Chiu et al. [14] and Chung and Genin [16][41]. However, comparisons with the simple moving force model (Fig. 6.2b) are only performed to a limited extent in the above references. Moreover, only a simply supported beam structure is studied in most of these references.

6.2.3 Numerical results

By means of the theory and analysis tools developed in Chapters 2 to 5 the present moving load problem, described in Subsec. 6.2.2, can be analysed. Numerical results from such an analysis are given in this subsection. Note that the two contact DOF in Fig. 6.2a are eliminated according to Sec. 2.4 giving structure-vehicle finite elements which contain the primary suspension springs.

Practically representative values of some of the nondimensional input parameters defined in Table 6.1 are given for air cushion vehicles by for instance Wormley et al. [14][110]. These are: $0 < \alpha < 1$, $0.1 < \kappa < 1.0$, $0.05 < \kappa_0 < 0.50$, $0.01 < \xi_i < 0.10$, $0.1 < \xi_v < 0.5$, $5 < \chi < 25$ and $1 < \Omega < 10$. In the present example the following input values are used: $\kappa = 0.5$, $\kappa_0 = 0.25$, $\kappa_1 = 1.0$, $\lambda = 0.5$, $\xi_i = 0.02$, $\xi_v = 0.125$, $\chi = 20$ and $\Omega = 3.0$. Thus, for instance, the vehicle axle distance ℓ equals half the span L, see Figs. 6.1 and 6.2. The velocity ratio α is set to different values in the range 0.1-0.8. Note that $\alpha = 1.0$ corresponds to a vehicle speed between about 400 to 1500 km/h depending on the type of structure, cf. the definition of α in Table 6.1.

The numerical results obtained from the models and parameter values above are given in terms of time histories and dynamic magnification factors. In order to determine the magnification factors and to simplify the time history presentation, the output results such as displacements and moments are normalized by the corresponding quasi-static ones (obtained by means of the moving force model and $v = 0^+$). In addition the time is normalized by the vehicle traversing time $\tau = 2L/v$, that is the time needed for a vehicle axle to pass one of the two span beams. ($t/\tau = 0$ when the vehicle enters the structure).

The time histories of the contact forces ($\alpha = 0.6$) are first presented, see Fig. 6.3. (The contact forces are set positive in compression). It can be seen from Fig. 6.3 that the contact forces deviate from half the vehicle dead weight by about $\pm$ 30% for the front axle and $\pm$ 20% for the rear axle. Although only three repetitive structural parts are included (Fig. 6.1a), an approaching steady state condition can be clearly distinguished from Fig. 6.3. According to Smith et al. [110], 5-10 repetitive parts must be included to reach a steady state vehicle motion. However, inclusion of so many parts causes undesirable computational complexity and costs. Popp et al. [95] presents a solution method, including periodic coefficients and periodically jumping states, to cope with this. In some cases, however, numerical problems appear in this method.

Next, pertinent time histories for the vertical vehicle contact displacements are given, see Fig. 6.4. From Fig. 6.4 it can be concluded that for $\alpha = 0.6$ the vehicle contact displacements significantly deviate from the quasistatic ones. Moreover, the main features of the actual displacements are well predicted by the simple moving force model. However, the dynamic magnification factor for $u_{vr}(t)$ in Fig. 6.4b is only 1.62 due to the moving force model while a value of 1.81 is predicted by the suspension model. It should also be noted that the suspension model response differs somewhat between the three two span units due to different initial vehicle motions, cf. Fig. 6.3.
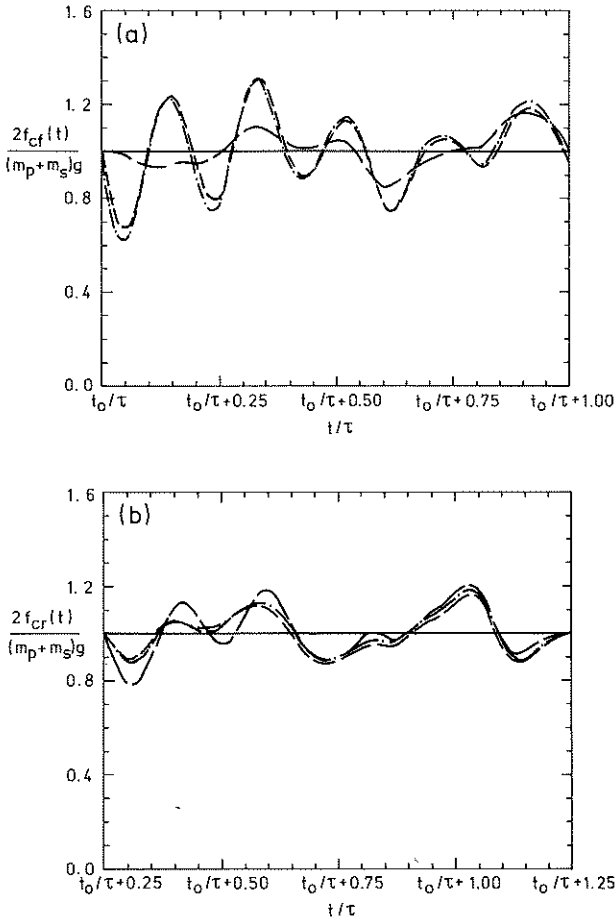
Figure 6.3. Time histories for normalized contact forces for the problem defined by Figs. 6.1 and 6.2, $0 \leq t/\tau \leq 3.25$, $\alpha = 0.6$, $\kappa = 0.5$, $\kappa_0 = 0.25$, $\kappa_1 = 1.0$, $\lambda = 0.5$, $\xi_i = 0.02$, $\xi_v = 0.125$, $\chi = 20$ and $\Omega = 3.0$. —— Moving force model; — — Suspension model, $t_0/\tau = 0$; — — — Suspension model, $t_0/\tau = 1$; —•—•— Suspension model, $t_0/\tau = 2$. (15 modes, $\Delta t = \tau/100$).
(a) Front contact force $f_{cf}(t)$.
(b) Rear contact force $f_{cr}(t)$.
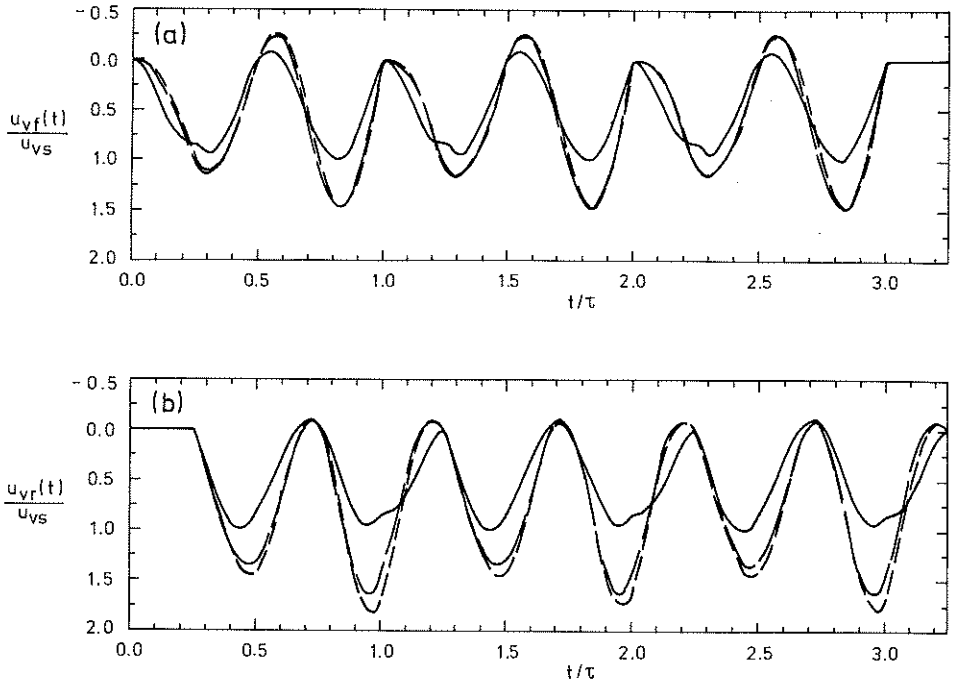
Figure 6.4. Time histories for normalized vehicle contact displace-
ments ($u_{vs} = 0.4280 \cdot PL^3/48\bar{E}I_y$) for the problem defined
by Figs. 6.1 and 6.2, $0 \leq t/\tau \leq 3.25$, $\alpha = 0.6$, $\kappa = 0.5$,
$\kappa_0 = 0.25$, $\kappa_1 = 1.0$, $\lambda = 0.5$, $\xi_i = 0.02$, $\xi_v = 0.125$,
$\chi = 20$ and $\Omega = 3.0$. ——— Quasistatic; —— Moving
force model; — — — Suspension model. (15 modes,
$\Delta t = \tau/100$).
(a) Front contact displacement $u_{vf}(t)$.
(b) Rear contact displacement $u_{vr}(t)$.

In contrast to the vehicle response the structural response is
transient in nature. The midspan displacement and moment histories
of Figs. 6.5 and 6.6 clearly demonstrate this. Once again it can be
seen from these figures that the dynamic response differs
considerably from the quasistatic one. Also the principal dynamic
behaviour of the structure is contained within the moving force
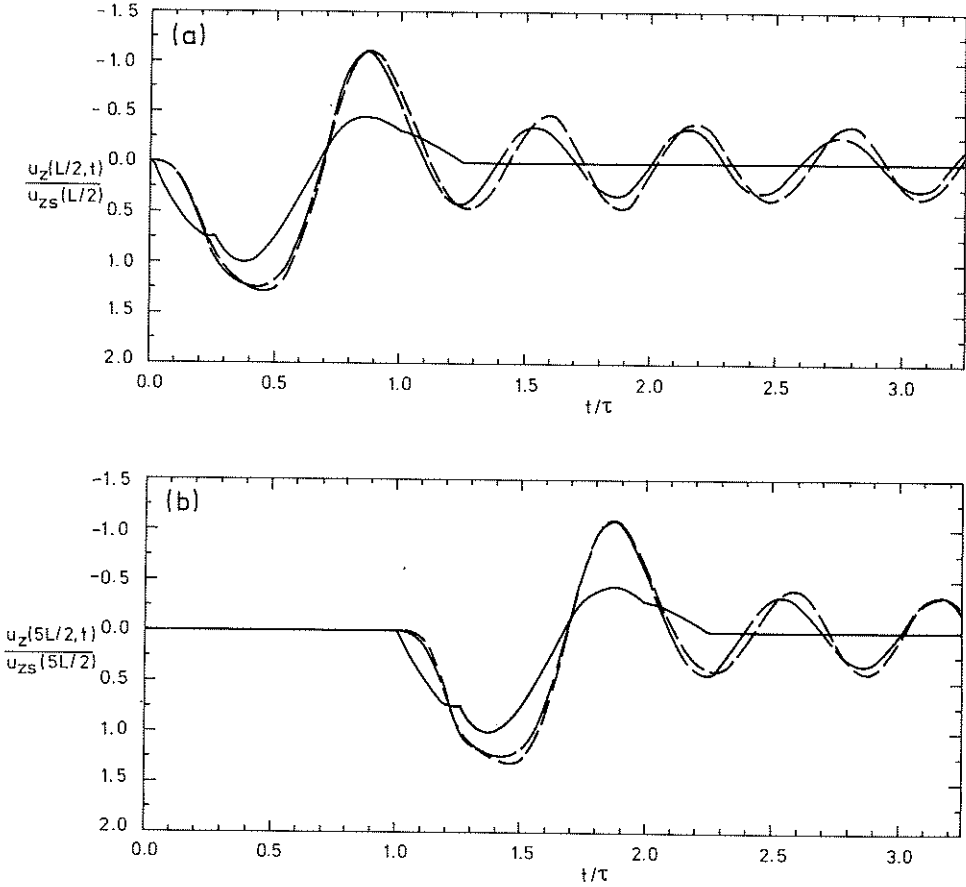
<u>Figure 6.5</u>. Time histories for normalized midspan displacements $(u_{zs}(L/2) = u_{zs}(5L/2) = 0.4768 \cdot PL^3/48\bar{\bar{E}}I_y)$ for the problem defined by Figs. 6.1 and 6.2, $0 \leq t/\tau \leq 3.25$. $\alpha = 0.6$, $\kappa = 0.5$, $\kappa_0 = 0.25$, $\kappa_1 = 1.0$, $\lambda = 0.5$, $\xi_i = 0.02$, $\xi_v = 0.125$, $\chi = 20$ and $\Omega = 3.0$. ———— Quasistatic; —— Moving force model; – – – Suspension model. (15 modes, $\Delta t = \tau/100$).

(a) Displacement $u_z(L/2, t)$.

(b) Displacement $u_z(5L/2, t)$.
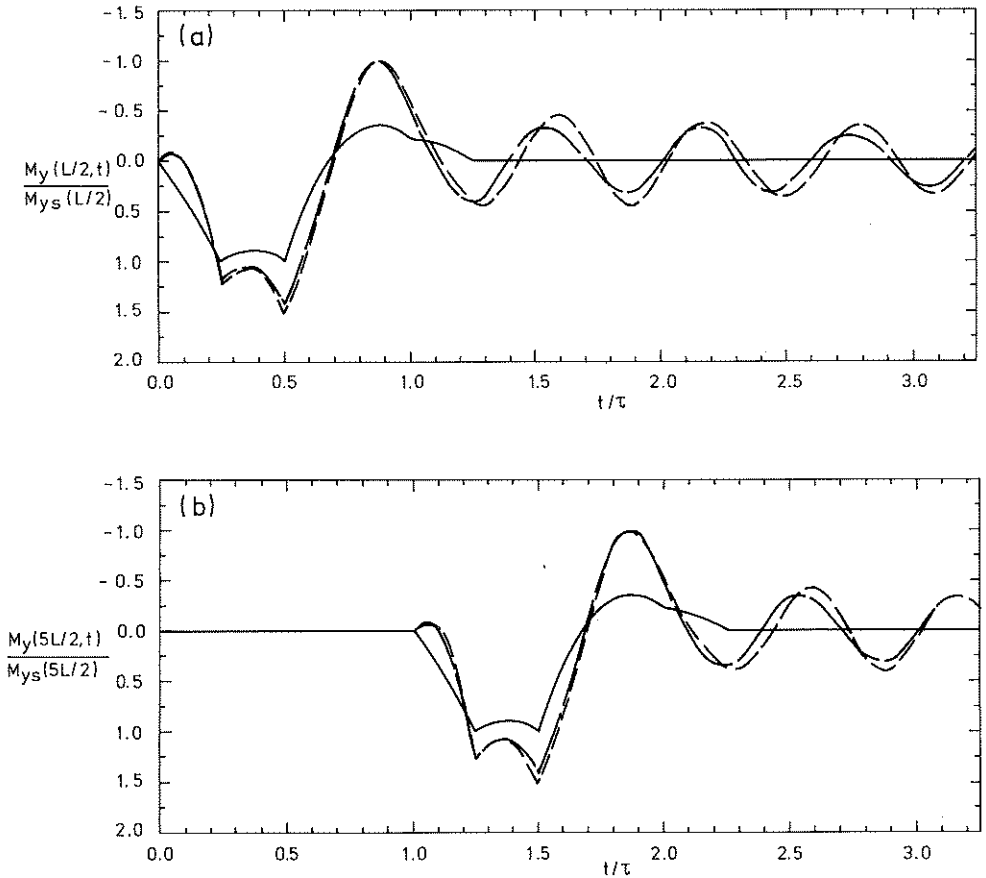
Figure 6.6. Time histories for normalized midspan moments ($M_{ys}(L/2)$ = $M_{ys}(5L/2)$ = 0.4063·PL/4) for the problem defined by Figs. 6.1 and 6.2, $0 \le t/\tau \le 3.25$. $\alpha = 0.6$, $\kappa = 0.5$, $\kappa_0 = 0.25$, $\kappa_1 = 1.0$, $\lambda = 0.5$, $\xi_i = 0.02$, $\xi_v = 0.125$, $\chi = 20$ and $\Omega = 3.0$. —— Quasistatic; — — Moving force model; — — — Suspension model. (15 modes, $\Delta t = \tau/100$).

(a) Moment $M_y(L/2, t)$.

(b) Moment $M_y(5L/2, t)$.

model. However, as for the displacement $u_{vr}(t)$ just mentioned the dynamic response here is greater for the suspension model. From Figs. 6.5 and 6.6 it is also noted how the free structural vibrations are slowly damped out ($\xi_i = 0.02$). In addition it is interesting to note that, except for the time lag, the curves in (b) only differ slightly from the curves in (a). This indicates that the relative vehicle motion present when the vehicle enters the second two span unit only gives rise to minor structural effects. Also note the great magnification for the negative moment at $t/\tau = 0.85$ in Fig. 6.6a ($t/\tau = 1.85$ in Fig. 6.6b).

In general the velocity parameter α is the most important parameter in describing the dynamic character of a moving load problem. Therefore, dynamic magnification factors for different values of α are given next in the present problem. The factors presented are the ones corresponding to the time histories in Figs. 6.5a and 6.6a. The dynamic magnification curves are given in Fig. 6.7.

From Fig. 6.7 it is seen that although the general trend is for the magnification factors to increase for an increased value of α, this is not always true locally (cf. Sec. D.2). It is also noted that the suspension vehicle model in most cases yields higher magnification values when compared with the values of the moving force model (cf. Sec. D.4).
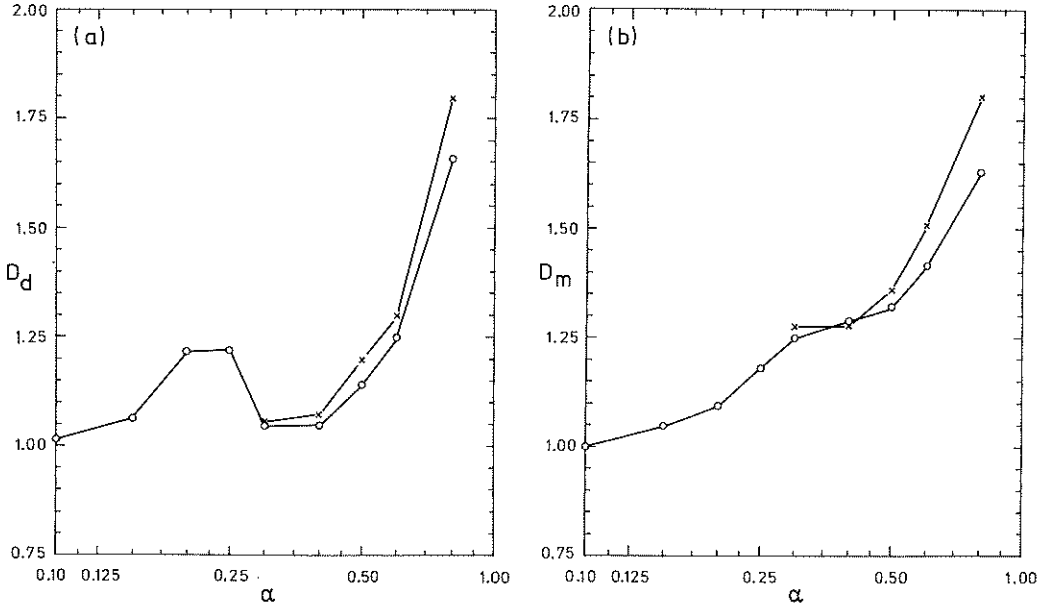
Figure 6.7. Dynamic magnification factors for midspan displacement and midspan moment for the problem defined by Figs. 6.1 and 6.2, $\alpha = 0.1$–0.8. $\kappa = 0.5$, $\kappa_0 = 0.25$, $\kappa_1 = 1.0$, $\lambda = 0.5$, $\xi_i = 0.02$, $\xi_v = 0.125$, $\chi = 20$ and $\Omega = 3.0$. o——o Moving force model; ×——× Suspension model. (15 modes, $\Delta t = \tau/100$).

(a) Displacement dynamic magnification factor

$$D_d = \max[u_z(L/2,t)]/u_{zs}(L/2).$$

(b) Moment dynamic magnification factor

$$D_m = \max[M_y(L/2,t)]/M_{ys}(L/2).$$

6.2.4 Discussion

From the numerical results given in Subsec. 6.2.3 it should be evident that the dynamic structural response due to moving loads may differ significantly from the quasistatic one. Still, effects due to structural irregularities (cf. Subsec. 2.4.3) are not considered. It can also be concluded that the principal structural response is well predicted by means of the moving force model for the cases studied. In most cases, however, the structural response is underestimated when the simple moving force model is used. Moreover, vehicle resonance effects arising in its steady state motion cannot be predicted by the moving force model, see for instance Wormley et al. [14] [110]. Thus, both advantages and disadvantages can be identified for the moving force model.

In order to limit the scope, only the input parameter α is varied in Subsec. 6.2.3. However, although α is the parameter of main interest, studies of the other eight parameters in Table 6.1 are also of interest. By performing such studies the structural results due to the two different vehicle models can be compared in more detail. Nevertheless, a rough guide for choosing an appropriate vehicle model can be given in terms of the parameters α, κ, κ_0 and Ω according to Table 6.2, cf. Dahlberg [23].

It can be seen in Table 6.2 that the moving force model is an appropriate model, thus neglecting structure–vehicle interaction, provided α or κ is low. For medium–high values of α and κ, however, other models should be more suitable unless κ_0 is low and Ω high, that is when most of the vehicle mass is suspended on weak secondary suspension springs. In Table 6.2 it is also seen that the moving mass model (cf. Secs. 4.3 and D.3) not studied in this section may also be of interest in some cases. A quantitative measure of low, medium and high parameter values for air cushion vehicles is

α \ κ	low	medium	high
low	MF	MF	MF
medium	MF	κ_0 \ Ω	low	medium	high
		low	MM	S	MF
		medium	MM	S	S
high	MF	high	MM	MM	MM

Table 6.2. Choice of vehicle model for low, medium and high values of the dimensionless parameters α, κ, κ_0 and Ω defined in Table 6.1. MF = Moving force model; MM = Moving mass model; S = Suspension model.

indicated at the beginning of Subsec. 6.2.3. See also Wormley et al. [14][110] and Frýba [38] for reference. It is believed that the four parameters in Table 6.2 may serve as a rough guide in the choice of vehicle model for many moving load problems.

It is also of interest to compare the dynamic magnification factors obtained in Subsec. 6.2.3 with design code curves and to discuss the merits of static contra dynamic structural analysis in moving load studies. A comparison of this type is illustrated in Fig. 6.8. The code magnification factors in Fig. 6.8 are described in, for instance, Machida and Matsuura [67]. The factors are based on numerical simulations and extensive laboratory and full-scale experiments. The ORE (Office of Research and Experiment) curve is defined as $D = 1+\alpha/(1-\alpha+\alpha^2)$ whereas the JNR (Japanese National Railways) curve is given by $D = 1+\alpha$. Note in Fig. 6.8 that these
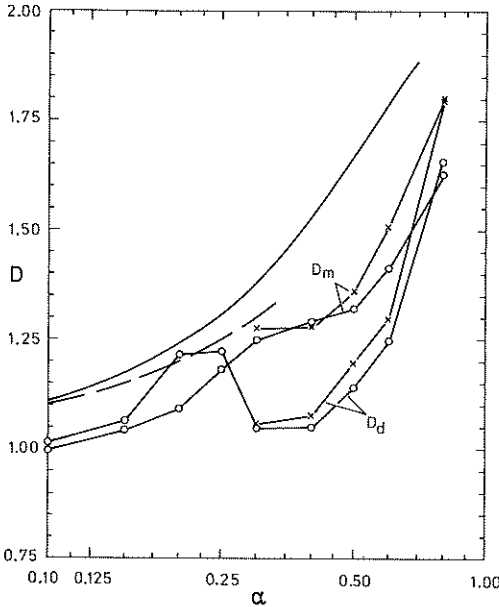
Figure 6.8. Dynamic magnification factor D, $\alpha = 0.1-0.8$. ——— Code, ORE ($\alpha \leq 0.7$); — — Code, JNR ($\alpha \leq 1/3$); o———o Present analysis, moving force model; x———x Present analysis, suspension model. D_d and D_m are displacement and moment dynamic magnification factors, respectively, according to Fig. 6.7.

expressions are not valid for the whole range of α. In addition, a contribution between about 0.1 to 0.4 shall be added to D in order to consider structural irregularities. A minor dimensional contribution of −L/1400 (span L in meter) is also not included in the D expression of the JNR code.

It is seen in Fig. 6.8 that the present magnification factors are almost without exception below the code factors. It is also the intention of, for instance, the ORE code to give an expression for D

on the safe side. Thus, although simple to undertake, a static structural analysis with a total vehicle load equal to the vehicle dead weight multiplied by D generally overdesigns the structure. Basically this is due to the fact that the dynamic character of a moving load problem is only roughly described by the single parameter α, see Fig. 6.8. For the problem studied in this section it is found that the moving force model well describes the principal structural behaviour. Therefore it is reasonable to argue that a dynamic moving force analysis should be an economically attractive alternative to a traditional static analysis in design studies. In a design situation, structure-vehicle interaction and structural irregularity effects may be taken into account approximately by making the magnitudes of the moving forces somewhat higher than the static values. Finally, it should be noted that the code curves in Fig. 6.8 may underdesign structures with lower capacity for negative moments than for positive ones, see Fig. 6.6.

6.3   Plane frame behaviour due to braking vehicle

6.3.1 General remarks

In this section the behaviour of a plane frame structure subjected to a braking vehicle is studied. The vehicle motion is thus non-inertial and a longitudinal structure-vehicle interaction is obtained in addition to the vertical interaction (cf. Sec. 6.2). The structure and vehicle models adopted are described in Subsec. 6.3.2 while numerical results are given in Subsec. 6.3.3. The results are given in terms of time histories of contact forces and structural displacements and moments. As in Sec. 6.2 the results due to the suspension vehicle model are compared with moving force and quasistatic results. Values of dynamic magnification factors are also indicated.

6.3.2 Structure and vehicle models

The frame structure studied consists of a two span beam rigidly connected to a column. The structural model with pertinent data is shown in Fig. 6.9. The plane and symmetric two span frame is modelled by 19 DOF: 12 basic DOF and 7 additional DOF. After considering boundary conditions and modal truncation the 19 DOF are reduced to seven. Note that eigenfrequencies and eigenmodes of the frame in Fig. 6.9 are studied in Sec. C.4 for the case of infinite axial stiffnesses.

(a)

(b)
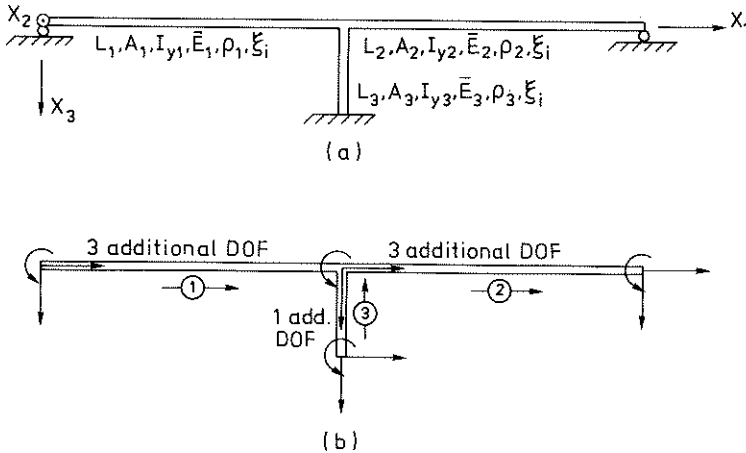
Figure 6.9. Structural model.

(a) The structure consists of a uniform two span beam rigidly connected to a uniform column. Global reference coordinate system (X_1, X_2, X_3). The frame is initially at rest. Data: $L_1 = L_2 = L = 20$ m, $L_3 = 5.66$ m, $A_1 = A_2 = 0.295$ m^2, $A_3 = 0.221$ m^2, $I_{y1} = I_{y2} = 0.0450$ m^4, $I_{y3} = 0.0225$ m^4, $\bar{E}_1 = \bar{E}_2 = \bar{E}_3 = 2 \cdot 10^{11}$ Pa, $\rho_1 = \rho_2 = \rho_3 = 7800$ kg/m^3 and $\xi_i = 0.02$.

(b) Finite element discretization. Three hierarchical (Euler–Bernoulli) beam elements with additional eigenfunctions in bending.
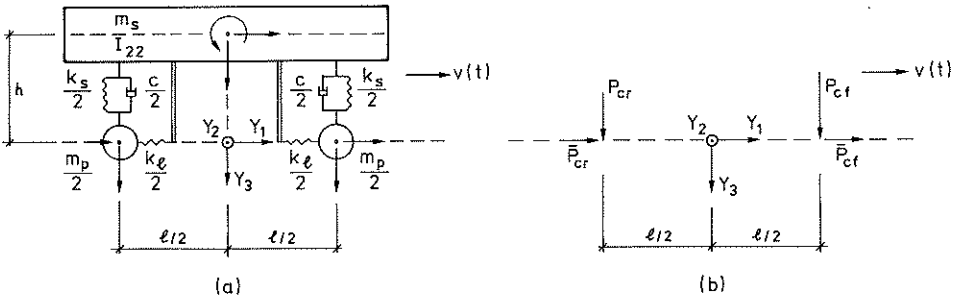
Figure 6.10. Vehicle models. The vehicle is moving at variable speed
v(t), see Fig. 6.11. Reference coordinate system
(Y_1, Y_2, Y_3). $\ell = 10$ m and h = 2 m.
(a) Suspension model. The seven nonzero DOF are indi-
icated. The vehicle is at rest (relative to Y)
when it enters the structure. Data: $m_p = 4 \cdot 10^3$ kg,
$m_s = 4 \cdot 10^4$ kg, $I_{22} = 3.333 \cdot 10^5$ kgm^2, c = $2 \cdot 10^5$
Ns/m, $k_\ell = 8 \cdot 10^8$ N/m and $k_s = 8 \cdot 10^6$ N/m.
(b) Moving force model. The magnitudes of the forces
correspond to steady state (constant) braking.
Data: $P_{cf} = 1.148 \cdot P/2$, $P_{cr} = 0.852 \cdot P/2$ and $\bar{P}_{cf} = \bar{P}_{cr} = 0.408 \cdot P/2$ (P = $(m_p + m_s)g$, a = -4.0 m/s^2).

Vehicle braking on the frame structure is modelled according to Fig.
6.10 (cf. Sec. 6.2). It may be noted that the suspension model in
Fig. 6.10a is an extension of the model shown in Fig. 4.4b. The
extension lies in two longitudinal springs and three longitudinal
DOF. Thus the model in Fig. 6.10a also takes into account longi-
tudinal structure–vehicle interaction. Note that the longitudinal
springs are much stiffer than the vertical ones. The vehicle speed
v(t) indicated in Fig. 6.10 is determined through the vehicle
acceleration a(t) and the initial speed v(0). The input quantity
a(t) as well as v(t) for the present example are given in Fig. 6.11.
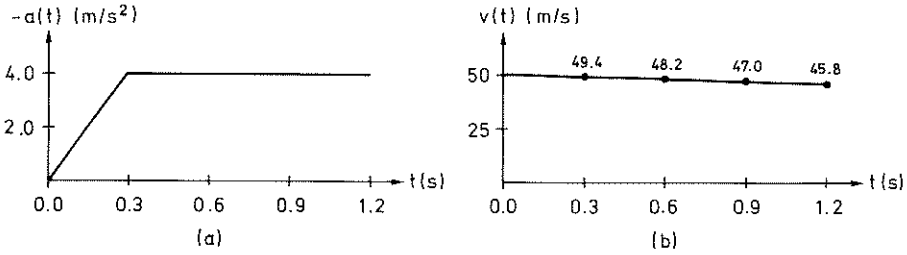
Figure 6.11. Vehicle motion (nominal). t = 0 when the vehicle enters the structure, cf. Figs. 6.9 and 6.10. t ≈ 1.03 on exit.

(a) Vehicle acceleration a(t) (ramp function).

(b) Vehicle speed v(t) (v(0) = 50 m/s = 180 km/h).

It is seen from Fig. 6.11 that although the vehicle braking is heavy the vehicle speed is only decreased somewhat during its passage over the structure. (If braking is continued the vehicle stops after 12.65 s and ~ 320 m). It is also recognized that the nominal vehicle motion is not only noninertial but also nonconstant noninertial due to the change in vehicle acceleration from 0 ($t \leq 0$) to -4.0 m/s^2. This also has the result that the suspension contact forces would have differed from the moving forces in Fig. 6.10b even in the case of an undeformable structure. (The noninertial load vector in Eq. (2.34) is activated through vehicle braking, cf. Sec. 5.4 and Appendix B).

Studies of vehicle braking in combination with structure–vehicle interaction have been undertaken by for instance Traill–Nash et al. [46][55] and by Mulcahy [77]. In these studies are neither frame structures nor longitudinal structure–vehicle interaction handled. This means that the longitudinal forces (braking forces) are assumed to be known in advance, cf. Fig. 6.10b. In addition, both a suspension and a moving force model (Fig. 6.10) are adopted in the present study.

6.3.3 Numerical results

As in Sec. 6.2 contact force results are first presented. However, vertical as well as longitudinal contact forces can be identified in this example. Time histories of the two vertical contact forces and one of the longitudinal forces (front) are given in Fig. 6.12. Note that the forces are normalized whereas the time is not and that two different force scales are used in Fig. 6.12b.

In Fig. 6.12 it is seen how the contact forces approach the steady state forces (moving forces). It may also be realized that the oscillations of the histories are closely related to entrance of the rear axle (t $\approx$ 0.20 s) on the structure and exit of the front axle (t $\approx$ 0.82 s). In fact, the oscillations of $\bar{f}_{cf}(t)$ immediately after t = 0.82 are severe. This is due to a substantial discontinuity in the longitudinal contact displacement, cf. Fig. 6.13. A second reason for the more pronounced longitudinal than vertical structure-vehicle interaction, is the large longitudinal suspension stiffness $(k_\ell/k_s = 100)$. The longitudinal contact force history of the vehicle rear axle is similar to that of the front axle.

The sway of the frame structure due to the braking vehicle is studied next. The time history for the longitudinal displacement $u_x(L,t)$ is given in Fig. 6.13 for three different cases. It should be noted that the reference system Y of the vehicle is assumed to move along the centroidal axis of the span beams so that the braking forces do not cause any concentrated moment loads on the structure.
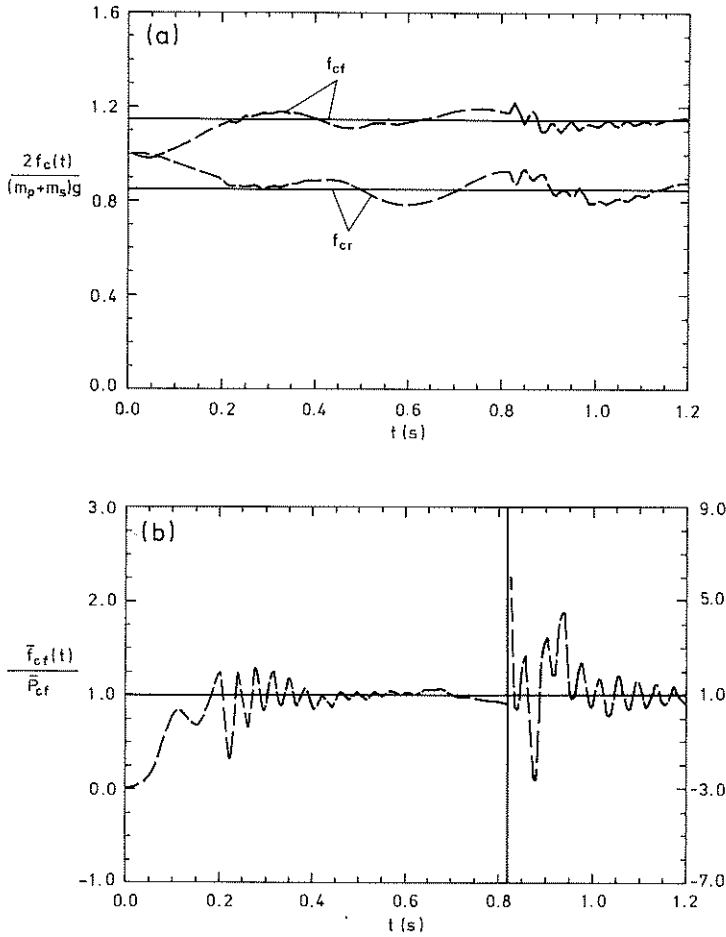
Figure 6.12. Time histories for normalized contact forces for the problem defined by Figs. 6.9 to 6.11, $0 \leq t \leq 1.2$ s. —— Moving force model; — — Suspension model. (7 modes, $\Delta t = 0.005$ s).
(a) Vertical contact forces (front and rear).
(b) Longitudinal contact force (front).
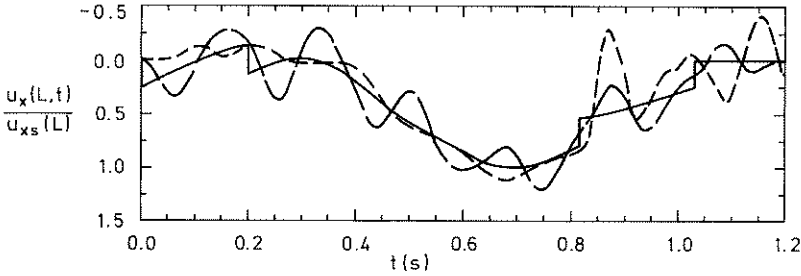
Figure 6.13. Time histories for normalized sway displacement ($u_{xs}(L)$ = $1.971 \cdot 10^{-3}$ m) for the problem defined by Figs. 6.9 to 6.11, $0 \leq t \leq 1.2$ s. ——— Quasistatic; — — Moving force model; — — — Suspension model. (7 modes, Δt = 0.005 s).

From Fig. 6.13 the dynamic displacement histories can be seen to oscillate about the quasistatic one. Note that discontinuities occur in the quasistatic history due to entrance and exit of braking forces. (Physical coordinates instead of a truncated number of modal coordinates have been used to describe these discontinuities correctly). For the suspension model history, it is seen that the sway displacement is rather large when the vehicle front axle leaves the structure ($t \approx 0.82$). Thus the discontinuity in longitudinal contact displacement at the structure exit ($u_x(2L,t) \approx u_x(L,t)$) is considerable causing severe oscillations of $\bar{f}_{cf}$, see Fig. 6.12b. In Fig. 6.13 the dynamic magnification factor is 1.20 for the moving force model and 1.11 for the suspension model.

As final numerical results, the time histories of the deflection and moment at midspan of the second span are presented, see Fig. 6.14. A pattern similar to that in Fig. 6.13 can be seen in Fig. 6.14. Since the dynamic character is not so pronounced in Fig. 6.14 the suspension model histories are excluded for clarity. The dynamic magnification factors in Figs. 6.14a and 6.14b are 1.04 and 1.09 respectively.
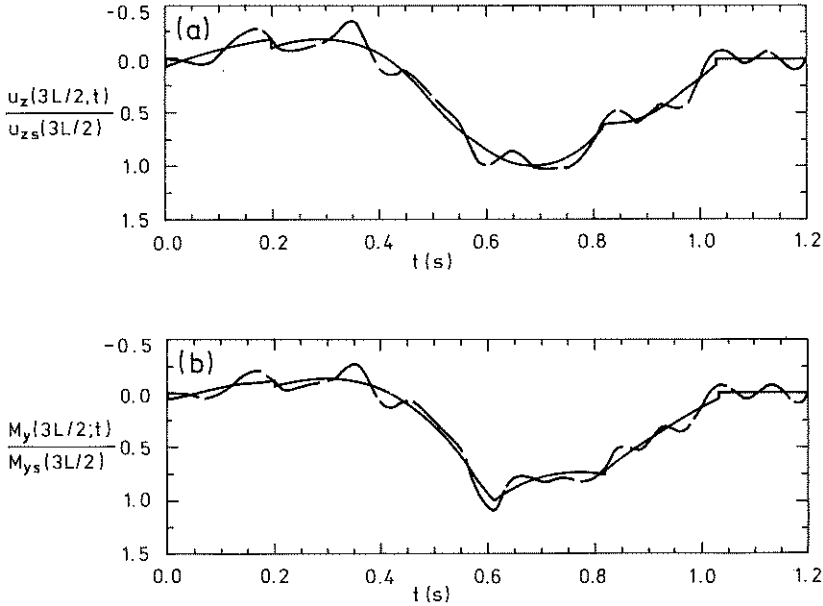
Figure 6.14. Time histories for normalized midspan displacement and moment ($u_{zs}(3L/2) = 4.072 \cdot 10^{-3}$ m, $M_{ys}(3L/2) = 1.052 \cdot 10^{6}$ Nm) for the problem defined by Figs. 6.9 to 6.11, $0 \leq t \leq 1.2$ s. ——— Quasistatic; — — Moving force model. (7 modes, $\Delta t = 0.005$ s).
(a) Displacement $u_z(3L/2, t)$.
(b) Moment $M_y(3L/2, t)$.

In this example the behaviour of a plane frame subjected to a braking vehicle has been studied. It can be concluded that the structure-vehicle interaction may be substantial in such a case, especially with regard to longitudinal (braking) contact forces. The dynamic magnification factors presented here are, however, rather low. (With $v = 50$ m/s, $\omega_1 = 38.47$ rad/s (cf. Sec. C.4) and $L = 20$ m the parameter α defined in Table 6.1 is ~ 0.20, cf. Figs. 6.7 and 6.8).

6.4   Bending-torsional behaviour of simple beam structure

6.4.1 General remarks

In the remaining two numerical examples the out-of-plane structural behaviour is studied. In this section the torsion of the structure is caused by a vehicle moving along a curved path. The present example is limited to a simple beam structure and a moving force vehicle model. The structure and vehicle models used are described in Subsec. 6.4.2 and numerical results are given in Subsec. 6.4.3. The results are mainly given in terms of time histories of beam cross sectional displacements and rotation as well as of bending and torsional moments. Values of different dynamic magnification factors are also given. In addition, structural eigenfrequencies are investigated.

6.4.2 Structure and vehicle models

The beam structure studied in this example is a horizontally curved bridge or guideway span. Since the radius of curvature R (cf. Chapter 2 and Appendix B) is as large as 2500 m, the structure is modelled here as a straight beam. The structural model and structural input data are given in Fig. 6.15. From Fig. 6.15 it is noticed that warping torsional effects have been neglected. For beams of closed cross section this is often justified, cf. Sec. 6.5. Moreover, the small discrepancies in structural properties between the slightly curved beam and the present straight beam model are verified in Subsec. 6.4.3 in terms of eigenfrequencies. The small changes in eigenfrequencies due to $z_p \neq 0$ are also indicated in that subsection.
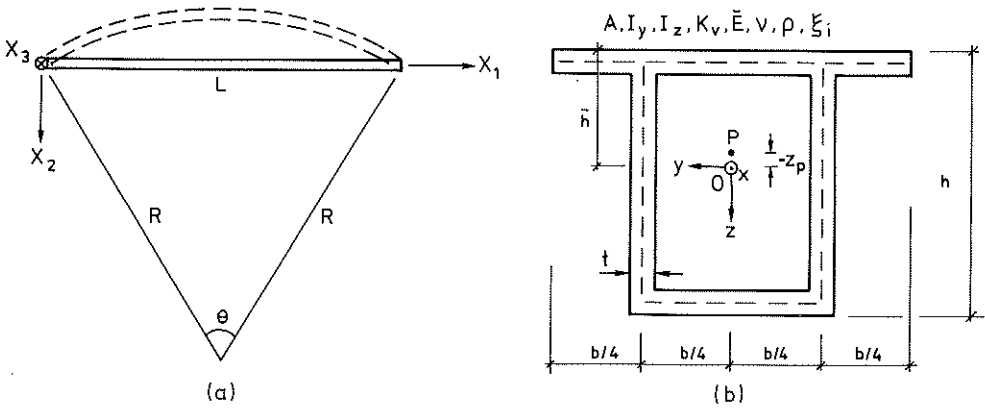
Figure 6.15. Structural model.

(a) Top view of horizontally curved structure (dashed lines) and assumed straight beam model. Global reference coordinate system (X_1, X_2, X_3). The model beam is simply supported with respect to bending.

Data: $L = 30$ m, $R = 2500$ m, $\theta \approx 0.69^{\circ}$ (the curvature is considerably exaggerated in the figure). The beam is modelled as a single hierarchical beam element with eight additional eigenfunctions in both (Euler-Bernoulli) bending actions and five functions in (Saint Venant) torsion.

(b) Cross sectional view. Local coordinate system (x, y, z). The origin O coincides with the centroid of the cross section while the pole P coincides with its shear centre. Data: $b = 3.0$ m, $h = 2.0$ m, $\bar{h} = 0.943$ m, $t = 0.20$ m, $z_p = -0.0135$ m, $A = 1.66 m^2$, $I_y = 1.097$ m^4, $I_z = 0.939$ m^4, $K_v = 1.033$ m^4, $\bar{E} = E = 3.2 \cdot 10^{10}$ Pa, $\upsilon = 0.15$, $\rho = 2400$ kg/m^3 and $\xi_i = 0.02$.

With regard to the vehicle only a moving force model is considered in this example. However, the magnitudes of the moving forces are determined from a suspension vehicle model moving in steady state curving on a smooth and rigid structure. The suspension model in question may be seen as a lateral analogy to the longitudinal model in Fig. 6.10a, cf. Fig. 4.3. Thus a one−axle vehicle model is considered here for convenience. The moving force model is shown in Fig. 6.16.

The magnitudes of the moving forces given in Fig. 6.16 have been calculated from Eqs. (2.34) and (B.23) ($\Omega_3 = \frac{v}{R}$, $\Omega_1 = \dot{\Omega}_1 = \Omega_2 = \dot{\Omega}_2 = \dot{\Omega}_3 = 0$) as well as from statics. Note that the magnitudes correspond to a structure with no superelevation ($Q = 0$). This overestimates the rotation of the structure. However, the dynamic magnification factors studied are not affected since a moving force model is chosen so that the principle of superposition can be applied. It should also be noted that the mass ratio κ is as low as 0.276, cf. Tables 6.1 and 6.2.

Studies of the bending−torsional behaviour of structures under moving loads have been performed by for instance Aida [1][2], Chaudhuri [11], Das [28], Dey and Balasubramanian [29], Frýba [38], Genin et al. [42], Joseph and Wilson [52], Rabizadeh et al. [97][98], Ramakrishnan and Kunukkasseril [99] and Tan and Shore [116][117]. See also the state−of−the−art review in Ref. [32]. The finite element method has been adopted only to a limited extent in these studies. Instead, analytical methods or the finite strip method, cf. Sec. 1.2, are used. In addition vertical, lateral and also torsional quantities are investigated in the present study.
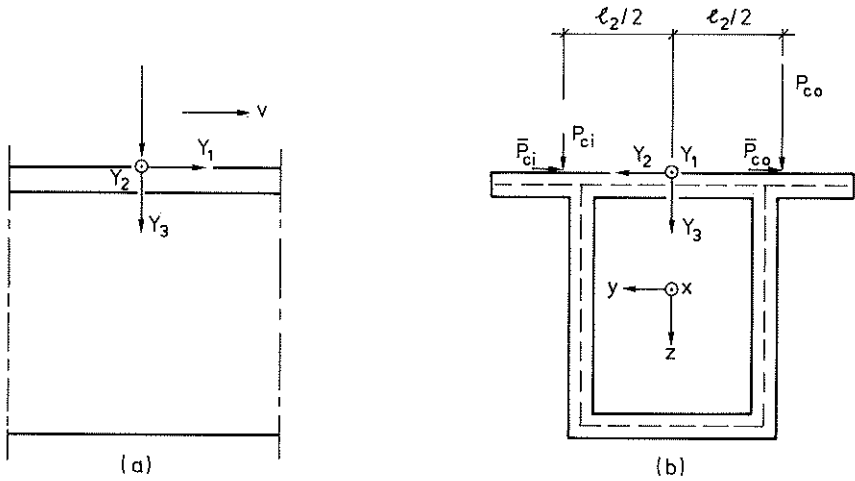
Figure 6.16. Vehicle model (moving forces). Reference coordinate system (Y_1, Y_2, Y_3).

(a) Side view (inner side). The one-axle vehicle is moving at constant speed $v = 100$ m/s (360 km/h).

(b) Front view. The magnitudes of the moving forces correspond to steady state (constant) curving. With a lateral analogy to the suspension model in Fig. 6.10a, $v = 100$ m/s, $R = 2500$ m, $m_p = 3 \cdot 10^3$ kg, $m_s = 3 \cdot 10^4$ kg, $\ell_2 = 1.8$ m and a vehicle height $h = 1.2$ m the following magnitudes are obtained: $P_{co} = 2.419 \cdot 10^5$ N, $P_{ci} = 0.819 \cdot 10^5$ N, $\bar{P}_{co} = \bar{P}_{ci} = 0.660 \cdot 10^5$ N (o = outer, i = inner).

6.4.3 Numerical results

Before moving force response quantities are shown the eigen-frequencies of the structure are studied. By means of these frequencies the discrepancy between different structural models can be evaluated. In addition, the natural frequencies help to under-stand the structural behaviour due to moving loads. Eigenfrequencies of the structure for four different cases are shown in Table 6.3. It can be seen that the numerical solution in the second column is in good agreement with the corresponding analytical one in the third column. It can also be recognized that the coupling effects due to

Mode	Present analysis		Exact [20][21]	
	$R=\infty, z_p=-0.0135$ m	$R=\infty$, $z_p=0$	$R=\infty$, $z_p=0$	$R=2500$ m, $z_p=0$
1	4.79319	4.79320	4.79320	–
2	5.18079	5.18079	5.18079	5.18062
3	19.1726	19.1728	19.1728	–
4	20.7232	20.7232	20.7232	20.7230
5	28.5836	28.5835	28.5835	28.5840
6	43.1387	43.1398	43.1388	–
7	46.6282	46.6282	46.6271	46.6269
8	57.1675	57.1670	57.1670	57.1673
9	76.6913	76.6960	76.6912	–
10	82.8978	82.8978	82.8926	82.8923
11	85.7526	85.7505	85.7505	85.7508
12	114.341	114.334	114.334	114.334
13	119.873	119.894	119.830	–
14	129.589	129.589	129.520	129.519
15	142.943	142.918	142.918	142.919

Table 6.3. Eigenfrequencies f_i (Hz) of the structure in Fig. 6.15. Four different cases. The middle two columns contain eigenfrequencies due to uncoupled vibrations: lateral vibrations (modes 1,3,6,9 and 13), vertical (2,4,7,10 and 14) and torsional (5,8,11,12 and 15). (Axial vibrations are not considered).

z_p = -0.0135 m (first column) and R = 2500 m (last column) are very small. Even for the case of R = 500 m (z_p = 0) the eigenfrequencies deviate less than 0.1 per cent from the uncoupled ones. Note that for $z_p \neq 0$ (R = ∞) the lateral-torsional modes are coupled while the vertical-torsional modes are coupled for R < ∞ (z_p = 0). In conclusion, the coupling effects due to z_p = -0.0135 m and R = 2500 m which arise in the present example may be ignored. Since the present beam element is capable of handling cases with $z_p \neq 0$, however, this coupling effect is retained in the analysis.

The structural response due to the moving forces in Fig. 6.16 is studied now. The midspan displacements $u_y(L/2,t)$ and $u_z(L/2,t)$, with reference to the pole P, as well as the midspan rotation $\theta_x(L/2,t)$ are investigated first. The quasistatic and dynamic moving force responses of these quantities are illustrated in Fig. 6.17. From Fig. 6.17 it can be seen that a significant dynamic magnification is obtained for u_y and u_z while the dynamic beam rotation is close to the quasistatic one. The dynamic magnification factors in Figs. 6.17a-c are 1.49, 1.43 and 1.01 respectively. The low factor for the rotation is not surprising since the lowest torsional eigenfrequency is high in comparison with the lowest bending eigenfrequencies, see Table 6.3. It may also be recognized from Fig. 6.17c that the dynamic solution oscillates about the quasistatic one at the lowest torsional eigenfrequency. (Note that an analytical solution for θ_x has been used to some extent to cope with the discontinuity of θ_x' at t/τ = 0.50 in Fig. 6.17c).

Next, the midspan moments corresponding to the quantities in Fig. 6.17 are studied. In Fig. 6.18 the moment time histories are given. A pattern similar to that in Fig. 6.17 can be seen in Fig. 6.18. (The dynamic oscillations have been somewhat exaggerated in Fig. 6.18c for clarity). The dynamic magnification factors in Figs. 6.18a-c are 1.40, 1.36 and 1.00 respectively.
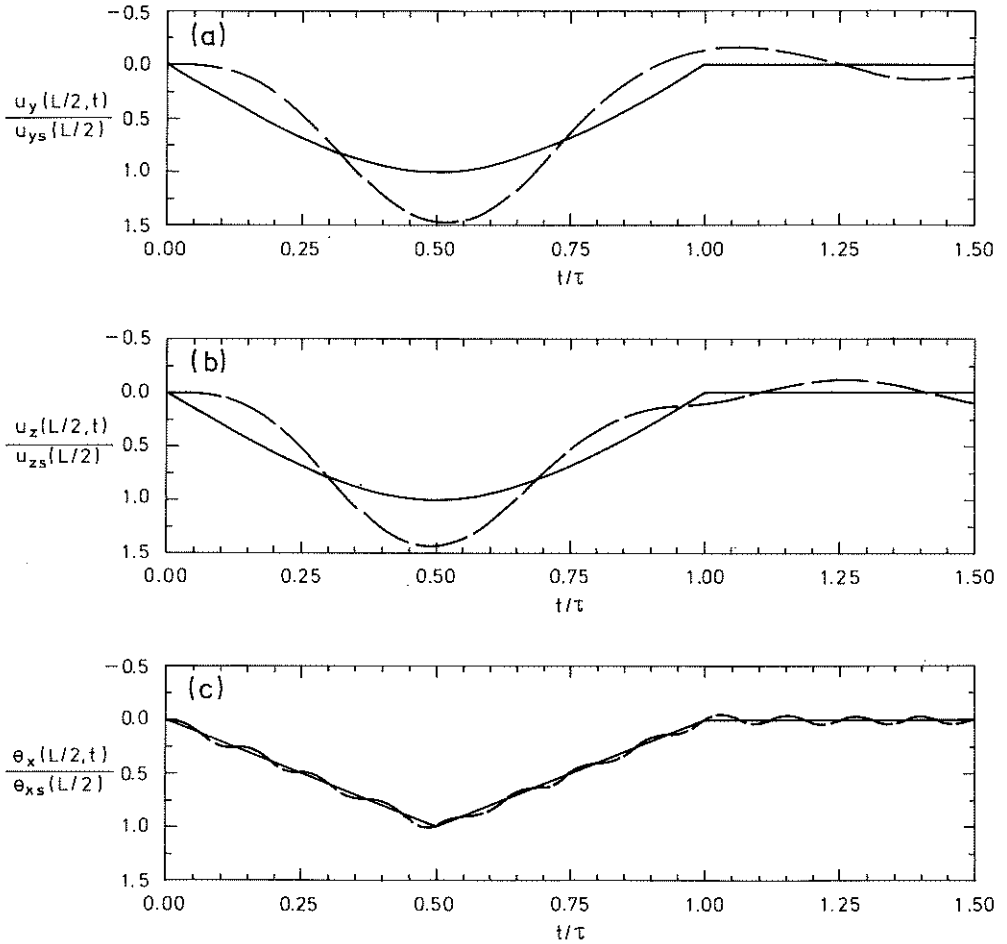
Figure 6.17. Time histories for normalized midspan displacements and rotation for the problem defined by Figs. 6.15 and 6.16, $0 \leq t/\tau \leq 1.5$. ——— Quasistatic; — — Moving force model. (15 modes, $\Delta t = 0.003$ s).

(a) Displacement $u_y(L/2, t)$ ($u_{ys}(L/2) = -2.471 \cdot 10^{-3}$ m).

(b) Displacement $u_z(L/2, t)$ ($u_{zs}(L/2) = 5.187 \cdot 10^{-3}$ m).

(c) Rotation $\theta_x(L/2, t)$ ($\theta_{xs}(L/2) = -1.392 \cdot 10^{-4}$ rad).
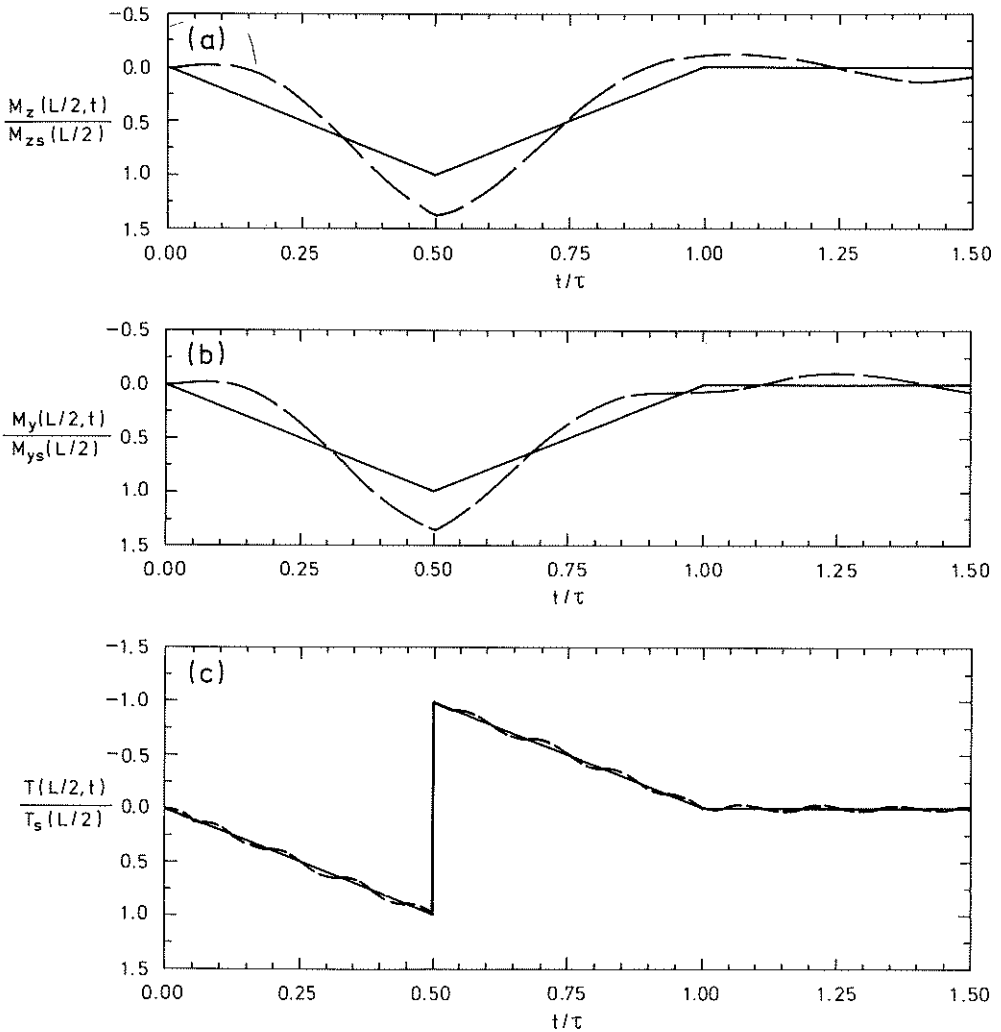
Figure 6.18. Time histories for normalized midspan moments for the problem defined by Figs. 6.15 and 6.16, $0 \leq t/\tau \leq 1.5$. ———— Quasistatic; — — Moving force model. (15 modes, $\Delta t = 0.003$ s).

(a) Bending moment $M_z(L/2, t)$ ($M_{zs}(L/2) = 0.990 \cdot 10^6$ Nm).

(b) Bending moment $M_y(L/2, t)$ ($M_{ys}(L/2) = 2.428 \cdot 10^6$ Nm).

(c) Torsional moment $T(L/2, t)$ ($T_s(L/2) = 1.334 \cdot 10^5$ Nm).

The bending-torsional behaviour of a simple beam structure under moving loads has been studied in this example. It can be concluded that the coupling effects for a slightly curved beam of closed cross section may be small. It is also recognized that the lowest eigenfrequency for each action (bending or torsion) constitutes a measure of the degree of dynamic magnification.

6.5   Large scale beam structure

6.5.1 General remarks

In the last numerical example, the behaviour of a large scale beam structure under moving loads is studied. The vehicle is modelled as both a moving force system and as a suspension system. In contrast to the example of Sec. 6.4, warping torsion of the structural members is considered here. Thus a rather general moving load problem is studied demonstrating some of the possibilities of the theory and tools developed. The structure and vehicle models are described in Subsec. 6.5.2 and numerical results are presented in Subsec. 6.5.3. The numerical results are mainly given in terms of time histories of contact forces, displacements, rotations and normal stresses. Dynamic magnification factors are also investigated. In particular, the magnification factors due to moving force and suspension vehicle models as well as code factors are compared.

6.5.2 Structure and vehicle models

The structural model considered in this example is a steel grid lying in a horizontal plane. The moving loads are acting on the structure in the vertical direction only, that is perpendicular to the plane of the grid. The structural model is shown in Fig. 6.19 and pertinent cross sectional data are given in Table 6.4.
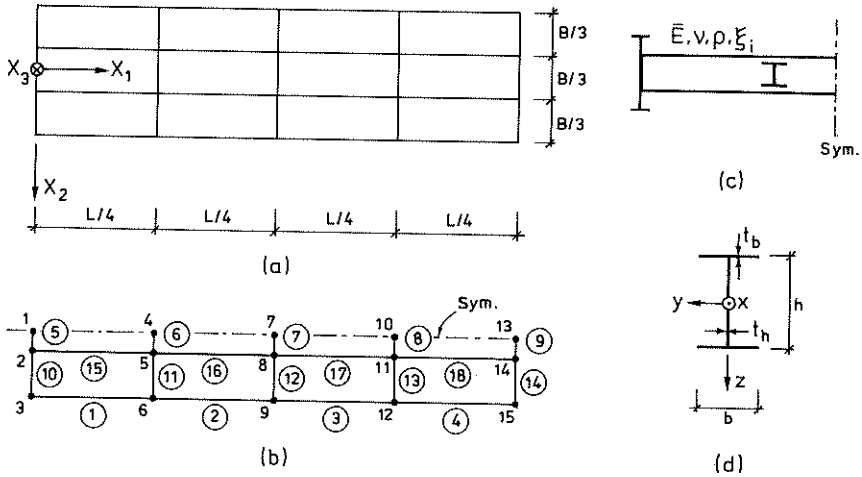
Figure 6.19. Structural model.

(a) Top view of symmetric steel grid structure. Global reference coordinate system (X_1, X_2, X_3). The members are rigidly connected to each other and the end cross beams are simply supported at their third points. The grid is initially at rest. Data: B = 5.4 m and L = 20 m.

(b) Finite element discretization (half structure). 18 uniform Euler–Bernoulli/Vlasov beam elements. One additional eigenfunction in torsion is included for the main and sleeper beam elements. For the sleeper beam elements one eigenfunction in bending is included as well (cf. Sec. C.3).

(c) Cross sectional view (half structure). Material data: $\bar{E} = E = 2.1 \cdot 10^{11}$ Pa, $\upsilon = 0.3$, $\rho = 7800$ kg/m^3 and $\xi_i = 0.02$ except for the sleeper beams which have $\rho = 15600$ kg/m^3 to take into account the non-structural mass of sleepers and rails.

(d) Cross sectional view of a single I-beam. The cross sectional data for the three different beam sections are given in Table 6.4.

Beams	Elements	b(m)	h(m)	t_b(m)	t_h(m)
Main beams (HEA 1000)	1 to 4	0.300	0.990	0.031	0.0165
Cross beams (HEA 500)	5 to 14	0.300	0.490	0.023	0.012
Sleeper beams (HEA 340)	15 to 18	0.300	0.330	0.0165	0.0095

Beams	$A(m^2)$ $\times 10^2$	$I_y(m^4)$ $\times 10^4$	$I_z(m^4)$ $\times 10^4$	$K_v(m^4)$ $\times 10^6$	$I_\Omega(m^6)$ $\times 10^6$
Main beams (HEA 1000)	3.468	55.38	1.400	8.250	32.10
Cross beams (HEA 500)	1.975	8.697	1.037	3.100	5.640
Sleeper beams (HEA 340)	1.335	2.769	0.744	1.280	1.820

Table 6.4. Cross sectional data for the I-beams in Fig. 6.19. Secondary warping is not included in the warping moment of inertia I_Ω.

As can be concluded from Fig. 6.19 and Table 6.4, in the present example warping torsion effects are considered in addition to Saint Venant torsion (mixed torsion). For beams of open cross section, which are adopted here, the warping torsional effect may be signifi- cant. As mentioned in Chapter 3, warping torsion of beams of open cross section is often referred to as Vlasov torsion and the inclusion of warping torsion gives rise to a rate of twist DOF at each beam element end. In this example restrained warping ($\theta_x' = 0$) is assumed at the beam ends while warping continuity is presupposed at the internal nodes of the beams, cf. Subsecs. 3.4.2 and 6.5.3. It should also be mentioned that the inclusion of secondary warping only increases I_Ω by about 0.1 per cent, cf. Table 6.4.

The fact that only half the structure in Fig. 6.19a is considered, see Figs. 6.19b-c, demands the moving loads to be symmetric with respect to the symmetry line indicated. This is also the case here since the vehicle is moving along the sleeper beams and the vehicle properties are symmetric. The vehicle models used in the present example are shown in Fig. 6.20, cf. Figs. 4.3 and 4.4. It should be recognized from Figs. 6.19 and 6.20 that the vehicle to structure mass ratio exceeds 2: $\kappa = 50000/23465 \approx 2.13$ (cf. the guide in Subsec. 6.2.4).
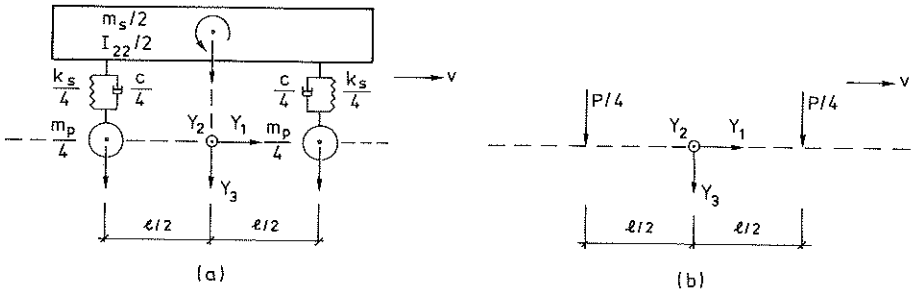
Figure 6.20. Vehicle models (half vehicle). The vehicle is moving at constant speed $v = 80$ m/s (288 km/h). Axle distance $\ell = 7.5$ m. Reference coordinate system (Y_1, Y_2, Y_3). The vehicle moves along the sleeper beam of Fig. 6.19b.

(a) Suspension model. The four nonzero DOF are indicated. The vehicle is at rest (relative to Y) when it enters the structure. Data: $m_p = 4 \cdot 10^3$ kg, $m_s = 4.6 \cdot 10^4$ kg, $I_{22} = 2.156 \cdot 10^5$ kgm^2, $c = 2 \cdot 10^5$ Ns/m and $k_s = 8 \cdot 10^6$ N/m.

(b) Moving force model. Vehicle dead weight $P = (m_p + m_s)g$.

6.5.3 Numerical results

As in all other examples of this study, modal coordinates are used for the structure here. Just as in Sec. 6.4 some comments are given on the structural eigenfrequencies associated with the modal coordinates, before presenting the moving load results.

The finite element model of Fig. 6.19b contains 59 unconstrained DOF. From this model, the lowest 12 (symmetric) eigenmodes and eigenfrequencies are determined to be used in the moving load analysis. The 12 eigenfrequencies range from f_1 = 5.73 Hz, f_2 = 19.3 Hz to f_{12} = 41.4 Hz. It should be mentioned that the first eigenmode contains almost exclusively pure bending of the main beams and sleeper beams. Using f_{10} as a comparison quantity, it is interesting to note that f_{10} is decreased from 40.5 Hz to 27.4 Hz if warping torsion of the structural members is neglected (i.e. pure Saint Venant torsion is assumed). Also note that f_{10} is decreased to 33.3 Hz if free warping of the beam ends is assumed (cf. Subsec. 6.5.2) and that it is almost identical, f_{10} = 40.4 Hz, when rotatory and warping inertia are taken into consideration.

In contrast to other moving load results of this study, the numerical results are not normalized in this example (except for the time parameter t/τ). This is because a more direct idea of the structural response is to be obtained. First, however, the suspension contact forces are compared with the moving force values, see Fig. 6.21. From Fig. 6.21 it may be seen that the overall pattern of the suspension contact forces is a decrease from the static value P/4 on the first half of the structure and an increase on the second half, cf. Sec. D.4. The cross beams give rise to the oscillations about this general trend. This can be clearly distinguished for the front contact force, see Fig. 6.21a. The discontinuity in the contact force when the axles (wheels) depart from the structure at t/τ = 1.0
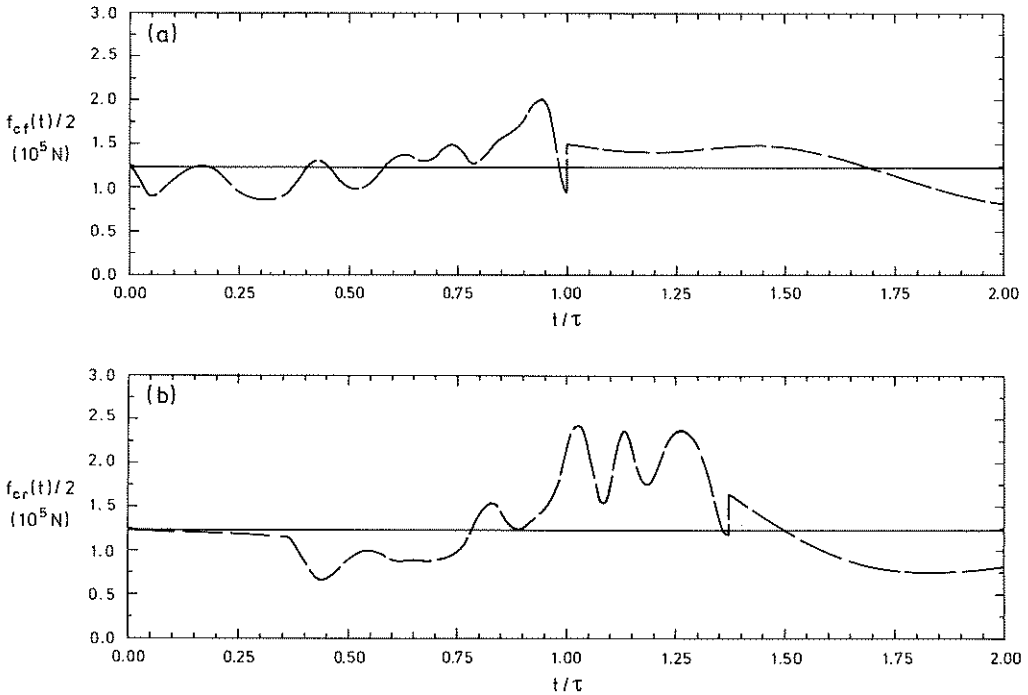
Figure 6.21. Time histories for contact forces of the front and rear
wheels for the problem defined by Figs. 6.19-20 and
Table 6.4, $0 \leq t/\tau \leq 2$. ——— Moving force model;
— — Suspension model. (12 modes, $\Delta t = 0.0025$ s).
(a) Front contact force $f_{cf}(t)$.
(b) Rear contact force $f_{cr}(t)$.

and $t/\tau = 1.375$ can also be identified. The real behaviour at the
exit (slope) discontinuity is very complex to describe and the
present vehicle model gives a less satisfactory description of this
effect. However, with the interest focused on the overall structural
behaviour due to moving loads this should be of minor importance. It
is also interesting to note that if the unsuspended mass is
increased from the present 8 per cent to about 14 per cent of the
total vehicle mass the contact is lost at the exit, cf. Secs. 2.4
and D.3.

Now the midspan deflection and rotation of the main beams are studied. Three different time histories for these quantities are shown in Fig. 6.22. It can be seen from Fig. 6.22a that the maximum midspan main girder deflection is quite large: almost 30 mm for all the three models. This maximum displacement is about 5 to 6 times greater than the corresponding ones in Secs. 6.3 and 6.4. (Together with the high mass ratio, $\kappa = 2.13$, this large deflection helps to explain the large contact force discrepancy in Fig. 6.21). In Fig. 6.22a the quasistatic maximum displacement 27.3 mm is increased to 29.7 mm for the moving force model (D = 1.09) and to 29.3 mm (D = 1.07) for the suspension model. The ORE code curve shown in Fig. 6.8, which is valid for main girders, suggests however a value as high as D = 1.45 ($\alpha \approx 0.35$). It is therefore reasonable to believe that the main girders are overdesigned if the ORE code is adopted for the present case.

With respect to the midspan rotation, Fig. 6.22b, a peak in the suspension model curve at about $t/\tau = 1.03$ makes it different from the other two curves. Absolute maximum values of midspan main beam rotation are: $1.79 \cdot 10^{-3}$ rad for the quasistatic case, $2.00 \cdot 10^{-3}$ rad for the moving force model (D = 1.12) and $2.74 \cdot 10^{-3}$ rad for the suspension model (D = 1.53). Thus the moving force model considerably underestimates the maximum dynamic response.

Finally, the time histories of a normal stress are investigated. The normal stress studied is that at the lower left corner of the cross section of to the centre cross beam at midspan (node 7). Results are presented for three different cases in analogy with Fig. 6.22. In addition, the present stress is decomposed into a bending moment part and a bimoment part. The results are shown in Fig. 6.23.
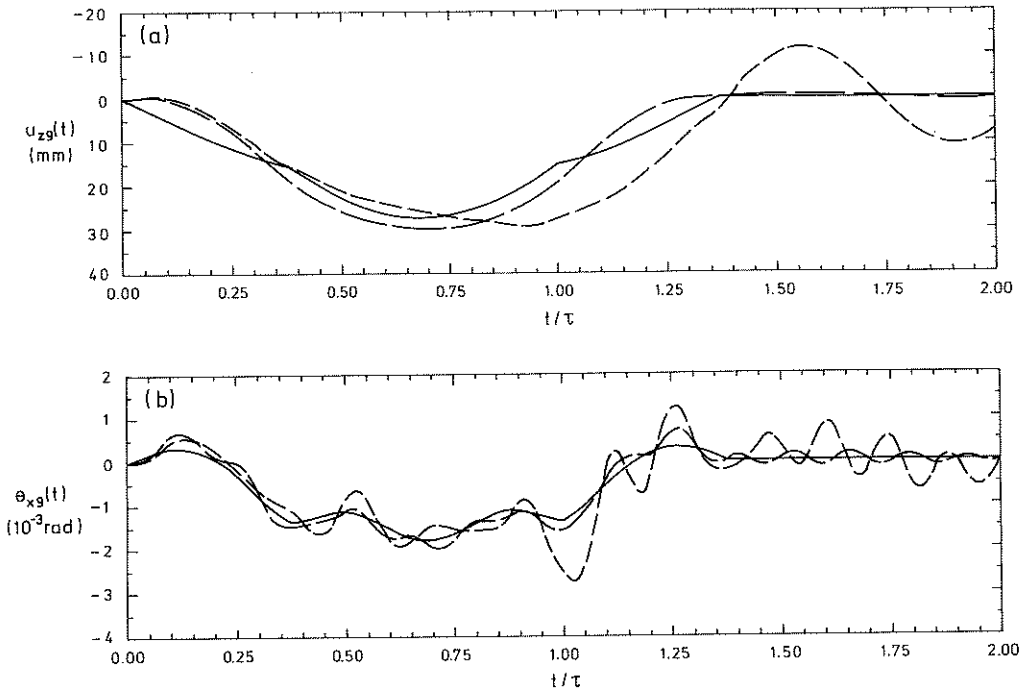
Figure 6.22. Time histories for midspan main beam displacements for the problem defined by Figs. 6.19–20 and Table 6.4, $0 \leq t/\tau \leq 2$. ——— Quasistatic; — — Moving force model; – – – Suspension model. (12 modes, $\Delta t = 0.0025$ s).
(a) Displacement $u_z(t)$ at node 9.
(b) Rotation $\theta_x(t)$ at node 9.

The pattern in Fig. 6.23a is similar to that in Fig. 6.22b with a peak in the suspension model curve. Maximum stresses are: 52.2 MPa for the quasistatic case, 56.2 MPa for the moving force model ($D = 1.08$) and 93.4 MPa ($D = 1.79$) for the suspension model. Once again it is thus evident that the moving force model considerably underestimates the maximum dynamic response. From Fig. 6.23b it is seen that the normal stresses over the actual cross section contribute more to the bending moment than to the bimoment. However the ratio $\max[\sigma(B)]/\max[\sigma(M_y)]$ is increased from 0.13 for the quasistatic case to 0.19 for the suspension model case.
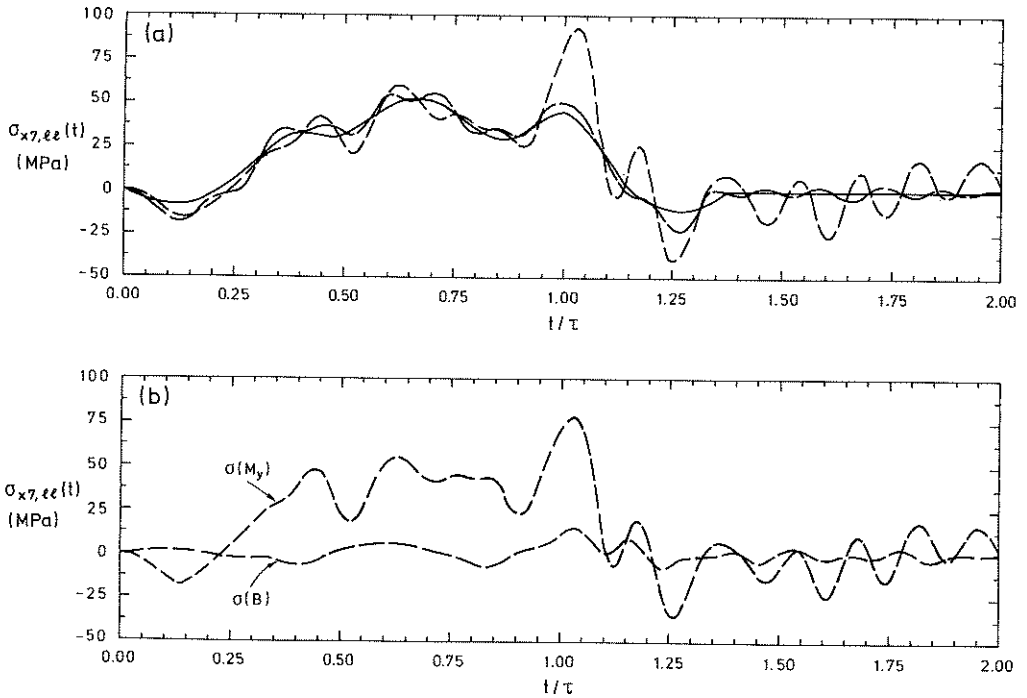
Figure 6.23. Time histories for normal stress at midspan of centre cross beam (lower left corner) for the problem defined by Figs. 6.19–20 and Table 6.4, $0 \leq t/\tau \leq 2$. ——— Quasistatic; — — Moving force model; — — — Suspension model. (12 modes, $\Delta t = 0.0025$ s).

(a) $\sigma_x(t)$ at node 7 (lower left corner).

(b) Decomposition of $\sigma_x(t)$: Bending moment part $\sigma(M_y)$ and bimoment part $\sigma(B)$.

In conclusion, some of the possibilities of the theory and tools developed in the present study have been shown in this example. It is also shown that the dynamic response predicted by the moving force vehicle model may be significantly in error, cf. Table 6.2 and note the large mass ratio here. The same may also apply to a design code. The problem of discontinuities of the structural surface and, as a consequence, the contact force histories is also touched upon.

7.   CONCLUDING REMARKS

7.1   Conclusions

The research work described in this thesis is concerned with analysis of structures subjected to moving loads. The main features of the work are structure–vehicle interaction, finite element formulations and numerical simulations.

The advantage of deriving the basic equations for the structure, the vehicle and their interaction within the finite element concept is indicated in Chapter 2. In particular, it is concluded that the structure–vehicle finite element derived serves as an efficient analysis tool. This interaction element is believed to be novel. From a number of verification examples it is found that an analysis by means of the present element gives results in good agreement with experimental results and results from other numerical simulations (Appendix D).

The limitation to beam structures, different beam theories and different finite beam element formulations are discussed in Chapter 3. It is concluded that the hierarchical finite beam element derived also serves as a good analysis tool. To the author's knowledge the present hierarchical formulation in terms of eigenfunctions has not appeared previously in the literature. The good performance of the proposed beam element is indicated by a number of verification examples (Appendix C).

In Chapter 4 different types of vehicle models are distinguished and their applicability is discussed (cf. Appendix D). It is found that especially the suspension models and the moving force models are useful. The importance of comparing structural effects due to different vehicle models is also made clear.

The time discretization and choice of solution algorithm for the present equations of motion are debated in the light of weighted residuals in Chapter 5 (cf. Subsec. 2.2.4). The usefulness of the computer program CAMFEM extended by problem-dependent commands is also emphasized in this chapter.

A number of numerical simulations of structures subjected to moving loads are treated in the present work. While introductory moving load problems are studied in Appendix D as verification, more complex problems are investigated in Chapter 6. In particular, the effect of dynamic magnification of structural quantities for different vehicle models and parameters is discussed in this chapter. It is concluded that four nondimensional parameters may serve as a rough guide in the choice of vehicle model for many moving load problems. For instance, it is seen that the moving force model may be sufficient for a low parameter value of the velocity ratio α or the mass ratio κ. It is also argued that the structural design would be more economic in some situations if the traditional quasistatic moving load analysis were extended or replaced by a dynamic analysis. Finally, it can be concluded that the longitudinal structure-vehicle interaction may be substantial for noninertial vehicle motion.

7.2   Future developments

Most of the assumptions introduced in the present research work are listed at the end of Secs. 2.1 and 3.1. It is therefore natural to utilize these lists when suggesting possible future developments. Such further research work is indicated below.

Geometric and material nonlinearities of the structure, neglected in Sec. 2.2, may be of importance when for instance special support arrangements or prestressed structures are used. Nonlinear damper and spring vehicle elements, active control elements and deformable

vehicle body elements should also be treated in order to determine the influence on the structural response. The same applies to contact loss – recontact and structural irregularities, cf. Sec. 2.4. In particular, simultaneously treatment of structure–vehicle interaction and structural irregularities is of interest in future research.

In many moving load analyses, beam structural models are relevant (Chapter 3). However, there is a need to compare different beam models with models based on plate and shell theories and beam theories which take into account deformable cross sections. It would also be of interest to apply the structure–vehicle finite element developed on structural elements other than beam elements.

Simple tools for determining the steady state motion of a vehicle travelling on a repetitive guideway structure are needed. Further, additional comparisons between structural responses obtained by means of moving force and suspension vehicle models respectively are also needed. Results of such comparisons should also be evaluated against quasistatic results in order to improve existing design codes.

APPENDIX A. NOTATIONS

Notations are explained in the text where they first occur. Most of the notations are given also in this appendix.

Latin letters

A	cross sectional area
A	additional (hierarchical) displacement field vector
A_b	spin tensor of vehicle body
a	vehicle acceleration
B	bimoment
b	vehicle body number ($b = 1,2\ldots n_b$); beam width
C_{IJKL}	material tensor components
C_{si}^m	modal damping coefficients of structure
$\bar{C}_s^e, C_s^e$	local/global damping matrix of structure element
$\bar{C}_v^e, C_v^e$	local/global damping matrix of vehicle element
c^e, c^{em}	nodal/modal damping matrix of structure–vehicle element
C_s	damping matrix of structure
C_v	damping matrix of vehicle
$C, {}^0C, {}^1C$	damping matrices of structure–vehicle system
c	vehicle damper viscosity (secondary)
D, D_d, D_m	dynamic magnification factors
D	material matrix
$D_\epsilon, D_\gamma, D_p, \bar{D}_p, D_s$	beam property matrices
$E, \bar{E}$	unmodified/modified elastic modulus
E	Green strain tensor
e_{Xi}, e_{Yi}, e_{Zbi}	unit base vectors
F_b, F_{qb}	force/load vector

F	deformation gradient tensor
$f_c, f_{cf}, f_{cr}, \bar{f}_{cf}$	contact forces
f_i	eigenfrequencies (Hz)
G	shear modulus
g	acceleration of gravity ($g = 9.81$ m/s^2)
H	vertical radius of curvature of vehicle path
H	beam transformation matrix
h	beam height, vehicle height
I_p	polar moment of inertia
I_y, I_z	moments of inertia
I_{yz}	product of inertia
I_Ω	warping moment of inertia
$I_{y\Omega}, I_{z\Omega}$	warping products of inertia
I_{11}, I_{22}, I_{33}	principal moments of inertia with respect to centre of gravity of vehicle body
I_{bo}	inertia tensor with respect to centre of gravity of vehicle body
K_v	Saint Venant torsion constant
$\bar{K}_s^e - {}^1K$	stiffness matrices analogous with $\bar{C}_s^e - {}^1C$
$\hat{K}$	effective stiffness matrix of structure-vehicle system
k_p, k_s, k_ℓ	vehicle spring stiffness (primary/secondary /longitudinal)
L	beam (element) length
ℓ, ℓ_1, ℓ_2	vehicle axle distance/length
M_y, M_z	bending moments
M_{ys}, M_{zs}	static bending moments
M_{si}^m	modal masses of structure
$\mathbf{M}_{bo}, \mathbf{M}_{qbo}$	moment/load vector
$\bar{M}_s^e - {}^1\mathbf{M}$	mass matrices analogous with $\bar{C}_s^e - {}^1C$

m,n	indices ranging from 1 to the number of degrees of freedom of the structure element
m, m_b	vehicle body mass
m_p, m_s	vehicle body mass (primary/secondary)
N	normal force
$\hat{N}_J, n_x, n_y, n_z$	direction cosines
$\left. {}^0N_u, {}^0N_{\dot{u}}, {}^0N_{\ddot{u}}, {}^1N_u \atop {}^0N, {}^1N \right\}$	shape functions (in time)
$\bar{N}, N^e$	local/global shape function matrix
N^e_c	value of shape function matrix at point of contact
$\bar{N}_{yz}, \bar{N}_x, \bar{\bar{N}}_x$	shape function matrices
$\bar{\bar{N}}_\alpha$	displacement function matrix
n_b	number of vehicle bodies
n	direction cosine matrix
0	origin
P	pole, dead weight of vehicle
$\left. P, P_{cf}, P_{cr}, \bar{P}_{cf}, \bar{P}_{cr} \atop P_{co}, P_{ci}, \bar{P}_{co}, \bar{P}_{ci} \right\}$	moving forces
P^m_{qsi}	modal loads of structure
$\bar{P}^e_{qs}, P^e_{qs}$	local/global load vector of structure element
$\bar{P}^e_{qv}, P^e_{qv}$	local/global load vector of vehicle element
P^e_q, P^{em}_q	nodal/modal load vector of structure-vehicle element
P_{qs}	load vector of structure
P_{qv}	load vector of vehicle
$P, {}^0P, {}^1P$	load vectors of structure-vehicle system
$\hat{P}$	effective load vector of structure-vehicle system

$\bar{P}^e_s - P^{em}$	force vectors analogous with $\bar{P}^e_{qs} - P^{em}_q$
$\bar{P}^e_Z, P^e_Z$	local/global noninertia load vector of vehicle element
P^e_Z, P^{em}_Z	nodal/modal noninertia load vector of structure-vehicle element
P_Z	noninertia load vector of vehicle
$\overset{=}{P}_{x\epsilon}, \overset{=}{P}_{x\gamma}, \overset{=}{P}_{x1}, \overset{=}{P}_{x2}$	stress resultant vectors
Q	superelevation angle
$\mathbf{Q}$	transformation matrix
$\overset{=}{\mathbf{q}}_{x1}, \overset{=}{\mathbf{q}}_{x2}$	distributed load vectors
R	horizontal radius of curvature of vehicle path
R_{XY}, R_{XZb}, R_{YZb}	reference translation vectors
r_b	absolute translation vector of vehicle body
r_{bo}	absolute translation vector of centre of gravity of vehicle body
$\tilde{r}^e_{sc}, r^e_{sc}$	irregularity vectors evaluated at point of contact
S, S^e	reference boundary surfaces of structure
S_y, S_z	static moments
$\bar{S}_y, \bar{S}_z$	modified static moments
S_Ω	warping static moment
S_{XY}, S_{XZb}, S_{YZb}	reference rotation tensors
s	vehicle path coordinate
s_b	absolute rotation tensor of vehicle body
T	torsional moment
T_s	static torsional moment
T_{sv}, T_w	Saint Venant/warping torsional moment
T, T_1, T_2	beam transformation matrices
T_{cu}, T_{cr}, T^m_{cu}	transformation matrices at point of contact
T_{XY}	transformation matrix relating basis Y to X

$\tilde{T}$	second Piola-Kirchhoff stress tensor
$\tilde{t}_I$	second Piola-Kirchhoff tractions
$t, \bar{t}, t_0, t_1$	time
t, t_b, t_h	beam wall thicknesses
U_i	global body loads
$\bar{U}_x, \bar{U}_y, \bar{U}_z$	local body loads
$\bar{U}, \bar{U}_\ell$	(local) body/traction load vectors
u_i	(global) displacement components
u_v, u_{vf}, u_{vr}	vehicle contact displacements
u_{vs}	static vehicle contact displacement
u_{xs}, u_{ys}, u_{zs}	static beam displacements
u_γ	warping displacement due to shear strains
$\bar{u}$	(local) displacement vector: $\bar{u} = [u\ v\ w]^T$
$\tilde{\bar{u}}_x$	beam displacement vector: $\tilde{\bar{u}}_x = [u_x\ u_y\ u_z\ \theta_x$ $u_y'\ u_z'\ \theta_x']^T$
$\bar{\bar{u}}_x$	beam displacement vector: $\bar{\bar{u}}_x = [u_x\ u_y\ u_z\ \theta_x]^T$
u_{si}^m	modal displacements of structure
$\bar{u}_s^e - {}^1u$	displacement vectors analogous with $\bar{P}_{qs}^e - {}^1P$
$\tilde{u}_{sc}^e, u_{sc}^e$	displacement vectors evaluated at point of contact
V, V^e	reference volumes of structure
V_y, V_z	shear forces
v	vehicle speed (m/s)
$v_{bo}, \dot{v}_{bo}$	absolute translational velocity/acceleration vector of centre of gravity of vehicle body
W_{imp}, W_{im}^X, W_p^t	weighting functions
$\bar{W}, \bar{W}_{yz}, \bar{W}_x$	weighting function matrices

$\mathbf{w}_b$	relative displacement vector of vehicle body
$\mathbf{w}_{bo}$	relative displacement vector of centre of gravity of vehicle body
X,Y,Z_b	reference frames
X,Z_b	reference position vectors (material coordinates)
x,y,z	(local) beam coordinates
x,z_b	current position vectors (spatial coordinates)
y_I,z_I	intermediate beam end coordinates
y_p,z_p	beam cross sectional coordinates of P relative O

Greek letters

A,B,Γ	rotation angles defining $\mathbf{S}_{XY}$
α	vehicle to structure velocity ratio
$\alpha_Z,\beta_Z,\gamma_Z$	Zienkiewicz time weighting parameters
$\bar{\alpha},\alpha,\beta,\gamma,\delta$	time weighting parameters
$\boldsymbol{\alpha}$	beam displacement coefficient vector
β_N,γ_N	Newmark step-by-step integration parameters
$\boldsymbol{\beta}_i$	displacement vectors
$\gamma_{xy},\gamma_{xz},\gamma_{yz}$	shear strains
$\Delta C,\Delta K,\Delta M$	incremental damping, stiffness and mass matrix
ΔP	incremental load vector
Δt	time step
δ_{IJ}	the Kronecker delta
$\epsilon_x,\epsilon_y,\epsilon_z$	normal strains
ϵ	beam strain vector
ζ_b	relative rotation tensor of vehicle body
θ	Wilson θ parameter, subtended angle of curved structure
θ_{xs}	static beam rotation
κ	vehicle to structural span mass ratio
κ_0	vehicle primary to secondary suspension mass ratio

κ_1	vehicle moment of inertia ratio
λ	vehicle axle distance to structural span ratio
λ, μ	Lamé elastic constants
υ	Poisson's ratio
ξ	time parameter
ξ_i	modal damping ratios
ξ_v	vehicle damping ratio
ρ	mass density
Σ	summation sign
$\sigma_x, \sigma_y, \sigma_z$	normal stresses
σ	beam stress vector
$\tilde{\sigma}$	stress vector
$\bar{\sigma}, \bar{\bar{\sigma}}$	stress resultant derivative vectors
τ	vehicle traversing time (each axle)
$\tau_{xy}, \tau_{xz}, \tau_{yz}$	shear stresses
ϕ_{svy}, ϕ_{svz}	Saint Venant shear strain functions
Φ, Φ^e	eigenvector matrices: $\Phi = [\varphi_1 \ \varphi_2 \ldots]$ etc.
φ_i	eigenvectors
χ	vehicle primary to secondary suspension stiffness ratio
χ_i	additional (cross sectional) beam displacements
ψ_i	additional (cross sectional) shape functions
ψ_b	relative rotation vector of vehicle body
Ω	structure to vehicle frequency ratio
$\bar{\Omega}, \Omega$	warping coordinates
$\Omega_{XY}, \Omega_{YZb}$	rotational (angular) velocity vectors of reference frames
ω_i	circular eigenfrequencies (rad/s)
ω_v	vehicle circular eigenfrequency (rad/s)
$\omega_b, \dot{\omega}_b$	absolute rotational (angular) velocity/acceleration vector of vehicle body

Other notations

$\mathscr{L}$	contour of beam cross section
$\mathbf{1}$	unit tensor, unit matrix
$\mathbf{0}$	zero vector, zero matrix, zero tensor
$\times$	cross product
$(\cdot)^T$	transpose of $(\cdot)$
$\dfrac{\partial}{\partial(\cdot)}$	partial derivative with respect to $(\cdot)$
$\dfrac{d}{d(\cdot)}$	material derivative with respect to $(\cdot)$
$d(\cdot)$	differential of $(\cdot)$
$(\dot{\cdot}),(\ddot{\cdot})$	first/second time derivative of $(\cdot)$
$(\cdot)',(\cdot)''$	first/second spatial derivative of $(\cdot)$
∇	operation matrices $(\tilde{\nabla},\ \nabla_a,\ \bar{\nabla}_a,\ \nabla_b,\ \bar{\nabla}_b,\ \nabla_\epsilon,\ \nabla_\gamma,$ $\nabla_p,\ \nabla_s,\ \nabla_{q1},\ \bar{\nabla}_{q1},\ \nabla_{q2})$

APPENDIX B.   VEHICLE ELEMENT MATRICES

B.1   Introduction

The vehicle in the present study consists of three different elements: rigid bodies, linear viscous dampers and linear elastic springs. The basic equations for these elements are given in Eqs. (2.34), (2.35a) and (2.35b) respectively. In this appendix explicit expressions are given for the matrices inherent in these equations. The pertinent vectors are also given. These matrices and vectors are closely connected with the kinematic quantities introduced in Subsec. 2.3.1. These quantities are therefore described to begin with (Sec. B.2). It should be noted that all relations in Subsec. 2.3.1 are described in terms of vectors and tensors without reference to any particular set of base vectors or components. In Sec. B.2, however, choices of such sets are necessary in order to develop explicit expressions.

B.2   Description of kinematic quantities

B.2.1 Displacements

The absolute translations and rotations of each rigid body are expressed in Subsec. 2.3.1 as

$$r_{bo} = R_{XY} + R_{YZb} + w_{bo} \tag{2.29a}$$

and

$$s_b = \zeta_b S_{YZb} S_{XY} \tag{2.29b}$$

respectively. The reference translation vectors R_{XY} and R_{YZb} are now expressed in component form as related to the base vectors e_{Xi} and

$\mathbf{e}_{Yi}$ respectively (see Fig. 2.1). Thus, with summation on i only

$$\mathbf{R}_{XY} = R_{XYi}\mathbf{e}_{Xi} \qquad (B.1a)$$

and

$$\mathbf{R}_{YZb} = R_{YZbi}\mathbf{e}_{Yi} \qquad (B.1b)$$

where the components R_{YZbi} are constant. Further, the relative translation vector $\mathbf{w}_{bo}$ in Eq. (2.29a) is expressed in $\mathbf{e}_{Zbi}$ $(= \mathbf{e}_{Yi})$ as

$$\mathbf{w}_{bo} = w_{boi}\mathbf{e}_{Zbi}. \qquad (B.1c)$$

As far as the rotations are concerned, the reference rotation tensor $\mathbf{S}_{XY}$ is related to the orthogonal transformation matrix T_{XY} defined by

$$\mathbf{e}_{Yj} = T_{XYji}\mathbf{e}_{Xi} \qquad (B.2)$$

as

$$S_{XYij} = T_{XYji} = \mathbf{e}_{Xi} \cdot \mathbf{e}_{Yj}. \qquad (B.3a)$$

Thus $\mathbf{S}_{XY}$ consists of nine direction cosine terms with reference to the base vectors $\mathbf{e}_{Xi}$ or $\mathbf{e}_{Yi}$. Analogously the components of $\mathbf{S}_{YZb}$, with reference to $\mathbf{e}_{Yi}$ or $\mathbf{e}_{Zbi}$, are given by

$$S_{YZbij} = \mathbf{e}_{Yi} \cdot \mathbf{e}_{Zbj}. \qquad (B.3b)$$

Since $e_{Zbi} = e_{Yi}$, according to Subsec. 2.3.1, $S_{YZb} = 1$ (in any base). The rotation tensor ζ_b in Eq. (2.29b) represents small relative rotations which means that, approximately,

$$\zeta_b = \begin{bmatrix} 1 & -\psi_{b3} & \psi_{b2} \\ \psi_{b3} & 1 & -\psi_{b1} \\ -\psi_{b2} & \psi_{b1} & 1 \end{bmatrix} \tag{B.3c}$$

where ψ_{bi} are the small relative rotations of the rigid body defining the rotation vector ψ_b as

$$\psi_b = \psi_{bi} e_{Zbi}. \tag{B.4}$$

In contrast to ζ_b the rotation tensor S_{XY} represents finite rotations and cannot be described by a corresponding rotation vector. Nevertheless, the nine direction cosines of S_{XY} are dependent due to the six orthogonality conditions (cf. Eq. (B.3a))

$$S_{XYij}S_{XYik} = \delta_{jk} \tag{B.5}$$

in which $\delta_{jk} = \delta_{kj}$ is the Kronecker delta. Hence three (independent) coordinates are sufficient to describe the finite rotations related to S_{XY}. In, for instance, Magnus [68] different ways of choosing three angles as coordinates are described. Here the angles referred to as cardan angles are chosen. In addition to the reference frames X and Y, two intermediate frames $\bar{X}$ and $\bar{Y}$ are used to describe the rotation angles. The rotations are denoted by A, B and Γ and illustrated in Fig. B.1.
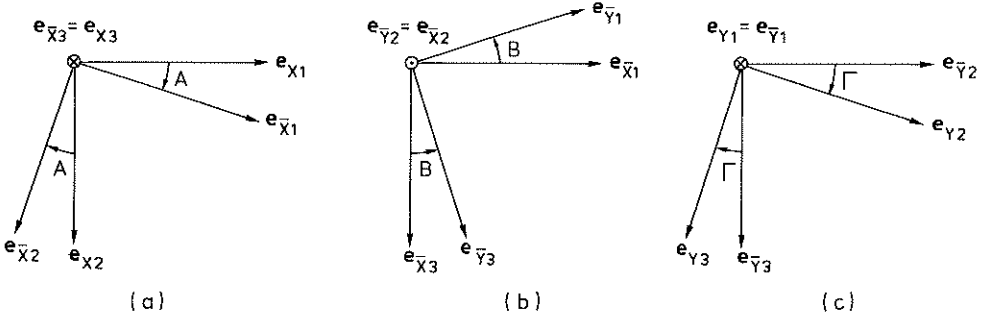
Figure B.1. Definition of rotation coordinates to represent the rotation tensor S_{XY}. Three consecutive rotations are defined.

(a) Positive rotation about $e_{\bar{X}3} = e_{X3}$ (A).

(b) Positive rotation about $e_{\bar{Y}2} = e_{\bar{X}2}$ (B).

(c) Positive rotation about $e_{Y1} = e_{\bar{Y}1}$ (Γ).

The change of basis from X to Y according to Fig. B.1 can be expressed by the three relations

$$
\begin{bmatrix} \bar{X}_1 \\ \bar{X}_2 \\ \bar{X}_3 \end{bmatrix} =
\begin{bmatrix} \cos A & \sin A & 0 \\ -\sin A & \cos A & 0 \\ 0 & 0 & 1 \end{bmatrix}
\begin{bmatrix} X_1 \\ X_2 \\ X_3 \end{bmatrix}
\tag{B.6a}
$$

$$
\begin{bmatrix} \bar{Y}_1 \\ \bar{Y}_2 \\ \bar{Y}_3 \end{bmatrix} =
\begin{bmatrix} \cos B & 0 & -\sin B \\ 0 & 1 & 0 \\ \sin B & 0 & \cos B \end{bmatrix}
\begin{bmatrix} \bar{X}_1 \\ \bar{X}_2 \\ \bar{X}_3 \end{bmatrix}
\tag{B.6b}
$$

and

$$
\begin{bmatrix} Y_1 \\ Y_2 \\ Y_3 \end{bmatrix} =
\begin{bmatrix} 1 & 0 & 0 \\ 0 & \cos \Gamma & \sin \Gamma \\ 0 & -\sin \Gamma & \cos \Gamma \end{bmatrix}
\begin{bmatrix} \bar{Y}_1 \\ \bar{Y}_2 \\ \bar{Y}_3 \end{bmatrix}
\tag{B.6c}
$$

where X_i are coordinates referring to e_{Xi} and so on. By means of Eqs. (B.6a–c), (B.2) and (B.3a) the explicit expression of S_{XY} in terms of A, B and Γ becomes

$$S_{XY} = \begin{bmatrix} \cos A \cos B & \cos A \sin B \sin \Gamma - \sin A \cos \Gamma & \cos A \sin B \cos \Gamma + \sin A \sin \Gamma \\ \sin A \cos B & \sin A \sin B \sin \Gamma + \cos A \cos \Gamma & \sin A \sin B \cos \Gamma - \cos A \sin \Gamma \\ -\sin B & \cos B \sin \Gamma & \cos B \cos \Gamma \end{bmatrix}$$

$$(B.7)$$

It should be noted that the finite rotation tensor in Eq. (B.7) turns into an infinitesimal one, analogous with ζ_b in Eq. (B.3c), when the rotations become small.

In general, it is inconvenient to describe the vehicle path and the inclination of the tangent plane to the structural surface at O_Y (see Fig. 2.1) in terms of the rotations A(s), B(s) and Γ(s). Instead two radii of curvature and a superelevation angle are introduced here according to Duffek et al. [30]. If e_{X3} is made vertical and downward, A, B and Γ can be evaluated from the relations

$$dA = \frac{ds \; \cos B}{R},$$

$$(B.8a)$$

$$dB = \frac{ds}{H}$$

$$(B.8b)$$

and

$$\tan\Gamma = \tan Q \cos B$$

$$(B.8c)$$

where R is the horizontal radius of curvature of the path, H the vertical radius of curvature in the vertical tangent plane and Q the
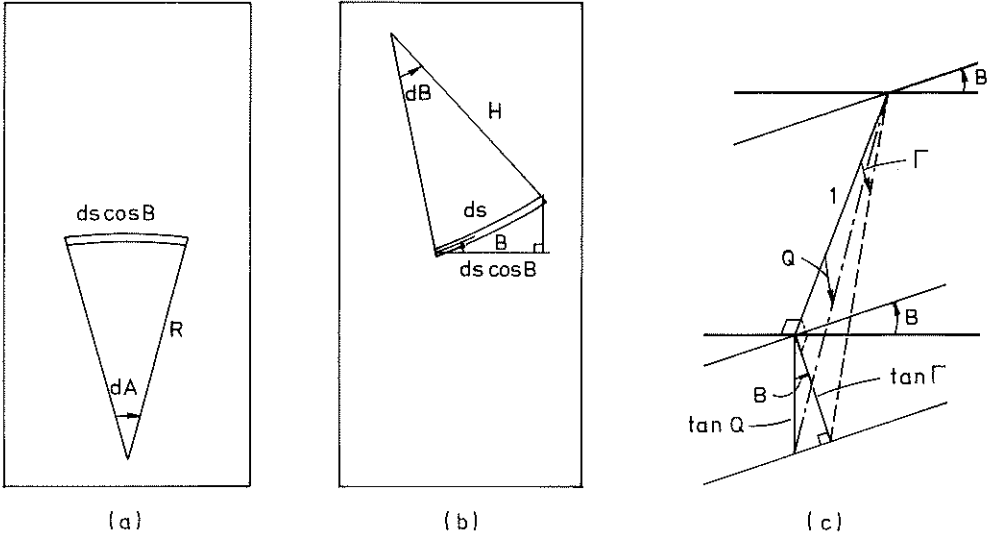
Figure B.2. Radii of curvature R and H of the path and superelevation angle Q as related to rotation angles A, B and Γ.
(a) Radius of curvature R (horizontal plane).
(b) Radius of curvature H (vertical tangent plane).
(c) Superelevation angle Q (perspective).

superelevation angle measured in the vertical plane perpendicular to the vertical tangent plane just mentioned. Equations (B.8a–c) are visualized in Fig. B.2 (cf. Fig. B.1).

Thus from given (prescribed) functions R(s), H(s) and Q(s) the rotation angles A(s), B(s) and Γ(s) can be determined and introduced in Eq. (B.7). (Since a straight vehicle path should also be manageable, it is more convenient to give the curvatures $\frac{1}{R}$ and $\frac{1}{H}$ instead of R and H as input data. In addition, initial rotation angles A_I and B_I must be given).

B.2.2 Velocities

The absolute translational and rotational velocities are given in Subsec. 2.3.1 as

$$\mathbf{v}_{bo} = (\frac{d}{dt} \mathbf{R}_{XY})_X + \mathbf{\Omega}_{XY} \times (\mathbf{R}_{YZb} + \mathbf{w}_{bo}) + (\frac{d}{dt} \mathbf{w}_{bo})_{Zb} \qquad (2.30a)$$

and

$$\mathbf{\omega}_b = \mathbf{\Omega}_{XY} + (\frac{d}{dt} \mathbf{\psi}_b)_{Zb} \qquad (2.30b)$$

respectively. Although $\mathbf{R}_{XY}$ is expressed in $\mathbf{e}_{Xi}$ in Eq. (B.1a), its first time derivative is most conveniently expressed in the base vectors $\mathbf{e}_{Yi}$ as

$$(\frac{d}{dt} \mathbf{R}_{XY})_X = \dot{\mathbf{R}}_{XY} = v\mathbf{e}_{Y1} + 0\mathbf{e}_{Y2} + 0\mathbf{e}_{Y3} \qquad (B.9)$$

where $v = v(t) = \frac{ds}{dt}$ is the vehicle speed, the fourth function that must be prescribed to define the nominal vehicle position. (The initial position s_0 must also be given). As can be noted from Eq. (B.9), the reference frame Y is defined so that the speed v only contributes in the direction of $\mathbf{e}_{Y1}$ (see Sec. 2.1). In Eqs. (2.30a-b) the rotational or angular velocity vector $\mathbf{\Omega}_{XY}$ is present. Thus, in contrast to the rotations of $\mathbf{S}_{XY}$, the angular velocities can be expressed as a vector. From the previous subsection it can be found that

$$\mathbf{\Omega}_{XY} = \dot{A}\mathbf{e}_{\overline{X}3} + \dot{B}\mathbf{e}_{\overline{Y}2} + \dot{\Gamma}\mathbf{e}_{Y1} \qquad (B.10)$$

where $\dot{A} = \dfrac{dA}{dt}$ and so on. Transformation of Eq. (B.10) to a common set of base vectors $\mathbf{e}_{Yi}$, according to Eqs. (B.6b–c), yields

$$\boldsymbol{\Omega}_{XY} = \Omega_1 \mathbf{e}_{Y1} + \Omega_2 \mathbf{e}_{Y2} + \Omega_3 \mathbf{e}_{Y3} \qquad (B.10')$$

where

$$\Omega_1 = -\dot{A}\sin B + \dot{\Gamma}, \qquad (B.11a)$$

$$\Omega_2 = \dot{B}\cos\Gamma + \dot{A}\cos B\sin\Gamma \qquad (B.11b)$$

and

$$\Omega_3 = -\dot{B}\sin\Gamma + \dot{A}\cos B\cos\Gamma \qquad (B.11c)$$

are the angular velocity components. Note that for small rotations $\Omega_1 = \dot{\Gamma}$, $\Omega_2 = \dot{B}$ and $\Omega_3 = \dot{A}$. From Eqs. (B.8a–c) it can be found that

$$\dot{A} = \frac{v}{R}\cos B, \qquad (B.12a)$$

$$\dot{B} = \frac{v}{H} \qquad (B.12b)$$

and

$$\dot{\Gamma} = vQ' \; \frac{\cos^2\Gamma\cos B}{\cos^2 Q} - \frac{v}{H}\cos^2\Gamma\tan Q\sin B. \qquad (B.12c)$$

Introduction of Eqs. (B.12a–c) into Eqs. (B.11a–c) gives Ω_1, Ω_2 and Ω_3 in terms of the functions $R(s)$, $H(s)$, $Q(s)$ and $v(t)$ as

$$\Omega_1 = -\frac{v}{R}\cos B \sin B + vQ' \, \frac{\cos^2\Gamma\cos B}{\cos^2 Q} - \frac{v}{H}\cos^2\Gamma\tan Q\sin B, \quad \text{(B.11a')}$$

$$\Omega_2 = \frac{v}{H}\cos\Gamma + \frac{v}{R}\cos^2 B\sin\Gamma \qquad\qquad\qquad \text{(B.11b')}$$

and

$$\Omega_3 = -\frac{v}{H}\sin\Gamma + \frac{v}{R}\cos^2 B\cos\Gamma \qquad\qquad\qquad \text{(B.11c')}$$

in which $Q' = \frac{dQ}{ds}$. For small rotations, or rotation about a single axis, it can be noted from Eqs. (B.11a'-c') that $\Omega_1 = \frac{vQ'}{\cos^2 Q}$, $\Omega_2 = \frac{v}{H}$ and $\Omega_3 = \frac{v}{R}$. Equations (2.30a-b) also contain the time derivatives of the fundamental unknowns w_{bo} and ψ_b. By means of Eqs. (B.1c) and (B.4) it is recognized that the relative velocities are given by

$$(\frac{d}{dt}\,w_{bo})_{Zb} = \dot{w}_{bo} = \dot{w}_{boi}e_{Zbi} \qquad\qquad\qquad \text{(B.13a)}$$

and

$$(\frac{d}{dt}\,\psi_b)_{Zb} = \dot{\psi}_b = \dot{\psi}_{bi}e_{Zbi}. \qquad\qquad\qquad \text{(B.13b)}$$

Note that the dots in Eqs. (B.13a-b) denote time differentiation with respect to the reference frame Z_b whereas the dot in Eq. (B.9) indicates time differentiation with respect to the frame X.

B.2.3 Accelerations

The absolute translational and rotational accelerations of each rigid body are given in Subsec. 2.3.1 as

$$\dot{v}_{bo} = (\frac{d^2}{dt^2} R_{XY})_X + (\frac{d}{dt} \Omega_{XY})_Y \times (R_{YZb} + w_{bo})$$

$$+ \Omega_{XY} \times (\Omega_{XY} \times (R_{YZb} + w_{bo})) + 2\Omega_{XY} \times (\frac{d}{dt} w_{bo})_{Zb} + (\frac{d^2}{dt^2} w_{bo})_{Zb}$$

$$(2.31a)$$

and

$$\dot{\omega}_b = (\frac{d}{dt} \Omega_{XY})_Y + \Omega_{XY} \times (\frac{d}{dt} \psi_b)_{Zb} + (\frac{d^2}{dt^2} \psi_b)_{Zb} \qquad (2.31b)$$

respectively. The second time derivative of R_{XY}, the first new vector in Eq. (2.31a), is given by

$$(\frac{d^2}{dt^2} R_{XY})_X = \ddot{R}_{XY} = (\frac{d}{dt} \dot{R}_{XY})_Y + \Omega_{XY} \times \dot{R}_{XY} =$$

$$= ae_{Y1} + v\Omega_3 e_{Y2} - v\Omega_2 e_{Y3} \qquad (B.14)$$

where $a = \frac{dv}{dt}$ is the vehicle acceleration and Ω_2 and Ω_3 the angular velocities given by Eqs. (B.11b–c) or Eqs. (B.11b'–c'). If Eqs. (B.11b'–c') are substituted into Eq. (B.14) it is found that

$$\ddot{\mathbf{R}}_{XY} = a\mathbf{e}_{Y1} + (- \frac{v^2}{H} \sin\Gamma + \frac{v^2}{R} \cos^2 B \cos\Gamma)\mathbf{e}_{Y2}$$

$$+ (- \frac{v^2}{H} \cos\Gamma - \frac{v^2}{R} \cos^2 B \sin\Gamma)\mathbf{e}_{Y3}. \tag{B.14'}$$

Once again it can be noted that for small rotations, or rotation about a single axis, the last two components in Eq. (B.14') yield $\frac{v^2}{R}$ and $- \frac{v^2}{H}$ respectively. Another new vector in this subsection is the angular acceleration vector $(\frac{d}{dt} \Omega_{XY})_Y$. It can be found from Eqs. (B.10') and (B.11a–c) that

$$(\frac{d}{dt} \Omega_{XY})_Y = \dot{\Omega}_{XY} = \dot{\Omega}_1 \mathbf{e}_{Y1} + \dot{\Omega}_2 \mathbf{e}_{Y2} + \dot{\Omega}_3 \mathbf{e}_{Y3} \tag{B.15}$$

where

$$\dot{\Omega}_1 = -\ddot{A}\sin B - \dot{A}\dot{B}\cos B + \ddot{\Gamma}, \tag{B.16a}$$

$$\dot{\Omega}_2 = \ddot{B}\cos\Gamma - \dot{B}\dot{\Gamma}\sin\Gamma + \ddot{A}\cos B\sin\Gamma - \dot{A}\dot{B}\sin B\sin\Gamma + \dot{A}\dot{\Gamma}\cos B\cos\Gamma \tag{B.16b}$$

and

$$\dot{\Omega}_3 = -\ddot{B}\sin\Gamma - \dot{B}\dot{\Gamma}\cos\Gamma + \ddot{A}\cos B\cos\Gamma - \dot{A}\dot{B}\sin B\cos\Gamma - \dot{A}\dot{\Gamma}\cos B\sin\Gamma \tag{B.16c}$$

are the angular acceleration components. As before these components can be expressed in R (or $\frac{1}{R}$), H (or $\frac{1}{H}$), Q and v by using Eqs. (B.12a–c) for the first derivatives of A, B and Γ and the following relations for the second derivatives

$$\ddot{A} = \frac{a}{R}\,\cos B + v^2(\frac{1}{R})'\cos B - \frac{v^2}{RH}\,\sin B, \tag{B.17a}$$

$$\ddot{B} = \frac{a}{H} + v^2(\frac{1}{H})' \tag{B.17b}$$

and

$$\ddot{\Gamma} = (aQ' + v^2 Q'')\,\frac{\cos^2\Gamma\cos B}{\cos^2 Q}$$

$$+ vQ'(-\frac{\dot{\Gamma}\sin 2\Gamma\cos B}{\cos^2 Q} - \frac{v}{H}\,\frac{\cos^2\Gamma\sin B}{\cos^2 Q} + 2vQ'\,\frac{\cos^2\Gamma\cos B\sin Q}{\cos^3 Q})$$

$$-(\frac{a}{H} + v^2(\frac{1}{H})')\cos^2\Gamma\tan Q\sin B \tag{B.17c}$$

$$- \frac{v}{H}(-\dot{\Gamma}\sin 2\Gamma\tan Q\sin B + vQ'\,\frac{\cos^2\Gamma\sin B}{\cos^2 Q} + \frac{v}{H}\,\cos^2\Gamma\tan Q\cos B).$$

Here $(\frac{1}{R})' = \frac{d}{ds}(\frac{1}{R})$, $(\frac{1}{H})' = \frac{d}{ds}(\frac{1}{H})$ and $Q'' = \frac{d^2 Q}{ds^2}$. Finally, the second time derivatives of w_{bo} and ψ_b in Eqs. (2.31a–b) are given in analogy with Eqs. (B.13a–b). Hence

$$(\frac{d^2}{dt^2}\,w_{bo})_{Zb} = \ddot{w}_{bo} = \ddot{w}_{boi}e_{Zbi} \tag{B.18a}$$

and

$$(\frac{d^2}{dt^2}\,\psi_b)_{Zb} = \ddot{\psi}_b = \ddot{\psi}_{bi}e_{Zbi}. \tag{B.18b}$$

B.3   Vehicle element matrices

B.3.1 Rigid body element

The basic equations for a rigid body element are given in Subsec. 2.3.2 in terms of its equations of motion

$$M_v^e \ddot{u}_v^e + C_v^e \dot{u}_v^e + K_v^e u_v^e = P_v^e + P_{qv}^e - P_Z^e. \tag{2.34}$$

In this subsection explicit expressions are given for the element matrices and vectors in Eq. (2.34). For this purpose the kinematic relations derived in Sec. B.2 are used as well as decomposition into submatrices and subvectors as

$$M_v^e = \left[\begin{array}{c|c} M_{vw}^e & 0 \\ \hline 0 & M_{v\psi}^e \end{array} \right], \quad C_v^e = \left[\begin{array}{c|c} C_{vw}^e & 0 \\ \hline 0 & C_{v\psi}^e \end{array} \right],$$

$$K_v^e = \left[\begin{array}{c|c} K_{vw}^e & 0 \\ \hline 0 & 0 \end{array} \right] \tag{B.19a,b,c}$$

and

$$u_v^e = \left[\begin{array}{c} w_{bo} \\ \hline \psi_b \end{array} \right], \quad P_v^e = \left[\begin{array}{c} F_b \\ \hline M_{bo} \end{array} \right], \quad P_{qv}^e = \left[\begin{array}{c} F_{qb} \\ \hline M_{qbo} \end{array} \right], \quad P_Z^e = \left[\begin{array}{c} P_{Zw}^e \\ \hline P_{Z\psi}^e \end{array} \right].$$

$$\tag{B.19d,e,f,g}$$

By comparing Eqs. (2.33a-b), (2.34) and (B.19a,d) one may write

$$\mathbf{M}^e_{vw} = \begin{bmatrix} m_b & 0 & 0 \\ 0 & m_b & 0 \\ 0 & 0 & m_b \end{bmatrix} \tag{B.20a}$$

and

$$\mathbf{M}^e_{v\psi} = \mathbf{I}_{bo} = \begin{bmatrix} I_{11} & 0 & 0 \\ 0 & I_{22} & 0 \\ 0 & 0 & I_{33} \end{bmatrix} \tag{B.20b}$$

where m_b is the mass of the body and I_{11}, I_{22} and I_{33} are the (time-independent) principal moments of inertia with respect to the principal axes through the centre of gravity of the body. Thus it is presupposed that the discrepancy between the (referential) Z_b-axes and the (body-fixed) principal axes can be neglected. The same applies to the reference point 0_{Zb} and the centre of gravity of the vehicle body. The restriction to principal axes is introduced here only to limit the length of the expressions that follow. Besides this aspect no special difficulties enter the analysis if the matrix in Eq. (B.20b) is full.

Further, it can be found that

$$\mathbf{C}^e_{vw}\dot{\mathbf{w}}_{bo} = 2m_b(\mathbf{\Omega}_{XY} \times \dot{\mathbf{w}}_{bo}) = 2m_b\begin{bmatrix} 0 & -\Omega_3 & \Omega_2 \\ \Omega_3 & 0 & -\Omega_1 \\ -\Omega_2 & \Omega_1 & 0 \end{bmatrix}\begin{bmatrix} \dot{w}_{bo1} \\ \dot{w}_{bo2} \\ \dot{w}_{bo3} \end{bmatrix} \tag{B.21a}$$

and

$$C_{v\psi}^{e}\dot{\psi}_{b} = I_{bo}(\Omega_{XY}\times\dot{\psi}_{b}) + \Omega_{XY} \times (I_{bo}\dot{\psi}_{b}) + \dot{\psi}_{b} \times (I_{bo}\Omega_{XY}) = \quad (B.21b)$$

$$= \begin{bmatrix} 0 & -(I_{11}+I_{22}-I_{33})\Omega_{3} & (I_{11}-I_{22}+I_{33})\Omega_{2} \\ (I_{11}+I_{22}-I_{33})\Omega_{3} & 0 & -(-I_{11}+I_{22}+I_{33})\Omega_{1} \\ -(I_{11}-I_{22}+I_{33})\Omega_{2} & (-I_{11}+I_{22}+I_{33})\Omega_{1} & 0 \end{bmatrix} \begin{bmatrix} \dot{\psi}_{b1} \\ \dot{\psi}_{b2} \\ \dot{\psi}_{b3} \end{bmatrix}$$

where the angular velocities Ω_{1}, Ω_{2} and Ω_{3} are given by Eqs. (B.11a-c) or Eqs. (B.11a'-c'). Note that the nonlinear term in Eq. (2.33b) has been omitted as described in the pertinent subsection. The rotational components contained in ψ_{b} do not contribute to the stiffness matrix K_{v}^{e} as indicated in Eq. (B.19c). The translational components of w_{bo}, however, are associated with the expression

$$K_{vw}^{e}w_{bo} = m_{b}(\Omega_{XY} \times (\Omega_{XY} \times w_{bo}) + \dot{\Omega}_{XY} \times w_{bo}) =$$

$$= m_{b} \begin{bmatrix} -\Omega_{2}^{2}-\Omega_{3}^{2} & \Omega_{1}\Omega_{2}-\dot{\Omega}_{3} & \Omega_{1}\Omega_{3}+\dot{\Omega}_{2} \\ \Omega_{1}\Omega_{2}+\dot{\Omega}_{3} & -\Omega_{1}^{2}-\Omega_{3}^{2} & \Omega_{2}\Omega_{3}-\dot{\Omega}_{1} \\ \Omega_{1}\Omega_{3}-\dot{\Omega}_{2} & \Omega_{2}\Omega_{3}+\dot{\Omega}_{1} & -\Omega_{1}^{2}-\Omega_{2}^{2} \end{bmatrix} \begin{bmatrix} w_{bo1} \\ w_{bo2} \\ w_{bo3} \end{bmatrix} \quad (B.22)$$

in which the angular accelerations $\dot{\Omega}_{1}$, $\dot{\Omega}_{2}$ and $\dot{\Omega}_{3}$ are given by Eqs. (B.16a-c). As mentioned previously, Eqs. (B.12a-c) and (B.17a-c) must be introduced into Eqs. (B.16a-c) if the accelerations are to be expressed as functions of R, H, Q and v. As is evident from Eqs. (B.20a-b), (B.21a-b) and (B.22), the rigid body element matrices C_{v}^{e} and K_{v}^{e} are in general both time-dependent and unsymmetric whereas M_{v}^{e} is time-independent and symmetric. With regard to the element vectors in Eqs. (B.19d-g), the displacement vector u_{v}^{e} is expressed by Eqs. (B.1c) and (B.4). Further, the element force vector P_{v}^{e} is eliminated when the rigid body element is assembled with other elements, see for instance Eq. (2.36) for the structure-vehicle

element. Since the element load vector P_{qv}^e refers to the point O_{Zb} and the frame Z_b, most element loads must be transformed to this point and the Z_b-axes. Transformation to the point O_{Zb} is shown in Subsec. B.3.4 whereas transformation to the Z_b-axes is performed by means of Eqs. (B.3a) and (B.7). For instance, the dead weight $m_b g$ of the body yields a load vector with constant components if related to the frame X while time-dependent components appear ,in general, if related to the frame Y or Z_b. The last vector in Eq. (2.34), the element noninertia load vector P_Z^e, is given by its subvectors as

$$P_{Zw}^e = m_b(\ddot{R}_{XY} + \Omega_{XY} \times (\Omega_{XY} \times R_{YZb}) + \dot{\Omega}_{XY} \times R_{YZb}) =$$

$$= m_b \begin{bmatrix} a \\ v\Omega_3 \\ -v\Omega_2 \end{bmatrix} + m_b \begin{bmatrix} -\Omega_2^2-\Omega_3^2 & \Omega_1\Omega_2-\dot{\Omega}_3 & \Omega_1\Omega_3+\dot{\Omega}_2 \\ \Omega_1\Omega_2+\dot{\Omega}_3 & -\Omega_1^2-\Omega_3^2 & \Omega_2\Omega_3-\dot{\Omega}_1 \\ \Omega_1\Omega_3-\dot{\Omega}_2 & \Omega_2\Omega_3+\dot{\Omega}_1 & -\Omega_1^2-\Omega_2^2 \end{bmatrix} \begin{bmatrix} R_{YZb1} \\ R_{YZb2} \\ R_{YZb3} \end{bmatrix} \quad \text{(B.23a)}$$

and

$$P_{Z\psi}^e = I_{bo}\dot{\Omega}_{XY} + \Omega_{XY} \times (I_{bo}\Omega_{XY}) =$$

$$= \begin{bmatrix} I_{11}\dot{\Omega}_1-(I_{22}-I_{33})\Omega_2\Omega_3 \\ I_{22}\dot{\Omega}_2-(I_{33}-I_{11})\Omega_3\Omega_1 \\ I_{33}\dot{\Omega}_3-(I_{11}-I_{22})\Omega_1\Omega_2 \end{bmatrix}. \quad \text{(B.23b)}$$

As before, the angular velocities and accelerations in Eqs. (B.23a-b) can be evaluated according to Sec. B.2. Expressions for the remaining two elements, the damper element and the spring element, are now given in the following two subsections.

B.3.2 Damper element

The basic equations for a damper element are expressed in Subsec. 2.3.3 as

$$C_v^e \dot{u}_v^e + K_v^e u_v^e = P_v^e - P_Z^e \qquad (2.35a)$$

in terms of the 12×1 global displacement vector u_v^e. The DOF in u_v^e are the six DOF at O_{Zb} of each of the two connected rigid body elements. A 6×1 local displacement vector, $\bar{u}_v^e$, is now introduced in order to simplify the derivation of an explicit expression of Eq. (2.35a). If the vector $\bar{u}_v^e$ contains the three translations of each of the ends of the connecting element one may write

$$\bar{u}_v^e = Q u_v^e \qquad (B.24)$$

where Q is a 6×12 transformation matrix depending on the position of the two element ends. Thus, if the basic equations for the damper element are given in terms of $\bar{u}_v^e$, that is

$$\bar{C}_v^e \dot{\bar{u}}_v^e + \bar{K}_v^e \bar{u}_v^e = \bar{P}_v^e - \bar{P}_Z^e \qquad (B.25)$$

the global quantities C_v^e, K_v^e, P_v^e and P_Z^e in Eq. (2.35a) become

$$C_v^e = Q^T \bar{C}_v^e Q, \qquad (B.26a)$$

$$K_v^e = Q^T \bar{K}_v^e Q, \qquad (B.26b)$$

$$P_v^e = Q^T \bar{P}_v^e \tag{B.26c}$$

and

$$P_Z^e = Q^T \bar{P}_Z^e \tag{B.26d}$$

respectively. In this subsection $\bar{C}_v^e$, $\bar{K}_v^e$ and $\bar{P}_Z^e$ are given in explicit form whereas Q is given in Subsec. B.3.4.

The translations of the two damper element ends can be described by (cf. Eq. (2.28))

$$r_1 = R_{XY} + R_{YZ1} + Z_1 + w_1 \tag{B.27a}$$

and

$$r_2 = R_{XY} + R_{YZ2} + Z_2 + w_2 \tag{B.27b}$$

where Z_1 and Z_2 are position vectors and w_1 and w_2 relative displacement vectors of the element ends. R_{YZ1} and R_{YZ2} define the reference position of 0_{Zb} of the two connected rigid body elements. The absolute translational velocities of the damper element ends are then given in analogy with Eq. (2.30a) as

$$v_1 = \dot{R}_{XY} + \Omega_{XY} \times (R_{YZ1} + Z_1 + w_1) + \dot{w}_1 \tag{B.28a}$$

and

$$v_2 = \dot{R}_{XY} + \Omega_{XY} \times (R_{YZ2} + Z_2 + w_2) + \dot{w}_2. \tag{B.28b}$$

The constitutive equations of the damper element may now be written in submatrices as

$$
\begin{bmatrix}
\bar{C}^e_{v11} & \vdots & \bar{C}^e_{v12} \\
\cdots & \vdots & \cdots \\
\bar{C}^e_{v21} & \vdots & \bar{C}^e_{v22}
\end{bmatrix}
\begin{bmatrix}
v_1 \\
\cdots \\
v_2
\end{bmatrix}
=
\begin{bmatrix}
\bar{P}^e_{v1} \\
\cdots \\
\bar{P}^e_{v2}
\end{bmatrix}
\tag{B.29}
$$

in which

$$
\bar{C}^e_{v11} = \bar{C}^e_{v22} = -\bar{C}^e_{v12} = -\bar{C}^e_{v21} = c
\begin{bmatrix}
n_1 n_1 & n_1 n_2 & n_1 n_3 \\
n_2 n_1 & n_2 n_2 & n_2 n_3 \\
n_3 n_1 & n_3 n_2 & n_3 n_3
\end{bmatrix}.
\tag{B.30}
$$

Here c is the damper viscosity and n_1, n_2 and n_3 direction cosines depending on the orientation of the damper relative to the base vectors e_{Zbi}. Introduction of Eqs. (B.28a-b) into Eq. (B.29) now yields Eq. (B.25) with

$$
\bar{u}^e_v =
\begin{bmatrix}
w_1 \\
\cdots \\
w_2
\end{bmatrix},
\tag{B.31a}
$$

$$
\bar{C}^e_v =
\begin{bmatrix}
\bar{C}^e_{v11} & \vdots & \bar{C}^e_{v12} \\
\cdots & \vdots & \cdots \\
\bar{C}^e_{v21} & \vdots & \bar{C}^e_{v22}
\end{bmatrix}.
\tag{B.31b}
$$

$$
\bar{K}^e_v \bar{u}^e_v =
\begin{bmatrix}
\bar{C}^e_{v11}(\Omega_{XY} \times w_1) + \bar{C}^e_{v12}(\Omega_{XY} \times w_2) \\
\cdots \\
\bar{C}^e_{v21}(\Omega_{XY} \times w_1) + \bar{C}^e_{v22}(\Omega_{XY} \times w_2)
\end{bmatrix},
\tag{B.31c}
$$

$$\bar{P}_v^e = \left[\begin{array}{c} \bar{P}_{v1}^e \\ \hline \bar{P}_{v2}^e \end{array} \right] \tag{B.31d}$$

and

$$\bar{P}_Z^e = \left[\begin{array}{c} \bar{C}_{v11}^e(\Omega_{XY} \times (R_{YZ1}+Z_1)) + \bar{C}_{v12}^e(\Omega_{XY} \times (R_{YZ2}+Z_2)) \\ \hline \bar{C}_{v21}^e(\Omega_{XY} \times (R_{YZ1}+Z_1)) + \bar{C}_{v22}^e(\Omega_{XY} \times (R_{YZ2}+Z_2)) \end{array} \right]. \tag{B.31e}$$

B.3.3 Spring element

The basic equations for a spring element are expressed in Subsec. 2.3.3 as

$$K_v^e u_v^e = P_v^e \tag{2.35b}$$

in terms of the 12×1 global displacement vector u_v^e. In analogy with the damper element, the basic equations for the spring element may be written in local displacements as (cf. Eq. (B.25))

$$\bar{K}_v^e \bar{u}_v^e = \bar{P}_v^e. \tag{B.32}$$

With the translations of the two spring element ends described by Eqs. (B.27a-b) the quantities in Eq. (B.32) can be identified directly as (cf. Subsec. B.3.2)

$$\bar{\mathbf{u}}_v^e = \left[\begin{array}{c} \mathbf{w}_1 \\ \hline \mathbf{w}_2 \end{array} \right], \qquad (B.33a)$$

$$\bar{\mathbf{K}}_v^e = \left[\begin{array}{c|c} \bar{\mathbf{K}}_{v11}^e & \bar{\mathbf{K}}_{v12}^e \\ \hline \bar{\mathbf{K}}_{v21}^e & \bar{\mathbf{K}}_{v22}^e \end{array} \right] \qquad (B.33b)$$

and

$$\bar{\mathbf{P}}_v^e = \left[\begin{array}{c} \bar{\mathbf{P}}_{v1}^e \\ \hline \bar{\mathbf{P}}_{v2}^e \end{array} \right]. \qquad (B.33c)$$

In Eq. (B.33b) the submatrices are given in analogy with Eq. (B.30), that is

$$\bar{\mathbf{K}}_{v11}^e = \bar{\mathbf{K}}_{v22}^e = -\bar{\mathbf{K}}_{v12}^e = -\bar{\mathbf{K}}_{v21}^e = k \left[\begin{array}{ccc} n_1 n_1 & n_1 n_2 & n_1 n_3 \\ n_2 n_1 & n_2 n_2 & n_2 n_3 \\ n_3 n_1 & n_3 n_2 & n_3 n_3 \end{array} \right] \qquad (B.34)$$

in which k is the spring stiffness.

B.3.4 Transformation matrix Q

In the previous two subsections the matrix **Q** is needed to transform the basic equations of the damper and spring elements from local to global displacement coordinates. In order to give an explicit expression for **Q**, Eq. (B.24) can be written in submatrices as

$$\left[\begin{array}{c} \mathbf{w}_1 \\ \hline \mathbf{w}_2 \end{array}\right] = \left[\begin{array}{c|c|c|c} 1 & \mathbf{Q}_1 & 0 & 0 \\ \hline 0 & 0 & 1 & \mathbf{Q}_2 \end{array}\right] \left[\begin{array}{c} \mathbf{w}_{1o} \\ \hline \psi_1 \\ \hline \mathbf{w}_{2o} \\ \hline \psi_2 \end{array}\right] \qquad (B.24')$$

where $\mathbf{w}_{bo}$ and ψ_b contain the translational and rotational DOF respectively of the connected rigid body element number b ($b = 1,2$). Note that $\mathbf{w}_{bo}$ refers to the centre of gravity of the body. If the connecting point at each body is given by (cf. Eqs. (B.27a-b))

$$Z_b = Z_{bi} e_{Zbi} \qquad\qquad (b = 1,2) \qquad\qquad (B.35)$$

it can be shown from geometrical considerations that $\mathbf{Q}_1$ and $\mathbf{Q}_2$ in Eq. (B.24') become

$$\mathbf{Q}_b = \left[\begin{array}{ccc} 0 & Z_{b3} & -Z_{b2} \\ -Z_{b3} & 0 & Z_{b1} \\ Z_{b2} & -Z_{b1} & 0 \end{array}\right]. \qquad (b = 1,2) \qquad\qquad (B.36)$$

A relation similar to Eq. (B.24') may be used to transform external loads $\mathbf{F}_{qb}$ and $\mathbf{M}_{qb}$ applied arbitrarily on a body to the point O_{Zb}. If the components of $\mathbf{F}_{qb}$ and $\mathbf{M}_{qb}$ refer to e_{Zbi} the load vector $\mathbf{P}_{qv}^e$, see Eq. (B.19f), is given by

$$\mathbf{P}_{qv}^e = \left[\begin{array}{c} \mathbf{F}_{qb} \\ \hline \mathbf{M}_{qbo} \end{array}\right] = \left[\begin{array}{c|c} 1 & 0 \\ \hline \mathbf{Q}_b^T & 1 \end{array}\right] \left[\begin{array}{c} \mathbf{F}_{qb} \\ \hline \mathbf{M}_{qb} \end{array}\right] \qquad\qquad (B.37)$$

where $\mathbf{Q}_b$ now contains the coordinates Z_{bi} of the point of application of the load.

APPENDIX C.   VERIFICATION EXAMPLES - FINITE BEAM ELEMENT

C.1   Introduction

In this appendix three examples are given to verify numerical results obtained by means of the finite beam element derived in Chapter 3. The examples are rather simple in scope in order to provide a physical insight into the different problems and to make a comparison with other theoretical solutions possible. The first two examples have been presented before, see the author [86][88]. In the last example, the structure in Sec. 6.3 is analysed. In all examples free vibrations are studied. Further applications of the present finite beam element have been presented by the author [86]. Summary and conclusions of this appendix are given in Sec. C.5.

C.2   Additional displacement functions

The purpose of this first verification example is to examine the efficiency of the two sets of additional (hierarchical) displacement functions, that is, eigenfunctions and polynomial terms. These p-refinements are compared with each other, the h-refinement and the exact (analytical) solution.

The problem studied is free undamped bending vibration of a uniform cantilever beam. The rotatory inertia according to Rayleigh which may be optionally included in the present beam element is neglected here. The lowest eight eigenfrequencies are determined for the above four cases. (The exact solution is easily found for this problem, see for example Clough and Penzien [17]).

In order to determine the eight eigenfrequencies numerically the cantilever beam is modelled as a single element with eight additional displacement functions (12 DOF in total) for the

p-refinements whereas it is modelled as five conventional cubic elements for the h-refinement. For all these three cases, 10 degrees of freedom are present after the boundary conditions have been considered. That is two more than the number of eigenfrequencies to be determined.

The results, in terms of normalized squared (circular) eigen-frequencies ω_1^2 to ω_8^2, are shown in Table C.1 below. (See also the author et al. [86][88][90]).

Mode	(a)	(b)	(c)	(d)
1	12.3624	12.3624	12.3624	12.3627
2	485.519	485.529	485.519	486.004
3	3806.55	3807.03	3806.55	3833.94
4	14617.3	14622.8	14617.8	14962.1
5	39943.8	39975.9	39954.4	41217.2
6	89135.4	89256.0	91907.5	113753
7	173881	174220	184942	243309
8	308208	308973	598932	511713

Table C.1. Normalized squared eigenfrequencies ω_i^2 (i = 1 to 8) of bending vibration of a uniform cantilever beam (the multiplication factor $\bar{E}I/\rho AL^4$ is set to unity). Exact results and results of three numerical cases. 10 DOF are used for the present numerical solutions.

(a) Exact.

(b) Single 12 DOF element (p-refinement based on eigen-functions).

(c) Single 12 DOF element (p-refinement based on poly-nomial terms).

(d) Five 4 DOF cubic elements (h-refinement).

The results in Table C.1 clearly show that a single element with additional displacement functions is considerably better than several conventional beam elements. It can also be seen that additional functions in the form of polynomial terms yield better results, in comparison with eigenfunctions, for modes 2 to 5 while eigenfunctions are far better for modes 6 to 8. In fact, the hierarchical element with additional polynomial terms gives a worse representation of mode 8 than the conventional elements. If an error in ω_i of 0.2 per cent is acceptable all the frequencies in (b) will do while only the five lowest frequencies in (c) are useful. This also means that the disadvantage of the element with additional eigenfunctions for modes 2 to 5 is of minor interest. Thus, at least for the present example, additional eigenfunctions should be chosen in preference to polynomial terms.

C.3   Coupled vibrations

As pointed out at the end of Subsec. 3.2.4 coupled beam vibrations occur when the shear centre axis does not coincide with the centroidal axis even though the reference axes and warping coordinate can be chosen so that $S_y = S_z = S_\Omega = I_{yz} = I_{y\Omega} = I_{z\Omega} = 0$. Such a case is studied in this verification example.

As in Sec. C.2 the eight lowest undamped eigenfrequencies for a uniform cantilever beam are calculated. The beam cross section is shown in Fig. C.1, see Friberg [37] and Gjelsvik [43]. From Fig. C.1 and Eq. (3.31') it can be concluded that bending in the xz–plane and torsion will be coupled whereas both the axial vibration and the bending vibration in the xy–plane are uncoupled. The eight lowest eigenfrequencies are shown in Table C.2 for four different cases.
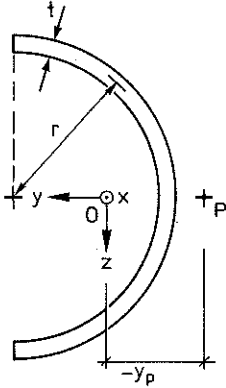
Figure C.1. Open thin–walled monosymmetric beam cross section. The origin O coincides with the centroid while the pole P coincides with the shear centre of the cross section. Data: $r = 24.5$ mm, $t = 4.0$ mm, $y_p = -15.5$ mm, $z_p = 0$, $L = 820$ mm, $A = 3.08 \cdot 10^{-4}$ m^2, $I_y = 9.26 \cdot 10^{-8}$ m^4, $I_z = 1.77 \cdot 10^{-8}$ m^4, $I_\Omega = 1.52 \cdot 10^{-12}$ m^6, $K_v = 1.64 \cdot 10^{-9}$ m^4, $\bar{E} = E = 6.89 \cdot 10^{10}$ Pa, $v = 0.3$ and $\rho = 2711$ kg/m^3.

In Table C.2 the modes 1, 4 and 7 are uncoupled bending modes in the xy–plane while the remaining modes listed are coupled bending–torsional modes as related above. Considering this is an open thin–walled beam the pure Saint Venant torsion result, case (a), is quite close to the mixed torsion result, case (b). As may be expected, the effects of rotatory/warping inertia and the static axial load are most accentuated in the higher and lower vibration modes, respectively. Although geometric effects are not included in the present study, see Subsec. 2.2.2, case (d) has been included for the sake of completeness (cf. the author [86][88]).

Mode	(a)	(b)	(c)	(d)
1	31.81	31.81 (31.81)	31.80 (31.80)	25.01 (25.01)
2	62.63	63.83 (63.79)	63.80 (63.76)	61.32 (61.28)
3	130.4	138.1 (137.7)	138.0 (137.5)	136.4 (136.0)
4	199.5	199.5 (199.3)	199.3 (199.0)	192.6 (192.4)
5	261.6	279.0 (278.4)	278.9 (278.2)	275.5 (274.9)
6	422.5	487.1 (484.8)	486.2 (483.9)	480.8 (478.5)
7	560.2	560.2 (558.1)	558.3 (556.3)	552.5 (550.7)
8	615.6	664.9 (663.8)	658.3 (657.3)	655.9 (654.8)

Table C.2. Eigenfrequencies f_i (Hz) of a uniform cantilever beam with cross section according to Fig. C.1. Four different cases. Present analysis results are compared with exact ones according to Friberg [37] (within parentheses) in cases (b), (c) and (d). In the present analysis a single finite element with 23 DOF (additional eigenfunctions) is used.

(a) Pure Saint Venant torsion.

(b) Case a + warping torsion (mixed torsion).

(c) Case b + rotatory and warping inertia effects.

(d) Case c + geometric effects due to a static axial load N = –1790 N.

The exact results given in Table C.2 (Friberg [37]) have been obtained by means of the dynamic stiffness method. The number of DOF in the present analysis, that is 23, has been chosen so that the error in the eight eigenfrequencies is less than 0.5 per cent. Note that additional eigenfunctions have been chosen since these yield better results than the polynomial terms (cf. Sec. C.2). The number of additional functions used is 0, 2, 3 and 6 in case (a) and 0, 2, 2, 5 in cases (b)–(d) for the actions of tension, bending in the xy–plane, bending in the xz–plane and torsion respectively. This indicates the relative importance of the torsional action.

Verification examples – finite beam element

For a chosen number of modes and an acceptable error percentage, here 8 and 0.5 respectively, the following two questions should be asked: How many DOF should be chosen? How should the additional DOF be distributed over the four different actions? In the present example the eigenfrequencies corresponding to the (uncoupled) additional eigenfunctions provide a guidance in answering both questions. The lowest eigenfunctions correspond to the eigen-frequencies 3074 Hz (tension), 202 Hz (xy-plane bending), 463 Hz (xz-plane bending), 232 Hz (pure Saint Venant torsion) and 99 Hz (pure warping torsion). The low torsional frequencies indicate, as pointed out above, the importance of the torsional action. The small increase in eigenfrequency between case (a) and (b) for the coupled modes, can also be better understood from the above frequencies: the warping torsion frequency, 99 Hz, is quite small as compared to the Saint Venant torsion frequency, 232 Hz, so that one should expect that the warping torsion stiffens the structure only to a limited extent. For an estimation of the number of DOF to be chosen the eigenfrequencies corresponding to higher eigenfunctions should be compared with the ones to be determined (if possible). In con-clusion, the additional eigenfunctions do not only give better results than the polynomial terms for most dynamic problems, but their corresponding eigenfrequencies, which can easily be calculated analytically, also serve as a tool for choosing appropriate DOF.

The present example shows that the finite beam element derived in Chapter 3 can be used in coupled vibration studies. In the example only the term $\bar{S}_z$, see Eqs. (3.31') and (3.32), gives rise to coupling effects. However, more general coupling problems can be handled as well, see the author [86]. If, for instance, the axial and transverse boundary conditions are not confined to the centroidal and shear centre axis, respectively, coupling effects occur.

C.4 Plane frame vibrations

In the third verification example of the present finite beam element, plane frame vibrations are considered. The frame structure studied is the one adopted in Sec. 6.3. Free undamped vibrations of this frame are investigated and the results are compared with the ones obtained by Popp [93][94]. Since infinite axial stiffnesses of the structural members are assumed by Popp, the frame properties in Sec. 6.3 are somewhat altered here. The frame studied is shown in Fig. C.2.
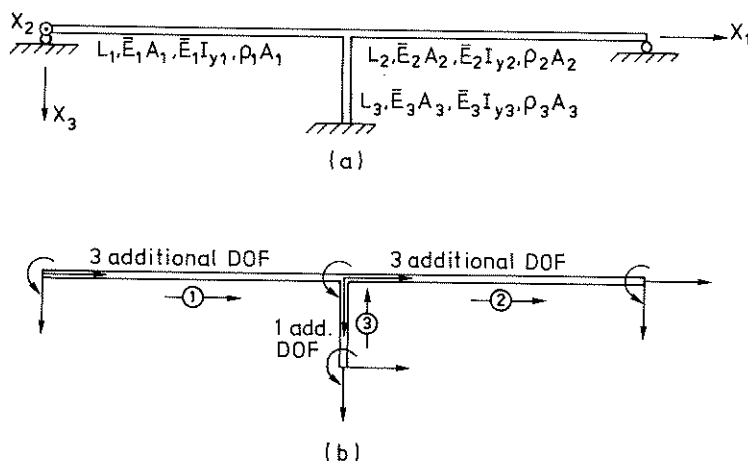
Figure C.2. Plane frame (cf. Sec. 6.3 and Popp [93][94]).

(a) Global coordinate system (X_1, X_2, X_3). Frame properties: $L_1 = L_2 = 20$ m, $L_3 = 5.66$ m, $\bar{E}_1 A_1 = \bar{E}_2 A_2 = \bar{E}_3 A_3 = \infty$, $\bar{E}_1 I_{y1} = \bar{E}_2 I_{y2} = 9.0 \cdot 10^9$ Nm^2, $\bar{E}_3 I_{y3} = 4.5 \cdot 10^9$ Nm^2, $\rho_1 A_1 = \rho_2 A_2 = 2300$ kg/m, $\rho_3 A_3 = 1725$ kg/m. The Euler–Bernoulli beam theory is assumed.

(b) Finite element discretization. Three hierarchical elements with additional eigenfunctions in bending.

From Fig. C.2b it is recognized that 19 DOF are introduced to model the frame structure: 12 basic DOF and 7 additional DOF. Six of the seven additional DOF are assigned to the relatively slender beam elements, cf. the guide in Sec. C.3. After considering the boundary conditions of the frame 14 of the 19 DOF remain. From these 14 DOF the five lowest eigenfrequencies are determined and compared with the exact ones obtained by Popp (dynamic stiffness method). The results are presented in Table C.3.

Mode	Popp [93][94]	Present analysis
1	6.14	6.14
2	10.54	10.55
3	12.13	12.14
4	33.18	33.21
5	39.33	39.34

Table C.3. Eigenfrequencies f_i (Hz) of the frame structure in Fig. C.2. The results of the present analysis are compared with exact ones according to Popp.

It can be concluded that the present results shown in Table C.3 are in good agreement with the exact ones. It should be kept in mind that 14 DOF are used in the present analysis while only seven DOF are needed in the exact dynamic stiffness method. As pointed out in Sec. 3.3, however, the dynamic stiffness method results in a nonlinear eigenvalue problem. It can also be noted that the eigenfrequencies of the frame in Sec. 6.3 (finite axial stiffnesses) are only somewhat lower than the ones given in Table C.3.

Finally, as an illustration of this verification example and the numerical example of Sec. 6.3, the three lowest eigenmodes of the frame are shown in Fig. C.3.
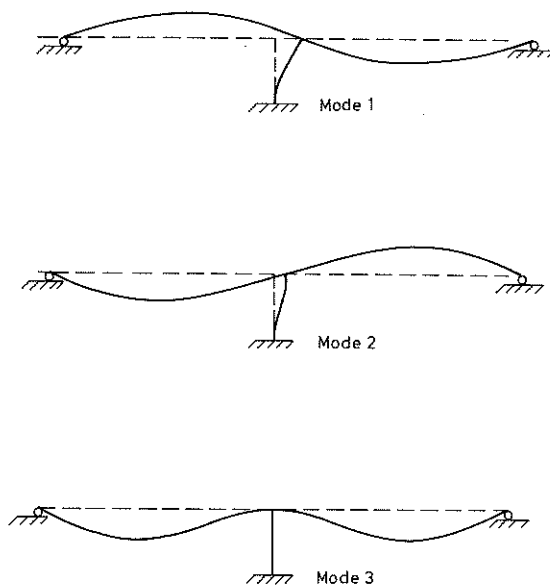
Figure C.3. Eigenmodes of the frame structure in Fig. C.2 (cf. Popp [93][94]).

C.5   Summary and conclusions

In this appendix three examples are given to verify numerical results obtained by means of the finite beam element derived in Chapter 3. In all examples eigenfrequencies of plane bending vibrations are used as verification quantity. In addition, coupled bending-torsional vibrations are studied in Sec. C.3.

The present results show good agreement with analytical results and numerical results of other investigators. It can also be concluded that hierarchical beam elements with additional eigenfunctions are especially powerful for the problems studied. Further verification examples of the present finite element are given by the author [86], see also Appendix D.

APPENDIX D. VERIFICATION EXAMPLES – STRUCTURE–VEHICLE FINITE ELEMENT

D.1   Introduction

The aim of this appendix is to verify the validity of the structure-vehicle finite element derived in Sec. 2.4. Here the finite beam element derived in Chapter 3 and verified in Appendix C is used as the structural part in the structure–vehicle element. Thus the present appendix also serves as a further verification of the beam element. In addition, the solution algorithm and the computer program described in Chapter 5 are tested.

The examples of this appendix can be divided into three groups corresponding to the three types of vehicle models described in Chapter 4. In this way Secs. D.2–D.4 are entitled moving force, moving mass and suspension vehicle models respectively. Thus the appendix is disposed so that the complexity of the vehicle models introduced is increased. Since the structural (beam) and vehicle models are still simple, Appendix D may also be seen as an introduction to analysis of structures subjected to moving loads. More advanced structure and vehicle models are treated in the examples of Chapter 6.

For clarity all input and output data of the examples in Secs. D.2–D.4 are given in terms of the nondimensional parameters introduced in Sec. 6.2. Output quantities such as normalized displacements, bending moments and contact forces are presented as time histories or as dynamic magnification factors. As in Chapter 6 the modal version of the structure–vehicle finite element is used in the present appendix. A summary and some conclusions of Appendix D are given in Sec. D.5.

D.2   Moving force vehicle models

The simplest dynamic vehicle models are the moving force models. For forces of constant magnitude the structure is affected dynamically through the moving character of the vehicle only. The consequences of neglecting the structure-vehicle interaction in these models may sometimes be minor. As expressed in nondimensional parameters in Sec. 6.2, the moving force models are most justified for low values of α or κ or for a combination of a low κ_0 value and a high Ω value.

The neglect of structure-vehicle interaction in this section means that the vehicle affects only the right-hand side of the structure-vehicle element equation (2.52) (or (2.44)). Nevertheless, the present section serves as an introduction to the moving load problem and the moving force model treated here constitutes a limiting case to the interactive models in Secs. D.3 and D.4.

The verification example studied in this section is the simplest possible moving load problem: a simply supported beam subjected to a constant force moving at constant speed, see Fig. D.1. The input quantities v, L, A, I_y, $\bar{E}$ and ρ given in Fig. D.1 can be represented by only one nondimensional parameter: the velocity ratio α, cf. Sec. 6.2. The modal damping ratios ξ_i are already nondimensional and the force P is included in the normalizing factors for output quantities. In this example output data are given in terms of time histories of midspan displacement and bending moment, $u_z(L/2, t)$ and $M_y(L/2, t)$, as well as of maximum values of these two quantities. The output data are normalized by the static midspan displacement $u_{zs}(L/2) = PL^3/48\bar{E}I_y$ and the static midspan moment $M_{ys}(L/2) = PL/4$ obtained when P is placed at midspan. In addition, the moving load traversing time $\tau = L/v$ is used to get a normalized time parameter t/τ ($t/\tau = 0$ when the load enters the structure).
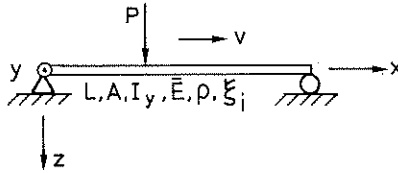
<u>Figure D.1</u>. Uniform, simply supported (Euler–Bernoulli) beam sub-
jected to a constant force P moving at constant speed v.
Local coordinate system (x,y,z). Beam length L, cross
sectional area A, moment of inertia I_y, elastic modulus
$\bar{E} = E$, mass density ρ and modal damping ratios ξ_i. The
beam is initially at rest.

The problem defined by Fig. D.1 has been studied by several authors.
Since analytical solutions are available for this problem many
classical studies exist, see Frýba [38]. More recent studies of this
case have been carried out by e.g. Dahlberg [23], Filho [35], the
author [83][85], Warburton [133] and Yoshida et al. [139][140] (cf.
references in Sec. 4.4). Before proceeding to the results of the
present study, time histories of midspan displacement and midspan
moment according to analytical (exact) expressions by Frýba [38] are
given. Time histories are given for five different velocity ratios
giving a good understanding of the moving load problem. The
histories are shown in Fig. D.2. It can be seen from Fig. D.2 that
for increasing velocity ratio α the curves deviate more and more
from the static ones $(\alpha = 0)$. The pattern is similar for both
displacement and moment. However, the moment curves are more
irregular and noticeable negative moment values are obtained when
the moving load (force) enters the structure (beam). Moreover, it
can be seen that for $\alpha = 0.125$ and $\alpha = 0.25$ more than one maximum is
obtained, in a mathematical sense, and that the maximum displacement
is obtained just as the force leaves the beam $(t/\tau = 1)$ for $\alpha = 1$.
Further comments on maxima and dynamic magnification factors are
given in connection with Fig. D.4 and Table D.1.
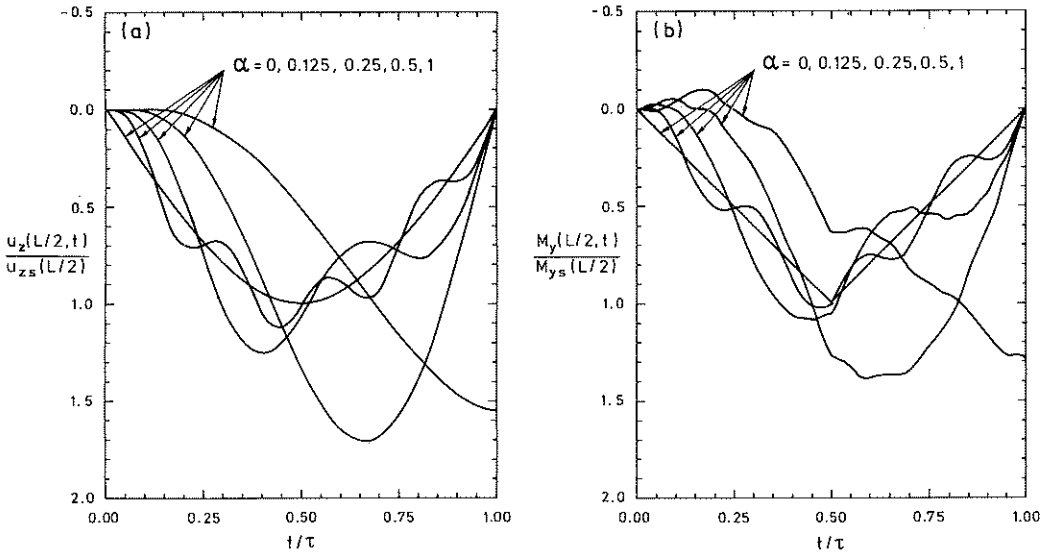
Figure D.2. Time histories for normalized midspan displacement and midspan moment for the problem defined by Fig. D.1, $0 \leq t/\tau \leq 1$. $\alpha = 0$, 0.125, 0.25, 0.5 and 1; $\xi_i = 0$. The curves are derived from Frÿba [38].
(a) Displacement $u_z(L/2, t)$.
(b) Moment $M_y(L/2, t)$.

In the present study, the beam element derived in Chapter 3 is used to solve the problem in Fig. D.1. The efficiency of using only one hierarchical beam element instead of many conventional ones is demonstrated in Sec. C.2 and is utilized here. Thus the beam in Fig. D.1 is modelled as a single beam element. Eight additional displacement functions (eigenfunctions) are used for the displacement component u_z. According to Persson and the author [90] the resulting 10 unconstrained DOF yield as much as eight natural frequencies (ω_1 to ω_8) with an error percentage less than 0.6. In Fig. D.3 obtained results are compared with the ones given by Fig. D.2 ($\alpha = 0.25$).
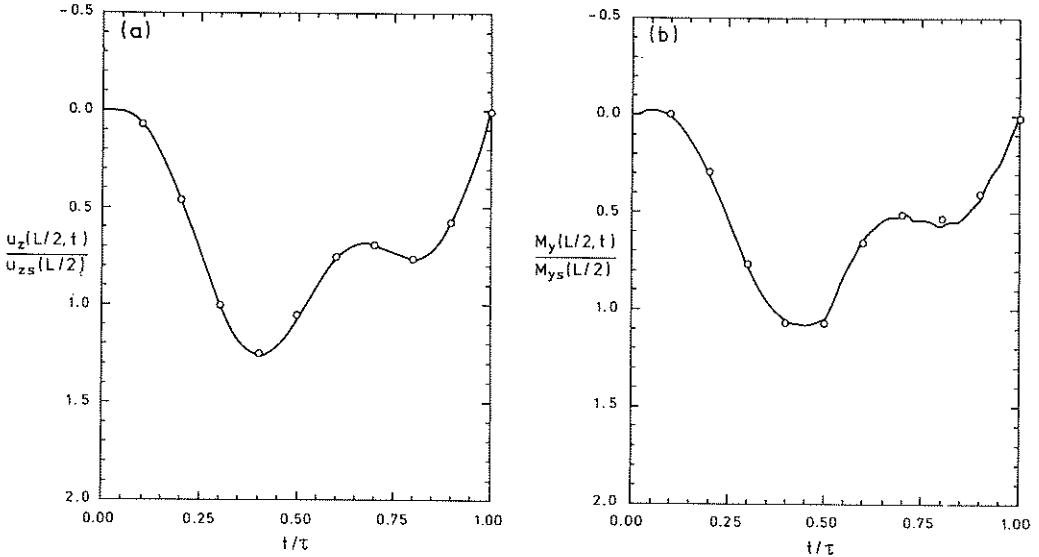
Figure D.3. Time histories for normalized midspan displacement and midspan moment for the problem defined by Fig. D.1, $0 \leq t/\tau \leq 1$. $\alpha = 0.25$ and $\xi_i = 0$. —— Frýba [38]; o Present analysis (one mode, $\Delta t = \tau/100$).
(a) Displacement $u_z(L/2, t)$.
(b) Moment $M_y(L/2, t)$.

Although the spatial and time discretizations are limited to only one mode and 100 time steps respectively, it can be seen from Fig. D.3 that the present results are in good agreement with those given by Frýba [38]. It should be kept in mind, however, that the moment results are not based on the second spatial derivative of the displacement field but on equations of motion for a beam lamina, see Subsec. 3.4.1.

In the remainder of this section, verification studies with respect to dynamic magnification factors of the problem in Fig. D.1 are performed. The factors in question are dynamic magnification for midspan displacement $D_d = \max[u_z(L/2, t)]/u_{zs}(L/2)$ and dynamic

magnification for midspan moment $D_m = \max[M_y(L/2, t)] / M_{ys}(L/2)$. Some comments are also given on magnification factors associated with u_z and M_y outside the midspan. As above the time interval studied is $0 \leq t/\tau \leq 1$, that is, the forced vibration era.

The dynamic magnification factors defined above are calculated for some values of α and compared with exact solutions in Fig. D.4, cf. Figs. D.2 and D.3.
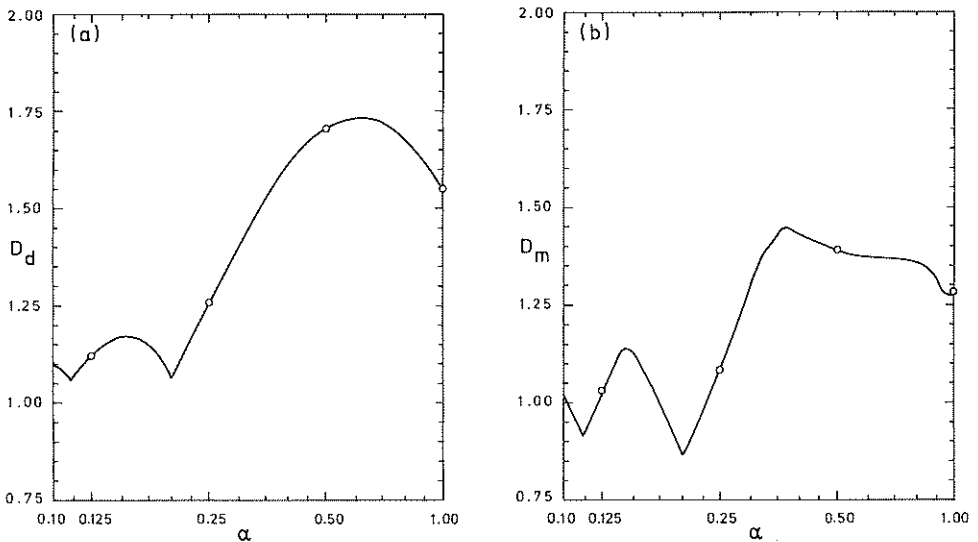
Figure D.4. Dynamic magnification factors for midspan displacement and midspan moment for the problem defined by Fig. D.1, $\alpha = 0.1$–1.0. $\xi_i = 0$ and $0 \leq t/\tau \leq 1$. ———— Frýba [38]; o Present analysis (three modes, $\Delta t = \tau/100$).

    (a) Displacement dynamic magnification factor

        $D_d = \max[u_z(L/2, t)]/u_{zs}(L/2)$; $\max(D_d) = 1.732$ for $\alpha = 0.619$ according to Frýba.

    (b) Moment dynamic magnification factor

        $D_m = \max[M_y(L/2, t)]/M_{ys}(L/2)$; $\max(D_m) = 1.449$ for $\alpha = 0.369$ according to Frýba.

Also in Fig. D.4 good agreement is obtained. Further, it should be noted that the main increases in D_d and D_m occur only in the intervals $0.20 \leq \alpha \leq 0.62$ and $0.20 \leq \alpha \leq 0.37$ respectively. For lower values of the velocity ratio, that is $\alpha < 0.20$, the curves for D_d and D_m are irregular due to the existence of many mathematical maxima; cf. Fig. D.2, Dahlberg [23] and Warburton [133]. For higher values of α, $\alpha > 0.62$ and $\alpha > 0.37$ respectively, D_d and D_m decrease. (It should be remembered that $\alpha = 1.0$ corresponds to a vehicle speed approximately between 400 and 1500 km/h). According to Warburton [133] the maximum midspan displacement occurs during the forced vibration era as long as $\alpha < 1.0$ even if damping is neglected ($\xi_i = 0$), cf. Fig. D.2a for $\alpha = 1.0$. The same cannot be said about the midspan moment. However, for most vehicle speeds and structure damping properties the free vibration era ($t/\tau > 1$) should be of minor interest.

The results for $\alpha = 0.125$, 0.25, 0.5 and 1 illustrated in Fig. D.4 are given numerically in Table D.1. In addition, these results are compared with two other references (D_d only). Once again the validity of the present analysis can be verified from Table D.1. In Yoshida et al. [139][140] also a modal formulation is used an the results obtained are quite good. Note that the study of Yoshida [139] was probably the first moving load study in which the finite element method was applied. It can also be seen that the results obtained by Falabella and referred by Filho [35] also are in good agreement with the exact solution by Frýba [38]. Note, however, that a geometric coordinate formulation with 8 DOF and $\Delta t = \tau/400$ was used by Falabella while 3 modal DOF and $\Delta t = \tau/100$ are used in the present analysis.

In Warburton [133] dynamic magnification factors defined as $\max[u_z(x,t)]/u_{zs}(L/2)$ and $\max[M_y(x,t)]/M_{ys}(L/2)$ are also studied. Thus x may differ from L/2 (midspan). Values of 1.738 ($\alpha = 0.625$, x/L = 0.53) and 1.550 ($\alpha = 0.525$, x/L = 0.636) are obtained for

	(a)				(b)	
α	Frýba [38]	Present analysis	Yoshida [139]	Filho [35]	Frýba [38]	Present analysis
0.125	1.121	1.122	1.112	–	1.027	1.031
0.250	1.258	1.259	1.251	1.258	1.089	1.082
0.500	1.705	1.706	1.700	1.707	1.389	1.390
1.000	1.548	1.550	1.540	1.547	1.273	1.286

Table D.1. Dynamic magnification factors for midspan displacement and midspan moment for the problem defined by Fig. D.1; α = 0.125, 0.25, 0.5 and 1. ξ_i = 0 and $0 \leq t/\tau \leq 1$. Three modes are included and $\Delta t = \tau/100$ for the present analysis. (Cf. Fig. D.4).

(a) Displacement dynamic magnification factor
$$D_d = \max[u_z(L/2,t)]/u_{zs}(L/2).$$

(b) Moment dynamic magnification factor
$$D_m = \max[M_y(L/2,t)]/M_{ys}(L/2).$$

these two quantities. Thus the displacement factor (1.738) is slightly larger than the one given in Fig. D.4 for x/L = 0.50 (1.732). The moment factor (1.550), however, more significantly exceeds the value in Fig. D.4 (1.449), see also Wilson [136]. According to Warburton [133] the value of $\max[M_y(x,t)]/M_{ys}(L/2)$ exceeds 1.45 for $0.36 \leq \alpha \leq 0.7$.

To sum up, the results of this section show that for the problem described in Fig. D.1 the theoretical formulation used in the present study is valid. Although the structure–vehicle interaction is neglected in this section it should serve as an introduction to the problem of structures subjected to moving loads. The neglect of interaction means, however, that the effect of many moving forces (multi–axle vehicle models) can be obtained by superposition.

D.3   Moving mass vehicle models

Another set of vehicle models is that of moving mass models. A moving mass vehicle model is the simplest model in which vehicle mass inertia effects and thus structure–vehicle interaction effects can be treated, cf. Sec. 4.3. For normal or high values of α and κ these models may be relevant provided κ_0 is high (most of the vehicle mass is unsuspended or suspended on stiff primary suspensions) or Ω is low (stiff secondary suspensions). If neither κ_0 nor Ω satisfies these requirements, suspension vehicle models and in some cases moving force models would be more appropriate. In general, neither of the requirements is satisfied for modern passenger vehicles. However, for freight vehicles moving mass models may be of interest.

In the present study the structure–vehicle interaction is handled by means of structure–vehicle finite elements, see Sec. 2.4. It should be realized that the moving mass interaction effects are represented by nonzero interaction part matrices in Eqs. (2.53b–d) (or 2.45b–d) since the mass matrix $\mathbf{M}_{vcc}^e$ is a nonzero matrix. Since T_{cu}^m (T_{cu}) and its derivatives are time-dependent the structure–vehicle element matrices become time-dependent as already mentioned in Sec. 2.4.

Two verification examples are studied in parallel in this section. The two problems are defined in Fig. D.5. As in Sec. D.2 the quantities v, L, A, I_y, $\bar{E}$ and ρ in Fig. D.5 can be represented by the velocity ratio α. Note that a given value of α corresponds to the same vehicle (mass) speed for the two cases above since the span L as well as the eigenfrequency ω_1 are identical for the single span and two span beams in Fig. D.5, cf. Sec. 6.2. In addition to α and ξ_i a third parameter, the mass ratio κ (Sec. 6.2), must be introduced for the above moving mass problems. A given value of κ corresponds to the same vehicle mass for the two beam types in Fig.
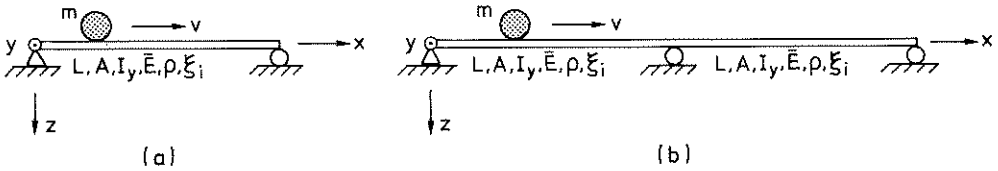
Figure D.5. Uniform (Euler–Bernoulli) beam subjected to a mass m moving at constant speed v. Local coordinate system (x,y,z). Beam cross sectional area A, moment of inertia I_y, elastic modulus $\bar{E} = E$, mass density ρ and modal damping ratios ξ_i. The beam is initially at rest.
(a) Single span beam (length L).
(b) Two span beam (length 2L).

D.5. In the present examples time histories of (vertical) vehicle mass displacement $u_v(t)$ and contact force $f_c(t)$ are studied in particular. Two different velocity ratios are investigated: $\alpha = 0.25$ and $\alpha = 0.5$. The parameter κ is set to 0.5 while damping is neglected ($\xi_i = 0$). $u_{zs}(L/2)$ serves as normalizing displacement factor, that is static midspan displacement (x = L/2) due to the dead weight P = mg of the mass placed at midspan (x = L/2). For the single span beam $u_{zs}(L/2) = PL^3/48\bar{E}I_y$ while $u_{zs}(L/2) = 23/32 \cdot PL^3/48\bar{E}I_y$ for the two span beam. The dead weight mg constitutes the normalizing contact force factor. As in Sec. D.2, t/τ is the nondimensional time parameter.

The problem of Fig. D.5a has been studied by many authors, see Frýba [38] for classical works. More recent investigations of this problem have been undertaken by e.g. Blejwas et al. [9][10], Dahlberg [23], Filho [35], the author [83][85], Ting et al. [122] and Yoshida et al. [139][140]. Both problems in Fig. D.5 have been studied experimentally by Ayre et al. [4]. The results of that laboratory study are used here to check the validity of the present structure-vehicle element and the moving mass model.
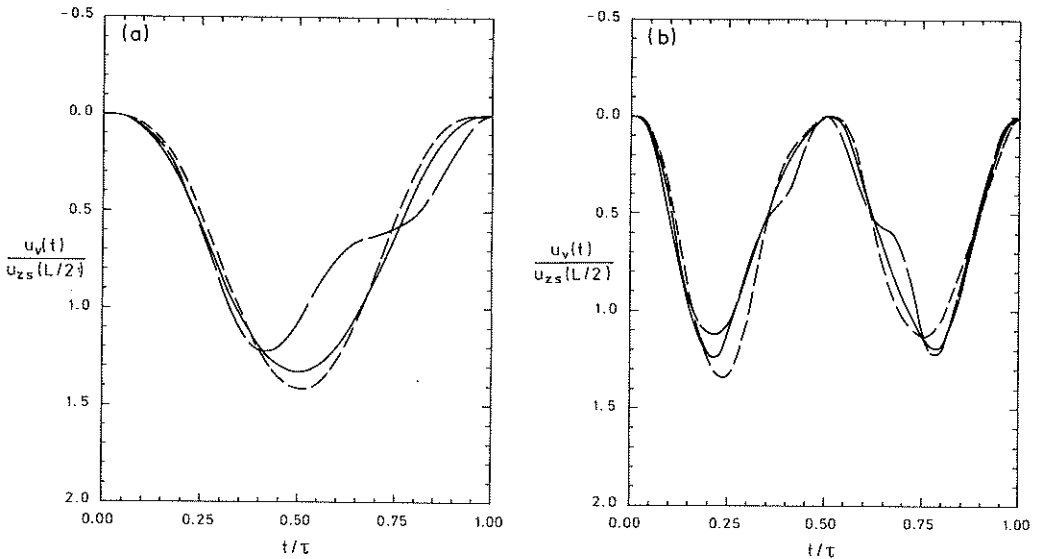
Figure D.6. Time histories for normalized vehicle mass displacement $u_V(t)/u_{zs}(L/2)$ for the problems defined by Fig. D.5, $0 \leq t/\tau \leq 1$. $\alpha = 0.25$, $\kappa = 0.5$ and $\xi_i = 0$. —— Ayre et al. [4] (experimental); — — Present analysis, moving force model; – – – Present analysis, moving mass model.

(a) Single span beam (five modes and $\Delta t = \tau/100$ for present analysis).

(b) Two span beam (five modes and $\Delta t = \tau/200$ for present analysis).

As in Sec. D.2 one single hierarchical finite beam element including eight additional eigenfunctions is used here to model a span. For the two span problem in Fig. D.5 this means that the problem is described in terms of one structure–vehicle element (including the vehicle mass) and one structural element (the unloaded span). For $\alpha = 0.25$, $\kappa = 0.5$ and $\xi_i = 0$ present results of the moving mass problems in Fig. D.5 are compared with the ones found experimentally by Ayre et al. [4], see Figs. D.6 and D.7. Note that a moving force model is also included.

Figure D.7. Time histories for normalized contact force $f_c(t)/mg$ for the problems defined by Fig. D.5, $0 \leq t/\tau \leq 1$. $\alpha = 0.25$, $\kappa = 0.5$ and $\xi_i = 0$. —— Moving force model; — — — Present analysis, moving mass model.

(a) Single span beam (five modes and $\Delta t = \tau/100$ for present analysis).

(b) Two span beam (five modes and $\Delta t = \tau/200$ for present analysis).

From Fig. D.6a it is evident that the moving mass model best describes what happens when the mass is moving over the simply supported beam. For the present two span problem, however, the moving force model is almost as good as the moving mass model, see Fig. D.6b. The reason for this is that the structural mass in question is doubled for the two span case so that the vehicle mass inertia effects are of less importance when compared with the structural ones. This can be seen in Fig. D.7 in which the two span contact force deviates less from the mass weight than the single span force does. The increase of the contact force around midspan and the decrease around the supports can also clearly be realized in

Figure D.8. Time histories for normalized vehicle mass displacement $u_v(t)/u_{zs}(L/2)$ for the problems defined by Fig. D.5, $0 \leq t/\tau \leq 1$. $\alpha = 0.5$, $\kappa = 0.5$ and $\xi_i = 0$. ———— Ayre et al. [4] (experimental); — — Present analysis, moving force model; – – – Present analysis, moving mass model.

(a) Single span beam (five modes and $\Delta t = \tau/100$ for present analysis).

(b) Two span beam (five modes and $\Delta t = \tau/200$ for present analysis).

Fig. D.7. A further verification is found in Filho [35]. For the single span beam and the actual set of parameters Filho finds the dynamic magnification factor for midspan displacement to be 1.418. The value found here is 1.419.

Now the same comparison is made for the doubled velocity ratio: $\alpha = 0.5$. A contact force comparison is also included. The results are shown in Figs. D.8 and D.9.
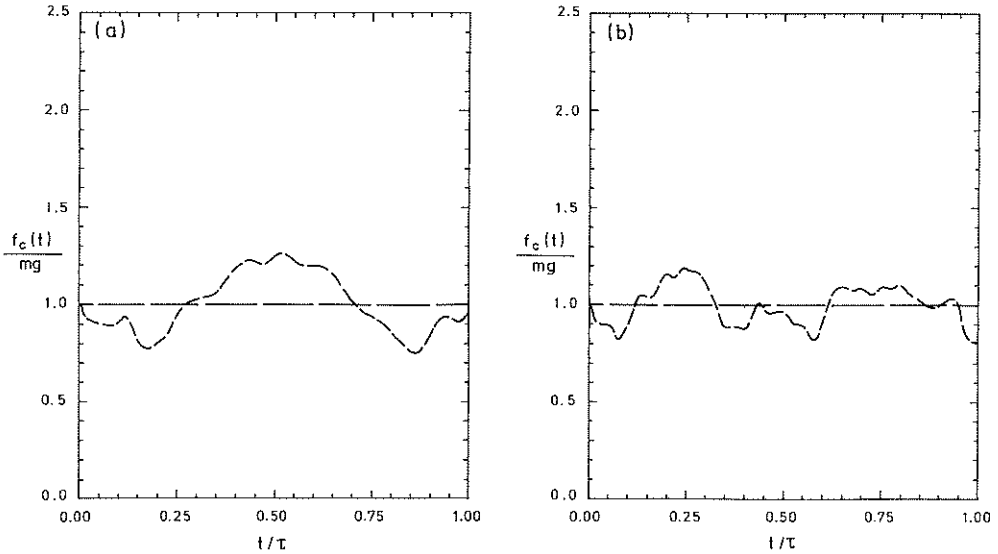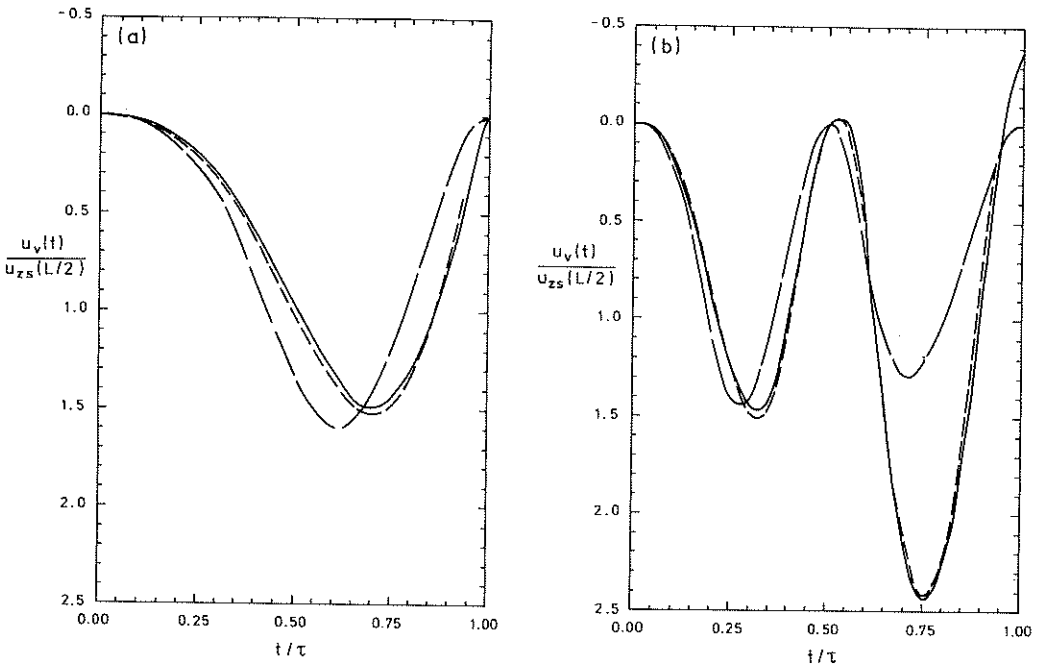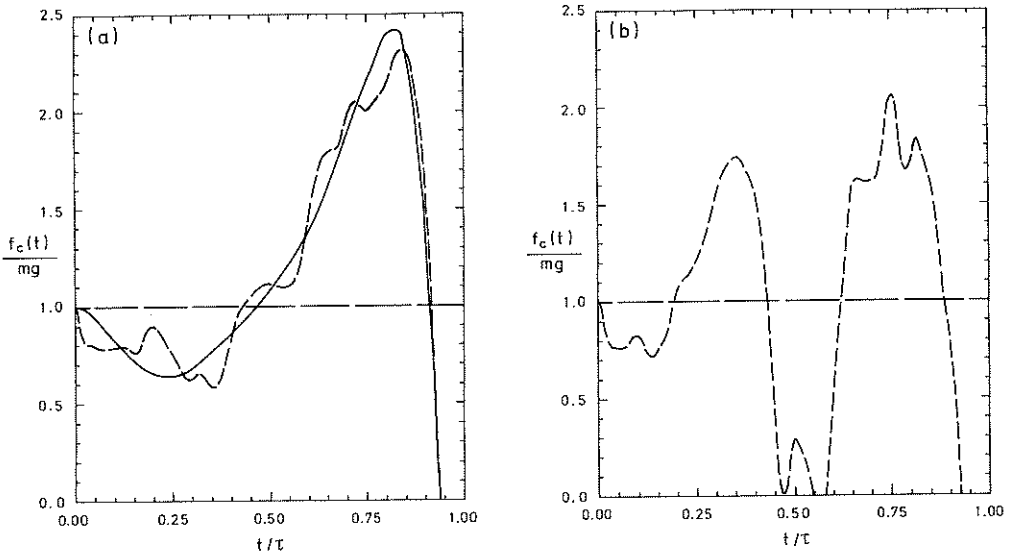
Figure D.9. Time histories for normalized contact force $f_c(t)/mg$ for the problems defined by Fig. D.5, $0 \leq t/\tau \leq 1$. $\alpha = 0.5$, $\kappa = 0.5$ and $\xi_i = 0$. ——— Dahlberg [23], moving mass model; —— Moving force model; — — — Present analysis, moving mass model.

(a) Single span beam (five modes and $\Delta t = \tau/100$ for present analysis).

(b) Two span beam (five modes and $\Delta t = \tau/200$ for present analysis).

It is evident from Fig. D.8 that the moving mass model, described by the structure-vehicle element, gives results in excellent agreement with the experimental ones. For both the single span and two span problem, the simple moving force model fails to describe the structure and vehicle behaviour. For both problems, however, the vehicle mass loses contact with the structure for this increased velocity ratio, see Fig. D.9. This is also found by Ayre and his co-workers. In the present analysis loss of contact and recontact cannot be treated, cf. Subsec. 2.4.1. Thus the dashed lines for the moving mass model in Fig. D.8 are ended when contact is lost.

However, the contact loss about midsupport illustrated in Fig. D.9b has been neglected since only a small tensile force over a short period of time is necessary to maintain contact.

In Fig. D.9a the calculated moving mass contact force has been compared with the one found by Dahlberg [23]. The overall time dependence of the force is similar but the curve obtained by Dahlberg is much smoother. The difference between the two curves is most probably due to the different number of structural modes included and to the special contact force assumption used by Dahlberg: three modes and a seven-term polynomial are used by Dahlberg. The increased irregularities of the contact force curve when more and more modes are included are shown by e.g. Blejwas et al. [9][10] and the author [83][85].

With regard to the dynamic magnification factor for midspan displacement (single span beam), the maximum occurs during the free vibration era for $\alpha = 0.5$. Filho [35] finds the value 2.047 and Dahlberg [23] the value 2.05 for this factor. In the previous work by the author [83], the value 2.045 was found. In the present analysis the free vibration era is not studied. The maximum obtained here during the forced vibration is somewhat smaller: 2.022 ($t/\tau = 0.85$). It should be remembered that the corresponding magnification factor for the moving force model is 1.705, see Table D.1 (Frýba). Thus a noticeable increase is obtained when the inertia effects of the moving mass cannot be neglected.

In conclusion, it is verified in this section that the moving mass model is well suited for the problems of Fig. D.5 and that the interaction can be described adequately by the structure-vehicle element developed. It is also realized that the strong interaction between structure and vehicle mass may result in contact losses which indicates that most of the vehicle mass must be suspended to satisfy comfort and wear requirements etc., see Sec. D.4.

D.4   Suspension vehicle models

The most realistic vehicle models are the suspension models, cf. Sec. 4.2. As indicated in Secs. 6.2 and D.2 the structural effects of suspension models approach those of moving force models for low values of α or κ or for a combination of a low κ_0 value and a high Ω value. On the other hand, the effects are similar to those predicted by moving mass models for high κ_0 values or low Ω values. Thus it is evident that moving force and moving mass models constitute limiting cases of suspension models.

In this section the problem of Fig. D.10, in which the vehicle is represented by a suspension model, is studied. Once again the quantities v, L, A, I_y, $\bar{E}$ and ρ are represented by the ratio α. In addition to α, ξ_i and κ used in Sec. D.3 the parameters κ_0, ξ_v and Ω are utilized for the present problem. These new parameters are related to the quantities m_p, m_s, c and k_s of the vehicle model in Fig. D.10 (cf. Fig. 4.4d) according to Sec. 6.2. Note that a one-axle vehicle model is used (cf. Chapter 6) thus demanding the vehicle length to be short as compared to the span. In this example the maximum value of midspan displacement and the point of time when the maximum occurs are studied for some sets of input parameters. Moreover, suspension contact force histories are compared with moving mass and moving force histories for two parameter sets. As before the normalizing factor for midspan displacement is $u_{zs}(L/2) =$ $PL^3/48\bar{E}I_y$ where now $P = (m_p+m_s)g$. The dead weight $(m_p+m_s)g$ of the vehicle is also used as the normalizing contact force factor.

The problem of Fig. D.10 has been studied by for instance Filho [35] and the author [83][85]. Studies of slightly modified versions of the present problem are reported by e.g. Chiu et al. [14], Dahlberg [22][23] and Frýba [38]. Unfortunately the values of some input
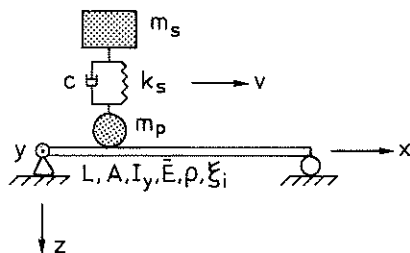
Figure D.10. Uniform, simply supported (Euler-Bernoulli) beam sub-
jected to suspension vehicle moving at constant speed
v. Local coordinate system (x,y,z). Beam length L,
cross sectional area A, moment of inertia I_y, elastic
modulus $\bar{E}=E$, mass density ρ and modal damping ratios
ξ_i. The beam is initially at rest. Vehicle (secondary)
suspension mass m_s, damping c and stiffness k_s.
Unsuspended (primary suspension) mass m_p. The vehicle
is initially at rest in the vertical direction.

parameters are not given in Filho [35]. Instead the work by Dahlberg
[22] and the previous work by the author [83] are used to verify the
validity of the present structure-vehicle element formulation.

As in Secs. D.2 and D.3 one single hierarchical finite beam element
with eight additional eigenfunctions is used here to model the beam
in Fig. D.10. By means of the computer commands BEAM3E, VEK3E,
VEC3EI and VEM3EI described in Sec. 5.4 the structure and vehicle
element matrices are created. Then the structure-vehicle element
matrices and vectors are generated by the commands SVE3EM and
SVE3EV. This means that the problem in Fig. D.10 is described in
terms of one structure-vehicle element and one vehicle mass element
(the suspended mass), cf. Fig. 2.2. It should be noted that the
present structure-vehicle element matrices contain interaction terms
not only due to the unsuspended mass, as in Sec. D.3, but also due
to the damper and spring, cf. Eqs. (2.45b-d) and (2.53b-d).

	(a)		(b)	
κ ⟍ Ω	1.0	2.0	1.0	2.0
0.5	1.36 (1.36)	1.38 (1.38)	0.84 (0.83)	0.64 (0.64)
1.0	1.55 (1.54)	1.15 (1.16)	0.94 (0.93)	0.62 (0.62)

Table D.2. Dynamic magnification factor for midspan displacement and point of time when the maximum occurs for the problem defined by Fig. D.10; $\kappa = 0.5$ and 1.0; $\Omega = 1.0$ and 2.0. $\alpha = 0.5$, $\kappa_0 = 0$, $\xi_i = 0$, $\xi_v = 0.1$ and $0 \leq t/\tau \leq 1$. Five modes included and $\Delta t = \tau/100$ for present analysis. Results by Dahlberg [22] within parentheses.

(a) Dynamic magnification factor

$$D_d = \max[u_z(L/2, t)]/u_{zs}(L/2).$$

(b) Point of time t/τ for maximum displacement.

The dynamic magnification factor for midspan displacement and the point of time when the maximum occurs are calculated for two values of κ and Ω and compared with the results of Dahlberg [22], see Table D.2. As can be seen from Table D.2 the present results are in good agreement with those of Dahlberg. The same quantities are also determined for two values of κ and α and compared with results obtained by the author [83], see Table D.3. It should be noted that conventional beam elements (cf. Sec. C.2) and Newmark's constant-average-acceleration time integration method, see Newmark [80], have been utilized in the previous study by the author [83].

Also in Table D.3 a good agreement can be seen. The value $D_d = 1.19$ in Table D.3a for $\alpha = 0.25$ and $\kappa = 0.5$ corresponds to $D_d = 1.26$ for a moving force model (Table D.1a) and $D_d = 1.42$ for a moving mass

|		(a)		(b)	
κ	α	0.25	0.50	0.25	0.50
0.5		1.19 (1.19)	1.59 (1.59)	0.42 (0.41)	0.70 (0.70)
1.0		1.13 (1.13)	1.51 (1.52)	0.43 (0.43)	0.74 (0.74)

Table D.3.   Dynamic magnification factor for midspan displacement
and point of time when the maximum occurs for the
problem defined by Fig. D.10; κ = 0.5 and 1.0; α = 0.25
and 0.50. κ_0 = 0.25, ξ_i = 0, ξ_v = 0.125, Ω = 3.0 and
$0 \le t/\tau \le 1$. Five modes included and $\Delta t = \tau/100$ for
present analysis. Results by the author [83] within
parentheses.
(a) Dynamic magnification factor
$D_d = \max[u_z(L/2,t)]/u_{zs}(L/2)$.
(b) Point of time t/τ for maximum displacement.

model (Sec. D.3). For α = 0.5 and κ = 0.5, Tables D.2a and D.3a give
three values of D_d: D_d = 1.36, 1.38 and 1.59 depending on the choice
of κ_0, ξ_v and Ω. The corresponding moving force and moving mass
values are here D_d = 1.71 (Table D.1a) and D_d = 2.02 (Sec. D.3)
respectively. (D_d = 2.05 for a moving mass model if the free
vibration era, $t/\tau > 1$, is considered as well). Thus for α = 0.25 or
0.5 and κ = 0.5 a moving mass model gives the highest D_d values
followed by a moving force model. For the present choices of κ_0, ξ_v
and Ω the suspension model in Fig. D.10 gives the lowest D_d values.
This relation between the results due to different vehicle models
may be better understood from Fig. D.11. In this figure contact
force time histories are plotted for the three different vehicle
models.
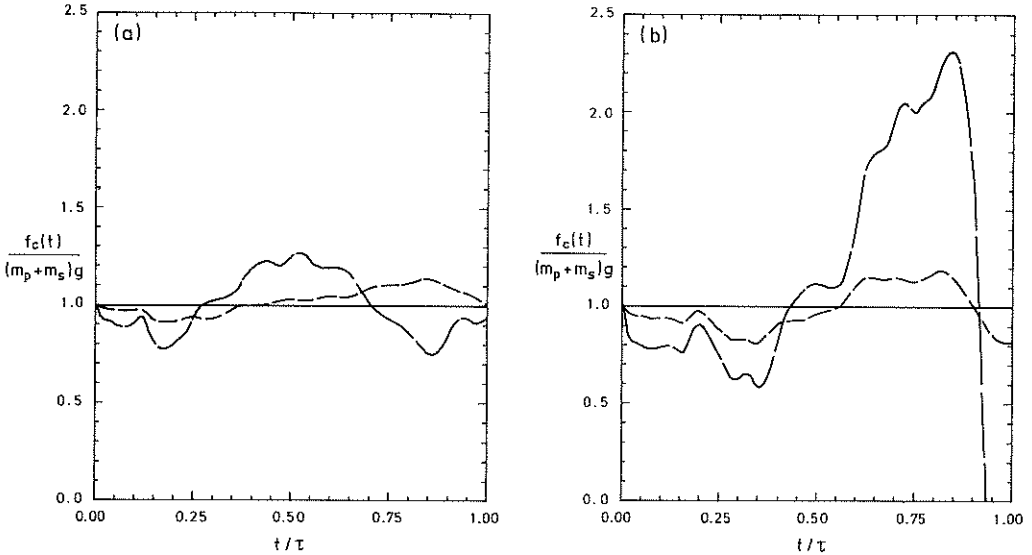
Figure D.11. Time histories for normalized contact force $f_c(t)/(m_p+m_s)g$ for the problem defined by Fig. D.10, $0 \le t/\tau \le 1$. $\kappa = 0.5$, $\kappa_0 = 0.25$, $\xi_i = 0$, $\xi_v = 0.125$ and $\Omega = 3.0$. ——— Moving force model; — — Present analysis, moving mass model; — — — Present analysis, suspension model. Five modes and $\Delta t = \tau/100$ for present analysis.

(a) $\alpha = 0.25$.

(b) $\alpha = 0.50$.

In both figures of Fig. D.11 it can be seen that the suspension contact force is less than the vehicle dead weight for about $0 \le t/\tau \le 0.5$. Although it exceeds $(m_p+m_s)g$ for $0.5 \le t/\tau \le 0.9$ ("uphill"), the resulting D_d value is less than that corresponding to the moving force model. The probable reason for this is that the normalized suspension contact force only exceeds unity by a small amount and that the vehicle has then already passed midspan. The moving mass contact force, however, is certainly less than the suspension one at beam entrance but then it becomes greater than the

suspension contact force. In fact, as high a value as $f_c/(m_p+m_s)g = 2.32$ is obtained at $t/\tau = 0.84$ for the case of $\alpha = 0.50$. Thus, in view of the histories in Fig. D.11, it should not come as a surprise that the highest D_d values are obtained for a moving mass model. Dynamic magnification factors for midspan displacement and midspan moment $(0 \le \alpha \le 1.0)$ of a simply supported beam are given for the three different vehicle models by the author [83][85].

In summary, the results of this section enhance the reliability of the present structure–vehicle element formulation. Attention is also paid to different contact force histories and thus different structural effects for the three vehicle models at hand.

D.5   Summary and conclusions

In this appendix a number of problems are studied in order to verify the validity of the structure–vehicle finite element formulated in Sec. 2.4. The problems refer to either of the three types of vehicle models introduced in Chapter 4. Input and output quantities are given in terms of nondimensional parameters as in Sec. 6.2. The present appendix may also be seen as an introduction to analysis of structures subjected to moving loads. More advanced structural and vehicle models are treated in Chapter 6.

The results obtained are generally in good agreement with the ones obtained by other investigators. This indicates that the structure–vehicle interaction is adequately described by the structure–vehicle element developed.

APPENDIX E. REFERENCES

[1] Aida T.: Dynamic stability of thin walled beams under traveling horizontal follower load systems, Journal of Sound and Vibration, Vol. 94, 3, 431–444, 1984.

[2] Aida T.: Combination resonance of beams under traveling follower load systems, Journal of Sound and Vibration, Vol. 95, 3, 415–422, 1984.

[3] Arpe R.: Dynamic response of bridges due to traffic loading (in Danish), Licentiate thesis, Part 1 and 2, Department of Structural Engineering, Technical University of Denmark, Lyngby, 1984.

[4] Ayre R.S., Jacobsen L.S. and Hsu C.S.: Transverse vibration of one- and two-span beams under the action of a moving mass load, Proceedings 1st US National Congress in Applied Mechanics, 81–90, 1951.

[5] Bathe K.J.: Finite element procedures in engineering analysis, Prentice-Hall, New Jersey, 1982.

[6] Bengtsson B.: Finite element analysis of thin-walled beams (in Swedish), Graduate work, Report TVSM-5008, Division of Structural Mechanics, Lund Institute of Technology, Lund, 1983.

[7] Benscoter S.U.: A theory of torsion bending for multicell beams, Journal of Applied Mechanics, 25–34, March 1954.

[8] Bhatt P.: Problems in structural analysis by matrix methods, The Construction Press, Harlow, Essex, 1981.

[9]   Blejwas T.E.: The simulation of vehicle and structure inter-
      action with nonlinear constraint conditions, Doctoral thesis,
      University of Colorado, 1978.

[10] Blejwas T.E., Feng C.C. and Ayre R.S.: Dynamic interaction of
      moving vehicles and structures, Journal of Sound and
      Vibration, Vol. 67, 4, 513-521, 1979.

[11] Chaudhuri S.K.: Dynamic response of horizontally curved
      I-girder highway bridges due to a moving vehicle, Doctoral
      thesis, University of Pennsylvania, 1975.

[12] Chen W.F. and Atsuta T.: Theory of beam-columns, Vol. 1 and 2,
      McGraw-Hill, New York, 1976 and 1977.

[13] Cheung Y.K.: Finite strip method in structural analysis,
      Pergamon Press, Sydney, 1976.

[14] Chiu W.S., Smith R.G. and Wormley D.N.: Influence of vehicle
      and distributed guideway parameters on high speed vehicle-
      guideway interaction, Journal of Dynamic Systems Measurements
      and Control, ASME, Vol. 93, 1, 25-34, 1971.

[15] Chu K-H., Garg V.K. and Dhar C.L.: Railway-bridge impact:
      Simplified train and bridge model, Journal of the Structural
      Division, ASCE, Vol. 105, ST9, 1823-1844, 1979.

[16] Chung Y.I. and Genin J.: Stability of a vehicle on a multispan
      simply supported guideway, Journal of Dynamic Systems Measure-
      ments and Control, ASME, Vol. 100, 4, 326-332, 1978.

[17] Clough R.W. and Penzien J.: Dynamics of structures, McGraw-
      Hill, New York, 1975.

[18] Cooperrider N.K. and Law E.H.: Rail vehicle dynamics, Course given at Chalmers University of Technology, Gothenburg, 1982.

[19] Craig R.R.: Structural dynamics – An introduction to computer methods, John Wiley and Sons, New York, 1981.

[20] Culver C.G.: Natural frequencies of horizontally curved beams, Journal of the Structural Division, ASCE, Vol. 93, ST2, 189–203, 1967.

[21] Culver C.G.: Horizontally curved girders – state of the art, Journal of the Structural Division, ASCE, Vol. 95, ST5, 853–870, 1969.

[22] Dahlberg T.: Vehicle-bridge interaction, Part I and II, Division of Solid Mechanics, Chalmers University of Technology, Gothenburg, 1984.

[23] Dahlberg T.: Vehicle-bridge interaction, Vehicle System Dynamics, 13, 187–206, 1984.

[24] Dahlblom O. and Peterson A.: CAMFEM – Computer aided modelling based on the finite element method, Report TVSM–3001, Division of Structural Mechanics, Lund Institute of Technology, Lund, 1982.

[25] Dahlblom O., Peterson A. and Petersson H.: CALFEM – A program for computer aided learning of the finite element method, Report TVSM–3007, Division of Structural Mechanics, Lund Institute of Technology, Lund, 1986.

[26] Dahlblom O.: Environmental influence on concrete structures: Constitutive modelling and finite element analysis, Doctoral thesis, Division of Structural Mechanics, Lund Institute of Technology, Lund. To be published.

[27] Dailey G., Caywood W.C. and O'Connor J.S.: A general purpose computer program for the dynamic simulation of vehicle-guideway interaction, AIAA Journal, Vol. 11, 3, 278-282, 1973.

[28] Das P.K.: Coupled vibration of a horizontally curved bridge subjected to simulated highway loadings, Doctoral thesis, University of Pennsylvania, 1971.

[29] Dey S.S. and Balasubramanian N.: Dynamic response of ortho-tropic curved bridge decks due to moving loads, Computers and Structures, Vol. 18, No. 1, 27-32, 1984.

[30] Duffek W., Kortüm W. and Wallrapp O.: A general purpose program for the simulation of vehicle-guideway interaction, IUTAM symposium, Vienna, 1977.

[31] Duffek W. and Jaschinski A.: Simulation des dynamischen Bogenlaufs von Rad/Schiene-Fahrzeugen mit dem Mehrkörper-programm MEDUSA, VDI-Berichte Nr. 510, 285-292, 1984.

[32] Dynamics of steel elevated guideways – An overview, By the Subcommittee on Vibration Problems Associated with Flexural Members on Transit Systems, Committee on Flexural Members of the Committee on Metals of the Structural Division, Journal of Structural Engineering, Vol. 111, 9, 1873-1898, 1985.

[33] Dössing O.: Dynamic design verification of a prototype rapid transit train using modal analysis, Brüel & Kjaer, 1984.

[34] Filho F.V.: Dynamic influence lines of beams and frames, Journal of the Structural Division, ASCE, Vol. 92, ST2, 371–386, 1966.

[35] Filho F.V.: Finite element analysis of structures under moving loads, Shock and Vibration Digest, Vol. 10, 8, 27–35, 1978.

[36] Fleming J.F. and Romualdi J.P.: Dynamic response of highway bridges, Journal of the Structural Division, ASCE, Vol. 87, ST7, 31–61, 1961.

[37] Friberg O.: Exact methods in coupled vibrations of beams and in dynamic substructure synthesis, Doctoral thesis, Division of Solid Mechanics, Chalmers University of Technology, Gothenburg, 1984.

[38] Frýba L.: Vibration of solids and structures under moving loads, Noordhoff International Publishing, Groningen, 1972.

[39] Garg V.K., Chu K.H. and Wang T.L.: A study of railway bridge/vehicle interaction and evaluation of fatigue life, Earthquake Engineering and Structural Dynamics, Vol. 13, 689–709, 1985.

[40] Genin J. and Maybee J.S.: Introduction to applied mathematics, Holt, Rinehart and Winston, New York, 1970.

[41] Genin J. and Chung Y.I.: Response of a continuous guideway on equally spaced supports traversed by a moving vehicle, Journal of Sound and Vibration, Vol. 67, 2, 245–251, 1979.

[42] Genin J., Ting E.C. and Vafa Z.: Curved bridge response to a moving vehicle, Journal of Sound and Vibration, Vol. 81, 4, 469–475, 1982.

[43] Gjelsvik A.: The theory of thin walled bars, John Wiley and Sons, New York, 1981.

[44] Greenwood D.T.: Classical dynamics, Prentice-Hall, Englewood Cliffs, 1977.

[45] Guide for evaluation of human exposure to whole body vibration, Draft International Standard ISO/DIS 2631, International Organization for Standardization, 1972/1978.

[46] Gupta R.K. and Traill-Nash R.W.: Bridge dynamic loading due to road surface irregularities and braking of vehicle, Earthquake Engineering and Structural Dynamics, Vol. 8, 83-96, 1980.

[47] Hillerborg A.: Dynamic influences of smoothly running loads on simply supported girders, Doctoral thesis, Institution of Structural Engineering and Bridge Building, Royal Institute of Technology, Stockholm, 1951.

[48] Hino J., Yoshimura T. and Konishi K.: A finite element method prediction of the vibration of a bridge subjected to a moving vehicle load, Journal of Sound and Vibration, Vol. 96, 1, 45-53, 1984.

[49] Houbolt J.C.: A recurrence matrix solution for the dynamic response of elastic aircraft, Journal of the Aeronautical Science, Vol. 17, 540-550, 1950.

[50] Howson W.P. and Williams F.W.: Natural frequencies of frames with axially loaded Timoshenko members, Journal of Sound and Vibration, Vol. 26, 4, 503-515, 1973.

[51] Huang T.: Vibration of bridges, Shock and Vibration Digest, 8, 61-76, 1976.

[52] Joseph T.P. and Wilson J.F.: Vibrations of curved spans for mass transit, Journal of the Engineering Mechanics Division, ASCE, Vol. 106, EM2, 255-272, 1980.

[53] Karaolides C.K. and Kounadis A.N.: Forced motion of a simple frame subjected to a moving force, Journal of Sound and Vibration, Vol. 88, 1, 37-45, 1983.

[54] Khouday A. and Proulx J.: Réaction dynamique des structures soumises aux charges mobiles, International Association for Bridge and Structural Engineering, 351, 103-133, 1975.

[55] Kishan H. and Traill-Nash R.W.: A modal method for calculation of highway bridge response with vehicle braking, Civil Engineering Transactions, 44-50, 1977.

[56] Kollbrunner C.F. and Hajdin N.: Wölbkrafttorsion dünnwandiger Stäbe mit geschlossenem Profil, Mitteilungen der Technischen Kommission, Heft 32, Schweizer Stahlbau-Vereinigung, Zürich, 1965.

[57] Kollbrunner C.F. and Hajdin N.: Dünnwandiger Stäbe, Band 1, Springer-Verlag, Berlin, 1972.

[58] Kolousek V.: Dynamics in engineering structures, Butterworths, London, 1973.

[59] Kortüm W. and Richter R.: Simulation of multibody vehicles moving over elastic guideways, Vehicle System Dynamics, 6, 21-35, 1977.

[60] Kortüm W. and Wormley D.N.: Dynamic interaction between travelling vehicles and guideway systems, Vehicle System Dynamics, 10, 285-317, 1981.

[61] Kortüm W.: Vehicle response on flexible track, Proceedings of the International Conference on MAGLEV Transport Now and in the Future, Solihull, England, 1984.

[62] Kortüm W. and Schiehlen W.O.: General purpose vehicle system dynamics software based on multibody formalisms, Vehicle System Dynamics, 14, 229–263, 1985.

[63] Krenk S.: A linear theory for pretwisted elastic beams, Journal of Applied Mechanics, Vol. 50, 137–142, 1983.

[64] Lees A.W. and Thomas D.L.: Unified Timoshenko beam finite element, Journal of Sound and Vibration, Vol. 80, 3, 355–366, 1982.

[65] Loo Y.C. and Cusens A.R.: The finite-strip method in bridge engineering, Viewpoint Publications, Alden Press, London,1978.

[66] Lundén R. and Åkesson B.: Damped second-order Rayleigh-Timoshenko beam vibration in space – An exact complex dynamic member stiffness matrix, International Journal for Numerical Methods in Engineering, Vol. 19, 431–449, 1983.

[67] Machida F. and Matsuura A.: Dynamic response of concrete railway bridges, Proceedings International Association for Bridge and Structural Engineering, IABSE Periodica, 2, 53–68, 1983.

[68] Magnus K.: Kreisel – Theorie und Anwendungen, Springer-Verlag, Berlin/Heidelberg, 1971.

[69] Magrab E.B.: Vibrations of elastic structural members, Sijthoff & Noordhoff, Alphen aan den Rijn, 1979.

[70] Malsch H.: Zur Berechnung von Durchsenkungen eines Balkens unter Folgen von wanderenden Lasten mit Finiten Raum-Zeit-Elementen, Ingenieur-Archiv, Vol. 47, 105-115, 1978.

[71] Malvern L.E.: Introduction to the mechanics of a continuous medium, Prentice-Hall, New Jersey, 1969.

[72] Matsuura A.: A reduced scale model test of dynamic response of railway bridge to the passage of railway car, Quarterly Report of the Railway Technical Research Institute, Vol. 12, 3, 127-132, 1971.

[73] Matsuura A.: Dynamic interaction between vehicle and girders in high speed railways, Quarterly Report of the Railway Technical Research Institute, Vol. 15, No. 3, 133-136, 1974.

[74] Mei C.: Coupled vibrations of thin-walled beams of open section using the finite element method, International Journal of Mechanical Sciences, Vol. 12, 883-891, 1970.

[75] Meirovitch L. and Baruh H.: On the inclusion principle for the hierarchical finite element method, International Journal for Numerical Methods, Vol. 19, 281-291, 1983.

[76] Meriam J.L.: Engineering mechanics – statics and dynamics, John Wiley and Sons, New York, 1980.

[77] Mulcahy N.L.: Bridge response with tractor-trailer vehicle loading, Earthquake Engineering and Structural Dynamics, Vol. 11, 649-665, 1983.

[78] Murray N.W.: Introduction to the theory of thin-walled structures, Clarendon Press, Oxford, 1984.

[79] Möller P.: Hierarchical and adaptive finite element for-
     mulation for second order elliptic problems, Licentiate
     thesis, Department of Structural Mechanics, Chalmers
     University of Technology, Gothenburg, 1985.

[80] Newmark N.M.: A method of computation for structural dynamics,
     Journal of the Engineering Mechanical Division, ASCE, Vol. 85,
     EM3, 67-94, 1959.

[81] Nilsson L.: Impact loading on concrete structures, Doctoral
     thesis, Department of Structural Mechanics, Chalmers
     University of Technology, 1979.

[82] Oden J.T. and Ripperger E.A.: Mechanics of elastic structures
     (2nd ed.), McGraw-Hill, New York, 1981.

[83] Olsson M.: Finite element analysis of structures subjected to
     moving loads, Report TVSM-3004, Division of Structural
     Mechanics, Lund Institute of Technology, Lund, 1983.

[84] Olsson M.: The finite element method in structural dynamics
     with applications to earthquake and moving load analysis,
     Licentiate thesis, Report TVSM-7015, Division of Structural
     Mechanics, Lund Institute of Technology, Lund, 1983.

[85] Olsson M.: Finite element, modal co-ordinate analysis of
     structures subjected to moving loads, Journal of Sound and
     Vibration, Vol. 99, 1, 1-12, 1985.

[86] Olsson M.: A finite element for analysis of beams and space
     frames, Report TVSM-3006, Division of Structural Mechanics,
     Lund Institute of Technology, Lund, 1985.

[87] Olsson M.: Study trip to West Germany 1985 (in Swedish), Report TVSM-7024, Division of Structural Mechanics, Lund Institute of Technology, Lund, 1985.

[88] Olsson M.: A finite element for dynamic analysis of beams and space frames, Proceedings 4th International Modal Analysis Conference, Union College, Schenectady, New York, 884–890, 1986.

[89] Paz M.: Structural dynamics – Theory and computation, Van Nostrand Reinhold Company, New York, 1980.

[90] Persson T. and Olsson M.: On approximations in structural dynamics (in Swedish), Report TVSM-7023, Division of Structural Mechanics, Lund Institute of Technology, Lund, 1984.

[91] Peterson A.: Finite element analysis of structures at high temperatures, Doctoral thesis, Report TVSM-1001, Division of Structural Mechanics, Lund Institute of Technology, Lund, 1984.

[92] Petersson H.: Analysis of beams of thin-walled open section (in Swedish), Division of Structural Mechanics, Lund Institute of Technology, Lund, 1984.

[93] Popp K.: Beiträge zur Dynamik von Magnetschwebefahrzeugen auf geständerten Fahrwegen, VDI Zeitschriften, Reihe 12, 35, Düsseldorf, 1979.

[94] Popp K.: Stochastic and elastic guideway models, CISM Courses and Lectures No. 274, 13–38, 1982.

[95] Popp K., Kraus A. and Heiss T.: Dynamical analysis of a simple vehicle on a periodic guideway, Vehicle System Dynamics, Vol. 11, 107–120, 1982.

[96] Przemieniecki J.S.: Theory of matrix structural analysis, McGraw-Hill, New York, 1968.

[97] Rabizadeh R.O.: Static and dynamic analysis of horizontally curved box girder bridges, Doctoral thesis, University of Pennsylvania, 1974.

[98] Rabizadeh R.O. and Shore S.: Dynamic analysis of curved box-girder bridges, Journal of the Structural Division, Vol. 101, ST9, 1899–1912, 1975.

[99] Ramakrishnan R. and Kunukkasseril V.X.: Response of circular bridge decks to moving vehicles, Earthquake Engineering and Structural Dynamics, Vol. 5, 377–394, 1977.

[100] Rayleigh J.W.S.: Theory of sound, McMillan and Co., London, 1894.

[101] Richardson H.H. and Wormley D.N.: Transportation vehicle/beam-elevated guideway dynamic interactions; A state-of-the-art review, Journal of Dynamic Systems Measurements and Control, ASME, Vol. 96, 2, 169–179, 1974.

[102] Ripegård G.: Dynamic analysis of beam subjected to moving load (in Swedish), Graduate work, Report TVSM-5004, Division of Structural Mechanics, Lund Institute of Technology, Lund, 1983.

[103] Sadek E.A.: On the dynamics of framed structures, Computers and Structures, Vol. 20, 6, 1013–1019, 1985.

[104] Sandberg G.: Finite element modelling of fluid-structure interaction, Doctoral thesis, Report TVSM-1002, Division of Structural Mechanics, Lund Institute of Technology, Lund, 1986.

[105] Schiehlen W.O. (ed.): Dynamics of high-speed vehicles, CISM Courses and Lectures No. 274, Springer-Verlag, Wien, 1982.

[106] Schiehlen W.O.: Modeling by multibody systems, CISM Courses and Lectures No. 274, 39-49, 1982.

[107] Schiehlen W.O.: Dynamics of complex multibody systems, Structural Mechanics Archives, 9, 159-195, 1984.

[108] Schneider H-J., Elf H.P. and Kölle P.: Modeling of travelling-loads and time-dependent masses with ADINA, Computers and Structures, Vol. 17, No. 5-6, 749-755, 1983.

[109] Segerlind L.J.: Applied finite element analysis, John Wiley and Sons, New York, 1976.

[110] Smith C.C., Gilchrist A.J. and Wormley D.N.: Multiple and continuous span elevated guideway-vehicle dynamic performance, Journal of Dynamic Systems Measurements and Control, ASME, Vol. 97, 1, 30-40, 1975.

[111] Smith J.W.: Finite strip analysis of the dynamic response of beam and slab highway bridges, Earthquake Engineering and Structural Dynamics, Vol. 1, 357-370, 1973.

[112] Spencer A.J.M.: Continuum mechanics, Longman Mathematical Texts, London, 1980.

[113] Srinivasan R.S. and Munaswamy K.: Dynamic response of skew bridge decks, Earthquake Engineering and Structural Dynamics, Vol. 6, 139-156, 1978.

[114] Stanisic M.M.: On a new theory of the dynamic behaviour of the structures carrying moving masses, Ingenieur-Archiv, Vol. 55, 176-185, 1985.

[115] Szabo B.A.: Some recent developments in finite element analysis, Computers and Mathematics with Applications, Vol. 5, 99-115, 1979.

[116] Tan C.P. and Shore S.: Dynamic response of a horizontally curved bridge, Journal of the Structural Division, ASCE, Vol. 94, ST3, 761-781, 1968.

[117] Tan C.P. and Shore S.: Response of horizontally curved bridge to moving load, Journal of the Structural Division, ASCE, Vol. 94, ST9, 2135-2151, 1968.

[118] Thelandersson S.: Computer structural analysis (in Swedish), Studentlitteratur, Lund, 1984.

[119] Thelandersson S.: Analysis of thin-walled elastic beams, Division of Structural Mechanics, Lund Institute of Technology, Lund, 1986.

[120] Timoshenko S.P.: Strength of materials - Part 1 (2nd ed.), D. Van Nostrand Company, New York, 1940.

[121] Timoshenko S.P. and Goodier J.N.: Theory of elasticity (2nd ed.), McGraw-Hill, Tokyo, 1951.

[122] Ting E.C., Genin J. and Ginsberg J.H.: A general algorithm for moving mass problems, Journal of Sound and Vibration, Vol. 33, 1, 49-58, 1974.

[123] Ting E.C., Genin J. and Ginsberg J.H.: Literature review – Dynamic interaction of bridge structures and vehicles, Shock and Vibration Digest, Vol. 7, 11, 61-69, 1975.

[124] Ting E.C. and Genin J.: Dynamics of bridge structures, Structural Mechanics Archives, Vol. 5, 3, 217-252, 1980.

[125] Ting E.C. and Yener M.: Vehicle-structure interactions in bridge dynamics, Shock and Vibration Digest, Vol. 15, 2, 3-9, 1983.

[126] Tralli A.: A simple hybrid model for torsion and flexure of thin-walled beams, Computers and Structures, Vol. 22, No. 4, 649-658, 1986.

[127] Truesdell C.: A first course in rational continuum mechanics – Volume 1, Academic Press, London, 1977.

[128] VDI-Berichte 510: Dynamik schneller Bahnsysteme – Rad/Schiene- und Magnetschwebetechnik, Verein Deutscher Ingenieure, VDI-Verlag, Düsseldorf, 1984.

[129] Veletsos A.S. and Huang T.: Analysis of dynamic response of highway bridges, Journal of the Engineering Mechanics Division, ASCE, Vol. 96, EM5, 593-620, 1970.

[130] Vichnevetsky R.: Computer methods for partial differential equations – Volume 1 (Elliptic equations and the finite element method), Prentice-Hall, Englewood Cliffs, 1981.

[131] Vlasov V.Z.: Thin-walled elastic beams (2nd ed.), Israel Program for Scientific Translations, Jerusalem, 1961.

[132] von Karman T. and Christensen N.B.: Methods of analysis for torsion with variable twist, Journal of the Aeronautical Sciences, 110-124, April 1944.

[133] Warburton G.B.: The dynamic behaviour of structures (2nd ed.), Pergamon Press, Oxford, 1976.

[134] Wilson J.F.: Model experiments for span-vehicle dynamics, Journal of the Engineering Mechanics Division, ASCE, Vol. 103, EM4, 701-715, 1977.

[135] Wilson J.F. and Barbas S.T.: Responses of continuous elastically supported beam guideways to transit loads, Journal of Dynamic Systems Measurements and Control, ASME, Vol. 102, 4, 247-254, 1980.

[136] Wilson J.F.: Optimal design methodology for elevated transit structures, Report UMTA-NC-11-0010-81-2, US Department of Transportation, 1981.

[137] Wood W.L.: On the Zienkiewicz four-time-level scheme for the numerical integration of vibration problems, International Journal for Numerical Methods in Engineering, Vol. 11, 1519-1528, 1977.

[138] Wood W.L.: A further look at Newmark, Houbolt, etc., time-stepping formulae, International Journal for Numerical Methods in Engineering, Vol. 20, 1009-1017, 1984.

[139] Yoshida D.M.: Dynamic response of beams and plates due to moving loads, Doctoral thesis, Stanford University, California, 1970.

[140] Yoshida D.M. and Weaver W.: Finite element analysis of beams and plates with moving loads, Publication International Association for Bridge and Structural Engineering, Vol. 31, 1, 179-195, 1971.

[141] Zienkiewicz O.C.: The finite element method (3rd ed.), McGraw-Hill, London, 1977.

[142] Zienkiewicz O.C., De S.R. Gago J.P. and Kelly D.W.: The hierarchical concept in finite element analysis, Computers and Structures, Vol. 16, No. 1-4, 53-65, 1983.

[143] Zienkiewicz O.C., Wood W.L., Hine N.W. and Taylor R.L.: A unified set of single step algorithms - Part 1: General formulation and applications, International Journal for Numerical Methods in Engineering, Vol. 20, 1529-1552, 1984.

[144] Åkesson B.: Handbook of torsion of beams (in Swedish), Vol. 1 and 2, Department of Structural Mechanics, Chalmers University of Technology, Gothenburg, 1969 and 1970.